Tetra-coordinated boron functionalized phenanthroimidazole and pyrazole based fluorophores: Synthesis, characterization, photocatalytic and sensing applications

By

Prakash Nayak

CHEM11201704004

National Institute of Science Education and Research Bhubaneswar, Odisha-752050

A thesis submitted to the

Board of Studies in Chemical Sciences

In partial fulfillment of requirements

for the Degree of

DOCTOR OF PHILOSOPHY

of

HOMI BHABHA NATIONAL INSTITUTE

January 2023

Homi Bhabha National Institute[1]

Recommendations of the Viva Voce Committee

As members of the Viva Voce Committee, we certify that we have read the dissertation prepared by **Prakash Nayak** entitled "**Tetra-coordinated boron functionalized phenanthroimidazole and pyrazole based fluorophores: Synthesis, characterization, photocatalytic and sensing applications**" and recommend that it may be accepted as fulfilling the thesis requirement for the award of Degree of Doctor of Philosophy.

Chairman: Prof. A. Srinivasan		Date: 02/05/2023
Guide: Prof. V. Krishnan		Date: 02/05/2023
Co-Guide: Prof. V. Chandrasekhar		Date: 02/05/2023
Examiner: Prof. R. Murugavel		Date: 02/05/2023
Member 1- Prof. U. Lourderaj		Date: 02/05/2023
Member 2- Prof. S. Peruncheralathan		Date: 02/05/2023
Member 3- Prof. P. Singru		Date: 02/05/2023

Final approval and acceptance of this thesis is contingent upon the candidate's submission of the final copies of the thesis to HBNI.
We hereby certify that we have read this thesis prepared under my/our direction and recommend that it may be accepted as fulfilling the thesis requirement.

Date: 02/05/2023   (Prof. V. Chandrasekhar)   (Prof. V. Krishnan)

Place: Bhubaneswar   Co-guide (if any)   Guide

---

[1] This page is to be included only for final submission after successful completion of viva voce.

STATEMENT BY AUTHOR

This dissertation has been submitted in partial fulfillment of requirements for an advanced degree at Homi Bhabha National Institute (HBNI) and is deposited in the Library to be made available to borrowers under the rules of the HBNI.

Brief quotations from this dissertation are allowable without special permission, provided that accurate acknowledgement of the source is made. Requests for permission for extended quotation from or reproduction of this manuscript in whole or in part may be granted by the Competent Authority of HBNI when in his or her judgment the proposed use of the material is in the interests of scholarship. In all other instances, however, permission must be obtained from the author.

Prakash Nayak

Prakash Nayak

DECLARATION

I, hereby declare that the investigation presented in the thesis has been carried out by me. The work is original and has not been submitted earlier as a whole or in part for a degree / diploma at this or any other Institution / University.

Prakash Nayak

Prakash Nayak

List of Publications arising from the thesis

Journal

1. "B-N coordinated phenanthroimidazole based zinc-salen as a photocatalyst for the synthesis of oxazolidinones using carbon dioxide as C1 source under mild conditions", Prakash Nayak, Anna Chandrasekar Murali, Venkateswara Rao Velpuri, Vadapalli Chandrasekhar* and Krishnan Venkatasubbaiah*, *Adv. Synth. Cat.,* **2023**, *365*, 230-237

2. "Tetra-coordinated boron functionalized phenanthroimidazole based Zinc-salen as a photocatalyst for the cycloaddition of CO_2 and epoxides", Prakash Nayak, Anna Chandrasekar Murali, Pradeep Kumar Pal, U. Deva Priyakumar,* Vadapalli Chandrasekhar,* and Krishnan Venkatasubbaiah*, *Inorg. Chem.,* **2022**, *61*, 14511-14516

3. "Tetra-coordinated boron-appended zinc(II)-salen: a highly selective fluorescence-based sensor for Sm^{3+} ions *via* sensitization", Prakash Nayak, Anna Chandrasekar Murali, Vadapalli Chandrasekhar,* and Krishnan Venkatasubbaiah* *Mater. Adv.,* **2022**, *3*, 5893–5899

Prakash Nayak

Prakash Nayak

Conferences

1. ''Synthesis and Functionalization of π-Extended B-N coordinated phenanthroimidazole polyaromatic hydrocarbons and study their optical properties'' - International Conference on Main Group Molecules to Materials – II, 2022, December 13-15, School of Chemical Sciences, NISER Bhubaneswar (Online poster presentation)

2. ''π-extended B$\leftarrow$N coordinated phenanthroimidazole dimers and their NLO properties''- 27th CRSI-National Symposium Chemistry held at the Novotel Hotel, Kolkata during September 26 –29, 2021 (Online poster presentation)

3. ''Synthesis of B$\leftarrow$N Coordinated Tetrahydrodibenzophenanthridine Polycyclic Aromatic Hydrocarbons and Study Their Optical Properties'' – Funtional Smart & Supramolecular Materials (FSSM-2020), January 29-30, 2020, IIT Kharagpur (Poster presentation)

Prakash Nayak

Prakash Nayak

*Dedicated to my mother **Mrs. Geeta Nayak***

ACKNOWLEDGEMENTS

CONTENTS

Synopsis

Organization of thesis

The present thesis has been divided into five chapters. The contents of the different chapters are briefly mentioned below.

Chapter 1: Introduction

This chapter describes a brief introduction to fluorescent boron compounds. Boron-based fluorophores are broadly divided into two groups, namely, (a) tri-coordinated boron compounds and (b) tetra-coordinated boron compounds.

Lewis acidity of tri-coordinated boron compounds is caused by the presence of an empty p_z-orbital. These compounds are susceptible to attack by Lewis bases like water due to the availability of an empty coordination site on the boron center. The tri-coordinated boron complexes are stabilized by sterically crowded aromatic groups such as mesityl, fluoro mesityl, and triisopropyl phenyl or by using π-donor substituents like alkoxy groups.[1]

Tetra-coordinated boron compounds often exhibit greater stability than tri-coordinated boron compounds. Therefore there has been much effort in the design and synthesis of tetra-coordinated boron compounds which have been widely used in optoelectronics including photoresponsive materials, OLEDs, OFETs, and sensory and biological imaging materials.[2] Due to coordinative saturation at the boron center, tetra-coordinated boron compounds exhibited increased chemical stability and rigidity with high fluorescence quantum yield. The luminescent tetra-coordinated boron compounds can be broadly classified into four different types based on the chelated donor atoms, namely, (a) O, O-chelate boron compounds, (b) N,C-chelate boron compounds, (c) N,O-chelate

boron compounds, and (d) N,N-chelate boron compounds. This thesis focuses on the N,C-chelated boron compounds and their applications.

Chapter 2: Tetra-coordinate boron appended Zinc(II)-salen: A highly selective fluorescence-based sensor for Sm^{3+} ion *via* sensitization

Selective detection of metal ions has emerged as an important area of research due to its implications in the area of environmental, biology, and clinical studies. Fluorescence-based probes or sensors have gained considerable attention due to their simplicity, selectivity, and sensitivity toward specific metal ions.[3] On the other hand, lanthanoids have found applications in the fields of magnetism, display, components of nuclear control rods, and even as catalysts.[4] Detection of lanthanoid ions is important due to their toxicity. Selective detection and discrimination of lanthanoid ions is a major challenge due to their similarity in size and chemical behavior.[5]
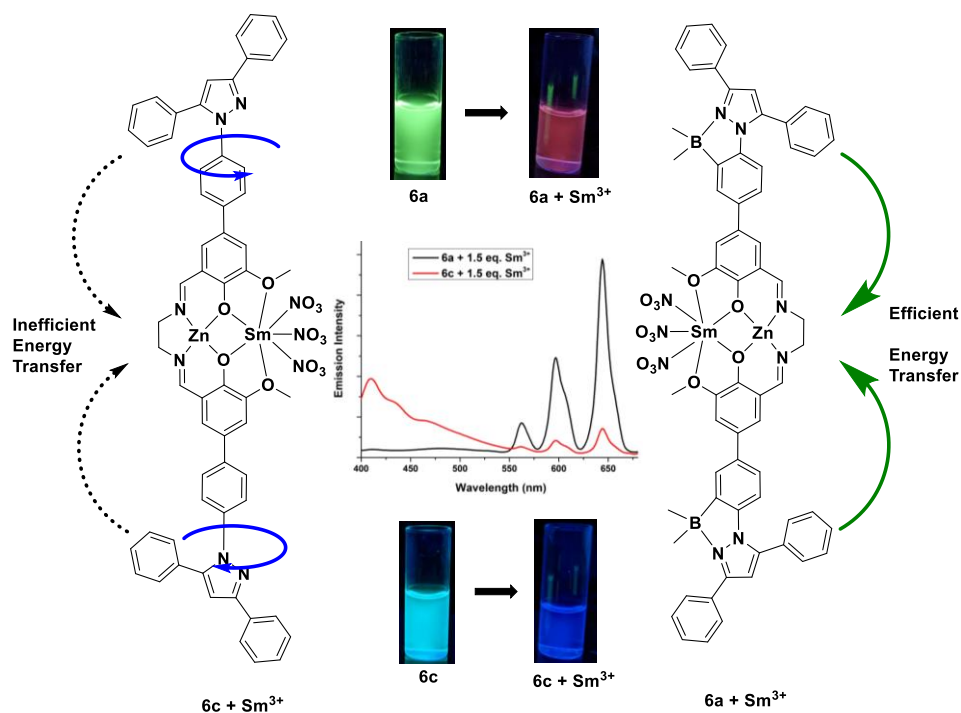
Taking advantage of the emissive and electron-transporting properties of the B-N coordinated fluorophores with the chelating ability of salen ligands which can find use in catalysis and materials chemistry, in this chapter I will present the synthesis of a tetra-coordinated boron-functionalized pyrazole based zinc-salen and it's potential in sensing Sm^{3+} ion selectively.

Chapter 3:

This chapter is divided into two parts.
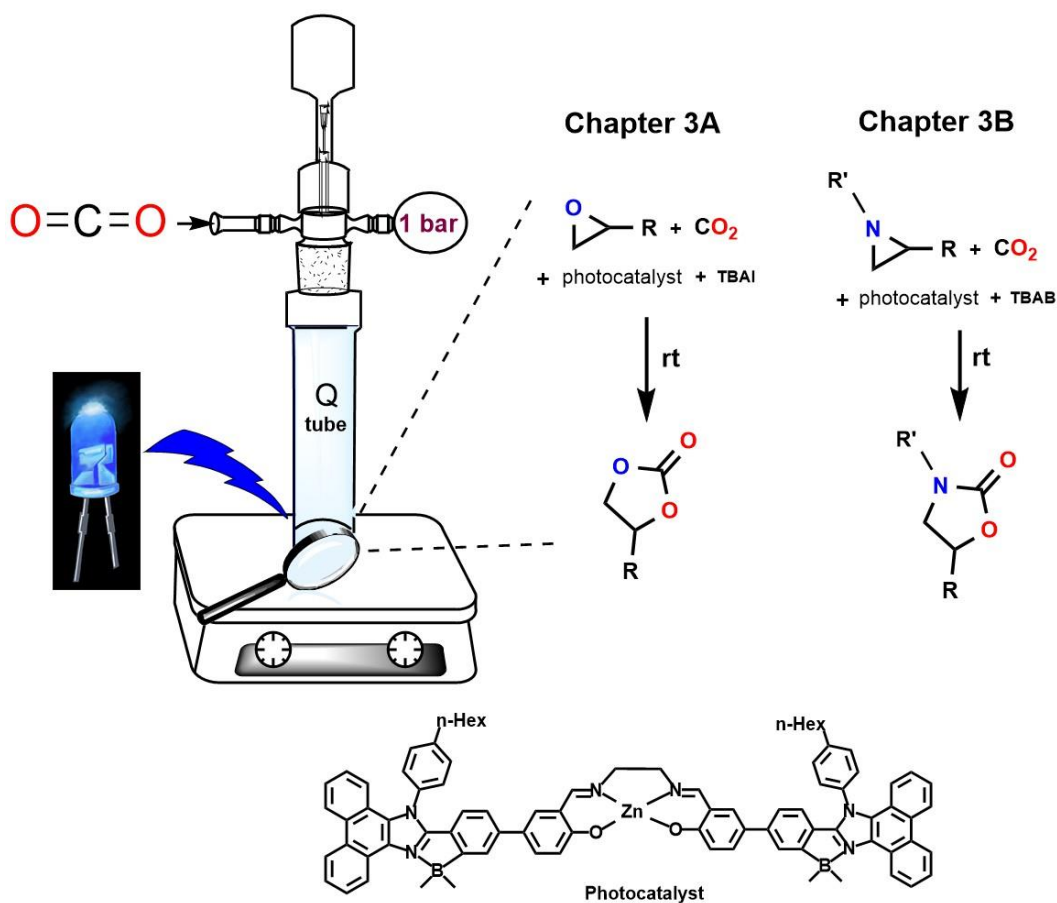
Chapter 3A: Cycloaddition of CO₂ and epoxides using B-N coordinated phenanthroimidazole based zinc-salen as a photocatalyst

This chapter describes the synthesis of a unique zinc salen complex based on B-N

coordinated phenanthroimidazole. The zinc catalyst was well characterized by multinuclear NMR, MALDI-MS, and single-crystal X-Ray diffraction analysis. The zinc-salen thus synthesized acts as a photocatalyst for the cycloaddition of carbon dioxide with terminal epoxides under ambient conditions under blue light irradiation. The effect of boron coordination to phenanthroimidazole moiety on catalysis reaction was also investigated. DFT study of the cycloaddition of carbon dioxide with terminal epoxide indicates the preference of the reaction pathway when photocatalyzed by zinc-salen.

Chapter 3B: Four coordinate boron functionalized phenanthroimidazole based zinc-salen as photocatalyst for cycloaddition of CO_2 and aziridines

This chapter describes the cycloaddition of carbon dioxide (CO_2) with aziridine using the zinc-salen photocatalyst with a B-N coordinated phenanthroimidazole motif at ambient temperature and 1 bar CO_2 pressure. The reaction was done in a solvent-free environment and blue light irradiation. The photocatalyst displayed high selectivity, tolerated a variety of substituted aziridines, and efficiently produced the oxazolidinones from aziridines under mild conditions.

Chapter 4: Tetracoordinated boron functionalized pyrazole based chiral zinc sensors for the enantioselective recognition of phenylalanine, alanine, and cysteine

Enantioselective discrimination of amino acids is highly demanded in various fields such as nutritional analysis and medical diagnosis of diseases.[6] In this chapter boron embedded pyrazole-based (*R,R*) and (*S,S*) zinc complexes were synthesized and fully characterized by NMR, MALDI-MS, CD spectroscopy, and X-ray crystallography. The synthesized chiral zinc complexes serve as fluorescent sensors for the enantioselective recognition of *D*/*L*-phenylalanine, alanine, and cysteine.
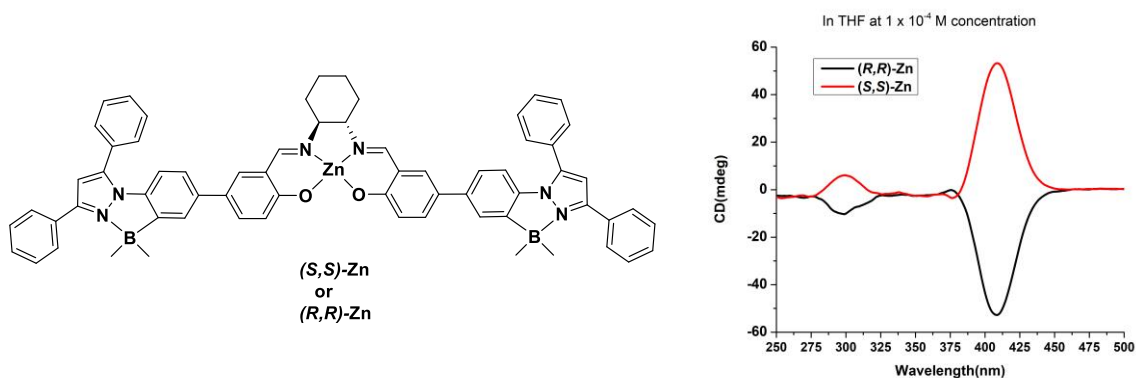
In THF at 1×10^{-4} M concentration

(S,S)-Zn
or
(R,R)-Zn

Chapter 5: Synthesis of B←N coordinated phenanthroimidazole based diphenyl-borane dimers and study of their photophysical and electrochemical properties

9

π =

Hexyl   Hexyl

10

Hexyl

11
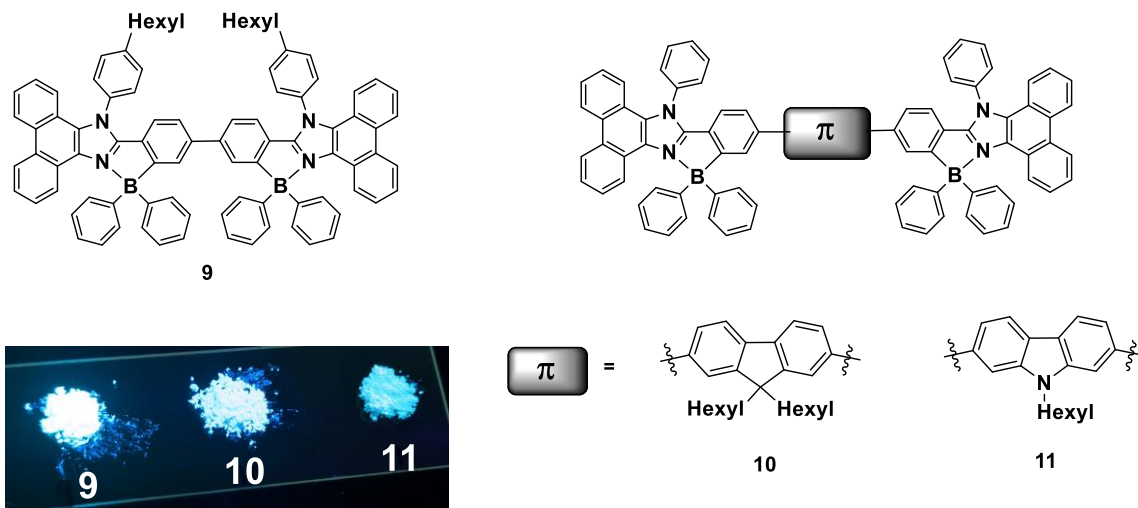
Boron substitution coordination is an effective method to tune the optoelectronic properties of the phenanthroimidazole based polyaromatic hydrocarbons (PAHs).[7] In this chapter we synthesized highly emissive π-extended diphenyl-borane doped phenanthroimidazole dimers and studied their photophysical and electrochemical properties. The diboron complexes were characterized by multinuclear NMR and single-crystal X-ray diffraction analysis. Photophysical studies showed that these dimers exhibit strong emission with excellent quantum yields in dichloromethane and moderate quantum yields in the solid state.

References

1. (a) F. Jäkle *Chem. Rev.*, **2010**, *110* , 3985 —4022 (b) J. He , F. Rauch , M. Finze and T. B. Marder , *Chem. Sci.*, **2021**, *12* , 128 —147

2. .Y.-L. Rao , H. Amarne and S. Wang , *Coord. Chem. Rev.*, **2012**, *256*, 759 —770

3. K. P. Carter, A. M. Young, A. E. Palmer , *Chem. Rev.*, **2014**, *114*, 4564 —4601

4. F. T. Edelmann *Chem. Soc. Rev.*, **2012**, *41*, 7649 —7964

5. T. Gorai and U. Maitra, *Angew. Chem., Int. Ed.*, **2017**, *56*, 10730 —10734

6. (a) Y. Zhou, J. Yoon, *Chem. Soc. Rev.* **2012**, *41*, 52–67 (b) L. Mutihac, J. H. Lee, J. S. Kim, J. Vicens, *Chem. Soc. Rev.* **2011**, *40*, 2777–2796

7. Yang, D.-T.; Mellerup, S. K.; Peng, J.-B.; Wang, X.; Li, Q.-S.; Wang, S., *J. Am. Chem. Soc.* **2016,** *138* (36), 11513-11516

List of figures

List o f tables

List of schemes

List of abbreviations

^{1}H NMR	Proton nuclear magnetic resonance
^{13}C NMR	Carbon-13 nuclear magnetic resonance
^{11}B NMR	Boron-11 nuclear magnetic resonance
^{31}P NMR	Phosphorous-31 nuclear magnetic resonance
^{19}F NMR	Fluorine-19 nuclear magnetic resonance
^{1}H-^{1}H COSY	Proton-proton correlated spectroscopy
UV-Vis	Ultraviolet-visible
ESI	Electrospray ionization
DFT	Density functional theory
HRMS	High-resolution mass spectrometry
IRF	Instrument response function
ICT	Intramolecular charge transfer
CD	Cyclic dichroism
CPL	Circularly polarized luminescence
CV	Cyclic voltammetry
XRD	X-ray diffraction
GOF	Goodness of fit
LED	Light emitting diode
OLEDs	Organic light emitting diodes
TADF	Thermally activated delayed fluorescence
HOMO	Highest occupied molecular orbital
LUMO	Lowest unoccupied molecular orbital

eV	Electronvolt
EL	Electroluminescence
ACQ	Aggregation caused quenching
AIEE	Aggregation induced enhanced emission
ppm	Parts per million
CH_2Cl_2	Dichloromethane
$CHCl_3$	Chloroform
DCE	1,2-Dichloroethane
MeOH	Methanol
EtOH	Ethanol
THF	Tetrahydrofuran
DMF	Dimethylformamide
$CDCl_3$	Deuterated chloroform
DMSO-d_6	Deuterated dimethyl sulphoxide
AcOH	Acetic acid
NaOAc	Sodium acetate
Na_2CO_3	Sodium carbonate
K_2CO_3	Potassium carbonate
TON	Turn over number
CaH_2	Calcium hydride
KBr	Potassium bromide
$AlCl_3$	Aluminium trichloride
BBr_3	Boron tribromide
$NaHCO_3$	Sodium hydrogen carbonate

PEG	Polyethylene glycol
IL	Ionic liquid
TBACl	Tetrabutylammonium chloride
TBAB	Tetrabutylammonium bromide
Bu_4NPF_6	Tetrabutylammonium hexafluorophosphate
$AlMe_3$	Trimethylaluminium
$(Bpin)_2$	Bis(pinacolato)diboron
$i-Pr_2Net$	N,N-Diisopropylethylamine
NBS	N-bromosuccinimide
NaH	Sodium hydride
$Pd(dppf)Cl_2$	[1,1'-bis(diphenylphosphino)ferrocene]dichloropalladium(II)
Mes	mesityl
N.D	Not detected
$Pd(PPh_3)_4$	Tetrakis(triphenylphosphine)palladium(0)

Chapter 1

Introduction

1.1 Fluorescent boron compounds

Organic emissive fluorophores have seen an increase in demand owing to their applications in organic field effect transistors (OFETs), organic light-emitting devices (OLED), nonlinear optics, organic solid-state lasers (OSLs), biomolecular probes, fluorescent sensors, etc.[1] An interesting method to adjust the electronic properties of organic emissive compounds is the incorporation of a heteroatom such as Al, B, P, Si, Sn or other elements into the backbone of the fluorophores.[2] Recently, many new functional materials with excellent photophysical and electronic properties have been developed by the incorporation of boron into conjugated organic framework. In general boron based fluorophores have been divided into tri- and tetra-coordinated boron compounds.

1.1.1 Tri- and tetra-coordinated boron compounds

Due to the presence of empty p-orbital, tri-coordinated boron compounds are lewis acidic and are prone to attack by lewis bases like water. As a result, the tri-coordinated boron is stabilized by sterically crowded aromatic groups like fluoro mesityl, mesityl, and triisopropyl phenyl as well as by utilizing π-donor substituents such as alkoxy groups. The stabilized tri-coordinated boron compounds thus synthesized have found uses as fluorescent indicators for bioimaging as well as OLEDs and OFETs.[3] In comparison to tri-coordinated boron compounds, tetra-coordinated boron compounds are more stable. Tetra-coordinated boron compounds have been employed extensively in optoelectronics, including photoresponsive materials, OFETs, OLEDs, sensory and biological imaging materials. As a result, the molecular design of these compounds has drawn a lot of attention.[4] Tetra-coordinated boron compounds have a coordinatively saturated boron center, which makes them rigid and stable and thereby increases the emission quantum yield. In tetra-coordinated boron compounds, the lowest unoccupied molecular orbital

(LUMO) is typically localized on the π-conjugated chelating ligand, while the highest occupied molecular orbital (HOMO), depending on the nature of the latter, is localized either at the chelating ligand or the R (aryl, alkyl, or halo) group. The luminescence characteristics of this class of compounds are typically due to the π–π* electronic transitions of the ligand or charge transfer transition from the R group to the ligand.
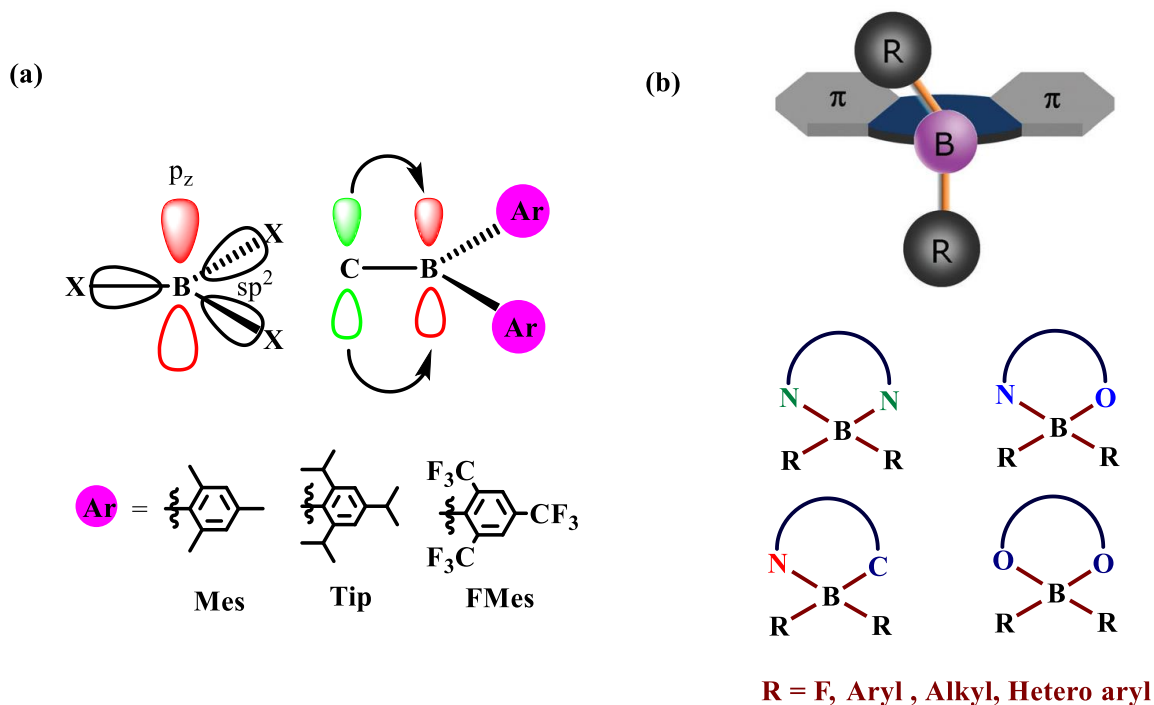
Figure 1.1: Schematic representation of (a) tri-coordinated boron (b) tetra-coordinated boron compounds

Therefore, modifications to the molecule's R group or chelating ligand would affect the HOMO-LUMO levels and, in turn, the color of emission. Based on the chelated donor atoms, the fluorescent tetra-coordinated boron compounds are broadly divided into four categories: (a) O,O- (b) N,C- (c) N,O and (d) N,N-chelate boron compounds (Fig 1.1). As the focus of this thesis is the development of different N,C-chelated B-N coordinated boron compounds, the most current developments and uses of N,C-chelate tetra-coordinated boron-based fluorophores will be covered in the next section.

1.1.2 N,C-chelate boron compounds

Although B–N coordinated N,C-chelated boron compounds were reported by Dewar and co-workers[5a] in 1958, the groundbreaking work reported by Yamaguchi and co-workers[5b] has attracted many groups to focus on the synthesis of different B-N coordinated boron compounds that act as fluorescent functional materials.
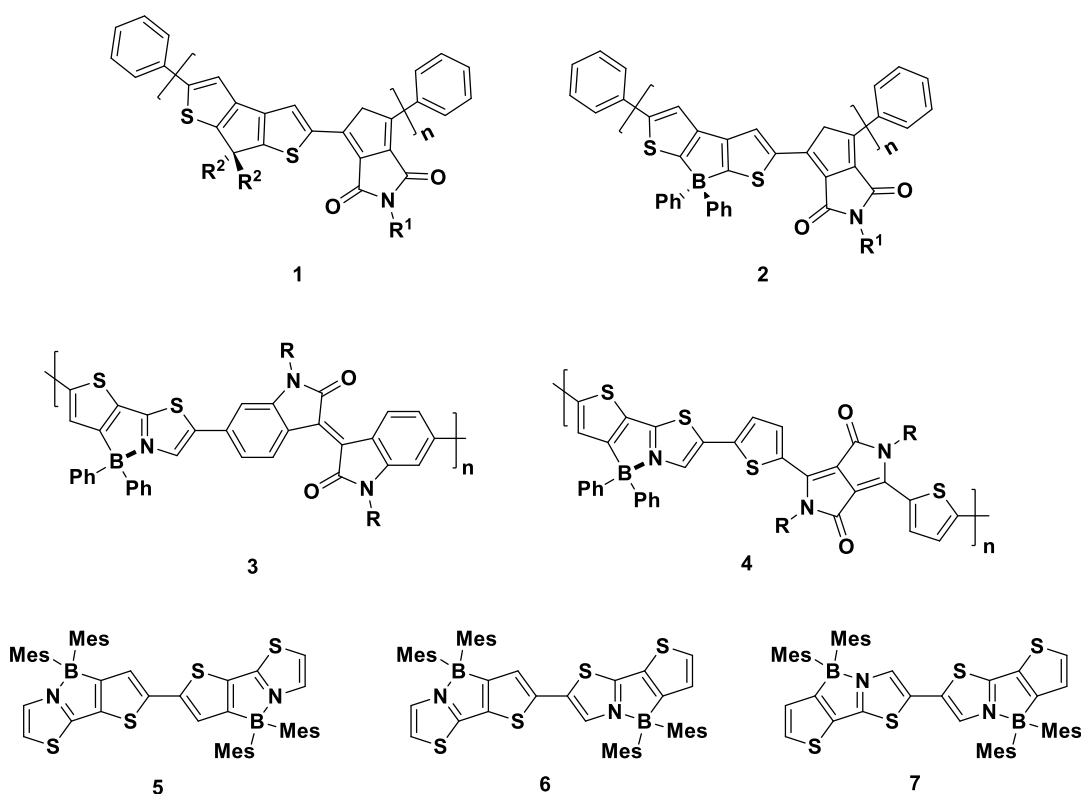
Figure 1.2: Structure of N,C-chelate boron compounds **1-7**

Wang and co-workers,[6] demonstrated the advantage of B-N based compounds over C-C based compounds which (**1** and **2**) helped to lower both HOMO and LUMO energy levels and transform the resulting polymer into an electron acceptor. Same group[7] in 2016 synthesized thenylthiazole based B–N framework to make polymers that were used in solar cells in combination with isoindigo and dithenyldiketopyrrolopyrrole units (**3** and **4**). The power conversion efficiency of the polymer-based solar-cell devices was greater

than 5.0%. Additionally, they demonstrated that B-N coordinated compounds used in the development of polymer-based solar cells which outperformed in comparison to C-C based compounds in terms of power conversion efficiency.[8] Wang and co-workers have extensively explored the effect of inner transition metal coordination on the photo-isomerization process of a number of N,C-chelated B–N coordinated compounds (**8–11**). Emission experiments and other techniques were used to monitor the photochromic activity.[9] The boryl-substituted thienylthiazole dimers (**5-7**) synthesized by Yamaguchi group[10] are also demonstrated to be potential electron-transporting materials because they form a -conjugated planar array via B-N coordination. In 2019, the Wang group[11] synthesized five pairs of regioisomers (**12–16**) based on the indolizino[3,4,5-*ab*]isoindole backbone as shown in Fig. 1.4 and with the help of ^{11}B-NMR, VT-^{1}H and TBAF titration experiments they proved that the strength of B-N bond depends on lewis acidity of N-heterocyclic units and the inductive effect of dichotomic units in isomers 'a' and 'b'. Taking advantage of the B–N coordination, they also prepared stimuli-responsive (mechanochromic and thermochromic) B-N Lewis pairs.[12] The same group also synthesized Pt(II) complexes with photochromic B(ppy)Mes$_2$ and dithienylethene (DTE) molecules (**17–19**).[13] It has been demonstrated through photophysical studies, NMR analyses, and DFT calculations that the photoisomerization reaction follows the triplet pathway through an effective energy transfer mechanism. In 2021, Wu and co-workers[14] synthesized 2-phenylpyridine type tetra-coordinated organoboron motif functionalized with Ir metal for OLED application. The prepared Ir-fused boron complexes (**20-22**) showed a high luminescence quantum yield ranging from 60 to 100% and excellent external quantum efficiency of 26% after device fabrication.
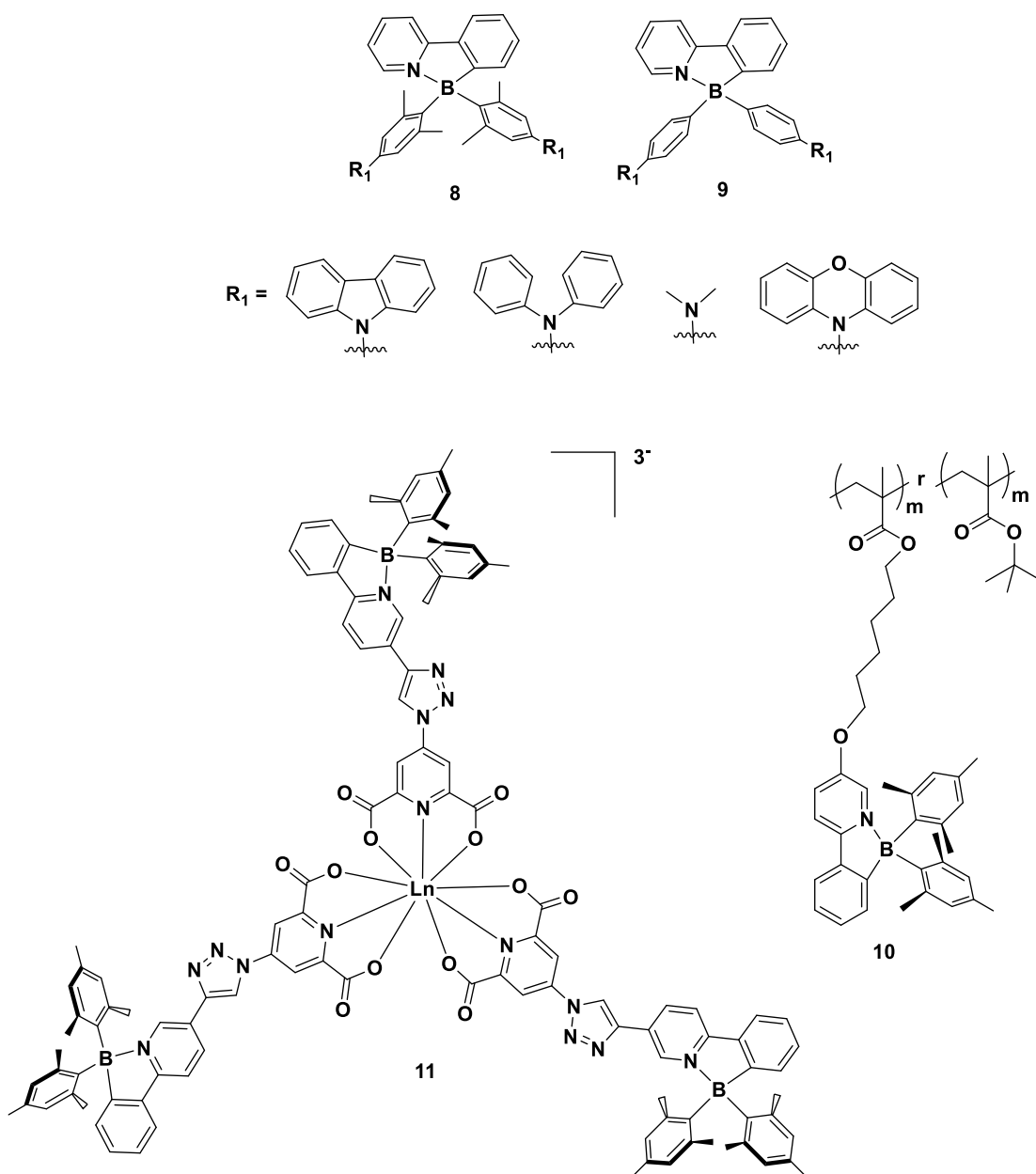
Figure 1.3: Structure of N,C-chelate boron compounds **8-11**

Jäkle and co-workers designed various B–N coordinated ladder-type compounds (**23**, **24**) as shown in Fig 1.5, and utilized them to make homo and co-polymers (**25**, **26**). In the solution state, the polymers displayed quantum yields up to 78%.[15] In 2019, they investigated the impact of electrochemical, photophysical, and structural properties of regioisomeric borylation on polyaromatic hydrocarbons fused pyrene-based compounds

(**27–30**).[16] Subsequently, they used electrophilic borylation to synthesize a series of B–N fused dipyridylanthracene derivatives with a methyl group at different positions on the pyridyl ring (**31**).[17] They further investigated the effect on the position of methyl group on oxygen sensing and its reversible release with temperature. They found that the endoperoxides form faster for the derivative which has methyl substitution close to anthracene moiety. In 2022, Jakle group showed the synthesis of linearly extended acene derivatives (**32-34**) Py-BR (R=Et, Ph, C_6F_5) *via* N-directed electrophilic borylation of 2,6-di(pyrid-2-yl)anthracene.[18] In comparison to diphenylanthracene or the pyridyl/quinolinyl-substituted precursors, the absorptions and emissions of the borylated species (**32-34**) are bathochromically shifted, indicating a significant impact of B-N lewis pair functionalization on the electronic structure. But the absorptions and emissions of Py-BR are blue-shifted, and the LUMO levels are more energetic than those of the corresponding laterally functionalized anthracenes (**31**). On the other hand, due to the N-ICT heterocycle's nature in the excited state, further conjugation of the Qu-Bet (**35**) N-heterocycle with seven six-membered rings in series results in longer wavelength absorptions and solvatochromic emissions. In contrast to laterally functionalized anthracenes A, photo-oxygenation investigations show that the new linearly B-N Lewis pair extended anthracenes are effective singlet oxygen sensitizers with a significantly decreased propensity for self-sensitized endoperoxide production. The incorporation of electron-withdrawing C_6F_5 substituents on boron in **34** leads to a particularly stable derivative, as demonstrated by the highly selective oxygenation of dimethylanthracene without considerable self-oxidation of the B-functionalized anthracene species.
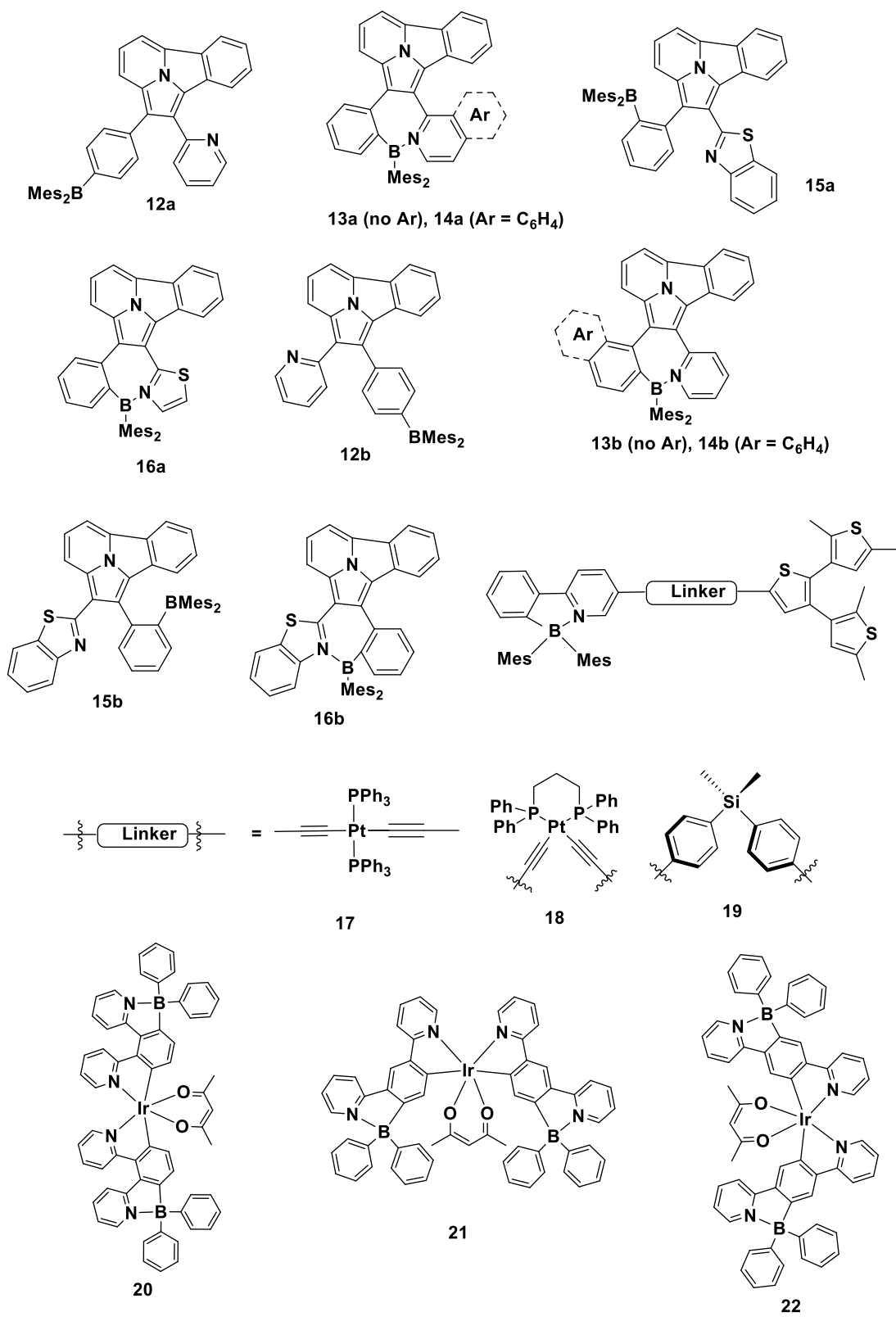
Figure 1.4: Structure of N,C-chelate boron compounds **12-22**

Electrochemical and DFT calculations reveal that the improved stability of **34** was caused by a reduction in the HOMO (and LUMO) levels. Comparing the conjugated systems to their C–C analogs, the incorporation of B–N units results in significant alterations to the electronic structure, including noticeably lower LUMO levels and significant reductions in the HOMO–LUMO gap. To demonstrate this, in 2022 the same group synthesized two new B-N-fused dianthracenylpyrazine compounds (**36, 37**) that have incredibly small HOMO-LUMO gaps.[19] As a result, the derivatives of borylated dianthracenylpyrazine exhibit notable absorbance at wavelengths greater than 700 nm. DFT calculations demonstrate the donor-acceptor-donor character of these B-N-fused dianthracenylpyrazines as evidenced in the spatial separation of the HOMO-LUMO orbitals and support the strong overall acceptor character. The nanostructured **37** exhibits a high power conversion efficiency of 41.8% due to intramolecular charge transfer and good photostability. The outstanding photothermal therapeutic efficacy and promising biocompatibility of **37** are confirmed by both *in-vitro* and *in-vivo* tests.

In 2017, the Ingleson and Turner groups[20] successfully studied the photophysical characteristics of ladder-type benzothiadiazole-arylamine D-A type N,C-chelated boron complexes synthesized using direct electrophilic C-H borylation (**38**) (Fig. 1.6). By varying the exocyclic boron substituents through transmetalation with various diaryl-zinc reagents, the emission characteristics can be altered. DFT studies further showed a narrow HOMO–LUMO gap supported by substantial red-shifted absorption band at >700 nm. Additional tuning with various aryl groups was also investigated. The utility of these compounds was realized when OLEDs were developed (**39**, **40**).[21] They also investigated donor-acceptor benzothiadiazole-arylamine compounds with twisting that showed delayed emission (**41**).[22] Using the post-polymerization technique, benzothiadiazole-

arylamine donor-acceptor compound polymers were also synthesized and borylated (**42**). The borylated polymers were investigated as near-IR emissive bio imaging agents and also to create near-IR-OLEDs.[23] The Turner and Ingleson groups[24] reported the synthesis of N-C chelate organoboron compounds based on benzoselenadiazole (BSe) and benzotriazole (BTz) (**43–46**) in 2019. When BSe and BTz were reacted with BCl_3, the C-H functionalization of neighboring aromatic units resulted in the formation of fused boracycles. The synthesis of air and moisture-stable boracycles was achieved by *in situ* arylation of boron using organotin or diarylzinc reagents. Photophysical analysis reveals that these boracycles exhibit a strong red shift in their absorption and emission spectra in both solution and film states. Borylated **43** and **44** were the only compounds to emit in the near-infrared spectrum in both solution and film forms. The synthesis of the dimesitylboryl (Mes_2B)-substituted benzothiadiazole derivative (**47**) was reported by the Wakamiya and Murata groups in 2017.[25] The reversible formation of the intramolecular B-N bond with a sterically bulky Mes_2B group helped compound **47** to exhibit thermo-, solvato-, and mechanochromism properties. The HOMO-LUMO gap is reduced by the B-N bond formation, which causes significant color change. By hydroborylation of 2-(*ortho*-styryl)pyridine with a variety of hydroboranes, the Pammer group in 2016 prepared a number of B-N coordinated organoboranes, including 9H-9-borabicyclo[3.3.1]nonyl (9HBBN), BH_3THF, $HBCl_2SMe_2$, $HB(C_6F_5)_2$, and 9H-9-borafluorene (**48-53**).[26] This method was used to synthesize compounds in good to outstanding yields with high regioselectivity under benign reaction conditions on a wide range of substrates. The results of the photophysical and DFT experiments demonstrated that the boron substituents can be changed to tailor the electronic properties of synthetic boranes.
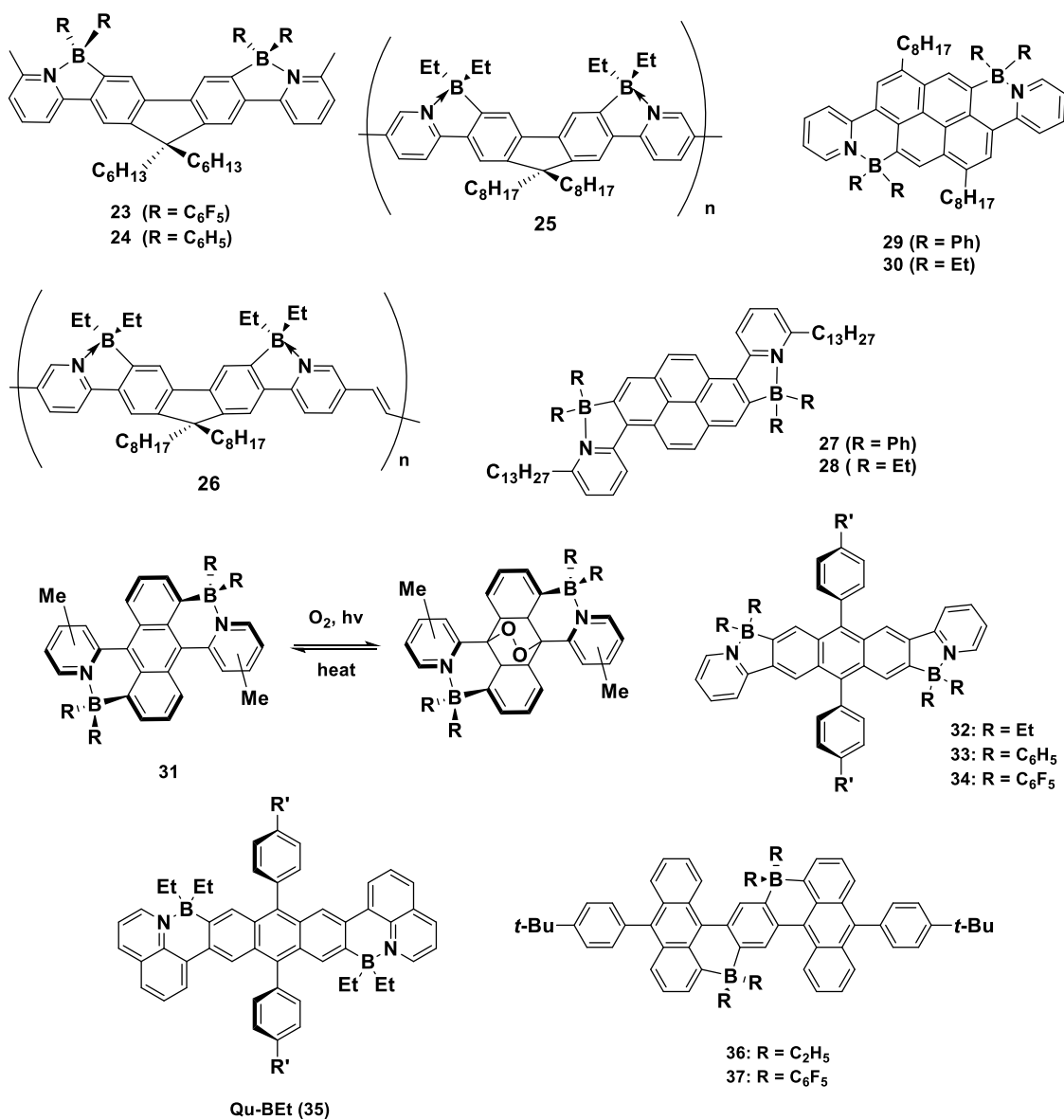
Figure 1.5: Structure of N,C-chelate boron compounds **23-37**

By performing a two-fold hydroboration process with quarterpyridine, pyrimidine, and 1,5-naphthyridine precursors along with 9H-BBN and Piers' boranes ($(C_6H_5)_2BH$), the same methodology was further extended to produce a series of conjugated ladder type B-N coordinated boranes (**54, 55**).[27]
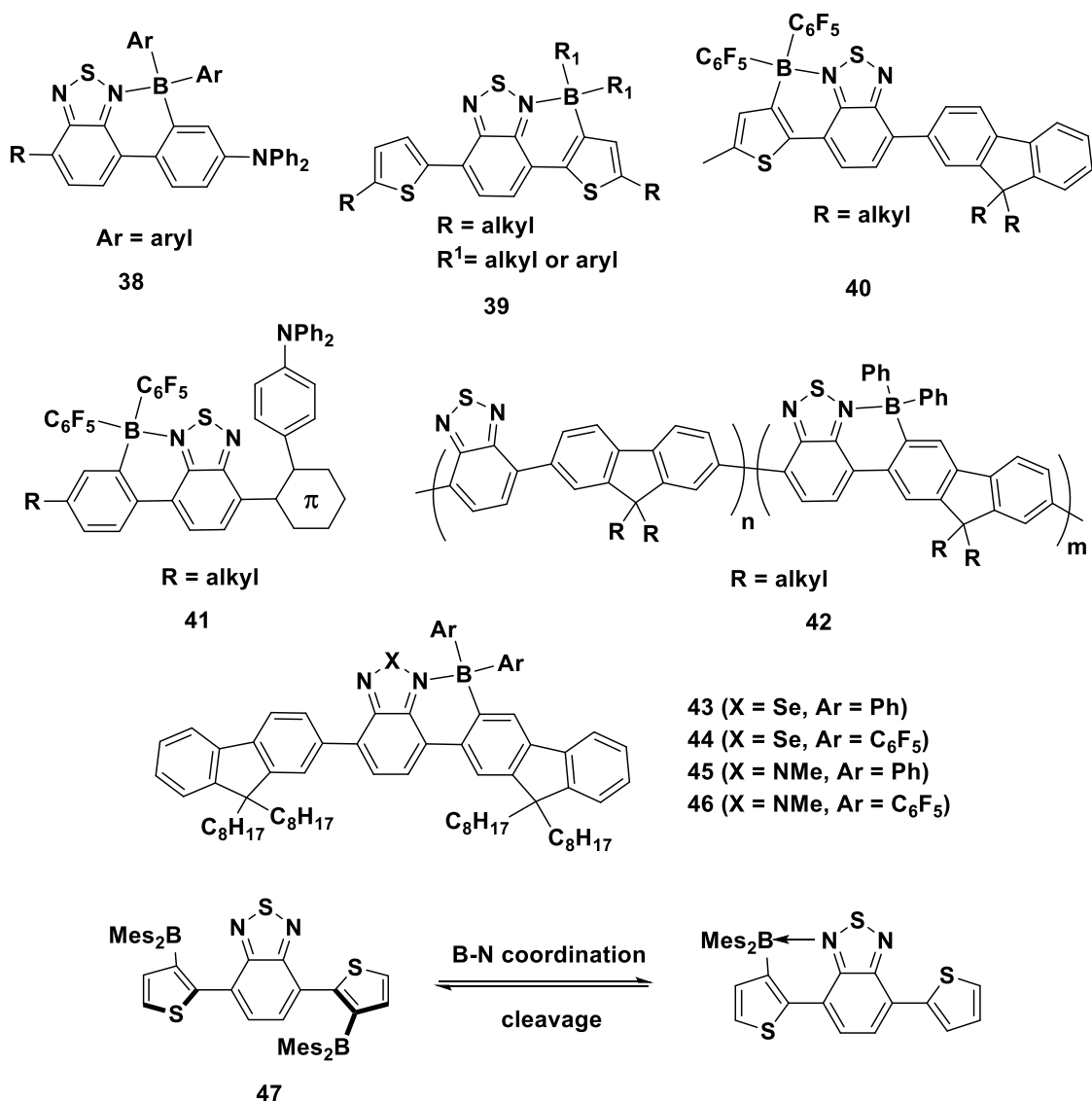
Figure 1.6: Structure of N,C-chelate boron compounds **38-47**

Photophysical and electrochemical studies reveal that these boranes have reduced optical band gaps and increased electron affinities of between 3.4 and 4 eV, which make them potential candidates for usage as n-type organic semiconductors. The post-modification hydroboration of alkenyl functionalized poly(biphenylene-pyrazinylene) and polypyridines utilizing various hydroboranes (9H-BBN, $(C_6H_5)_2$B-H (BPF-H), Cl_2B-H) was also used to synthesize ladder type intramolecular B-N coordinated polymers (**56-**

58).[28] The possible applicability of these polymers as electron acceptors was investigated. In 2017, the Pammer group[29] synthesized a number of B-N coordinated boranes (monomers) and polymers based on aryl triazoles (**59–61**). The absorption and emission characteristics of several aromatic groups (**61**) were thoroughly investigated. Thermal exchange between open non-coordinated and closed B-N coordinated conformers was detected by ^{1}H and ^{11}B studies. The impact of substituents is revealed by fluorescence experiments on monomeric units.[30]

The Yam group in 2016 designed and synthesized a number of spirofluorene ladder-type boracycles (**62, 63**) based on thiophene and investigated their electrochemistry and photophysical properties.[31] Experiments on absorption and emission show intramolecular charge transfer from thiophene to the pyridine-borane unit. A structureless band attributed to an intramolecular charge transfer transition was visible in the emission spectra. It's interesting to note that these boron compounds show high emission quantum yields, reaching up to 81% in the solution state and 86% in the thin film state. Some of the molecules were employed to create OLEDs with EQEs up to 1.3% and with tuneable red, green, and blue emissions. In 2022, the same group reported a new family of four-coordinate boron compounds with an auxiliary N-C ligand and a photochromic dithienylethene-containing C-C ligand (**69-74**).[32] These substances exhibit thermally induced upconversion from the lower excited state to the higher excited state, as well as reversible photochromism upon photoexcitation and easily tuneable photocycloreversion quantum yields.
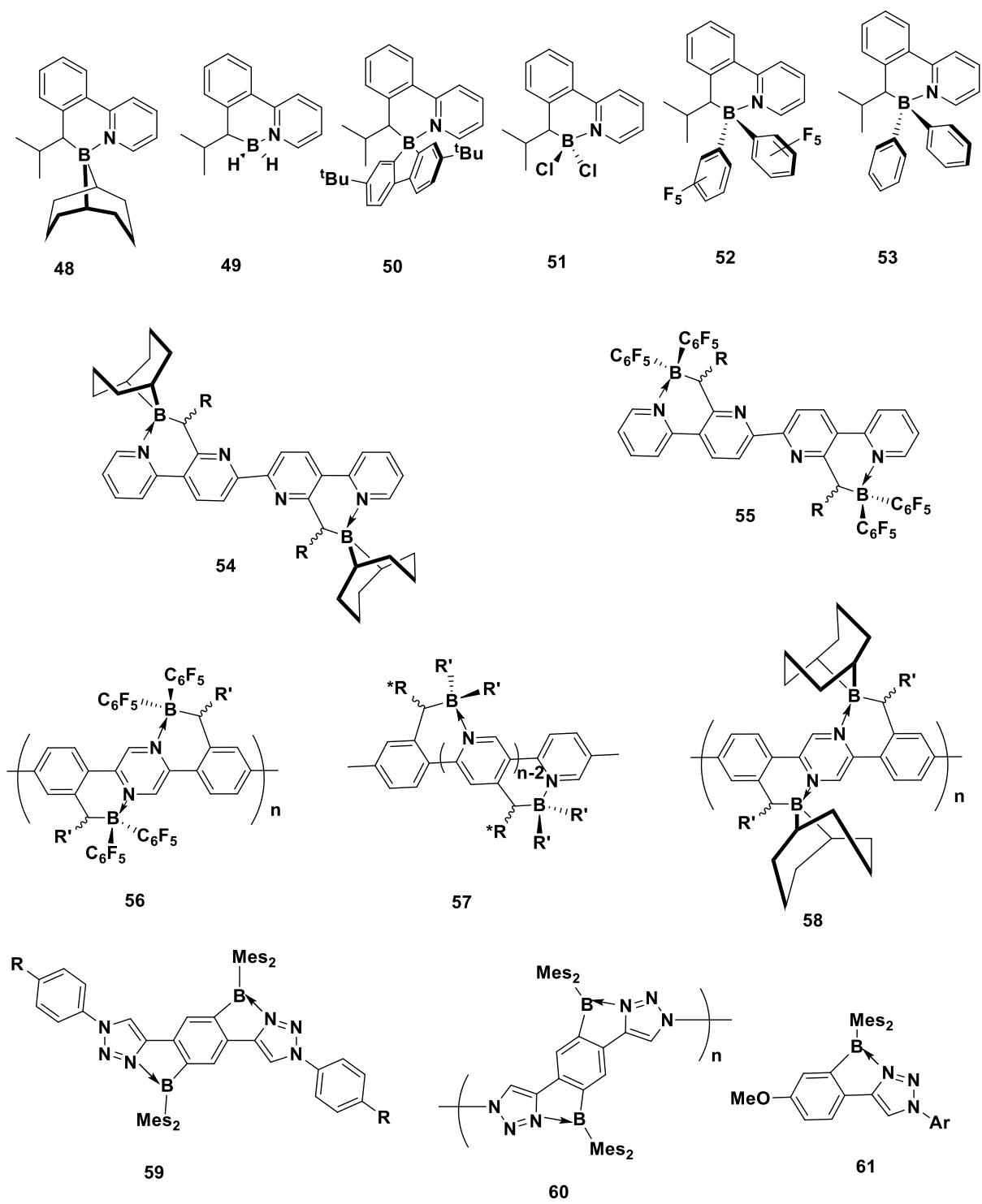
Figure 1.7: Structure of N,C-chelate boron compounds **48-61**

In 2017, the Chi group[33] prepared donor-acceptor type boron compounds (**64-66**) using triphenyl carbazole/triphenyl amine as the electron donor (D) and phenylpyridine as the electron acceptor (A). The TADF characteristics of these D-A units using boron as a linker were examined in a variety of solvents. The OLED device made from these N,C-chelated tetra-coordinated compounds makes them efficient TADF OLED materials. N,C-chelated boron complexes based on donor-spiro-acceptors also function as promising TADF materials.[34] Novak-krol and co-workers synthesized two donor-bridge-acceptor (D-π-A) compounds (**67, 68**) based on 2-(3-boryl-2-thienyl)thiazole π-linker and indandione as acceptor moiety and studied their solvatochromic activity.[35] To understand the impact of two distinct highly electron-donating hydrazonyl groups on the solvatochromic and luminescence behavior of these compounds, DFT/TDDFT calculations were carried out in conjunction with steady-state absorption and fluorescence data, as well as electrochemical experiments. Based on the obtained spectroscopic characteristics in solvents of different polarity, the Lippert-Mataga equation was used to determine the difference in dipole moments (Dm) between excited and ground states, and the data were validated by theoretical investigations.

In 2018, borylated arylisoquinoline skeletons with a helicene-like structure (**75**) were reported by Ros and co-workers.[36] The electronic circular dichroism (ECD) and circularly polarised luminescence (CPL) of the helicene enantiomers were remarkably strong, and the dissymmetry factor was also quite high. The intrinsic relationship between helicenes and circulenes is of fundamental interest and importance in molecular engineering. By incorporating a boryl unit into the terminals of two helicenes, the Marder group demonstrated the electrophilic borylation of aza[5]helicenes generated from phenanthroline to produce quasi-[7]circulenes (**81**).[37] X-ray diffraction reveals their
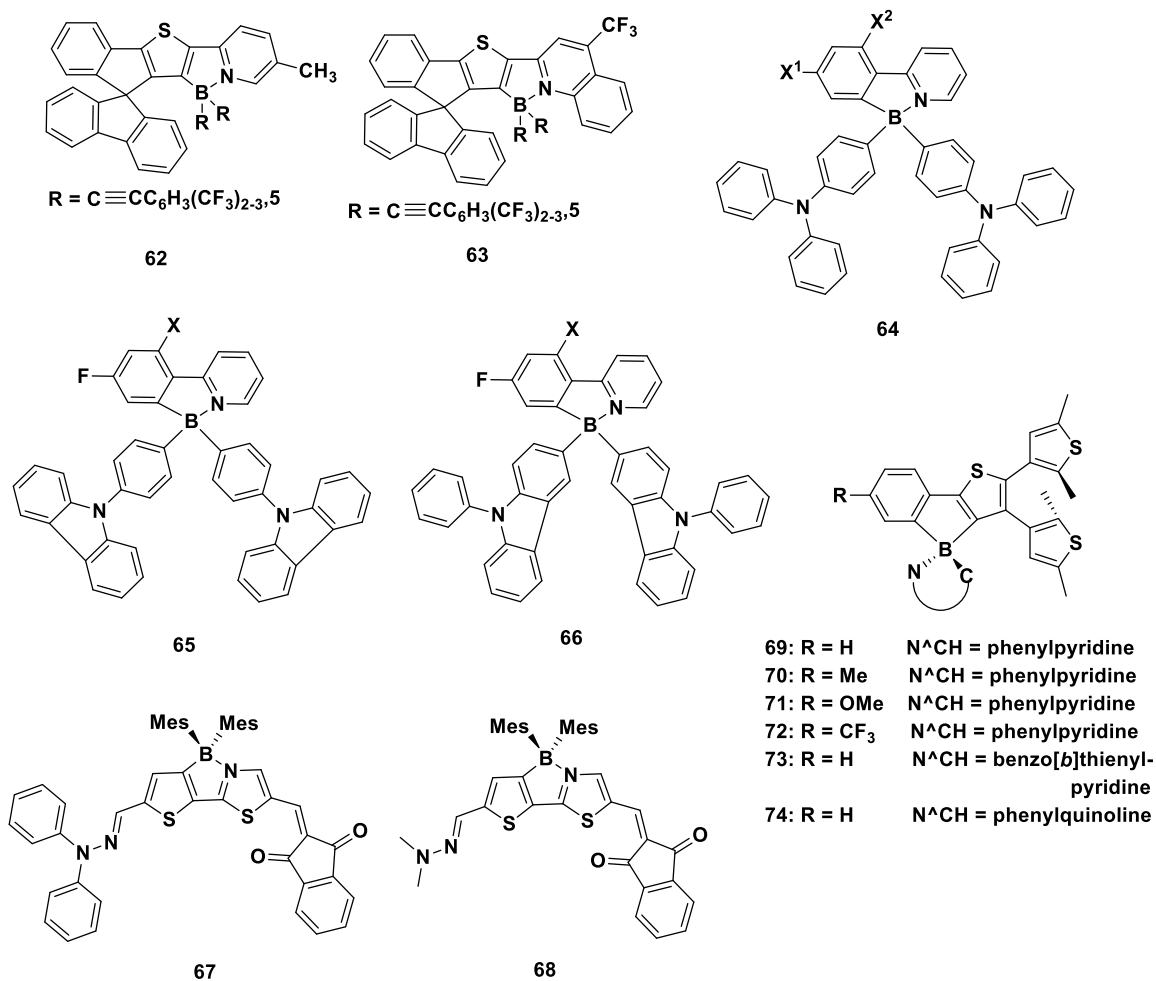
Figure 1.8: Structure of N,C-chelate boron compounds **62-74**

bowl-like shapes. Their electronic characteristics were studied by UV-vis absorption, fluorescence spectroscopy, electrochemical experiments, and DFT computations. VT ^{1}H-NMR showed bowl-to-bowl inversion at normal temperature and bowl-to-helix equilibrium at high temperature, demonstrating the critical function of B-N bond strength in adjusting their dynamic characteristics A modular strategy was recently used by the Nowak-Krol group to isolate two different types of helically chiral molecules with one and two boron atoms (**76**, **77**). [38] Azabora[7]helicenes have solution state quantum yields that range from 18 to 24% and display blue or green fluorescence. In the solid state, they
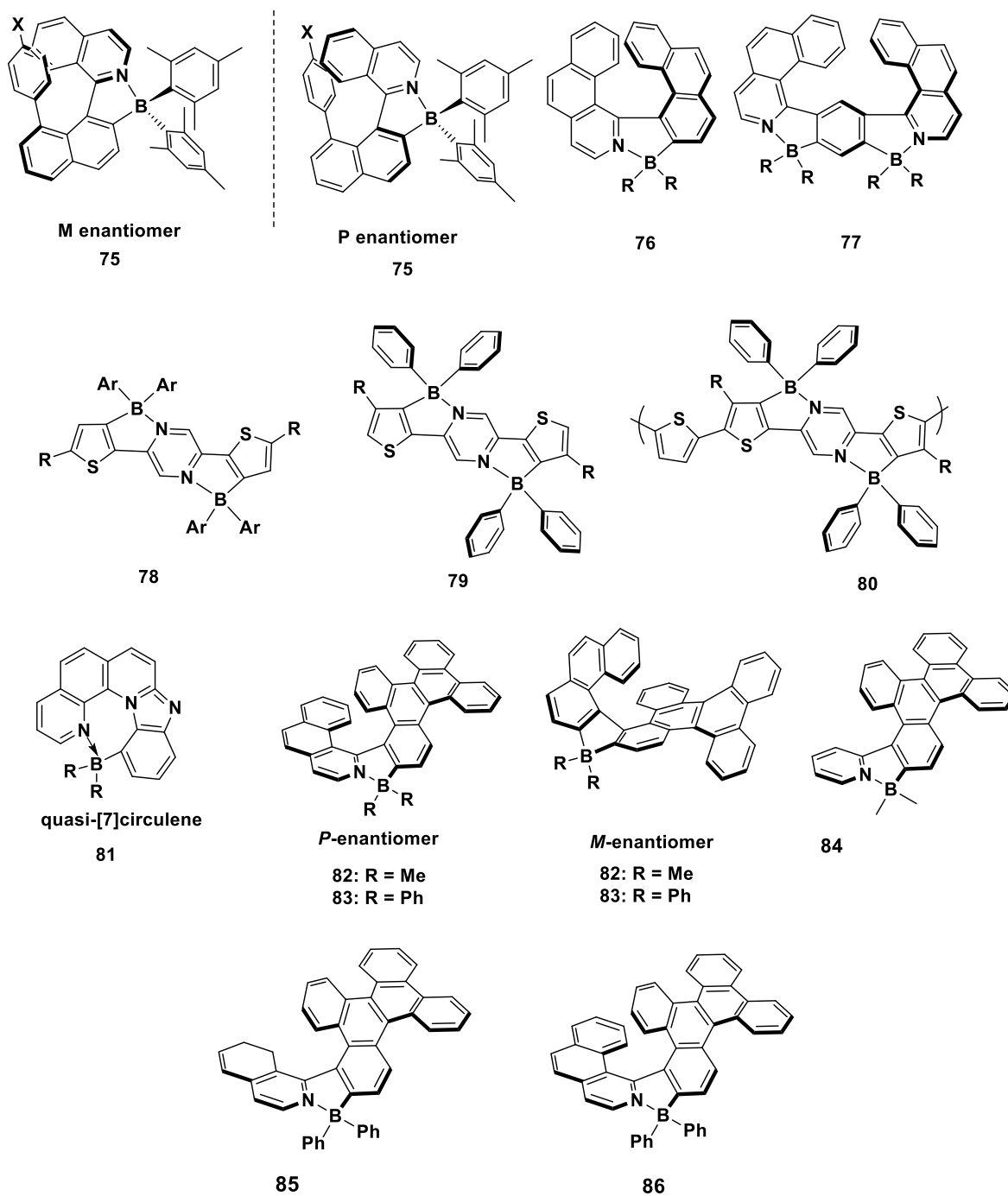
Figure 1.9: Structure of N,C-chelate boron compounds **75-86**

also, display green or yellow emissions with a quantum yield of up to 23%. With quantum yields of up to 47% in the solution state and 25% in the solid state, azabora[9]helicenes exhibit blue fluorescence. The same group also developed a stereoselective synthesis of azaborole helicenes (**82, 83**) by transferring chirality from axially chiral biaryls.[39] Various studies were carried out experimentally to gain insight into the chiroptical characteristics and configurational stability of the heterobiaryls. X-ray examination of a single crystal clearly established the structure of the phenyl-substituted helicene. In 2022, they explained how laterally extended azabora[5]-, -[6]-, and -[7]helicenes (**84-86**) were made using the building blocks of N-heteroaromatic and dibenzo[g,p]chrysene.[40] Formally, the phenanthrene unit was added to the conjugated systems of the original azaborole helicenes, resulting in compounds with a significant increase in luminescence quantum yields and dissymmetry factors as well as large Stokes shifts (glum). Helical elongation had the same positive impact on optical characteristics. A compound with green emission and the highest quantum yield and stability among the series of π-extended azaborahelicenes as well as superior emission intensity and the chiroptical response was produced by the combined effects of lateral and helical extensions. This study demonstrates that lateral and helical expansions of π-conjugated systems enhance the properties of azaborole helicenes. Adachi and co-workers[41] designed and synthesized spiro-type N-C chelate B-N coordinated boron derivatives based on 2-phenylpyridinato and demonstrated the significance of excited-state energy alignment. Several investigations have shown that the triplet excited state of the donor and acceptor units is critical for high quantum yields of exciplexes. Further studies showed that efficient TADF can be accomplished when the energy levels of the triplet charge-transfer excited state and the triplet local excited state are in alignment to permit reverse

intersystem crossing (RISC). The Huang group reported thiophene-pyrimidine-based ladder-type compounds with B-N coordination (**78**).[42] Low-lying energy levels, red-shifted absorbance, and ambipolar transport properties were achieved *via* the polymerization of the same backbone. The efficiency of all-polymer solar cells with the B-N coordinated thiophene-pyrimidine conjugated polymer as the acceptor reached up to 8%. (**79**, **80**).[43]

In recent years, our group has also conducted substantial research on N,C-chelate boron compounds. In 2019, we prepared a number of polycyclic aromatic hydrocarbons based on tetrahydrodibenzo[a,i]phenanthridine that was N-C chelated (**87-89**).[44] Photophysical investigations showed that absorption maxima fall between 368 and 420 nm, and exhibit moderate molar extinction coefficients ranging from 15800 to 38700 $M^{-1}cm^{-1}$. Complexes exhibit a red-shifted band in emission spectra in comparison to their ligands. With a similar methodology, we prepared phenanthroimidazole-based boron compounds (**90**) which showed moderate to good quantum yields in the solution and solid state.[45] In addition, we explored the synthesis of N,C-chelated B-N coordinated dimers based on triaryl pyrazole and phenanthroimidazole (**91–94**).[46] Due to the longer conjugation chains, the absorption spectra of dimers based on phenanthroimidazole and triaryl pyrazole were noticeably more red-shifted than those of monomeric borylated complexes. Excellent quantum yields up to 99% in the solution state and moderate quantum yields in the solid state were achieved with phenanthroimidazole dimers. This shows that dimers lose very little energy *via* non-radiative processes. Additionally, we investigated the phenanthroimidazole dimer's nonlinear optical characteristics and demonstrated the relationship between the conjugation length and two-photon absorption cross-section. All

the B-N coordinated pyrazole dimers exhibit good molar absorption coefficients and quantum yields of up to 94% in the solution state.[47] The nonlinear optical (NLO) properties of the B-N coordinated pyrazole dimers were further investigated because of a significant change in the excited state dipole moment. Additional research reveals that these compounds exhibited outstanding NLO properties. The two-photon-
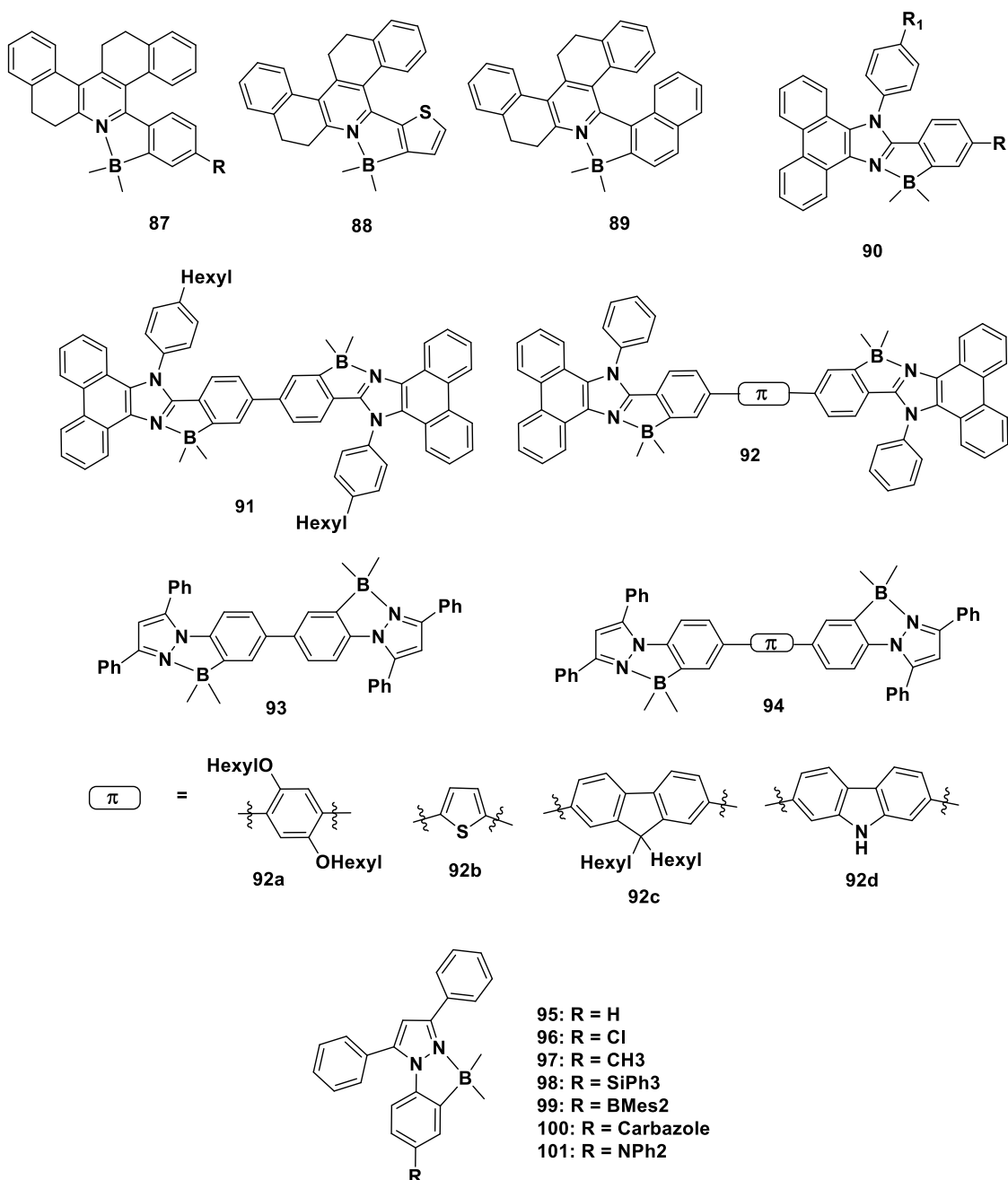
Figure 1.10: Structure of N,C-chelate boron compounds **87-101**

absorption (TPA) cross-section is strongly affected by dimer symmetry and the presence of acceptor or donor motifs. In addition, the studies show that the conjugation length in all dimer types has a significant influence on the nonlinear optical properties. Pischel and co-workers designed and synthesized B-N coordinated monomeric and dimeric aryl isoquinoline-based system with good photostability and a TPA cross section up to 220 GM at 700 nm.[48] Recently we reported a group of B-N coordinated boron complexes (**95–101**) based on triaryl pyrazoles that were produced using an electrophilic aromatic borylation approach.[49] The photoluminescence studies of these compounds showed that the emission maxima were dependent on the modification on N-phenyl. Theoretical calculations provided additional support for the photophysical and electrochemical features. Investigations using Z-scan technique at the 515 nm pump wavelength demonstrated that adding an electron-deficient moiety to these compounds increased the nonlinear absorption (two-photon absorption, or TPA) due to B-N coordination. Additionally, it has been noted that the right choice of moiety facilitates the most effective manipulation of the π-system's molecular polarizability, which helps to manage the third order nonlinear optical response.

1.2 References

1. (a) J. E. Anthony, *Chem. Rev.*, **2006**, *106*, 5028–5048. (b) V. Coropceanu, J. Cornil, D. A. Da Silva Filho, Y. Olivier, R. Silbey and J.-L. Bredas, *Chem. Rev*., **2007**, *107*, 926–952. (c) A. Mishra, C.-Q. Ma and P. Baeuerle, *Chem. Rev.,* **2009**, *109*, 1141–1276. (d) L. R. Dalton, P. A. Sullivan and D. H. Bale, *Chem. Rev.,* **2010**, *110*, 25–55. (e) N. J. Hestand and F. C. Spano, Chem. Rev., **2018**, *118*, 7069–7163

2. (a) A. Fukazawa and S. Yamaguchi, *Chem. – Asian J.*, **2009**, *4*, 1386–1400. (b) A. Narita, X.- Y. Wang, X. Feng and K. Muellen, *Chem. Soc. Rev.*, **2015**, *44*, 6616–6643. (c) A. Wakamiya and S. Yamaguchi, *Bull. Chem. Soc. Jpn.*, **2015**, *88*, 1357–1377. (d) M. Stepien, E. Gonka, M. Zyla and N. Sprutta, *Chem. Rev.*, **2017**, *117*, 3479–3716

3. (a) Z. M. Hudson and S. Wang, *Acc. Chem. Res.,* **2009**, *42*, 1584–1596 (b) F. Jäkle, *Chem. Rev.*, **2010**, *110*, 3985–4022 (c) L. Ji, S. Griesbeck and T. B. Marder, *Chem. Sci.*, **2017**, *8*, 846–863 (d) E. von Grotthuss, A. John, T. Kaese and M. Wagner, *Asian J. Org. Chem.*, **2018**, *7*, 37–53 (e) S. K. Mellerup and S. Wang, *Chem. Soc. Rev.,* **2019**, *48*, 3537–3549 (f) J. He, F. Rauch, M. Finze and T. B. Marder, *Chem. Sci.,* **2021**, *12*, 128–147

4. (a) Y.-L. Rao, H. Amarne and S. Wang, *Coord. Chem. Rev*., **2012**, *256*, 759–770 (b) D. Li, H. Zhang and Y. Wang, *Chem. Soc. Rev.*, **2013**, *42*, 8416–8433 (c) D. Frath, J. Massue, G. Ulrich and R. Ziessel, *Angew. Chem., Int. Ed.,* **2014**, *53*, 2290–2310 (d) K. Tanaka and Y. Chujo, *NPG Asia Mater.*, **2015**, *7*, e223 (e) P.-Z. Chen, L.-Y. Niu, Y.-Z. Chen and Q.-Z. Yang, *Coord. Chem. Rev.*, **2017**, *350*, 196–216 (f) M. Gon, K. Tanaka and Y. Chujo, *Bull. Chem. Soc. Jpn.,* **2019**, *92*, 7–18 (g) J. Massue, D. Jacquemin and G. Ulrich, *Organics*, **2021**, *2*, 365–375

5. (a) M. J. S. Dewar , V. P. Kubba and R. Pettit , *J. Chem. Soc.*, **1958**, 3073 —3076 (b) A. Wakamiya , T. Taniguchi and S. Yamaguchi , *Angew. Chem., Int. Ed.*, **2006**, *45* , 3170 —3173

6. C. Dou , Z. Ding , Z. Zhang , Z. Xie , J. Liu and L. Wang , *Angew. Chem., Int. Ed.*, **2015**, *54*, 3648 —3652

7. R. Zhao , C. Dou , Z. Xie , J. Liu and L. Wang , *Angew. Chem., Int. Ed.*, **2016**, *55*, 5313 —5317

8. Z. Zhang , Z. Ding , C. Dou , J. Liu and L. Wang , *Polym. Chem.*, **2015**, *6*, 8029 — 8035

9. (a) S. K. Mellerup , K. Yuan , C. Nguyen , Z.-H. Lu and S. Wang , *Chem. – Eur. J.*, **2016**, *22*, 12464 —12472 (b) J. Wang , B. Jin , N. Wang , T. Peng , X. Li , Y. Luo and S. Wang , *Macromolecules*, **2017**, *50*, 4629 —4638 (c) C. Li , S. K. Mellerup , X. Wang and S. Wang , *Organometallics*, **2018**, *37*, 3360 —3367 (d) S. K. Mellerup , C. Li , X. Wang and S. Wang , *J. Org. Chem.*, **2018**, *83*, 11970 —11977 (e) S. K. Mellerup , G. Yousefalizadeh , S. Wang and K. G. Stamplecoskie , *J. Phys. Chem. A*, **2018**, *122*, 9267 —9274 (f) N. Wang , J. Wang , D. Zhao , S. K. Mellerup , T. Peng , H. Wang and S. Wang , *Inorg. Chem.*, **2018**, *57*, 10040 —10049 (g) S. Wang , K. Yuan , M.-F. Hu , X. Wang , T. Peng , N. Wang and Q.-S. Li , *Angew. Chem., Int. Ed.*, **2018**, *57*, 1073 —1077 (h) Z.-C. He , S. K. Mellerup , L. Liu , X. Wang , C. Dao and S. Wang , *Angew. Chem., Int. Ed.*, **2019**, *58*, 6683 —6687 (i) Z. He , L. Liu , Z. Zhao , S. K. Mellerup , Y. Ge , X. Wang , N. Wang and S. Wang , *Chem. – Eur. J.*, **2020**, *26*, 12403 —12410

10. A. Wakamiya , T. Taniguchi and S. Yamaguchi , *Angew. Chem., Int. Ed.*, **2006**, *45*, 3170 —3173

11. C. Zeng , K. Yuan , N. Wang , T. Peng , G. Wu and S. Wang , *Chem. Sci.*, **2019**, *10*, 1724 —1734

12. Q. Hou , L. Liu , S. K. Mellerup , N. Wang , T. Peng , P. Chen and S. Wang , *Org. Lett.*, **2018**, *20*, 6467 —6470

13. X. Li , Y. Shi , N. Wang , T. Peng and S. Wang , *Chem. – Eur. J.*, **2019**, *25*, 5757 —5767

14. Z. Feng , Y. Yu , X. Yang , Y. Sun , D. Zhong , X. Deng , G. Zhou and Z. Wu , *J. Mater. Chem. C*, **2021**, *9*, 12650 —12660

15. (a) M. Yusuf , K. Liu , F. Guo , R. A. Lalancette and F. Jäkle , *Dalton Trans.*, **2016**, *45*, 4580 —4587 (b) A. F. Alahmadi , R. A. Lalancette and F. Jäkle , *Macromol. Rapid Commun.*, **2018**, *39*, 1800456

16. M. Vanga , R. A. Lalancette and F. Jäkle , *Chem. – Eur. J.*, **2019**, *25*, 10133 —10140

17. (a) K. Liu , R. A. Lalancette and F. Jäkle , *J. Am. Chem. Soc.*, **2017**, *139* , 18170 —18173 (b) K. Liu , R. A. Lalancette and F. Jäkle , *J. Am. Chem. Soc.*, **2019**, *141*, 7453 —7462

18. M. Vanga, A. Sahoo, R. A. Lalancette and F. Jäkle , *Angew. Chem., Int. Ed.*, **2022**, *61*, e202113075

19. K. Liu, Z. Jiang, R. A. Lalancette, X. Tang and F. Jäkle, *J. Am. Chem. Soc.*, **2022**, *144*, 18908 —18917

20. D. L. Crossley , R. Goh , J. Cid , I. Vitorica-Yrezabal , M. L. Turner and M. J. Ingleson , *Organometallics*, **2017**, *36*, 2597 —2604

21. D. L. Crossley , I. A. Cade , E. R. Clark , A. Escande , M. J. Humphries , S. M. King , I. Vitorica-Yrezabal , M. J. Ingleson and M. L. Turner , *Chem. Sci.*, **2015**, *6*, 5144 —5151

22. D. L. Crossley , P. Kulapichitr , J. E. Radcliffe , J. J. Dunsford , I. Vitorica-Yrezabal , R. J. Kahan , A. W. Woodward , M. L. Turner , J. J. W. McDouall and M. J. Ingleson , *Chem. – Eur. J.*, **2018**, *24*, 10521 —10530

23. D. L. Crossley , L. Urbano , R. Neumann , S. Bourke , J. Jones , L. A. Dailey , M. Green , M. J. Humphries , S. M. King , M. L. Turner and M. J. Ingleson , *ACS Appl. Mater. Interfaces*, **2017**, *9*, 28243 —28249

24. B. P. Dash , I. Hamilton , D. J. Tate , D. L. Crossley , J.-S. Kim , M. J. Ingleson and M. L. Turner , *J. Mater. Chem. C*, **2019**, *7*, 718 —724

25. H. Shimogawa , O. Yoshikawa , Y. Aramaki , M. Murata , A. Wakamiya and Y. Murata , *Chem. – Eur. J.*, **2017**, *23*, 3784 —3791

26. M. Grandl , T. Kaese , A. Krautsieder , Y. Sun and F. Pammer , *Chem. – Eur. J.*, **2016**, *22*, 14373 —14382

27. (a) M. Grandl , Y. Sun and F. Pammer , *Org. Chem. Front.*, **2018**, *5*, 336 —352 (b) F. Pammer , J. Schepper , J. Gloeckler , Y. Sun and A. Orthaber , *Dalton Trans.*, **2019**, *48*, 10298 —10312

28. M. Grandl , J. Schepper , S. Maity , A. Peukert , E. von Hauff and F. Pammer , *Macromolecules*, **2019**, *52*, 1013 —1024

29. S. Schraff , Y. Sun and F. Pammer , *J. Mater. Chem. C*, **2017**, *5*, 1730 —1741

30. R. Koch , Y. Sun , A. Orthaber , A. J. Pierik and F. Pammer , *Org. Chem. Front.*, **2020**, *7*, 1437 —1452

31. B. Y.-W. Wong , H.-L. Wong , Y.-C. Wong , M.-Y. Chan and V. W.-W. Yam , *Chem. – Eur. J.*, **2016**, *22*, 15095 —15106

32. T. C.-H. Fong, C.-L. Wong, W.-K. Tang, M.-Y. Leung, K.-H. Low and V. W.-W. Yam, *Chem. Comm.*, **2022**, *58*, 4231-4234

33. Y.-J. Shiu , Y.-T. Chen , W.-K. Lee , C.-C. Wu , T.-C. Lin , S.-H. Liu , P.-T. Chou , C.-W. Lu , I. C. Cheng , Y.-J. Lien and Y. Chi , *J. Mater. Chem. C*, **2017**, *5*, 1452 —1462

34. M. Stanoppi and A. Lorbach , *Dalton Trans.*, **2018**, *47*, 10394 —10398

35. M. J. Wildervanck, R. Hecht, A. Nowak-Krol , *Molecules*, **2022**, *27*, 5510

36. Z. Dominguez , R. Lopez-Rodriguez , E. Alvarez , S. Abbate , G. Longhi , U. Pischel and A. Ros , *Chem. – Eur. J.*, **2018**, *24*, 12660 —12668

37. X. Zhang, F. Rauch, J. Niedens, R. B. da Silva, A. Friedrich, A. Nowak-Krol, S. J. Garden, and T. B. Marder, *J. Am. Chem. Soc.* **2022**, *144*, 22316−22324

38. J. Full, S. P. Panchal , J. Goetz , A.-M. Krause and A. Nowak-Krol , *Angew. Chem., Int. Ed.*, **2021**, *60*, 4350 —4357

39. Felix Full, Martijn J. Wildervanck, Daniel Volland, and Agnieszka Nowak-Król, *Synlett,* **2022**, *33*, A–F

40. F. Full, Q. Wolflick, K. Radacki, H. Braunschweig, and A. Nowak-Krol, *Chem. Eur. J.*, **2022**, *28*, e202202280

41. M. Mamada , G. Tian , H. Nakanotani , J. Su and C. Adachi , *Angew. Chem., Int. Ed.*, **2018**, *57*, 12380 —12384

42. Y. Li , B. Pang , H. Meng , Y. Xiang , Y. Li and J. Huang , *Tetrahedron Lett.*, **2019**, *60*, 151286

43. Y. Li , H. Meng , T. Liu , Y. Xiao , Z. Tang , B. Pang , Y. Li , Y. Xiang , G. Zhang , X. Lu , G. Yu , H. Yan , C. Zhan , J. Huang and J. Yao , *Adv. Mater.*, **2019**, *31*, 1904585

44. D. Kunchala, S. Sa , P. Nayak , J. Ponniah S and K. Venkatasubbaiah , *Organometallics*, **2019**, *38* , 870 —878

45. K. Dhanunjayarao , S. Sa , B. P. R. Aradhyula and K. Venkatasubbaiah , *Tetrahedron*, **2018**, *74* , 5819 —5825

46. M. Vanga , S. Sa , A. Kumari , A. C. Murali , P. Nayak , R. Das and K. Venkatasubbaiah , *Dalton Trans.*, 2020, **49** , 7737 —7746; V. Mukundam , S. Sa , A. Kumari , R. Das and K. Venkatasubbaiah , *J. Mater. Chem. C*, **2019**, *7*, 12725 — 12737

47. V. Mukundam , S. Sa , A. Kumari , R. Das and K. Venkatasubbaiah , *J. Mater. Chem. C*, **2019**, *7*, 12725 —12737

48. Z. Dominguez , V. F. Pais , D. Collado , P. Vazquez-Dominguez , F. N. Albendin , E. Perez-Inestrosa , A. Ros and U. Pischel , *J. Org. Chem.*, **2019**, *84*, 13384 —13393

49. V. Mukundam, S. Sa, A. Kumari, T. T. Ponduru, R. Das, and K. Venkatasubbaiah, *Chem Asian J.,* **2022**, *17*, e202200291

Chapter 2

Tetra-coordinate boron appended zinc(II)-salen:

A highly selective fluorescence based sensor for

Sm^{3+} ion *via* sensitization

2.1 Introduction

In recent years, the design and synthesis of tri- and tetra-coordinated boron compounds have received considerable attention due to their applications in diverse fields such as light-emitting devices, photovoltaics, sensors, and organic field-effect transistors.[1] The ability to attain planar conformation, stability due to saturation of Lewis acidity, and rigidity of the basic structure makes tetra-coordinated boron-based fluorophores as more favorable alternatives over three-coordinated boron compounds. Among the different tetra-coordinated boron compounds, B-N coordinated compounds secured considerable attention because of their widespread applications.[2] We and others have recently shown that B-N coordinated compounds can show oxygen sensing behavior, photochromism, non-linear optical properties, *etc*.[2a,2g,2i,2l,2m,3]

Selective detection of metal ions has emerged as an important area of research due to its implications in the area of environmental, biological, and clinical studies. Several probes or sensors have been reported for the detection of different metal ions employing colorimetric and/or fluorometric techniques.[4] Fluorescence-based probes or sensors received considerable attention owing to their simplicity, selectivity, and sensitivity towards specific metal ions. Among the different metal ions, lanthanoid ions constitute a family with very similar and non-discriminative coordination behavior. On the other hand, the use of lanthanoids in industrial applications is ever-burgeoning. To name a few in magnetism, display, components of nuclear control rods, and even as catalysts.[5] As some or many of the lanthanoid ions are toxic in nature their detection is an important task. Although there are reports on the detection of different lanthanoid ions,[6] selective discrimination and detection of lanthanoid ions is a major challenge in view of their

similarity in terms of size and chemical behavior. Taking advantage of the emissive and electron-transporting properties of the B-N coordinated fluorophores with the chelating ability of salen ligands which can find use in catalysis and materials chemistry, we designed a tetra-coordinated boron-functionalized pyrazole-based salen ligand (Fig. 2.1). We envisioned that this molecular architecture will enable the selective detection of Zn^{2+} using pocket 1 and also further expected that pocket 2 will discriminate lanthanoid ions.
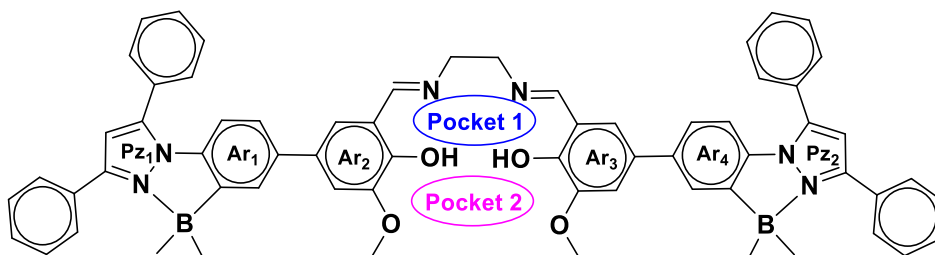
Figure 2.1: Structure of ligand used in this study

2.2 Results and discussion

Selective detection of zinc ions plays a vital role in the chemical and biological sciences owing to its important role in gene expression, apoptosis, cellular metabolism, and neurotransmission.[7] A number of analytical techniques such as UV/Vis, fluorescence, atomic absorption spectroscopy, and electrochemical methods are used for the detection of Zn^{2+} ions.[8] Among the different methods, fluorescent sensors showed superior sensitivity. This motivated us to investigate the coordinating ability of boron-functionalized compound **5a** as a luminescent probe for Zn^{2+}. The synthetic route to pyrazole-based boron functionalized imine ligand **5a** is outlined in Scheme 2.1.
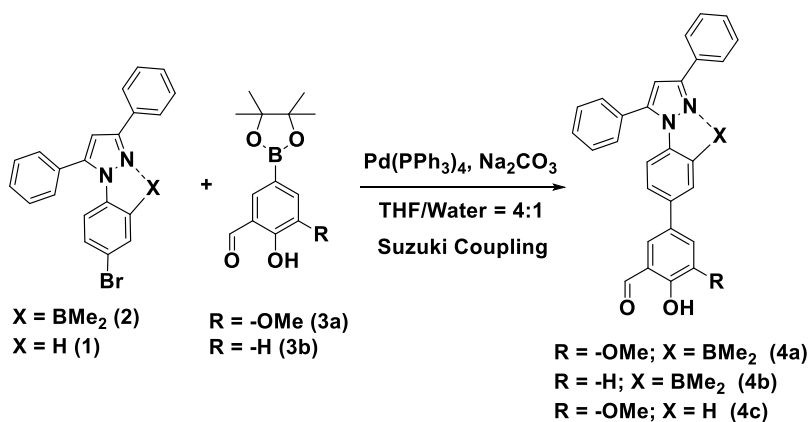
Scheme 2.1: Synthesis of compounds **4a**-**4c**
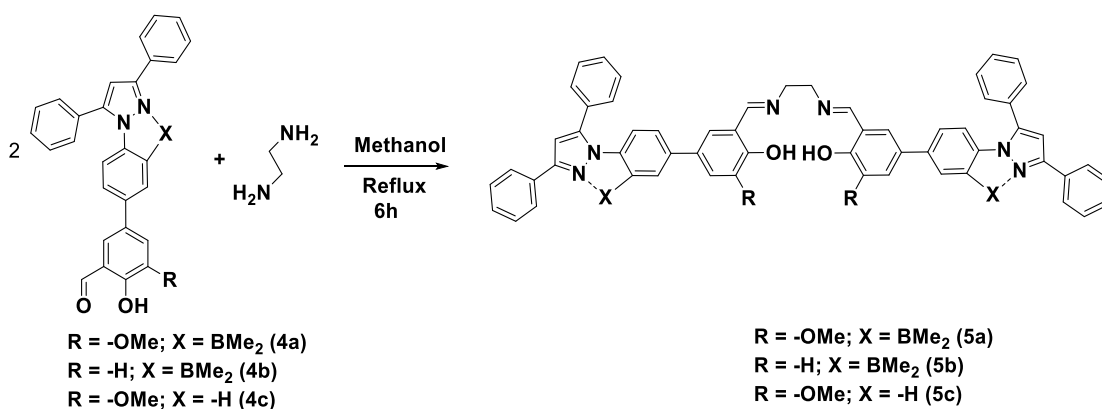
Scheme 2.2: Synthesis of ligands **5a**-**5c**

Compounds **1**-**3** were prepared according to the literature-reported methods.[3g] Treatment of **2** and **3a** (Scheme 2.1) with Na_2CO_3 and a catalytic amount of $Pd(PPh_3)_4$ under Suzuki coupling conditions resulted in a moderate yield (61%) of **4a**. Synthesis of the required ligand **5a** (Scheme 2.2) was achieved in an excellent yield (92 %) by a simple condensation reaction of 2 equivalents of **4a** with ethylene diamine in dry methanol solvent. Compound **5a** was characterized using multi-nuclear NMR and HRMS. Furthermore, compound **5a** was also analyzed using ^{1}H-^{1}H COSY (Fig 2.2). The UV/Vis absorption and fluorescence spectra of **5a** (10 μM) reveal an absorption maximum at 330 nm and an emission maximum at 464 nm. To understand the sensing properties of **5a**, the
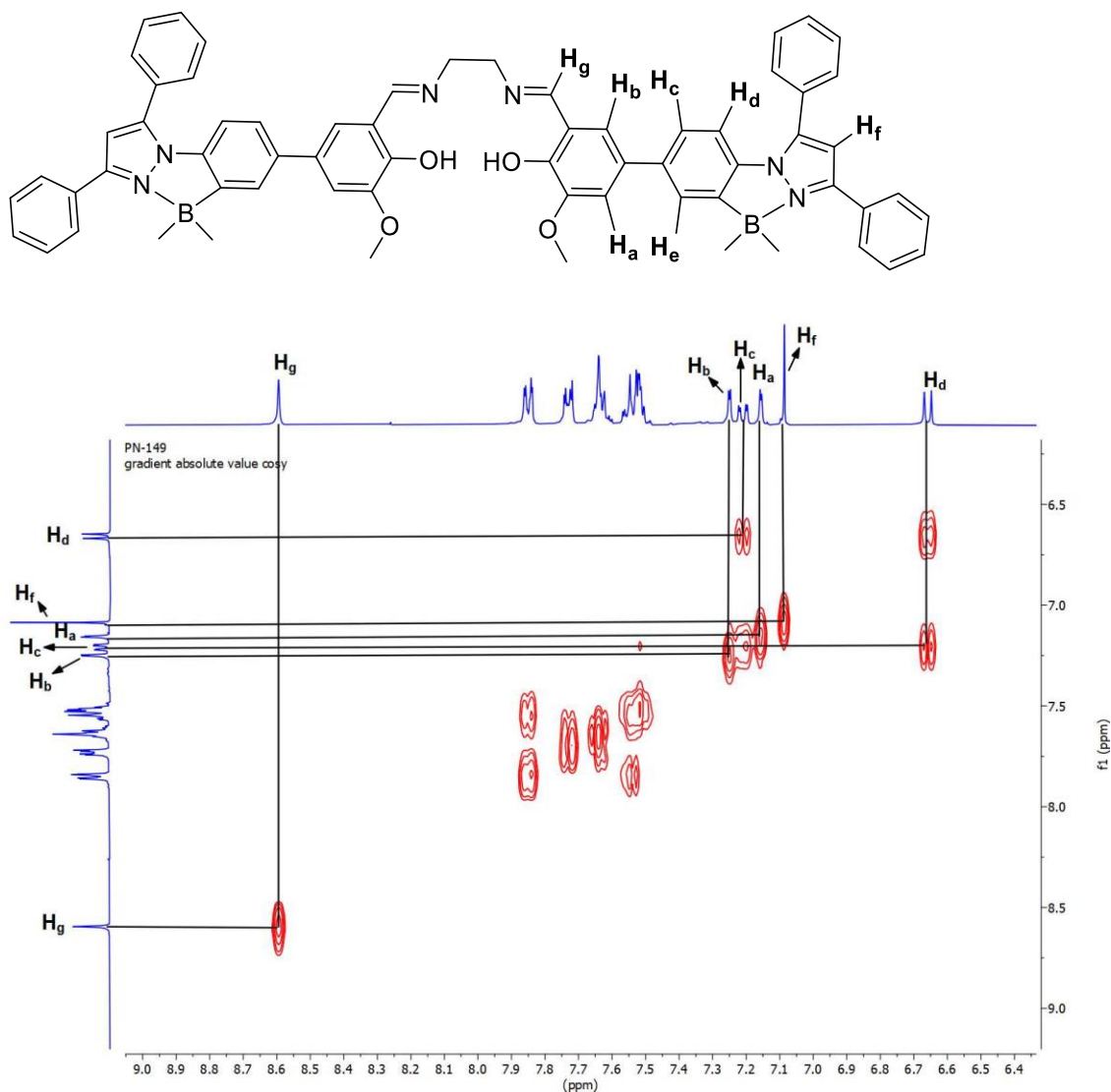
Figure 2.2: ^1H-^1H COSY NMR of compound **5a** in DMSO-d_6.

absorption and fluorescence spectra of **5a** were recorded with different amounts of Zn^{2+} ions. Sequential addition of Zn^{2+} ions (0 - 2.4 equiv.) to **5a** resulted in a new absorption peak at 353 nm with an isosbestic point at 339 nm (Fig 2.3). As shown in figure 2.3(b), the fluorescence intensity gradually increased with the sequential addition of Zn^{2+} ions (0 - 2.4 equiv.). Furthermore, a selectivity test was performed using various cations such as Cd^{2+}, Co^{2+}, Fe^{3+}, Fe^{2+}, Hg^{2+}, K^+, Mn^{2+}, Cr^{3+}, Na^+, $Ni^{2+,}$ and Mg^{2+} to investigate the binding interaction of **5a** (10 µM). As shown in figure 2.3(d), only Zn^{2+} caused an
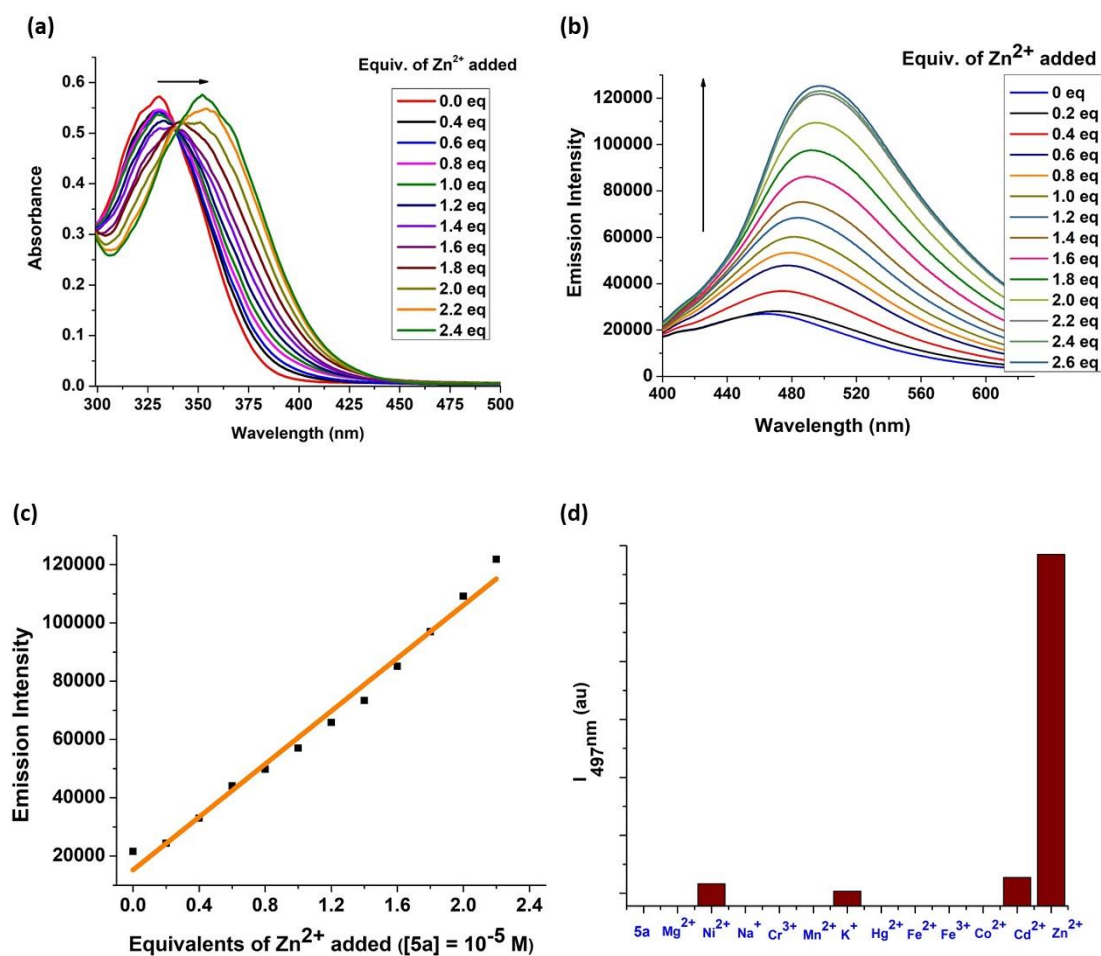
Figure 2.3: (a) Absorbance and (b) Fluorescence spectra (λ_{ex} = 330 nm) of **5a** (10 μM) with 2.2 equiv. of NaOAc upon addition of 0 – 2.4 equiv of Zn^{2+} in (10:90) Methanol/THF solvent system. (c) Linear increase of the fluorescence intensity at 497 nm of **5a** (10 μM) upon addition of 0 – 2.4 equiv of Zn^{2+} (λ_{ex} = 330 nm). (d) Fluorescence intensity profile changes of **5a** in presence of various metal ions

enhanced emission while other cations were silent. This result indicates that **5a** discriminates Zn^{2+} from other cations which can be detected by a green emission.

To investigate the binding mode of the zinc ion with salen, we independently synthesized (Scheme 2.3) the Zn-salen and characterized using different techniques like ^1H, ^{13}C, ^{11}B. The disappearance of OH peak at 13.61 ppm of the ligand **5a** and upfield shifting of four
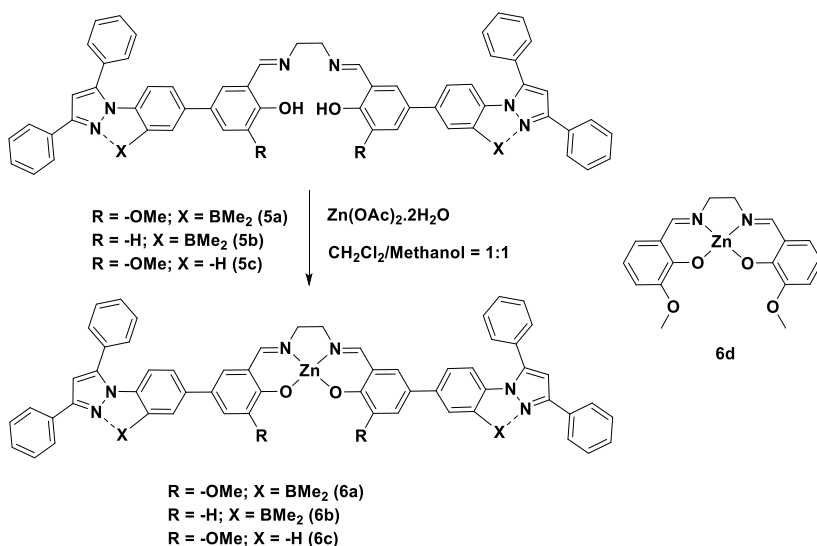
Scheme 2.3: Synthesis of zinc complexes **6a**, **6b**, **6c** and structure of complex **6d** used in this study

ethylene protons from 3.94 ppm in **5a** to 3.74 ppm in **6a** confirms the formation of Zn^{2+} complex, **6a**. To our delight, X-Ray quality crystals of complex **6a** could be grown in DMF/CH₃CN solvent system. The crystal structure confirms a 1:1 binding of **5a** with Zn^{2+} (Fig 2.5).

The detection limit for Zn^{2+} was calculated and found to be 72 nM. These results reveal the applicability of **5a** in determining Zn^{2+} ion with high selectivity. Benesi Hildebrand (B-H) plot[9] was used to estimate the binding constant of **5a** with Zn^{2+}.

The binding constant was calculated using the Eq. (i) from the fluorescence titration data for **5a** with Zn^{2+} complex.

$$1/\Delta I = 1/\Delta I_{max} + 1/(K\Delta I_{max})(1/[Zn^{2+}]) \qquad \qquad ....(i)$$

Here $\Delta I = I - I_{min}$ and $\Delta I_{max} = I_{max} - I_{min}$, where I_{min}, I, and I_{max} are the emission intensities of receptor considered in the absence of Zn^{2+}, at an intermediate Zn^{2+} concentration, and at a concentration of complete saturation where K is the binding constant and $[Zn^{2+}]$ is

the Zn^{2+} concentration respectively. From the plot of $[1 / (I - I_{min})]$ against $1/[Zn^{2+}]$ for

5a, the value of K has been determined from the slope (Fig 2.4). The binding constant

(K) was found to be $1.9 \times 10^4\ M^{-1}$ for **5a**-Zn^{2+}.
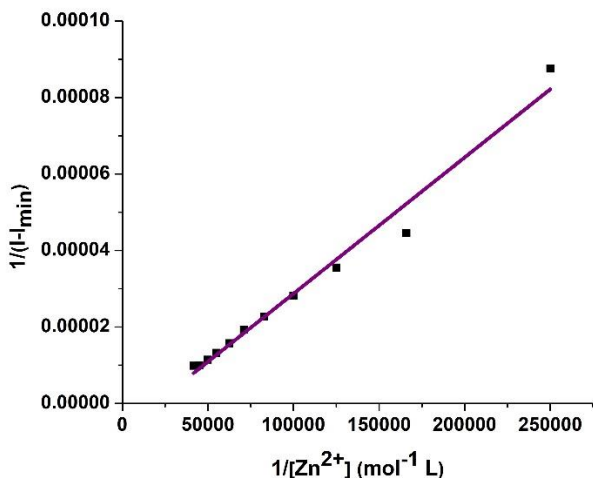
Figure 2.4: B-H plot assuming 1:1 stoichiometry for complexation between **5a** and Zn^{2+}

ions

A calibration curve representing emission intensity vs concentration of zinc ions showed

excellent linearity with a high coefficient ($R^2 = 0.98$) in the range from 0 to 24 μM (Fig

2.4). The detection limit of **5a** for Zn^{2+} is 72 nM which was calculated using the

calibration curve. These results showed the valuable applicability of probe **5a** in

quantitative determination of Zn^{2+} with high sensitivity.

Complex **6a** crystallizes in a triclinic P-1 space group. The molecular structure revels that

the zinc atom adopts a five-coordinate distorted square pyramidal geometry. The zinc

atom is 0.447 Å above the plane formed by the N_2O_2 coordination from the salen motif.

The axial position is occupied by a water molecule with a bond length of 2.066 Å. The

Zn-O/N bond distances and angles observed for compound **6a** are consistent with previously reported Zn^{2+}-salen complexes.[10] The pyrazole (Figure 2.1, Pz_1 and Pz_2) and the N-phenyls (Figure 2.1, Ar_1 and Ar_4) forms a three-cycle co-planarized system *via* B-N coordination. The torsional angles observed for Ar3-Ar4 and Ar2-Ar1 are 18.5 ° and 32.3 ° respectively, which indicates that Zn-salen and B-N coordinated pyrazole moieties have a slight deviation from planarity.
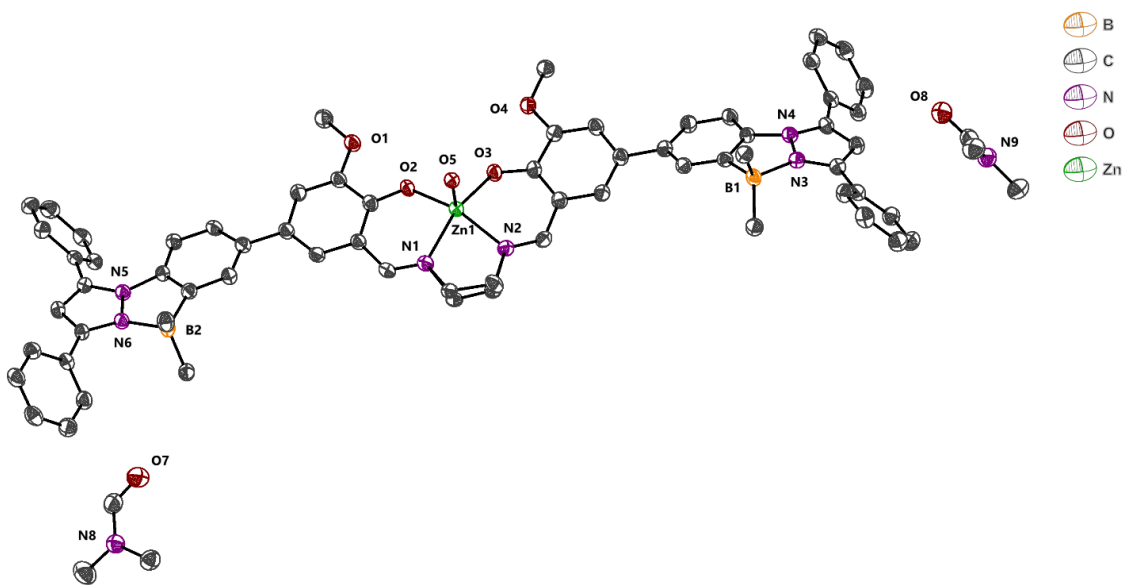
Figure 2.5: Crystal Structure of complex **6a**. Thermal ellipsoids are drawn at 50% probability level. Hydrogen atoms and water molecules are removed for clarity.

With this success, we further investigated the coordination ability of pocket 2 in **6a** towards lanthanoid ions. To our surprise complex **6a** discriminate lanthanoid ions and was able to detect Sm^{3+} ion selectively using pocket 2. We examined the emission spectra of complex **6a** upon addition of 1.2 equiv. of various lanthanoid ions such as Sm^{3+}, Ce^{3+}, Dy^{3+}, Er^{3+}, Eu^{3+}, Gd^{3+}, Ho^{3+}, La^{3+}, Pr^{3+}, Tb^{3+}, Tm^{3+} and Yb^{3+}. Except for Sm^{3+} ion, all other ions showed a weak fluorescence quenching at 500 nm (Fig 2.6). However, a strong fluorescence quenching at 500 nm and enhanced emission peaks at 560 nm, 602 nm, and

645 nm were observed on the addition of 1.2 equivalents of Sm^{3+} ion to complex **6a**. This could be due to an efficient energy transfer from **6a** to Sm^{3+} center upon complexation. These are characteristic peaks of Sm^{3+} emission resulting from the deactivation of the $^4G_{5/2}$ excited state to the ^6H_J ground state ($J = 9/2, 7/2, 5/2$).[11] To know the capability of **6a** to detect Sm^{3+} in the aqueous medium, 1.5 equivalents of Sm^{3+} ion in water were added to **6a** in THF solution which showed an emission reminiscent to the Methanol/THF system. This result suggests that **6a** can also be used to discriminate lanthanoid ions in THF/H_2O medium.
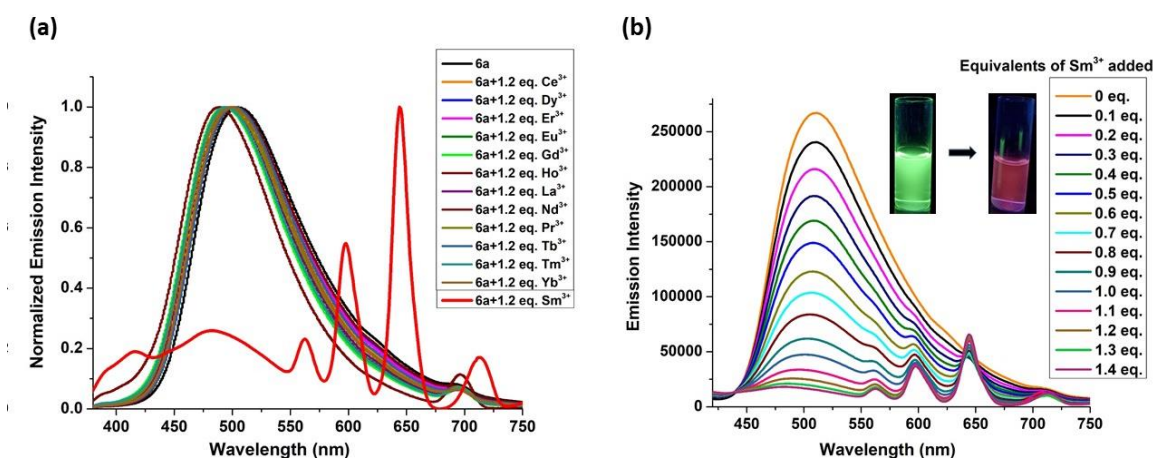
Figure 2.6: (a) Normalized fluorescence spectra of **6a** (10 μM) upon the addition of different lanthanoide ions (1.2 equiv) in (10:90) Methanol/THF (λ_{ex} = 357). (b) Emission spectra of **6a** + Sm^{3+} in (10:90) Methanol/THF with increasing concentrations of **Sm^{3+} ion (6a concentration of 1 x 10^{-5} M); (inset)** Color change under a UV lamp of **6a** and **6a** + 1.2 eq. Sm^{3+} at 1 x 10^{-5} M concentration in (10:90) Methanol/THF

In general, lanthanoid ion sensitization process takes place from the triplet state of the sensitizer.[12] To understand the electronic properties of complex **6a**, and the sensitization phenomenon, TD-DFT calculations were performed using the optimized ground-state geometry of **6a**. The T_1 triplet energy of complex **6a** was predicted using the

corresponding TD-DFT calculation results of **6a**, which gives an energy of 1053 nm/9497 cm-1 (Table 2.1).
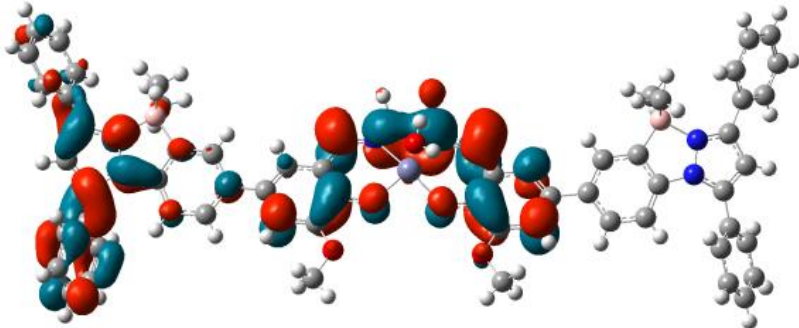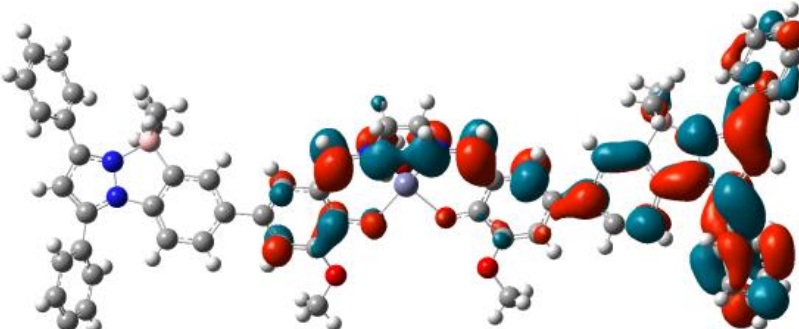
The triplet state energy of **6a** is lower than the emissive state of Sm^{3+} ion (558 nm/17900 cm-1) which proves that the sensitization of Sm^{3+} by **6a** is not taking place from triplet state. Previous reports have also shown that the sensitization of Ln^{3+} centers can occur from the singlet state of the sensitizers.[13] From TD-DFT calculations it was calculated that the S1 singlet state energy of **6a** (388 nm/25773 cm^{-1}) is above the emissive state $^4G_{5/2}$ of Sm^{3+}. Thus, complex **6a** is expected to sensitize Sm^{3+} emission from its singlet S1 state.
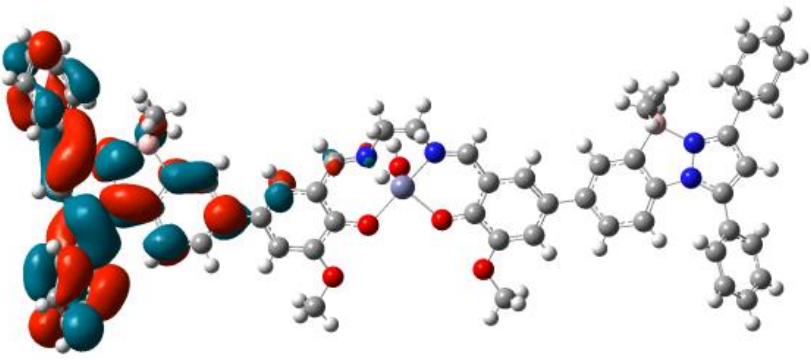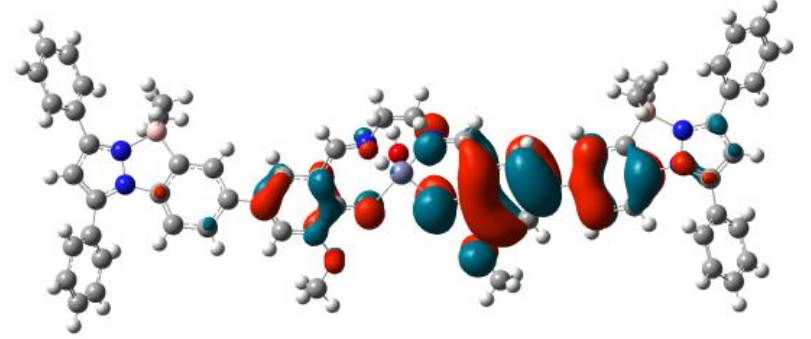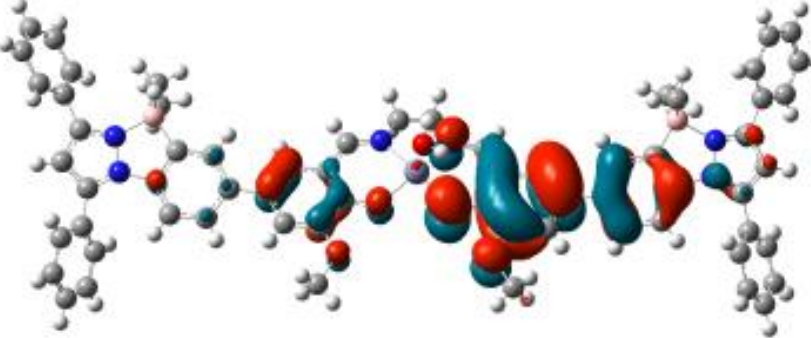
Table 2.1: Calculated electronic transitions for compound **6a** from TD-DFT (B3LYP) calculations

Compound	Transition	MO contributions	Energy gap eV (nm)	Oscillator strength/f
6a	$S_0{\rightarrow}S_1$	HOMO-1→LUMO(10%) HOMO→LUMO(27%) HOMO→LUMO+1(59%) HOMO→LUMO+2(11%)	2.59 (477)	0.1706
	$S_0{\rightarrow}S_2$	HOMO-1→LUMO(33%) HOMO→LUMO(53%)	2.72 (454)	0.1291
	$S_0{\rightarrow}S_3$	HOMO→LUMO+1(27%) HOMO-1→LUMO+1(13%)	2.79 (433)	0.2901

	$T_1 \rightarrow S_0$	HOMO→LUMO+1(16%)	1.33 (929)	0.0146
		HOMO→LUMO+2(65%)		
		HOMO→LUMO(70%)		

Table 2.2: Computed orbitals from DFT (B3LYP:6-31G) calculations for complexes **6a** (color red indicates negative and blue indicates positive)

Compound	6a
LUMO+2	
	0.075 eV
LUMO+1	
	0.0029 eV

LUMO	
	-0.1499 eV
HOMO	
	-4.250 eV
HOMO-1	
	-5.680 eV

| HOMO-2 | |
| | -6.780 eV |
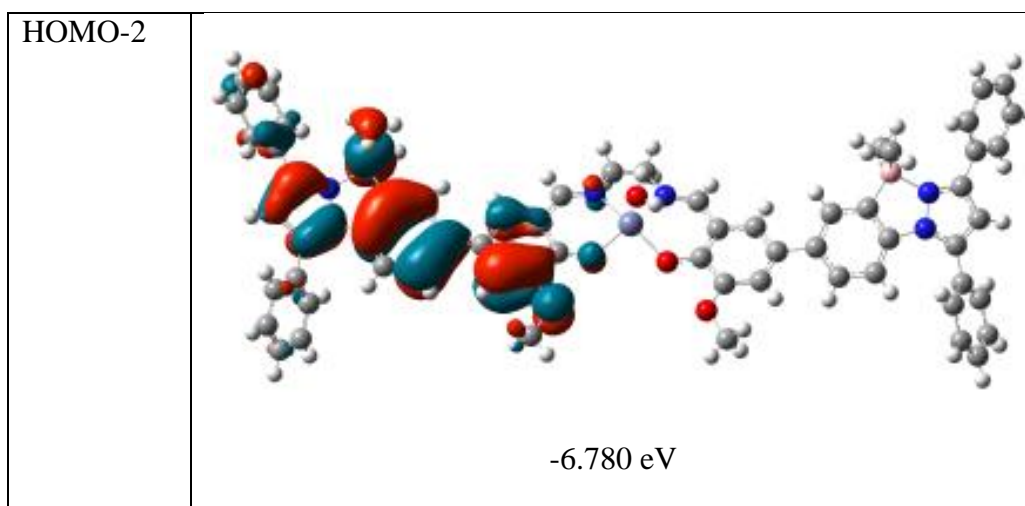
In order to investigate the interactions between **6a** and Sm^{3+}, we reacted complex **6a** with $Sm(NO_3)_3.6H_2O$ in 1:1.5 ratio in $CHCl_3$/EtOH solvent system at room temperature and isolated pure **6a.Sm^{3+}** complex as a yellow precipitate. Single crystals of **6a·Sm^{3+}** were grown by slow evaporation of DMF and methanol. To our delight, single-crystal X-ray diffraction analysis revealed the formation of a 1:1 adduct, in which Sm^{3+} forms a ten coordinated complex with **6a** (Fig 2.7). Complex **6a.Sm^{3+}** crystallizes in the monoclinic system with a space group of $P2_1$/c. The complex **6a** is bound to the samarium ion through four oxygen atoms, in which Sm1-O4 (2.667(4) Å) and Sm1-O5 (2.770(4) Å) bond distances are significantly longer than Sm1-O1 (2.372(4) Å) and Sm1-O2 (2.357(3) Å) bond distances. Samarium ion is further coordinated to three nitrate ions adopting a distorted square pyramidal structure achieving a coordination number of ten. The zinc ion adopts a distorted square pyramidal coordination environment in the heterometallic complex. The Sm···Zn distance is 3.454 Å, suggesting that there is no direct Sm···Zn bond.
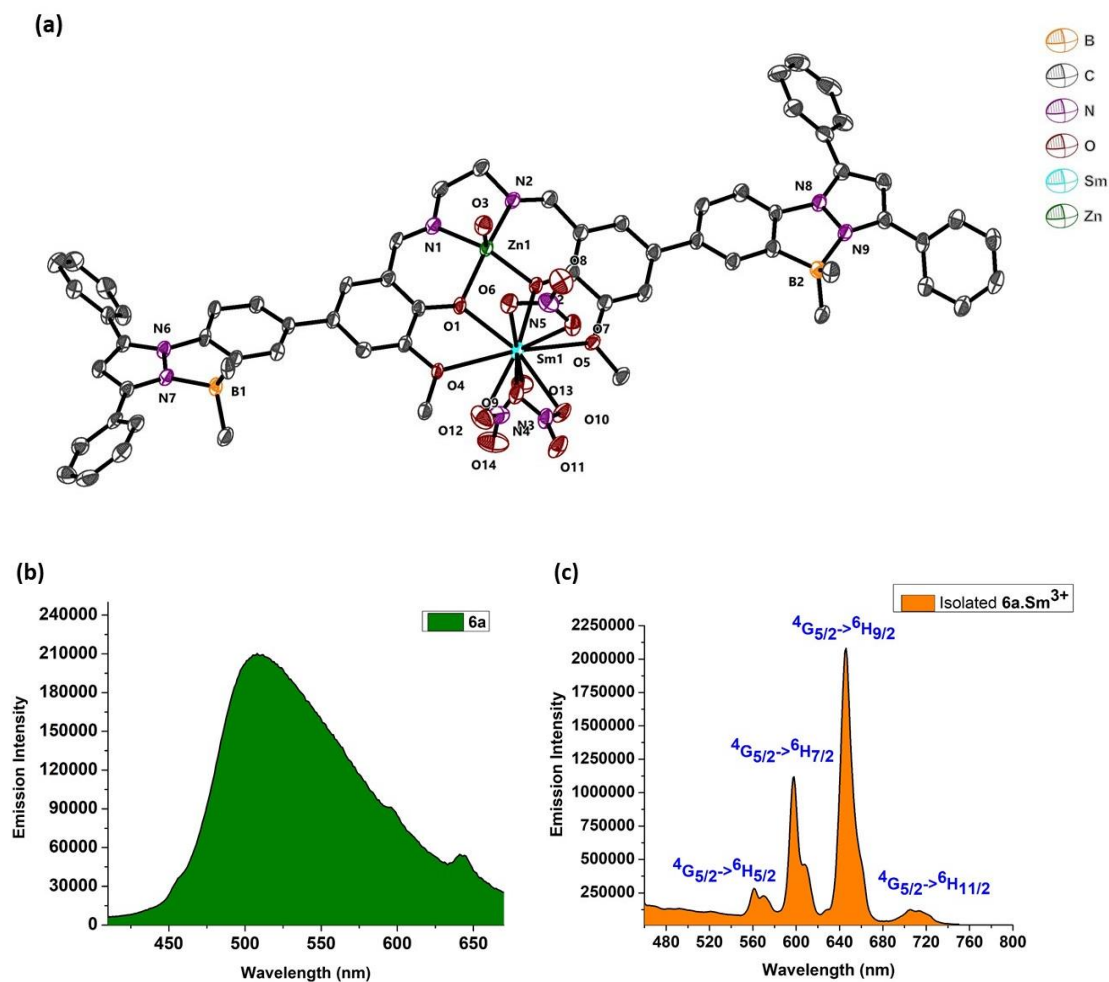
Figure 2.7: (a) Crystal Structure of complex **6a**. Thermal ellipsoids are drawn at 50% probability level. Hydrogen atoms and water molecules are removed for clarity. Solid state emission spectra of complex (b) **6a** and (c) **6a.Sm^{3+}**

Table 2.3: Crystal data and structure refinement for complex **6a** and compounds **6a.Sm^{3+}**

Identification code	Complex **6a**	Complex **6a.Sm^{3+}**
Empirical formula	$C_{70}H_{72}B_2N_8O_7Zn$	$C_{64}H_{70}B_2N_9O_{20}SmZn$
Formula weight	1224.34	1522.63
Temperature/K	100.0	100.00(10)
Crystal system	triclinic	monoclinic

Space group	P-1	P2$_1$/c
a/Å	11.8935(3)	24.2907(6)
b/Å	13.7058(3)	12.6115(4)
c/Å	23.2005(5)	22.4062(7)
α/°	79.5340(10)	90
β/°	76.7020(10)	92.615(2)
γ/°	77.6310(10)	90
Volume/Å^3	3560.05(14)	6856.8(3)
Z	2	4
ρ$_{calc}$g/cm^3	1.142	1.475
μ/mm^{-1}	0.912	1.276
F(000)	1288.0	3116.0
Crystal size/mm^3	0.28 × 0.25 × 0.23	0.19 × 0.17 × 0.15
Radiation	CuKα (λ = 1.54178)	MoKα (λ = 0.71073)
2Θ range for data collection/°	6.668 to 136.61	6.626 to 49.998
Index ranges	-14 ≤ h ≤ 14, -16 ≤ k ≤ 16, -27 ≤ l ≤ 27	-28 ≤ h ≤ 26, -13 ≤ k ≤ 14, -26 ≤ l ≤ 26
Reflections collected	118979	41152
Independent reflections	13012 [R$_{int}$ = 0.0674, R$_{sigma}$ = 0.0335]	11843 [R$_{int}$ = 0.0513, R$_{sigma}$ = 0.0480]
Data/restraints/parameters	13012/0/824	11843/0/899
Goodness-of-fit on F^2	1.046	1.073

To know the solid state emission properties of the **6a.Sm^{3+}** complex, we excited the complex at 350 nm. The solid state emission of **6a.Sm^{3+}** shows well resolved peaks at 562 nm, 598 nm, 646 nm and 712 nm which corresponds to the transitions, $^4G_{5/2} \rightarrow {}^6H_{5/2}$, $^4G_{5/2} \rightarrow {}^6H_{7/2}$, $^4G_{5/2} \rightarrow {}^6H_{9/2}$ and $^4G_{5/2} \rightarrow {}^6H_{11/2}$ respectively. Among the emission peaks, the most intense emission at 645 nm corresponds to the $^4G_{5/2} \rightarrow {}^6H_{9/2}$ transition (Fig 2.7). The complex **6a** showed green emission whereas **6a.Sm^{3+}** shows red emission in solid state (Fig 2.7).
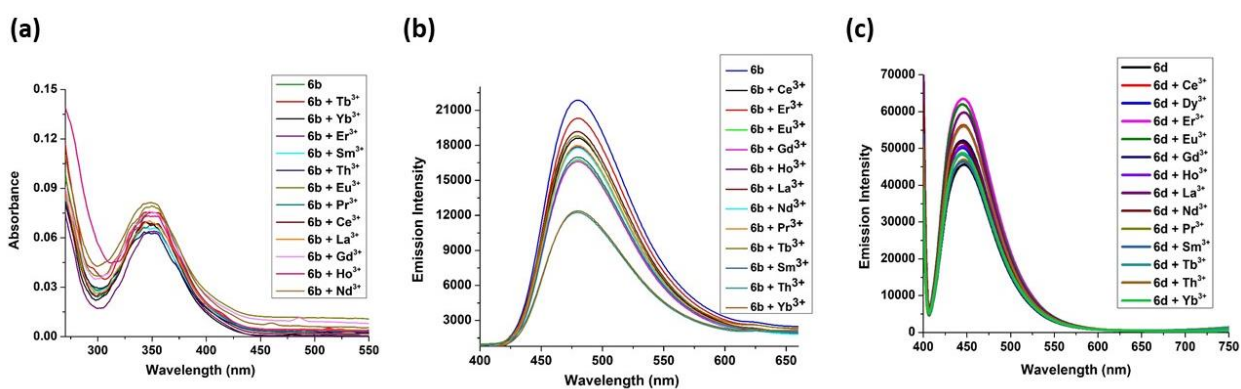
Figure 2.8: (a) Absorbance and (b) Fluorescence Spectra of **6b** (1 x 10^{-5} M) upon the addition of different lanthanide ions (1.2 equiv) excitation wavelength, 350 nm in (10:90) Methanol/THF (c) Fluorescence Spectra of **6d** (1 x 10^{-5} M) upon the addition of different lanthanide ions (1.2 equiv) excitation wavelength, 350 nm in (10:90) Methanol/THF

The –OMe functionality plays an important role in forming the complex with Sm^{3+} ion. To test our hypothesis, we made compound **6b** (Scheme 2) which does not have any –OMe functionality. As expected, the emission of compound **6b** did not alter upon addition of Sm^{3+} ion (Fig 2.8). To investigate the importance of boron coordination, we synthesized complex **6c** (Scheme 2.3) which does not have boron on the framework, and characterized it using ^{1}H and ^{13}C spectroscopy. Complex **6c** showed a blue-shifted absorption and emission with respect to **6a** (Fig 2.9). This signifies that boron

coordination increases the rigidity of the pyrazole moiety which resulted in slightly higher quantum yield and higher emission intensity for **6a** with respect to **6c** (Table 2.4).

Table 2.4: Photophysical data of complexes **6a** and **6c**

	Complex	**λ_{max} (nm)**	**λ_{ems} (nm)**	**ε (mol^{-1} L cm^{-1})**	**ΔE (cm^{-1}) Stokes Shift**	**ϕ^a**
THF	**6a**	344	527	48670	10094	3.68
	6c	334	500	48346	9940	3.19

^{a} relative quantum yield
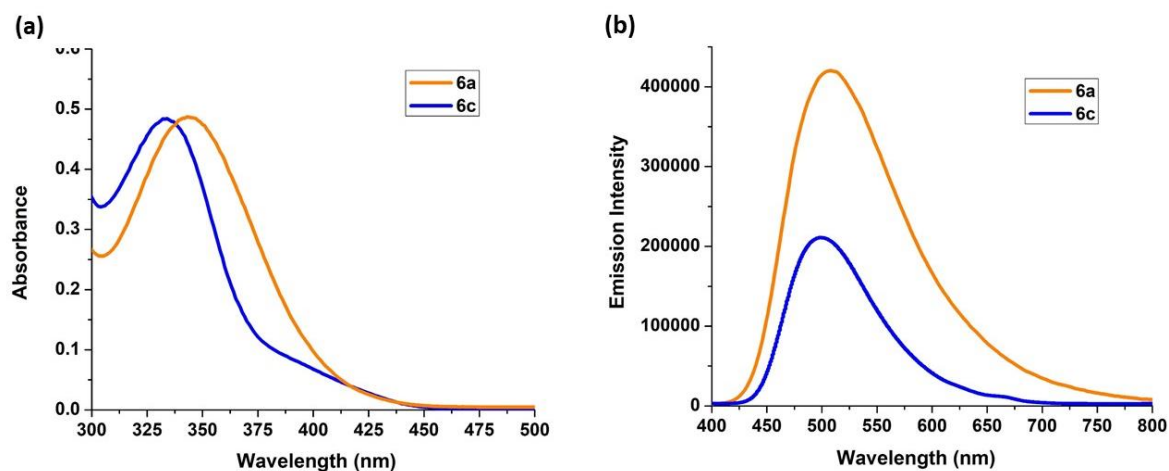
Figure 2.9: (a) Absorbance and (b) emission spectra of complexes **6a** and **6c** at 1 x 10^{-5} M concentration in THF
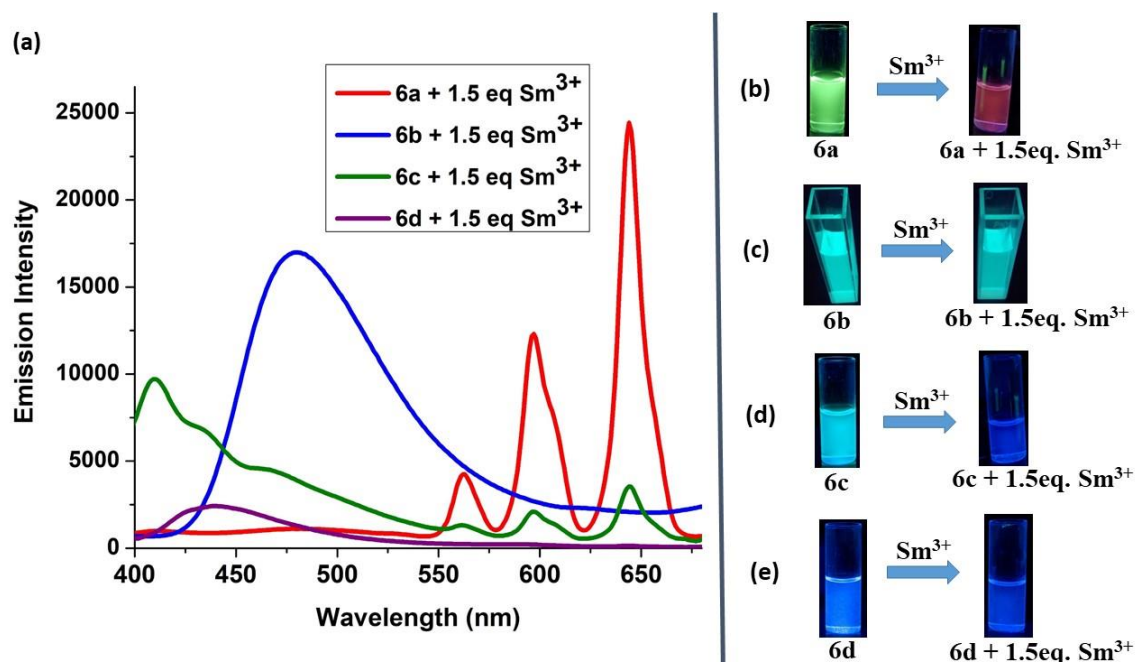
Figure 2.10: (a) Fluorescence spectra of **6a-6d** with 1.5 equiv of Sm^{3+} ion in (10:90) Methanol/THF Concentration = 1 x 10^{-5} M. (b-e) Color change under a UV lamp of **6a** and **6a** + 1.5 eq Sm^{3+}; **6b** and **6b** + 1.5 eq Sm^{3+}; **6c** and **6c** + 1.5 eq Sm^{3+}; **6d** and **6d** + 1.5 eq Sm^{3+} at 1 x 10^{-5} M concentration ion in (10:90) Methanol/THF.

When 1.5 equivalent of Sm^{3+} was added to **6c** (1 x 10^{-5} M), we observed very less intense Sm^{3+} characteristic peaks in the emission spectrum and some residual emission from **6c** (Fig 2.10). When the solution was kept under hand held UV-lamp, no red emission was observed unlike complex **6a** (Fig 2.10). When 1.5 eq. of Sm^{3+} was added to **6a**, we observed intense Sm^{3+} characteristic peaks in emission spectrum with no residual emission from **6a** and intense red emission under hand held UV-lamp (Fig 2.10). We believe that non-radiative decay due to lack of rigidity in complex **6c** resulted in less intense red emission with respect to **6a**. The lack of rigidity in **6c** also resulted in inefficient energy transfer from tri-phenyl pyrazole moiety to Sm^{3+} center and thus caused relatively less intense red emission.
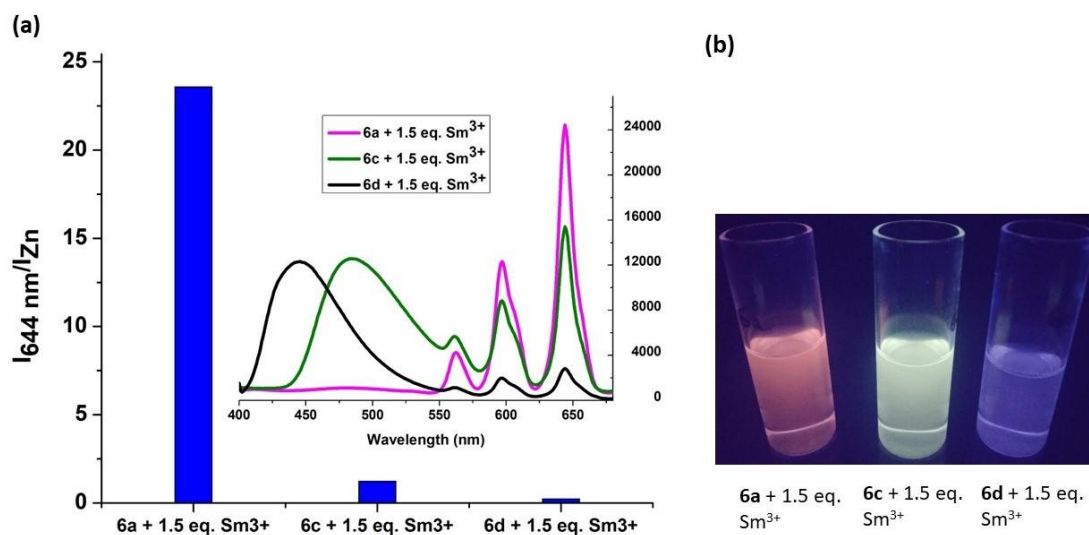
Figure 2.11: (a) Comparing the energy transfer process in **6a**, **6c**, and **6d** with addition of 1.5 eq. of Sm^{3+} at 5 x 10^{-5} M concentration ion in (10:90) Methanol/THF. (b) Comparison of **6a**, **6c** and **6d** with 1.5 eq. Sm^{3+} at 5 x 10^{-5} M concentration under hand held UV-lamp

Dong and co-workers[6h] reported a bimetallic Zn-Sm complex derived from a Salamo-type ligand and also observed selective sensitization of the Sm^{3+} ions. Although structural characterization and emission for Zn(II)-Sm(III) complex was presented, there is no discussion about the concentration of the solution used for this study. We synthesized compound **6d** which is analogues to Dong and co-workers complex and analyzed its potential to test Sm^{3+} under identical conditions that we used in our study. Use of **6d** as a probe did not show any emission color change (conc. 1 x 10^{-5} M), when 1.5 eq. of Sm^{3+} was added to the THF/Methanol solution of **6d** (Fig 2.10). At the same time, **6a** made it possible to detect Sm^{3+} at 1 x 10^{-5} M concentration. In order to compare the energy transfer in **6a**, **6c** and **6d**, we increased the concentration from 1 x 10^{-5} M to 5 x 10^{-5} M and plotted I_{644nm}/I_{Zn} (I_{Zn}=emission maximum of the respective zinc complex) for all complexes with the addition of 1.5 eq. Sm^{3+} ion. It was observed that I_{644nm}/I_{Zn} ratio for

6a + 1.5 eq. Sm^{3+} is almost 100 times higher than **6d** and 20 times higher than **6c** at the same concentration. The inset emission spectrum, shown in figure 2.11 reveals the presence of residual emission from **6c** at 484 nm and **6d** at 444 nm. This residual emission from **6c** and **6d** mask the red emission from Sm^{3+} which can be observed under hand held UV-Lamp (Fig 2.11). From these studies we conclude that our design has the advantage to discriminate the Sm^{3+} ion at a very low concentration.

2.3 Conclusion

To conclude, we have successfully synthesized a tetracoordinated boron based salen ligand which exhibits excellent selectivity for the detection of Zn^{2+} ion using pocket 1. Furthermore, the zinc complex **6a**, showed remarkable luminescence response at a very low concentration upon the addition of Sm^{3+} ions and discriminates it from other lanthanoid ions. X-rays crystallography and other studies reveal that pocket 2 is responsible for the selective binding and sensitization of Sm^{3+} ion *via* a cooperative use of B-N coordinated pyrazole motif and the –OMe functionality. The sensitivity of **6a** was found to be 100 fold than that of **6d**. The design described here will be an excellent lead for further development of ligands for selective discrimination of metal ions.

2.4 Experimental section:

2.4.1 General information:

All reagents were used as received from Spectrochem, Alfa-aesar and Sigma-Aldrich unless otherwise noted. Dichloromethane and toluene were dried using calcium hydride and Na/benzophenone respectively. The substrates and complexes were characterized by

multinuclear NMR data. All ^{1}H (400 MHz), ^{13}C (100 MHz), and ^{11}B (128 MHz) NMR were recorded at room temperature on Bruker ARX 400 MHz spectrometer. Residual protonated solvents were used as internal standards for ^{1}H and ^{13}C NMR. ^{11}B NMR spectra were referenced externally to $BF_3 \cdot Et_2O$ in $CDCl_3$ ($\delta = 0$ ppm). ESI mass spectra were recorded with Bruker micro TOF-QII mass spectrometer. MALDI was recorded on Bruker UltrafleXtreme MALDI TOF/TOF analyzer equipped with a nitrogen UV laser. Matrix and target mixed solution (v/v: 1/1) was dropped onto the MALDI plate and analyzed in positive ion reflection mode with the mass range of m/z 400–2500 Da. Each point was collected using 1000 laser shots and results were analyzed by Bruker flexAnalysis software. Elemental analyses of the compounds were performed using a Euro Vector EA instrument (CHNS-O, model EuroEA3000). Rigaku Oxford X-ray diffractometer having Cu-Kα radiation (1.54184 Å) and Mo-Kα radiation (0.71073 Å) was used for collecting single crystal X-ray diffraction data. SADABS absorption corrections were applied. Olex were used for structure solving and refinement. Anisotropic refinements were used for non-hydrogen atoms. The H atoms were placed at calculated positions and were refined as riding atoms (CCDC no. 2152949-2152950). UV-Visible spectra were recorded on JASCO V-730 UV/Visible spectrometer. The fluorescence spectra were recorded with a Edinburgh Instruments FS5 Spectrofluorometer. DFT calculations were performed with the Gaussian 16 program.[14] The structures were optimized using B3LYP with LANL2DZ basis set for Zn and 6-31G basis set for other atoms. Frequency calculations confirmed the optimized structures to be local minimum structures. Excitation data were determined using TD-DFT (CAM-B3LYP/631g)–calculations. Compound **6d**, synthesized following the literature reported method.[15]

Synthesis of compound 4a:
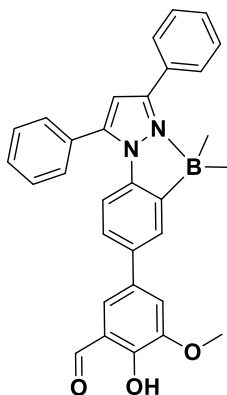
To an oven dried two neck 250 mL RB, compound **2a** (2.41 mmol, 1.00 g, 1.0 equiv.), compound **3a**, (2.65 mmol, 0.737 g, 1.1 equiv.), Na_2CO_3 (7.23 mmol, 0.765 g, 3.0 equiv.) and $Pd(PPh_3)_4$ (0.072 mmol, 0.083 g, 3 mol%) were loaded under nitrogen atmosphere. To this mixture, degassed THF (40 mL) and water (10 mL) in 4:1 ratio was added and the reaction mixture was refluxed for 24 h. The progress of the reaction was monitored through TLC. After completion of the reaction, the whole mixture is cooled to room temperature. Dichloromethane (50 mL) and water (50 mL) were added to the reaction mixture; organic layer was separated and the aqueous layer was extracted using CH_2Cl_2 (3x20 mL). The combined organic layer was washed with brine, dried over Na_2SO_4 and concentrated under reduced pressure. The crude product was purified by column chromatography (1:20 of EtOAc : *n*-hexane) on silica gel to afford the corresponding coupled product **4a.** Yield: 61% (0.715 g). ^{1}H NMR (400 MHz, CDCl$_3$) δ 11.00 (s, 1H), 9.97 (s, 1H), 7.87 – 7.77 (m, 2H), 7.70 – 7.65 (m, 2H), 7.64 – 7.56 (m, 4H), 7.55 – 7.46 (m, 3H), 7.38 (s, 1H), 7.34 (s, 1H), 7.12 (d, *J* = 8.6 Hz, 1H), 6.82 (d, *J* = 8.0 Hz, 1H), 6.61 (s, 1H), 3.98 (s, 3H), 0.15 (s, 6H). ^{13}C NMR (101 MHz, CDCl$_3$) δ 196.9, 150.9, 148.8, 148.6, 140.2, 138.0, 138.0, 133.8, 130.5, 129.8, 129.7, 129.6, 129.2, 129.1, 128.7, 128.5, 127.9, 123.7, 122.9, 120.9, 117.3, 112.2, 110.9, 56.6, 9.3. ^{11}B NMR (128 MHz, CDCl$_3$) δ -1.95. HRMS (ESI+, m/z) calcd for $C_{31}H_{27}BN_2O_3Na$, [M+Na]$^+$ m/z = 509.2012, found 509.1989.

Synthesis of compound 5a:
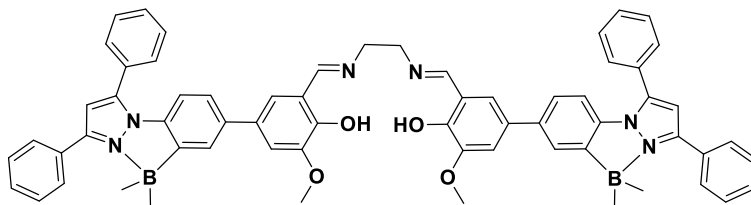
To 100 mL one neck RB, compound **4a** (1.0 mmol, 0.50 g, 2.0 equiv.) and ethylene diamine (0.51 mmol, 34 μL, 1.0 equiv.) were added to dry methanol and refluxed overnight. The reaction mixture was filtered and the resultant yellow precipitate of compound **5a** was collected. Yield: 92% (0.467 g) ^{1}H NMR (400 MHz, DMSO-d_6) δ 13.61 (s, 2H), 8.65 (s, 2H), 7.93 – 7.86 (m, 4H), 7.82 – 7.73 (m, 4H), 7.71 – 7.65 (m, 6H), 7.62 – 7.53 (m, 8H), 7.29 (d, J = 2.2 Hz, 2H), 7.26 (d, J = 2.1 Hz, 2H), 7.24 (d, J = 1.86 Hz, 2H), 7.20 (d, J = 2.1 Hz, 2H), 7.13 (s, 2H), 6.70 (d, J = 8.0 Hz, 2H), 3.94 (s, 4H), 3.81 (s, 6H), 0.08 (s, 12H). ^{13}C NMR (101 MHz, DMSO-d_6) δ 9.7, 55.7, 58.1, 111.3, 111.5, 113.1, 118.1, 121.0, 123.4, 126.7, 128.0, 128.6, 128.6, 128.9, 129.2, 129.7, 129.9, 130.6, 136.8, 137.9, 140.1, 148.0, 148.4, 151.6, 167.4. ^{11}B NMR (128 MHz, DMSO-d_6) δ 0.45. HRMS (ESI+, m/z) calcd for $C_{64}H_{59}B_2N_6O_4$, $[M+H]^+$ m/z = 997.4736, found 997.4716.

Synthesis of complex 6a:
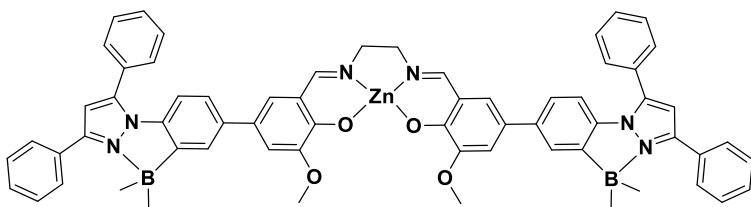
To 100 mL one neck RB, compound **5a** (0.200 g, 0.2 mmol, 1.0 equiv.) was dissolved in 10 mL of CH$_2$Cl$_2$ and a solution of Zn(OAc)$_2$.2H$_2$O (0.049 g, 0.22 mmol, 1.1 equiv.) in 10 mL dry methanol was added dropwise. The greenish-yellow solution was refluxed for 12 h. Light green color crystals of complex **6a** with a coordinated solvent molecule were collected

after 1 week. Yield: 73% (155 mg) ^{1}H NMR (400 MHz, DMSO-d_6) δ 8.56 (s, 2H), 7.93 –

7.88 (m, 4H), 7.82 – 7.75 (m, 4H), 7.71 – 7.66 (m, 6H), 7.62 – 7.53 (m, 8H), 7.24 (d, J =

8.0 Hz, 2H), 7.15 – 7.11 (m, 4H), 7.06 (s, 2H), 6.70 (d, J = 8.5 Hz, 2H), 3.80 (s, 6H),

3.75 (s, 4H), 1.80 (s, 6H), 0.09 (s, 12H). ^{13}C NMR (101 MHz, DMSO-d_6) δ 176.7, 168.5,

155.5, 152.7, 147.8, 139.9, 138.9, 136.0, 130.5, 129.7, 129.2, 129.0, 128.6, 128.1, 125.9,

123.9, 123.3, 122.5, 118.4, 111.5, 111.1, 55.9, 55.2, 22.4, 9.8. ^{11}B NMR (128 MHz,

DMSO-d_6) δ -3.12. MALDI-MS calcd for $C_{64}H_{60}B_2N_6O_5Zn$, $[M+H_2O+2H]^{2+}$ m/z =

1080.2, found 1080.3. Anal. Calcd for $C_{64}H_{58}B_2N_6O_5Zn$: C, 71.29; H, 5.42; N, 7.79.

Found: C, 71.00; H, 5.05; N, 8.21.

Synthesis of compound 4b:
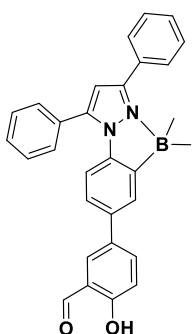
To an oven dried two neck 250 mL RB, compound **2a** (2.41 mmol, 1.00

g, 1.0 equiv.), compound **3b**, (2.65 mmol, 0.659 g, 1.1 equiv.), Na_2CO_3

(7.23 mmol, 0.766 g, 3.0 equiv.) and Pd(PPh$_3$)$_4$ (0.072 mmol, 0.083 g, 3

mol%) were loaded under nitrogen atmosphere. To this mixture,

degassed THF (40 mL) and water (10 mL) in 4:1 ratio was added and

the reaction mixture was refluxed for 24 h. The progress of the reaction was monitored

through TLC. After completion of the reaction, the whole mixture is cooled to room

temperature. Dichloromethane (50 mL) and water (50 mL) were added to the reaction

mixture; organic layer was separated and the aqueous layer was extracted using CH_2Cl_2

(3x20 mL). The combined organic layer was washed with brine, dried over Na_2SO_4 and

concentrated under reduced pressure. The crude product was purified by column

chromatography (1:20 of EtOAc : *n*-hexane) on silica gel to afford the corresponding

coupled product **4b.** Yield: 58% (0.637 g). ^{1}H NMR (400 MHz, CDCl$_3$) δ 10.99 (s, 1H),

9.96 (s, 1H), 7.85 – 7.80 (m, 2H), 7.79 – 7.75 (m, 2H), 7.70 -7.64 (m, 2H), 7.65 – 7.58 (m, 4H), 7.54 -7.48 (m, 3H), 7.12 (dd, J = 8.4, 1.6 Hz, 1H), 7.08 – 7.02 (m, 1H), 6.83 (d, J = 8.4 Hz, 1H), 6.61 (s, 1H), 0.15 (s, 3H). ^{13}C NMR (101 MHz, CDCl$_3$) δ 196.9, 160.9, 148.8, 140.1, 137.9, 137.6, 135.9, 133.8, 131.9, 130.5, 129.8, 129.7, 129.6, 129.2, 129.1, 128.7, 128.5, 127.8, 123.5, 120.8, 118.1, 112.2, 110.9, 9.3. ^{11}B NMR (128 MHz, CDCl$_3$) δ 0.54. HRMS (ESI+, m/z) calcd for C$_{30}$H$_{26}$BN$_2$O$_2$, [M+H]$^+$ m/z = 457.2045, found 457.2073

Synthesis of compound 5b:
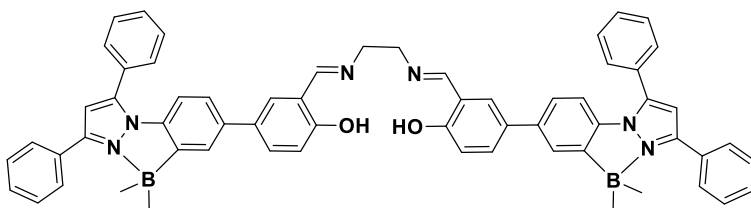
To 100 mL one neck RB, compound **4b** (1.0 mmol, 0.50 g, 2.0 equiv.) and ethylene diamine (0.51 mmol, 34 μL, 1.0 equiv.) were added to dry methanol and refluxed overnight. The reaction mixture was filtered and the resultant yellow precipitate of compound **5b** was collected. Yield: 88% (0.421 g) ^{1}H NMR (400 MHz, DMSO-d_6) δ 13.45 (s, 2H), 8.69 (s, 2H), 7.89 (d, J = 7.2 Hz, 4H), 7.81 – 7.72 (m, 6H), 7.71 – 7.63 (m, 7H), 7.62 – 7.47 (m, 11H), 7.22 (d, J = 7.4 Hz, 2H), 7.14 (s, 2H), 6.91 (d, J = 8.0 Hz, 2H), 6.72 (d, J = 8.0 Hz, 2H), 3.95 (s, 4H), 0.08 (s, 12H). ^{13}C NMR (101 MHz, DMSO-D_6) δ 167.2, 160.2, 148.0, 140.2, 137.6, 136.9, 130.7, 129.7, 129.2, 128.9, 128.6, 128.6, 128.0, 126.7, 123.2, 118.7, 117.1, 111.7, 111.4, 58.8, 9.8. ^{11}B NMR (128 MHz, DMSO-d_6) δ 0.84. HRMS (ESI+, m/z) calcd for C$_{62}$H$_{55}$B$_2$N$_6$O$_2$, [M+H]$^+$ m/z = 937.4586, found 937.4457

Synthesis of complex 6b
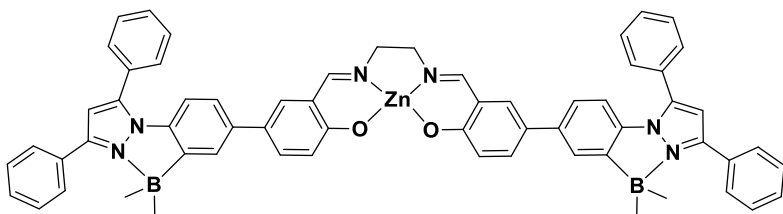
To 100 mL one neck RB, compound **5b** (0.187 g, 0.20 mmol, 1.0 equiv.) was dissolved in 10 mL of CH$_2$Cl$_2$ and a solution of Zn(OAc)$_2$.2H$_2$O (0.049 g, 0.22 mmol, 1.1 equiv.) in 10 mL dry methanol was added dropwise. The greenish-yellow solution was refluxed for 12 h. Light green color precipitate of complex **6b** was collected after the reaction. Yield: 78% (156 mg) ^{1}H NMR (400 MHz, DMSO-d_6) δ 8.56 (s, 2H), 7.91 – 7.86 (m, 4H), 7.79 – 7.75 (m, 4H), 7.70 – 7.64 (m, 6H), 7.61 – 7.49 (m, 10H), 7.46 (d, J = 8 Hz, 2H), 7.19 (dd, J = 8.0, 1.8 Hz, 2 Hz), 7.10 (s, 2H), 6.70 (d, 8.0 Hz, 2 Hz), 6.68 (d, 8.0 Hz, 2 Hz), 3.71 (s, 4H), 0.08 (s, 12 H). ^{13}C NMR (101 MHz, DMSO-d_6) δ 171.1, 168.7, 156.3, 148.3, 140.2, 139.0, 136.6, 133.0, 131.7, 130.9, 130.0, 129.6, 129.5, 129.1, 128.9, 128.6, 126.4, 125.0, 123.9, 122.6, 119.7, 112.1, 111.5, 56.4, 10.2. ^{11}B NMR (128 MHz, DMSO-d_6) δ -2.86. MALDI-MS calcd for C$_{64}$H$_{59}$B$_2$N$_6$O$_3$SZn, [M+(CH$_3$)$_2$SO+H]$^+$ m/z = 1079.2, found 1079.2. Anal. Calcd for C$_{62}$H$_{52}$B$_2$N$_6$O$_2$Zn: C, 74.46; H, 5.24; N, 8.40. Found: C, 74.76; H, 4.77; N, 8.68.

Synthesis of compound 4c:

To an oven dried two neck 250 mL RB, compound **2b** (2.66 mmol, 1.00 g, 1.0 equiv.), compound **3a**, (2.93 mmol, 0.815 g, 1.1 equiv.), Na$_2$CO$_3$ (7.98 mmol, 0.845 g, 3.0 equiv.) and Pd(PPh$_3$)$_4$ (0.0798 mmol, 0.092 g, 3.00 mol%) were loaded under nitrogen atmosphere. To this mixture, degassed THF (40 mL) and water (10 mL) in 3:1 ratio was added and the reaction mixture was refluxed for 24 h. The progress of the reaction was

monitored through TLC. After completion of the reaction, the whole mixture is cooled to room temperature. Dichloromethane (50 mL) and water (50 mL) were added to the reaction mixture; organic layer was separated and the aqueous layer was extracted using CH_2Cl_2 (3x20 mL). The combined organic layer was washed with brine, dried over Na_2SO_4 and concentrated under reduced pressure. The crude product was purified by column chromatography (1:20 of EtOAc: *n*-hexane) on silica gel to afford the corresponding coupled product **4c.** Yield: 69% (0.819 g) ^{1}H NMR (400 MHz, CDCl$_3$) δ 11.09 (s, 1H), 9.99 (s, 1H), 7.96 (d, *J* = 8.0 Hz, 2H), 7.55 (d, *J* = 8.0 Hz, 2H), 7.51 – 7.43 (m, 4H), 7.41 – 7.30 (m, 8H), 6.86 (s, 1H), 4.00 (s, 3H). ^{13}C NMR (101 MHz, CDCl$_3$) δ 196.7, 152.2, 151.4, 148.8, 144.6, 139.4, 138.7, 132.8, 132.2, 130.6, 128.9, 128.8, 128.8, 128.7, 128.6, 128.3, 127.2, 125.9, 125.7, 122.7, 120.9, 116.8, 105.7, 56.6. HRMS (ESI+, m/z) calcd for $C_{29}H_{23}N_2O_3$, [M+H]$^+$ m/z = 447.1703, found 447.1729.

Synthesis of compound 5c:
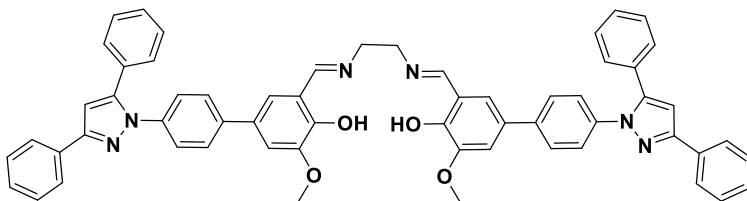
To 100 mL one neck RB, compound **4c** (1.11 mmol, 0.50 g, 2.0 equiv.) and ethylene diamine (0.56 mmol, 37 μL, 1.0 equiv.) were added to dry methanol and refluxed overnight. The reaction mixture was filtered and the resultant orange precipitate of compound **5c** was collected. Yield: 88% (0.447 g) ^{1}H NMR (400 MHz, DMSO-*d$_6$*) δ 13.75 (s, 2H), 8.65 (s, 2H), 7.94 (d, *J* = 8 Hz, 4H), 7.72 (d, *J* = 8.0 Hz, 4H), 7.47 (t, *J* = 8.0 Hz, 4H), 7.42 – 7.28 (m, 20H), 7.18 (s, 2H), 3.98 (s, 4H), 3.85 (s, 6H). ^{13}C NMR (101 MHz, DMSO-*d$_6$*) δ 166.9, 152.1, 151.2, 148.5, 144.3, 138.7, 138.3, 128.4, 128.4, 127.8,

126.4, 125.3, 125.1, 121.2, 112.6, 105.2, 58.7, 55.7. HRMS (ESI+, m/z) calcd for $C_{60}H_{49}N_6O_4$, $[M+H]^+$ m/z = 917.3815, found 917.3878.

Synthesis of complex 6c:
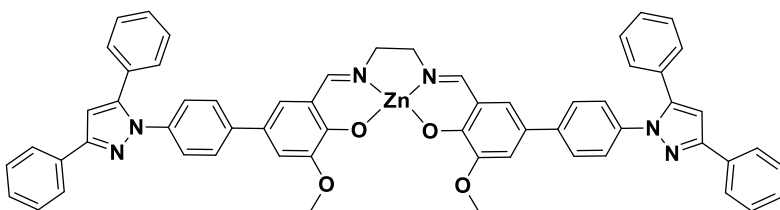
To 100 mL one neck RB, compound **5c** (0.200 g, 0.22 mmol, 1.0 equiv.) was dissolved in 10 mL of CH_2Cl_2 and a solution of $Zn(OAc)_2.2H_2O$ (0.053 g, 0.24 mmol, 1.1 equiv.) in 10 mL methanol was added dropwise. The greenish-yellow solution was refluxed for 12 h. Light green powder was collected and washed with methanol multiple times before drying the remaining solvent completely. Yield: 71% (153 mg) ^{1}H NMR (400 MHz, DMSO) δ 8.65 (s, 2H), 7.94 (d, J = 8.0 Hz, 4H), 7.70 (d, J = 8.2 Hz, 4H), 7.47 (t, J = 8.0 Hz, 5H), 7.43 – 7.32 (m, 14H), 7.24 (s, 2H), 7.18 (s, 4H), 3.84 (s, 6H), 3.77 (s, 4H). ^{13}C NMR (101 MHz, DMSO) δ 168.3, 162.1, 152.9, 150.9, 144.1, 139.8, 137.4, 132.7, 130.1, 128.8, 128.7, 128.6, 128.1, 125.6, 125.5, 125.4, 121.6, 118.4, 111.1, 105.3, 56.1, 55.3. MALDI-MS Calcd for $C_{60}H_{49}N_6O_5Zn$, $[M+H_3O]^+$ m/z = 999.4, found 999.4. Anal. Calcd for $C_{60}H_{46}N_6O_4Zn$: C, 73.50; H, 4.73; N, 8.57. Found: C, 73.34; H, 4.93; N, 8.39

Synthesis of complex 6a.Sm³⁺:
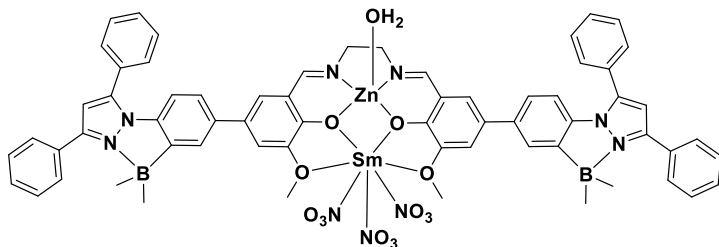
To 50 mL one neck RB, complex **6a** (0.05 g, 0.046 mmol, 1.0 equiv.) was dissolved in 5 mL of $CHCl_3$

and a solution of $Sm(NO_3)_3.6H_2O$ (0.031 g, 0.069 mmol, 1.5 equiv.) in 5 mL dry ethanol was added dropwise. The green solution was stirred for 6 h at room temperature. The solution was kept undisturbed for few days. Light green crystals of **6a.Sm^{3+}** were collected after one week. Yield: 53% (0.034 g). Anal. Calcd for $C_{64}H_{58}B_2N_9O_{14}SmZn$: C, 54.34; H, 4.13; N, 8.91. Found: C, 54.06; H, 4.18; N, 8.91

2.5 References:

1. (a) F. Jäkle, *Chem. Rev.* **2010**, *110*, 3965-4022; *(b)* Y.-L. Rao, H. Amarne, S. Wang, *Coord. Chem. Rev.* **2012**, *256*, 759-770; *(c)* D. Li, H. Zhang, Y. Wang, *Chem. Soc. Rev.* **2013**, *42*, 8416-8433; *(d)* Z. M. Hudson, S. Wang, *Acc. Chem. Res.* **2009**, *42*, 1584-1596 *(e)* D. Frath, J. Massue, G. Ulrich, R. Ziessel, *Angew. Chem. Int. Ed.* **2014**, *53*, 2290-2310; *(f)* K. Tanaka, Y. Chujo, *NPG Asia Mater.* **2015**, *7*, e223-e223; *(g)* P.-Z. Chen, L.-Y. Niu, Y.-Z. Chen, Q.-Z. Yang, *Coord. Chem. Rev.* **2017**, *350*, 196-216; *(h)* L. Ji, S. Griesbeck, T. B. Marder, *Chem. Sci.* **2017**, *8*, 846-863; *(i)* E. von Grotthuss, A. John, T. Kaese, M. Wagner, *Asian. J. Org. Chem.* **2018**, *7*, 37-53; *(j)* T. W. Hudnall, C.-W. Chiu, F. P. Gabbaï, *Acc. Chem. Res.* **2009**, *42*, 388–397; *(k)* J. F. Araneda, W. E. Piers, B. Heyne, M. Parvez, R. McDonald, *Angew. Chem., Int. Ed.*, **2011**, *50*, 12214–12217; *(l)* X. Su, T. A. Bartholome, J. R. Tidwell, A. Pujol, S. Yruegas, J. J. Martinez, C. D. Martin, *Chem. Rev.*, **2021**, *121*, 4147-4192; *(m)* R. R. Maar, R. Zhang, D. G. Stephens, Z. Ding, J. B. Gilroy, *Angew. Chem., Int. Ed.*, **2019**, *58*, 1052-1056; (n) R. Zhao, C. Dou, Z. Xie, J. Liu, L. Wang, *Angew. Chem., Int. Ed.*, 2016, **55**,

5313-5317 (o) S. Sa, A. C. Murali, P. Nayak, K. Venkatasubbaiah, *Chem. Commun.*, **2021**, *57*, 10170-10173.

2. *(a)* A. Wakamiya, T. Taniguchi, S. Yamaguchi, *Angew. Chem. Int. Ed.* **2006**, *45*, 3170-3173; (*b*) D. L. Crossley, I. A. Cade, E. R. Clark, A. Escande, M. J. Humphries, S. M. King, I. Vitorica-Yrezabal, M. J. Ingleson, M. L. Turner, *Chem. Sci.* **2015**, *6*, 5144-5151; *(c)* M. Grandl, T. Kaese, A. Krautsieder, Y. Sun, F. Pammer, *Chem. Eur. J.* **2016**, *22*, 14373-14382; *(d)* S. K. Mellerup, K. Yuan, C. Nguyen, Z. H. Lu, S. Wang, *Chem. Eur. J.* **2016**, *22*, 12464-12472; *(e)* M. Yusuf, K. Liu, F. Guo, R. A. Lalancette, F. Jäkle, *Dalton. Trans.* **2016**, *45*, 4580-4587; *(f)* D. L. Crossley, R. Goh, J. Cid, I. Vitorica-Yrezabal, M. L. Turner, M. J. Ingleson, *Organometallics* **2017**, *36*, 2597-2604; *(g)* K. Liu, R. A. Lalancette, F. Jäkle, *J. Am. Chem. Soc.* **2017**, *139*, 18170-18173; *(h)* S. Schraff, Y. Sun, F. Pammer, *J. Mater. Chem. C* **2017**, *5*, 1730-1741; *(i)* J. Wang, B. Jin, N. Wang, T. Peng, X. Li, Y. Luo, S. Wang, *Macromolecules* **2017**, *50*, 4629-4638; *(j)* M. Mamada, G. Tian, H. Nakanotani, J. Su, C. Adachi, *Angew. Chem. Int. Ed.* **2018**, *57*, 12380-12384; *(k)* S. Wang, K. Yuan, M. F. Hu, X. Wang, T. Peng, N. Wang, Q. S. Li, *Angew. Chem. Int. Ed.* **2018**, *57*, 1073-1077; *(l)* B. P. Dash, I. Hamilton, D. J. Tate, D. L. Crossley, J.-S. Kim, M. J. Ingleson, M. L. Turner, *J. Mater. Chem. C* **2019**, *7*, 718-724; *(m)* Y. Li, H. Meng, T. Liu, Y. Xiao, Z. Tang, B. Pang, Y. Li, Y. Xiang, G. Zhang, X. Lu, G. Yu, H. Yan, C. Zhan, J. Huang, J. Yao, *Adv. Mater.* **2019**, *31*, e1904585; *(n)* K. Liu, R. A. Lalancette, F. Jäkle, *J. Am. Chem. Soc.* **2019**, *141*, 7453-7462; *(o)* J. Full, S. P. Panchal, J. Gotz, A. M. Krause, A. Nowak-Krol, *Angew. Chem. Int. Ed.* **2021**, *60*, 4350-4357. *(p)* A. C. Murali, P. Nayak, K. Venkatasubbaiah, *Dalton. Trans.* **2022***, 51*, 5751-5771; *(q)* Z. Dominguez, R.

Lopez-Rodriguez, E. Alvarez, S. Abbate, G. Longhi, U. Pischel, A. Ros, *Chem. Eur. J.* **2018**, *24*, 12660-12668;

3. *(a)* C. Li, S. K. Mellerup, X. Wang, S. Wang, *Organometallics* **2018**, *37*, 3360-3367; *(b)* S. K. Mellerup, C. Li, X. Wang, S. Wang, *J. Org. Chem.* **2018**, *83*, 11970-11977; *(c)* X. Li, Y. Shi, N. Wang, T. Peng, S. Wang, *Chem. Eur. J.* **2019**, *25*, 5757-5767; *(d)* Z. He, L. Liu, Z. Zhao, S. K. Mellerup, Y. Ge, X. Wang, N. Wang, S. Wang, *Chem. Eur. J.* **2020**, *26*, 12403-12410; *(e)* M. Vanga, S. Sa, A. Kumari, A. C. Murali, P. Nayak, R. Das, K. Venkatasubbaiah, *Dalton. Trans.* **2020**, *49*, 7737-7746. *(f)* D. Kunchala, S. Sa, P. Nayak, J. Ponniah S, K. Venkatasubbaiah, *Organometallics* **2019**, *38*, 870-878. *(g)* V. Mukundam, S. Sa, A. Kumari, R. Das, K. Venkatasubbaiah, *J. Mater. Chem. C*, **2019**, *7*, 12725—12737

4. *(a)* K. P. Carter, A. M. Young, A. E. Palmer, *Chem. Rev.* **2014**, *114*, 4564-4601; *(b)* L. Wang, X. Gong, Q. Bing, G. Wang, *Microchem. J.* **2018**, *142*, 279-287; *(c)* P. Ravichandiran, A. Boguszewska-Czubara, M. Masłyk, A. P. Bella, S. A. Subramaniyan, P. M. Johnson, K. S. Shim, H. G. Kim, D. J. Yoo, *ACS Sustain. Chem. Eng.* **2019**, *7*, 17210-17219; *(d)* N. Yadav, A. K. Singh, *J. Electrochem. Soc.* **2019**, *166*, B644-B653; *(e)* A. Gul, M. Oguz, A. N. Kursunlu, M. Yilmaz, *Dyes Pig.* **2020**, *176*; *(f)* M. Sahu, A. Kumar Manna, K. Rout, J. Mondal, G. K. Patra, *Inorganica Chim. Acta* **2020**, *508*; *(g)* Y. Zhang, W. Wang, R. Li, E. Zhang, Z. Li, L. Tang, B. Han, X. Hou, J. J. Wang, *Spectrochim. Acta A Mol. Biomol. Spectrosc.* **2020**, *230*, 118050; *(h)* T. Samanta, R. Shunmugam, *Mater. Adv.* **2021**, *2*, 64-95.

5. *(a)* F. T. Edelmann, *Chem. Soc. Rev.* **2012**, *41*, 7649-7964; *(b)* J. Kido, Y. Okamoto, *Chem. Rev.* **2002**, *102*, 2357-2368; *(c)* S. Faulkner, S. J. A. Pope, B. P. Burton-Pye, *Applied Spectroscopy Reviews* **2005**, *40*, 1-31; *(d)* C. Andraud, O. Maury, *Eur. J. Inorg. Chem.* **2009**, 4357-4371; *(e)* C. J. Weiss, T. J. Marks, *Dalton. Trans.* **2010**, *39*, 6576-6588; *(f)* S. D. Bennett, B. A. Core, M. P. Blake, S. J. Pope, P. Mountford, B. D. Ward, *Dalton. Trans.* **2014**, *43*, 5871-5885; *(g)* Z. Ahmed, K. Iftikhar, *Inorg. Chem.* **2015**, *54*, 11209-11225; *(h)* V. V. Utochnikova, N. N. Solodukhin, A. N. Aslandukov, L. Marciniak, I. S. Bushmarinov, A. A. Vashchenko, N. P. Kuzmina, *Org. Electron.* **2017**, *44*, 85-93; *(i)* F. Zinna, M. Pasini, F. Galeotti, C. Botta, L. Di Bari, U. Giovanella, *Adv. Funct. Mater.* **2017**, *27*; *(j)* Y. Qiao, E. J. Schelter, *Acc. Chem. Res.* **2018**, *51*, 2926-2936; *(k)* Y. Zhang, S. Liu, Z.-S. Zhao, Z. Wang, R. Zhang, L. Liu, Z.-B. Han, *Inorg. Chem. Front.* **2021**, *8*, 590-619; *(l)* P. Kalita, J. Goura, J. M. Herrera, E. Colacio, V. Chandrasekhar, *ACS Omega* **2018**, *3*, 5202–5211; *(m)* A. K. Bar, P. Kalita, M. K. Singh, G. Rajaraman, V. Chandraselkar*, Coord. Chem. Rev.* **2018**, *367*, 163-216; *(n)* P. Kalita, N. Ahmed, A. K. Bar, S. Dey, A. Jana, G. Rajaraman, J-P Sutter, V. Chandrasekhar, *Inorg. Chem.* **2020**, *59*, 6603- 6612; *(o)* V. V. Utochnikova, E. V. Latipov, A. I. Dalinger, Y. V. Nelyubina, A. A. Vashchenko, M. Hoffmann, A. S. Kalyakina, S. Z. Vatsadze, U. Schepers, S. Bräse, N. P. Kuzmina, *J. Lumines.* **2018**, *202*, 38-46; (p) L. Wang, Z. Zhao, C. Wei, H. Wei, Z. Liu, Z. Bian, C. Huang, *Adv. Optical Mater.* **2019**, *7*, 1801256.

6. *(a)* D. A. Chowdhury, T. Ogata, S. Kamata, *Anal. Chem.* **1996**, *68*, 366-370; *(b)* C. E. Lisowski, J. E. Hutchison, *Anal. Chem.* **2009**, *81*, 10246-10253; *(c)* C. Han, L. Zhang, H. Li, *Chem. Commun.* **2009**, 3545-3547; *(d)* P. Das, A. Ghosh, A. Das,

Inorg. Chem. **2010**, *49*, 6909-6916; *(e)* T. Gorai, U. Maitra, *Angew. Chem. Int. Ed.* **2017**, *56*, 10730-10734; *(f)* P. Harvey, A. Nonat, C. Platas-Iglesias, L. S. Natrajan, L. J. Charbonniere, *Angew. Chem. Int. Ed.* **2018**, *57*, 9921-9924; *(g)* G. I. Vargas-Zuniga, J. L. Sessler, Sensors for Lanthanides and Actinides. In The Rare Earth Elements: Fundamentals and Applications, Atwood, D. A., Ed. Wiley: 2012; pp 561-573. (h) S-S. Zheng, W-K. Dong, Y. Zhang, L. Chen*,* Y.-J. Ding, *New J. Chem.*, **2017**, *41*, 4966-4973.

7. *(a)* M. P. Cuajungco, G. J. Lees, *Neurobiol. dis.* **1997**, *4*, 137-169; *(b)* D. Beyersmann, H. Haase, *Biometals* **2001**, *14*, 331-341; *(c)* D. Beyersmann, *Mat.-wiss. u. Werkstofftech* **2002**, *33*, 764-769; *(d)* S. G. Bell, B. L. Vallee, *Chembiochem.* **2009**, *10*, 55-62; *(e)* W. Maret, *Biometals* **2011**, *24*, 411-418; *(f)* W. Maret, *Adv. Nutr.* **2013**, *4*, 82-91; *(g)* S. Triboulet, C. Aude-Garcia, L. Armand, A. Gerdil, H. Diemer, F. Proamer, V. Collin-Faure, A. Habert, J. M. Strub, D. Hanau, N. Herlin, M. Carriere, A. Van Dorsselaer, T. Rabilloud, *Nanoscale* **2014**, *6*, 6102-6114; *(h)* T. Kambe, T. Tsuji, A. Hashimoto, N. Itsumura, *Physiol. Rev.* **2015**, *95*, 749-784; *(i)* W. Maret, *Metallomics* **2015**, *7*, 202-211; *(j)* L. C. Costello, R. B. Franklin, *Arch. Biochem. Biophys.* **2016**, *611*, 100-112; *(k)* K. Grüngreiff, D. Reinhold, H. Wedemeyer, *Ann. Hepatol.* **2016**, *15*, 7-16; *(l)* W. Maret, *Int. J. Mol. Sci.* **2017**, *18*; *(m)* X. Yang, H. Wang, C. Huang, X. He, W. Xu, Y. Luo, K. Huang, *Sci. Rep.* **2017**, *7*, 14669; *(n)* W. Maret, *Free Radic. Biol. Med.* **2019**, *134*, 311-326.

8. *(a)* K. Hanaoka, K. Kikuchi, H. Kojima, Y. Urano, T. Nagano, *Angew. Chem. Int. Ed.* **2003**, *42*, 2996-2999; *(b)* Y. Xu, J. Meng, L. Meng, Y. Dong, Y. Cheng, C. Zhu, *Chem. Eur. J.* **2010**, *16*, 12898-12903; *(c)* Z. Xu, K.-H. Baek, H. N. Kim, J.

Cui, X. Qian, D. R. Spring, I. Shin, J. Yoon, *J. Am. Chem. Soc.* **2010**, *132*, 601-610.

9. H. A. Benesi, J. H. Hildebrand, *J. Am. Chem. Soc.* **1949**, *71*, 2703–2707.

10. *(a)* M. E. Germain, T. R. Vargo, P. G. Khalifah, M. J. Knapp, *Inorg. Chem.* **2007**, *46*, 4422-4429; *(b)* X.-Q. Song, Y.-Q. Peng, G.-Q. Cheng, X.-R. Wang, P.-P. Liu, W.-Y. Xu, *Inorganica Chim. Acta* **2015**, *427*, 13-21.

11. Y. Hasegawa, Y. Kitagawa, T. Nakanishi, *NPG Asia Materials* **2018**, *10*, 52-70.

12. (*a*) E. A. Varaksina , I. V. Taydakov , S. A. Ambrozevich , A. S. Selyukov , K. A. Lyssenko , L. T. Jesus and R. O. Freire , *J. Lumin.*, **2018**, *196*, 161—168. (*b*) Z. Ahmed and K. Iftikhar *, Dalton Trans.*, **2019**, *48*, 4973 —4986. (*c*) F. P. Aguiar , I. F. Costa , J. G. P. Espínola , W. M. Faustino , J. L. Moura , H. F. Brito , T. B. Paolini , M. C. F. C. Felinto and E. E. S. Teotonio , *J. Lumin.*, **2016**, *170*, 538 —546. (*d*) Z. Li, P. Li, Q. Xu and H. Li, *Chem. Commun.*, **2015**, *51*, 10644 —10647. (*e*) J.-C. G. Bünzli *Coord. Chem. Rev.*, **2015**, *293–294*, 19—47. (*f*) L. Sun, Y. Qiu, T. Liu, J. Feng, W. Deng and L. Shi, *Luminescence*, **2015**, *30*, 1071 —1076. (g) P. Kalita, P. Nayak, N. Ahmed, J. M. Herrera, K. Venkatasubbaiah, E. Colacio, V. Chandrasekhar, *Dalton. Trans.* **2020**, *49*, 15404-15416.

13. *(a)* A. Guenet, F. Eckes, V. Bulach, C. A. Strassert, L. De Cola, M. W. Hosseini, *Chemphyschem* **2012**, *13*, 3163-3171; *(b)* E. Kasprzycka, V. A. Trush, V. M. Amirkhanov, L. Jerzykiewicz, O. L. Malta, J. Legendziewicz, P. Gawryszewska, *Chem. Eur. J.* **2017**, *23*, 1318-1330. *(c)* J. R. G. Thorne, J. M. Rey, R. G. Denning, S. E. Watkins, M. Etchells, M. Green, V. Christon, *J. Phys. Chem. A* **2002**, *106*, 4014-4021.

14. Gaussian 16, Revision A.03, M. J. Frisch, G. W. Trucks, H. B. Schlegel, G. E. Scuseria, M. A. Robb, J. R. Cheeseman, G. Scalmani, V. Barone, G. A. Petersson, H. Nakatsuji, X. Li, M. Caricato, A. V. Marenich, J. Bloino, B. G. Janesko, R. Gomperts, B. Mennucci, H. P. Hratchian, J. V. Ortiz, A. F. Izmaylov, J. L. Sonnenberg, D. Williams-Young, F. Ding, F. Lipparini, F. Egidi, J. Goings, B. Peng, A. Petrone, T. Henderson, D. Ranasinghe, V. G. Zakrzewski, J. Gao, N. Rega, G. Zheng, W. Liang, M. Hada, M. Ehara, K. Toyota, R. Fukuda, J. Hasegawa, M. Ishida, T. Nakajima, Y. Honda, O. Kitao, H. Nakai, T. Vreven, K. Throssell, J. A. Montgomery, Jr., J. E. Peralta, F. Ogliaro, M. J. Bearpark, J. J. Heyd, E. N. Brothers, K. N. Kudin, V. N. Staroverov, T. A. Keith, R. Kobayashi, J. Normand, K. Raghavachari, A. P. Rendell, J. C. Burant, S. S. Iyengar, J. Tomasi, M. Cossi, J. M. Millam, M. Klene, C. Adamo, R. Cammi, J. W. Ochterski, R. L. Martin, K. Morokuma, O. Farkas, J. B. Foresman, and D. J. Fox, Gaussian, Inc., Wallingford CT, **2016**.

15. O. V. Amirkhanov, O. V. Moroz, K. O. Znovjyak, T. Y. Sliva, L. V. Penkova, T. Yushchenko, L. Szyrwiel, I. S. Konovalova, V. V. Dyakonenko, O. V. Shishkin, V. M. Amirkhanov, *Eur. J. Inorg. Chem.* **2014**, 3720–3730.

Chapter 3A

Cycloaddition of CO$_2$ and epoxides using a B-N coordinated phenanthroimidazole-based zinc-salen as a photocatalyst

3A.1 Introduction

Polycyclic aromatic hydrocarbons (PAHs) have attracted significant attention due to their wide range of applications.[1] In-corporation of main-group elements has helped to overcome the shortcomings of PAHs and impart properties like extended stability and performance.[2] Boron-incorporated PAHs especially tetra-coordinated boron-embedded PAHs have gained attraction owing to their tunable optical properties.[3] For instance, B-N coordinated tetra-coordinated PAHs have been explored as photochromic, enhanced acceptor, NIR-emissive, oxygen sensors, and π-conjugated donor-acceptor materials.[4]

Global climate change is one of the most debated topics in recent times and the increasing atmospheric carbon dioxide (CO_2) levels are linked to the change in the earth's climate. Carbon capture and sequestration are considered one of the most practical methods to reduce the CO_2 content in the atmosphere.[5] While this can be done by many methods[6] a promising methodology involves the chemical conversion of CO_2 into useful products such as its reaction with oxiranes affording cyclic carbonates.[7] Salen ligands possessing a N_2O_2 coordination sphere have been widely used to prepare complexes with Al(III),[8] Zn(II),[9] Cr(III),[8c,10] and Co(II)[11] which have been utilized for the CO_2 fixation reaction. Developing highly efficient catalysts for the coupling of oxiranes and CO_2 at low pressure and temperature is still a challenging problem.[9b, 9d, 9e, 12] We propose a new strategy to use light energy to induce the chemical transformation of CO_2 and oxiranes to produce cyclic carbonates.

We recently reported monomers and dimers of tetra-coordinated boron functionalized phenanthroimidazole compounds and studied their linear and non-linear optical properties.[13] We have now coupled this tetra-coordinated boron motif with a zinc(II) salen and utilized the hybrid system for the chemical transformation of CO_2 and oxiranes

to produce cyclic carbonates using visible light.

3A.2 Results and discussion

3A.2.1 *Synthesis*

Compounds **1**–**3** were prepared according to the previously reported procedures.[13] Treatment of **2** and **3** in the presence of Na_2CO_3 and a catalytic amount of $Pd(PPh_3)_4$ under Suzuki coupling conditions produced compound **4a** in moderate yield (64%).(Scheme 3A.1) The synthetic route to phenanthroimidazole B-N coordinated imine ligand **5a** and its corresponding Zn(II) complex **6a** is outlined in Scheme 3A.2. Starting materials used for the synthesis of ligands **5a** & **5b** were prepared according to the previously reported procedures.[13] The ligand **5a** was synthesized with excellent yield (93 %) by a simple condensation reaction of **4a** with ethylenediamine in dry methanol. The Zn(II) complex **6a** was synthesized in good yield (84%) by reacting equimolar amounts of **5a** and $Zn(OAc)_2 \cdot 2H_2O$ in CH_2Cl_2-CH_3OH under reflux conditions for 12 hours. To examine the effect of B-N coordination, we have synthesized a complex that does not have this motif, *viz.*, the Zn(II) complex, **6b**. A similar methodology as described above was used for the preparation of **4b**, **5b**, and **6b** (Scheme 3A.1 & 3A.2).
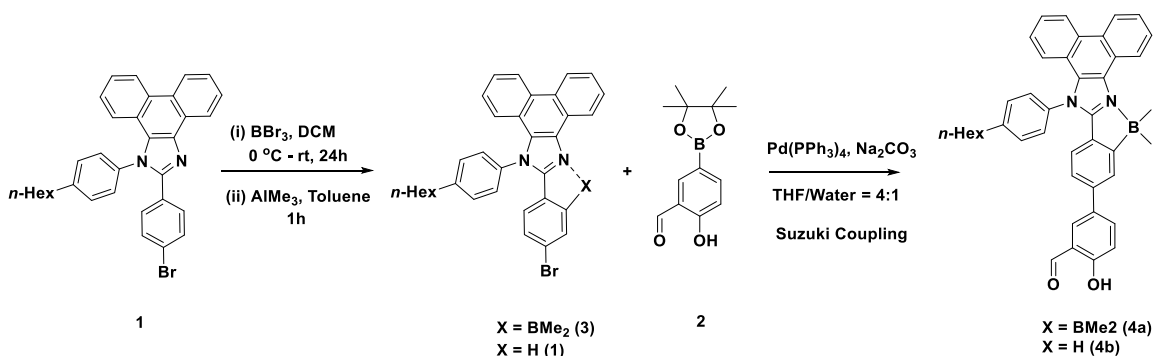
Scheme 3A.1: Synthetic procedure for complex **4a** and **4b**
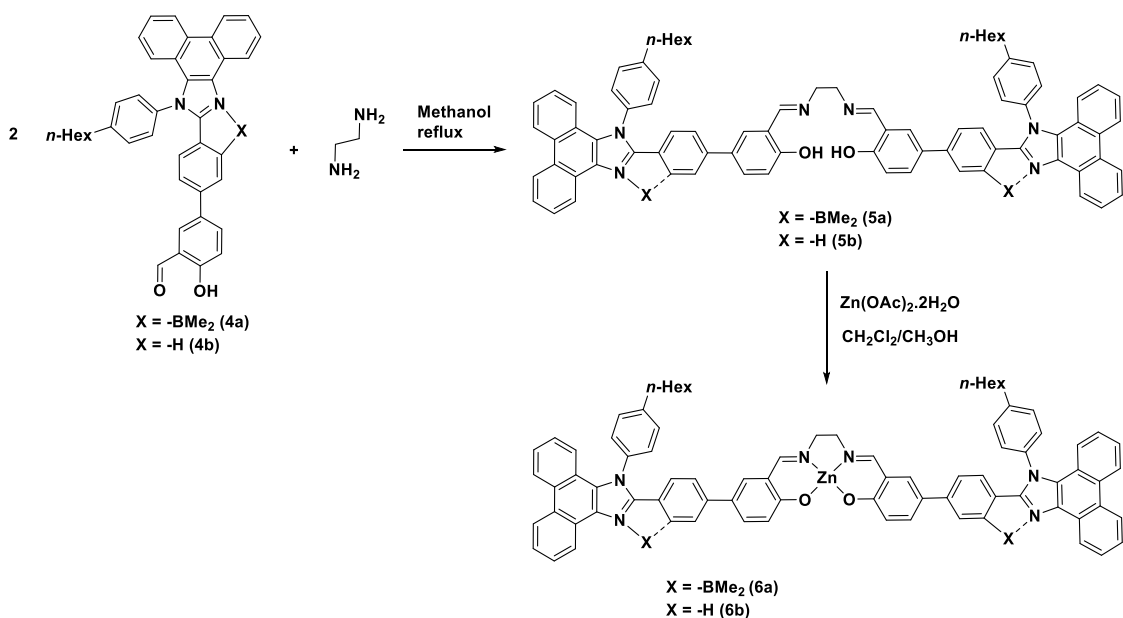
Scheme 3A.2: Synthetic procedure for complex **6a** and **6b**

Ligand **5a** and complex **6a** were characterized by multi-nuclear NMR, MALDI-MS, and X-ray crystallography (in the case of complex **6a**). Boron coordination in **5a** and **6a** was confirmed by ^{11}B-NMR. Singlets at 0.46 and 0.38 ppm in the ^{1}H-NMR of ligand **5a** and complex **6a** respectively represent 12 protons from four methyl groups attached to the B center. The disappearance of the OH peak at 13.28 ppm of ligand **5a** and upfield shift of four ethylene protons from 4.0 ppm in **5a** to 3.80 ppm in **6a** confirms the formation of Zn(II) complex, **6a**.

3A.2.2 *X-ray crystal structure analysis*

X-ray quality crystals of complex **6a** were obtained by slow evaporation of its solution in a DMF-DCM-methanol mixture. The molecular structure of complex **6a** was determined by single crystal X-ray diffraction analysis and is presented in Figure 3A.1. The molecular structure of complex **6a** reveals that the zinc atom is in a distorted square pyramidal geometry with a coordination environment consisting of two imino nitrogen

atoms, two phenolate oxygen atoms and one oxygen from a dimethyl formamide molecule. The zinc atom is 0.43 Å above the mean plane of the N_2O_2 coordination, as reported by Atwood for the pyridine-coordinated zinc complex, and to the value of 0.41 Å reported by Lin and co-workers.[14] Also, the Zn-N/O bond distances and angles (Table 3A.1) for complex **6a** are in well agreement with previously reported Zn(II) salen complexes.[14a] The axial position is occupied by a dimethyl formamide molecule with Zn1-O1 bond length of 2.053(2) Å. The tetra-coordinate boron center adopts a typical distorted tetrahedral geometry. The B–N and B–C distances are consistent with those of other reported B ← N chelated tetra-coordinate boron complexes in the literature.[3h, 15] (Table 3A.1)
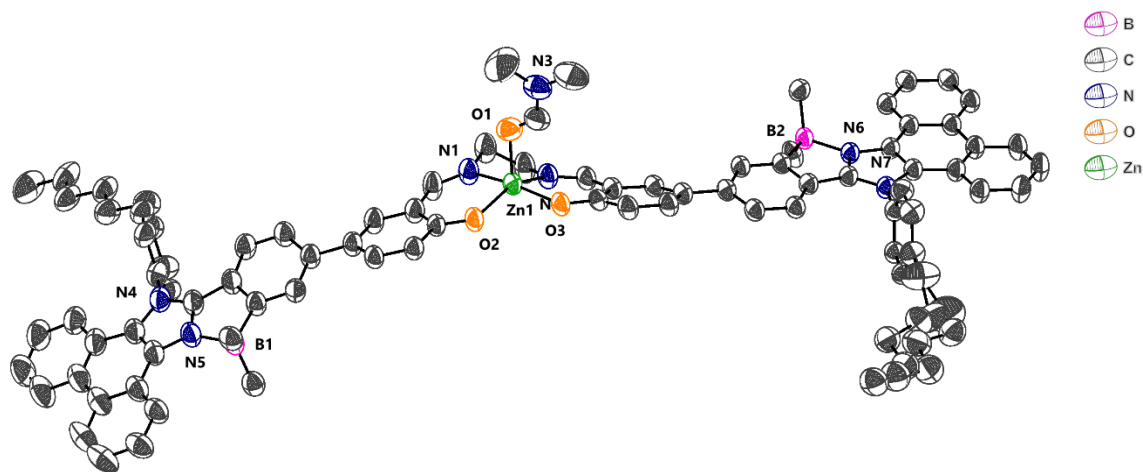
Figure 3A.1: Crystal structure of complex **6a.** Thermal ellipsoids are drawn at 50% probability level. Hydrogens are removed for clarity.

Table 3A.1: Selected bond lengths and bond angles of complex **6a**

	Bond lengths (Å)		Bond Angles (°)
Zn1-O1	2.053(2)	O2-Zn1-O1	106.7(9)
Zn1-O2	1.9545(2)	O2-Zn1-N2	144.7(1)
Zn1-O3	1.9874(2)	O2-Zn1-N1	88.7(9)
Zn1-N1	2.081(3)	O1-Zn1-N2	107.5(1)
Zn1-N2	2.075(2)	O1-Zn1-N1	96.6(1)
B1-C11	1.617(4)	N2-Zn1-N1	79.1(1)
B1-C17	1.619(5)	C11-B1-N5	95.5(2)
B1-C16	1.622(4)	C11-B1-C17	110.6(2)
B1-N5	1.641(4)	C11-B1-C16	110.6(3)
B2-C62	1.619(4)	C17-B1-N5	108.8(2)
B2-C61	1.618(4)	C17-B1-C16	116.5(2)
B2-C59	1.621(3)	C16-B1-N5	113.0(2)
B2-N6	1.656(3)	C59-B2-N6	95.2(2)
	Bond Angles (°)	C61-B2-N6	110.6(2)
O3-Zn1-O1	96.05(9)	C61-B2-C59	111.4(2)
O3-Zn1-N2	89.22(8)	C61-B2-C62	114.7(2)
O3-Zn1-N1	164.88(1)	C62-B2-N6	110.9(2)
O2-Zn1-O3	95.52(8)	C62-B2-C59	112.4(2)

3A.2.3 *Photophysical properties*
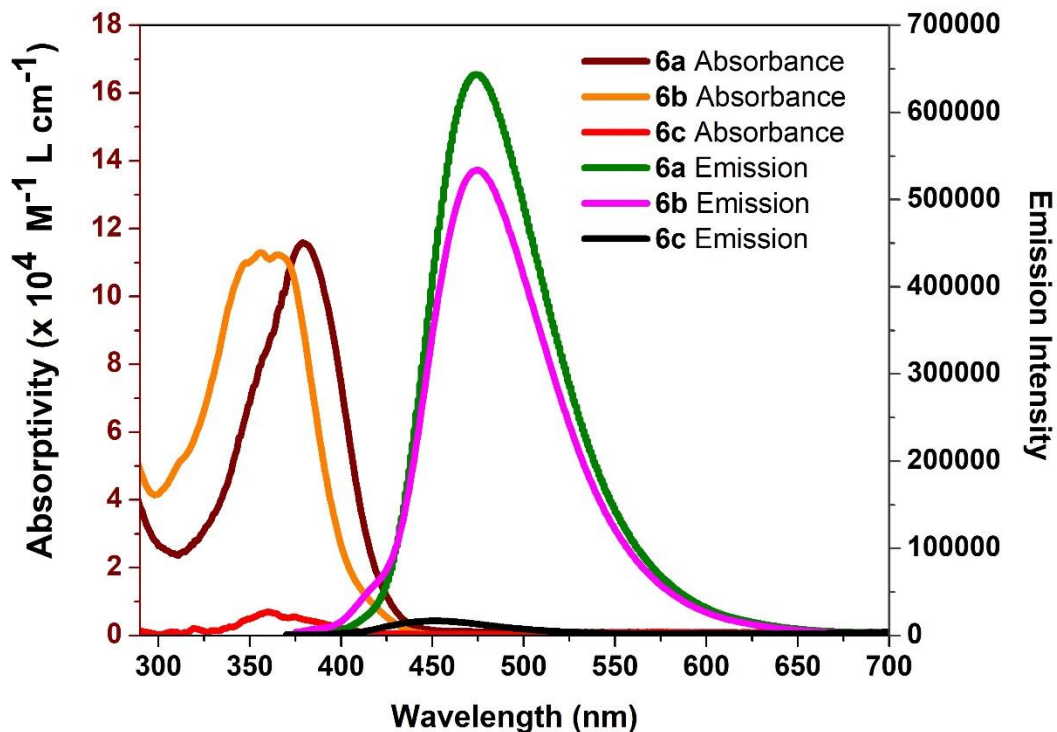
Figure 3A.2: Absorption and emission spectra of complex **6a, 6b** and **6c** in THF at 5 x

10^{-6} M concentration

Table 3A.2: Photophysical data of complexes **6a**, **6b** and **6c**

Solvent	Complex	$\lambda_{max}{}^{a}$ (nm)	$\lambda_{ems}{}^{b}$ (nm)	ε x 10^5 (M^{-1} L cm^{-1})	Stokes Shift (cm^{-1})	ϕ^{c}	τ (ns)
THF	**6a**	380	473	1.15	5174	11.0	1.64
	6b	365	473	1.12	6255	10.0	1.74
	6c	361	447	0.017	5166	4.7	4.7

^{a} concentration = 5 x 10^{-6} M, *^{b}* excited at λ_{max}, *^{c}* Absolute quantum yield in solution using

integrating sphere module

The photophysical data of complex **6a** recorded in THF is displayed in Figure 3A.2. When complex **6a** was irradiated at its longer wavelength absorption maxima, it exhibited moderate fluorescence emission. The absorption and emission spectra of the non-boron analog **6b** are shown in Figure 3A.2.
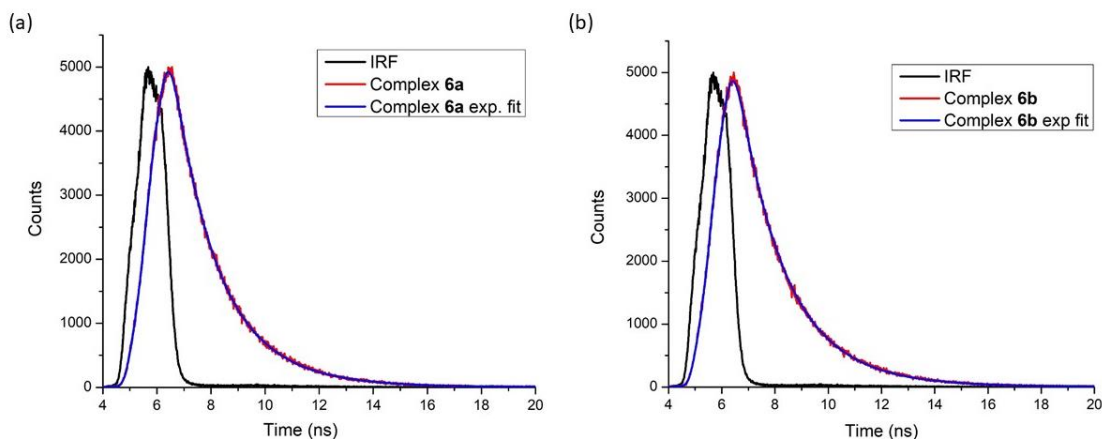
Figure 3A.3: Fluorescence lifetime decay profiles of complexes **6a** and **6b** in THF

Complex **6b** displayed a lower absorption maximum than complex **6a** which signifies the effect of boron coordination (Table 3A.2). Complex **6a** showed intense emission and slightly better quantum yields over **6b**. Borylation in **6a** helps to planarize the two rings which promote effective energy transfer along the structure which is restricted in **6b** due to the non-planarity of imidazole and phenyl rings. Both **6a** and **6b** showed single exponential decay with lifetimes in nanoseconds in THF solution (Figure 3A.3). UV-Visible spectra of compound **6a** obtained from theoretical calculations at B3LYP[16] level of theory and 6-31G(d) basis functions compares well with the experimental spectrum and shows a peak at 376 nm.

3A.2.4 *CO$_2$ fixation reaction*

Table 3A.3: *Optimization table*
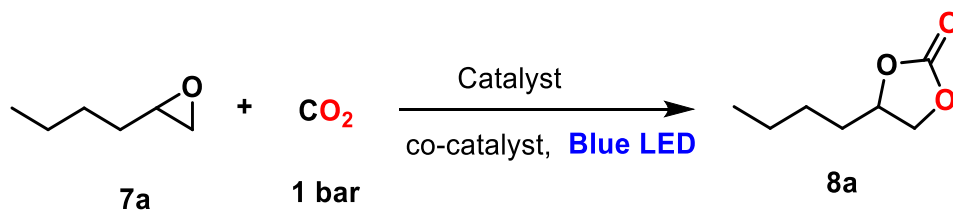
Sl. No.	Catalyst (mol%)	Co-Catalyst (mol %)	pCO$_2$ (bar)	Time (h)	Conv. (%)	Yield (%)
1.	**6a** (0.2)	TBAI (0.5)	1	19	49	42
2.	**6a** (0.2)	TBAI (1.0)	1	19	81	74
3.	**6a** (0.2)	TBAI (1.0)	2	19	75	70
4.	**6a** (0.2)	TBAI (1.5)	1	19	76	73
5.	**6a** (0.5)	TBAI (1.5)	1	19	78	70
6.	**6a** (0.5)	TBAI (1.5)	1	24	77	70
7.	**6a (0.5)**	**TBAI (2.5)**	**1**	**24**	**> 99**	**92**
8.	**6a** (0.5)	TBAI (2.5)	1	24	51	48 (dark)
9.	**6a** (0.5)	TBAI (3.0)	1	24	96	90
10.	**6a** (0.75)	TBAI (3.75)	1	24	96	91
11.	**6a** (0.5)	TBAI (2.5)	2	24	88	84
12.	**6a** (0.5)	TBAB (2.5)	1	24	74	66
13.	**6a** (0.5)	TBACl (2.5)	1	24	Trace	Trace
14.	----------------	TBAI (2.5)	1	24	ND	ND
15.	**6a** (0.5)	---------------	1	24	ND	ND

16.	**6a** (0.5)	^{n}Bu$_4$NPF$_6$ (2.5)	1	24	ND	ND
17.	**6a** (0.5)	NaI (2.5)	1	24	ND	ND
18.	**6a** (0.5)	Et$_4$NCl (2.5)	1	24	ND	ND
19[a].	**6a** (0.5)	TBAI (2.5)	1	24	10	09
20[b].	**6a** (0.5)	TBAI (2.5)	1	24	56	40
21[c].	**6a** (0.5)	TBAI (2.5)	1	24	26	25
22[d].	**6a** (0.5)	TBAI (2.5)	1	24	ND	ND
23[e].	**6a** (0.5)	TBAI (2.5)	1	24	ND	ND
24[f].	**6a** (0.5)	TBAI (2.5)	1	24	ND	ND
25.	**6b (0.5)**	**TBAI (2.5)**	**1**	**24**	**41**	**24**
26.	**6c** (0.5)	TBAI (2.5)	1	24	45	36

[a]CH$_2$Cl$_2$ Solvent, [b]THF solvent, [c]Toluene solvent, [d]DMSO solvent, [e]MeOH solvent, [f]EtOH

Motivated by the interesting photophysical properties of complex **6a**, we investigated its photocatalytic activity for the synthesis of cyclic carbonates using CO_2 under the irradiation of 6 W blue LED. Our initial investigation was started using 1,2-epoxy hexane as a substrate, complex **6a** as a photocatalyst (0.2 mol%), TBAI (0.5 mol%) as the co-catalyst under 1 bar CO_2 pressure at room temperature. Under blue light, 49% conversion of 1,2-epoxy hexane was observed after 19 h (Table 3A.3, entry1). Encouraged by this result, control experiments with different catalysts and co-catalyst (Table 3A.3, entries 2-7) loading were performed. It was found that 0.5 mol% of photocatalyst (**6a**), 2.5 mol% of co-catalyst (TBAI), at 1 bar CO_2 pressure under blue light full conversion (> 99%) of 1,2-epoxy hexane was observed (Table 3A.3, entry 7). There was no significant impact

on the catalytic activity on a further increase of catalyst or co-catalyst loading (Table 3A.3, entries 9-10). The significance of catalyst **6a** under blue light was realized when the reaction was performed without light, which resulted in only 51% conversion of 1,2-epoxy hexane (Table 3A.3, entry 8). Neither catalyst **6a** nor the tetrabutylammonium iodide salt alone was able to catalyze the reaction (Table 3A.3, entries 14 and 15). Among the different tetrabutylammonium halides tested, iodide showed superior activity and the order of the catalytic activity was found to be I > Br > Cl (Table 3A.3, entries 7, 12, and 13 respectively). Other co-catalysts such as $^nBu_4NPF_6$, NaI, and Et_4NCl proved to be less efficient (Table 3A.3, entries 16 - 18). Increasing the pressure to 2 bar does not have any significant impact on the catalytic activity. (Table 3A.3, entry 11). The catalytic activity decreases significantly using catalyst **6b** (Table 3A.3, entry 25) which shows the importance of boron coordination. A high degree of planarity was achieved after boron coordination which helps in the effective extension of conjugation. We believe that the effective conjugation observed in **6a** plays a crucial role in driving the cycloaddition reaction between epoxides and CO_2. We also synthesized a simple Zinc-salen[17] **6c** (Scheme 3A.2) and studied its catalytic activity under the optimized reaction conditions mentioned above (entry 26). Catalyst **6c** gave a low yield of 36% which further indicates the significance of the boron-coordinated phenanthroimidazole moiety.

3A.2.5 *Kinetic analysis*
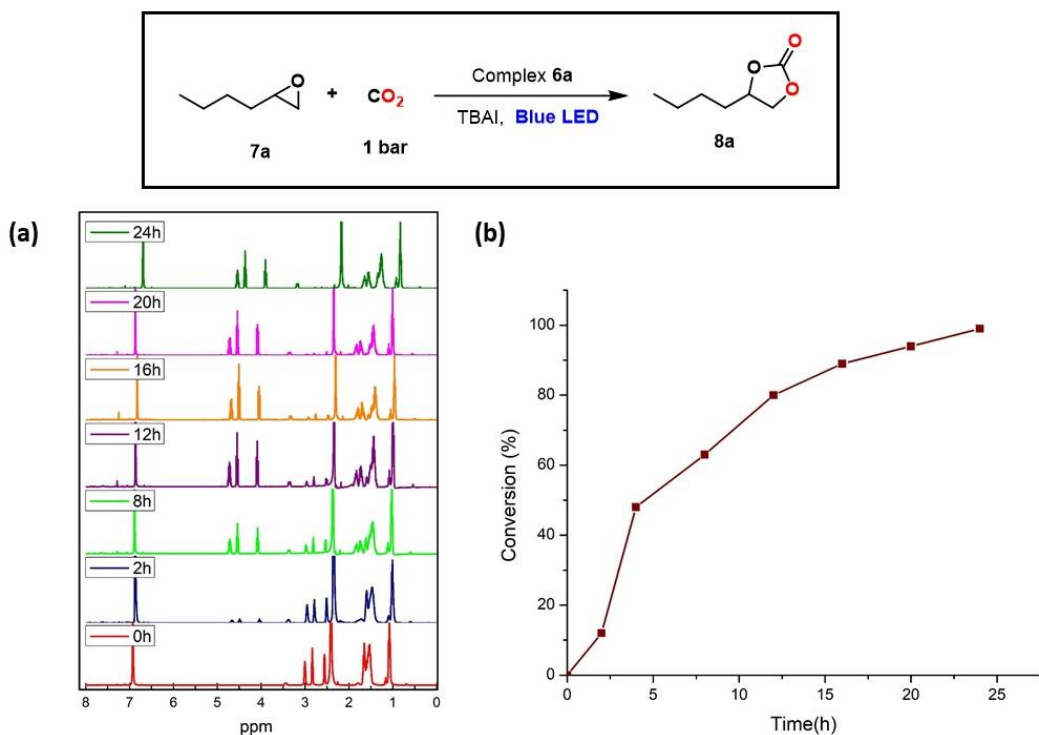
Figure 3A.4: (a) Stacked NMR spectra of the reaction mixture (mesitylene is used as an internal standard) in CDCl$_3$ at different time intervals. (b) Conversion of 1, 2-epoxy hexane to carbonate **8a** at 1 bar CO$_2$ pressure as a function of time at room temperature under blue LED.

The progress of the reaction of 1,2-epoxy hexane under the optimized conditions was monitored by NMR spectroscopy. The disappearance of 1,2-epoxy hexane was observed with the formation of the cyclic carbonate product as the reaction progresses. The NMR studies reveal that only starting materials and/or the cyclic carbonate product signals were present. Characteristic NMR peaks of the product appear between 4.0-4.8 ppm and starting material peaks appear between 2.4 – 3.0 ppm (Figure 3A.4). Almost 50 % conversion was observed in 4 hours of the reaction time and it took almost 24 hours for the full conversion of the reactant to form the desired cyclic carbonate. Conversion vs time plot is provided in Figure 3A.4 along with NMR spectra.

Table 3A.4: Scope of cycloaddition of terminal epoxides and CO_2

8a (91%) 8b (71%) 8c (87%) 8d (88%)

8e (63%) 8f (87%) 8g (72%) 8h (72%)

8i (89%) 8j (90%)

8k (88%) 8l (62%) 8m (90%)

8n (76%) 8o (83%)

8p (71%)
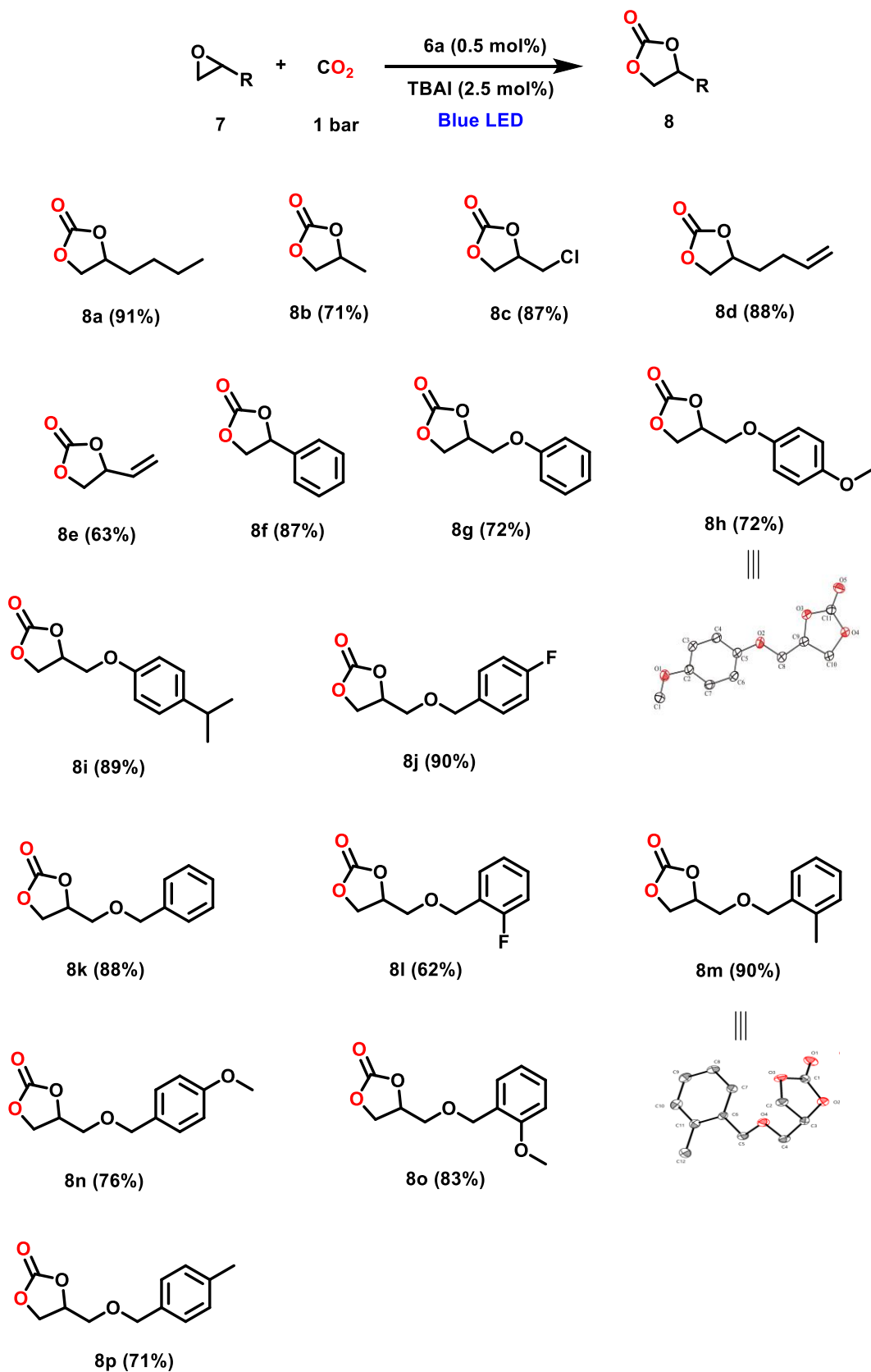
With the optimized conditions in hand, the scope of the reaction was studied using a series of functionalized terminal epoxides to investigate the applicability of our newly synthesized photocatalyst **6a** (Table 3A.4). All the terminal epoxides with different substituents produced the corresponding cyclic carbonates in good to excellent isolated yields (Table 3A.4, **8a-8p**). Unlike other reported zinc salen complexes, the photocatalyst **6a** showed a good reactivity for styrene oxide (Table 3A.4, **8f**) under mild reaction conditions.[9b, 9e, 18] Substituted phenoxy methyl oxiranes (Table 3A.4, **8g-8i**) and substituted benzyloxy methyl oxiranes (**8j-8p**) afforded good isolated yields of the desired cyclic carbonates.

Table 3A.5: Crystal data and structure refinement for complex **6a** and compounds **8h** and **8m**

	Complex **6a**	Compound **8h**	Compound **8m**
Empirical formula	$C_{89}H_{87}B_2N_7O_3Zn$	$C_{11}H_{12}O_5$	$C_{12}H_{14}O_4$
Formula weight	1389.64	224.21	222.23
Temperature/K	100(10)	10010)	99(2)
Crystal system	monoclinic	monoclinic	triclinic
Space group	I2/a	P21/c	P-1
a/Å	28.8831(2)	11.3939(4)	6.24087(19)
b/Å	16.8850(10)	14.7672(4)	8.8198(3)
c/Å	36.1216(3)	6.2697(2)	20.2377(6)
α/°	90	90	99.795(3)
β/°	95.8430(10)	104.037(3)	98.296(3)
γ/°	90	90	90.027(2)

Volume/Å3	17524.7(2)	1023.41(6)	1085.86(6)
Z	8	4	4
ρcalcg/cm3	1.053	1.455	1.359
µ/mm-1	0.756	0.984	0.102
F(000)	5872.0	472.0	472.0
Crystal size/mm3	$0.27 \times 0.26 \times 0.18$	$0.17 \times 0.14 \times 0.12$	$0.17 \times 0.15 \times 0.12$
Radiation	CuKα (λ = 1.54184)	CuKα (λ = 1.54184)	MoKα (λ = 0.71073)
2Θ range for data collection/°	7.478 to 163.906	7.998 to 155.058	7.1 to 63.474
Index ranges	$-36 \leq h \leq 29$, $-21 \leq k \leq 21$, $-45 \leq l \leq 45$	$-14 \leq h \leq 14$, $-18 \leq k \leq 17$, $-7 \leq l \leq 5$	$-8 \leq h \leq 8$, $-11 \leq k \leq 12$, $-29 \leq l \leq 29$
Reflections collected	77623	7974	22579
Independent reflections	18771 [Rint = 0.0278, Rsigma = 0.0229]	2110 [Rint = 0.0527, Rsigma = 0.0333]	6222 [R_{int} = 0.0454, R_{sigma} = 0.0344]
Data/restraints/parameters	18771/1251/927	2110/258/146	6222/516/292
Goodness-of-fit on F2	1.057	1.116	1.150
Final R indexes [I>=2σ (I)]	R1 = 0.0784, wR2 = 0.2385	R1 = 0.0509, wR2 = 0.1380	R_1 = 0.1267, wR_2 = 0.3246
Final R indexes [all data]	R1 = 0.0845, wR2 = 0.2462	R1 = 0.0578, wR2 = 0.1412	R_1 = 0.1316, wR_2 = 0.3264

Largest diff. peak/hole / e Å-3	2.13/-1.14	0.28/-0.33	1.41/-0.55

3A.2.6 Theoretical calculations

Theoretical calculations using the DFT functional B3LYP and 6-31G(d) U SDD basis functions have been done to understand the reaction pathway involved in the synthesis of cyclic carbonate using **6a**. The calculated energy difference between the ES and GS of [**6a.PO**] is 52.71 kcal/mol which is less than the energy difference between the ES and GS of the [**6c.PO**] (63.9 kcal/mol). Formation of the excited state [**6a.PO**]* is more
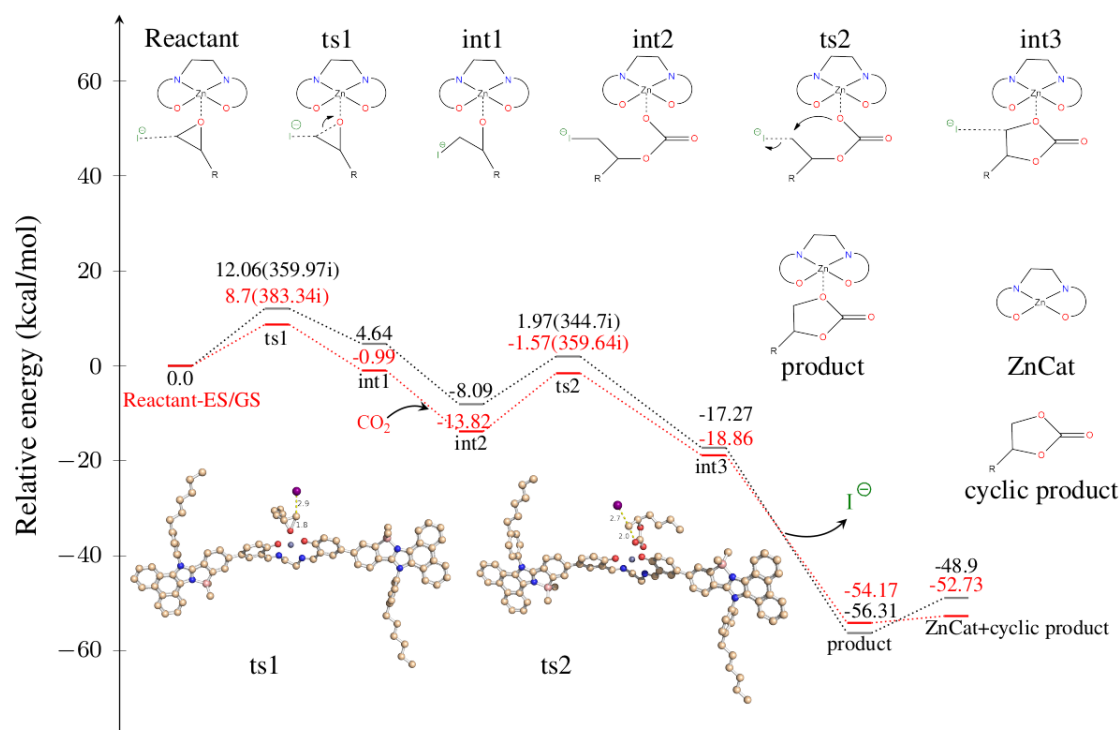
Figure 3A.5: Reaction energy profile of the mechanism with **6a**. Black indicates energies at ground state and Red indicates energies at excited state.

favorable than the excited state [**6c.PO**]* which we believe is the crucial step in this reaction. These findings further suggest that the formation of cyclic carbonate is favorable by around 52.73 kcal/mol when the catalyst was irradiated with blue light and 48.9 kcal/mol when the catalyst was at the ground state in the absence of any irradiation. The interaction of epoxide to **6a** is exothermic for both the ground state and excited state but is slightly more favorable in the ground state by around 1 kcal/mol than the excited state. The reaction has been studied with iodide having a long-range interaction with epoxide bound catalyst as the reactant. The penultimate step in the reaction, where the iodide is released, is the most exothermic step with 39.04 and 35.31 kcal/mol being released by the complex at the ground state and excited state respectively. Insertion of CO_2 into the epoxide-bound catalyst is a concerted step. Potential energy scan along the reaction coordinate $C(CO_2) - O(epoxide)$ for **6c** indicates the absence of any transition state for this step. A detailed mechanism of the reaction is presented in figure 3A.5.

3A.2.7 *Plausible mechanism*

A possible catalytic cycle for the cycloaddition of CO_2 and epoxides is proposed as shown in figure 3A.6. The catalytic cycle can be thought of as being initiated with the binding of epoxide O-atom with the Lewis acidic zinc center in its excited state and thereby activating the epoxide ring to form the species A. Intramolecular nucleophilic attack by the iodide anion on the less-hindered side of the activated epoxide leads to the ring-opened epoxide, affording an intermediate of metal-bound alkoxide species B. CO_2 insertion allowed the formation of species C which subsequently undergoes intramolecular nucleophilic (S_N2) reaction to give the corresponding cyclic carbonate and regenerates the excited state catalyst **6a**. A comparative study reveal that aluminum

complexes showed superior activity over other metal complexes (Table 3A.6). Most of the zinc complexes failed to form cyclic carbonates in high yield under mild conditions and in some instances the substrate scope is limited; however, our system showed good activity under mild conditions.
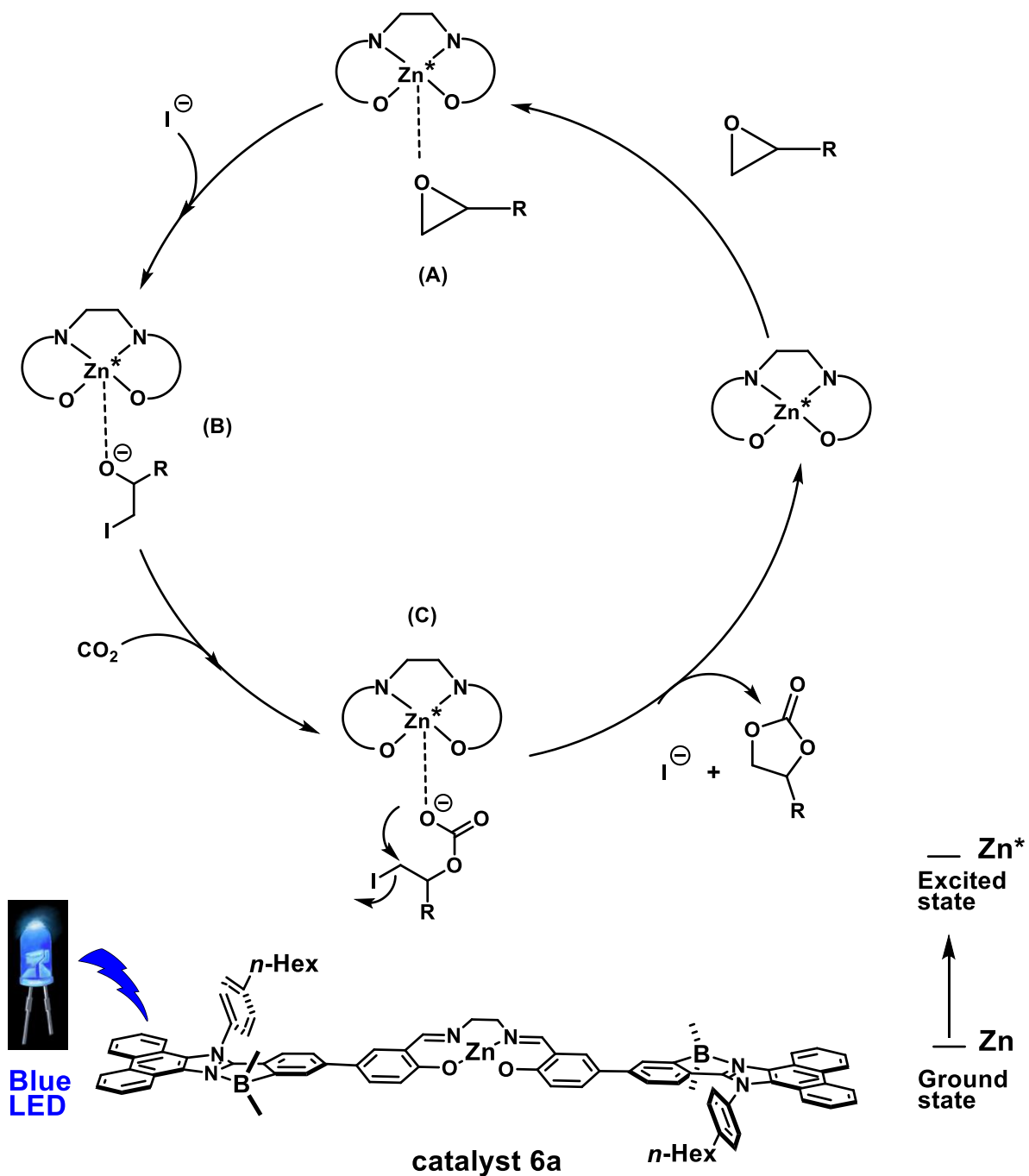
Figure 3A.6: Plausible catalytic cycle

3A.3 Conclusion

In summary, we have synthesized a tetra-coordinated boron functionalized phenanthroimidazole based zinc salen complex and characterized it with multinuclear NMR spectroscopy and single-crystal X-ray diffraction. Under blue light irradiation, the newly synthesized zinc salen complex successfully catalyzes the coupling of CO_2 with terminal epoxides under atmospheric pressure to form cyclic carbonates. Theoretical studies reveal that the formation of **6a.PO** is favored over **6c.PO** which is one of the crucial steps in this reaction. This approach will open up a new methodology for the conversion of CO_2 to useful starting materials and may have a high industrial impact as well.

Table 3A.6: Comparison of catalyst **6a** with previously reported Zn-salen catalysts
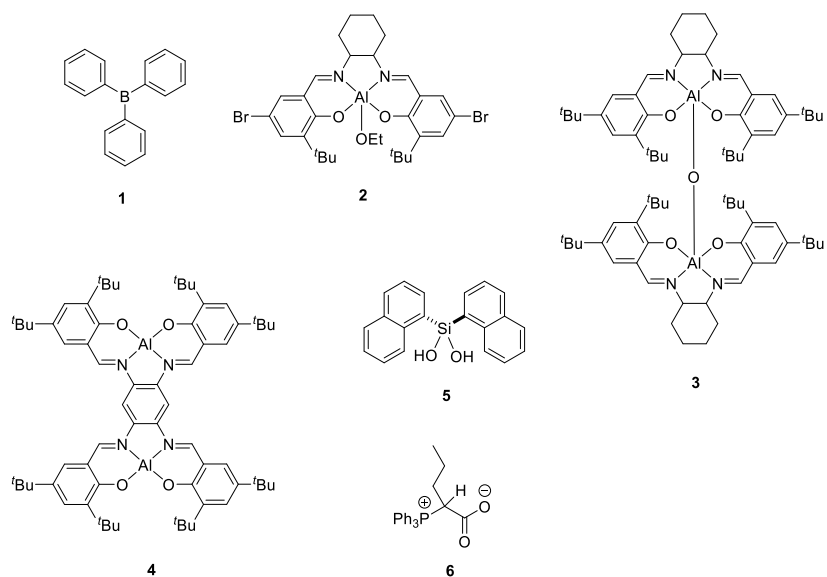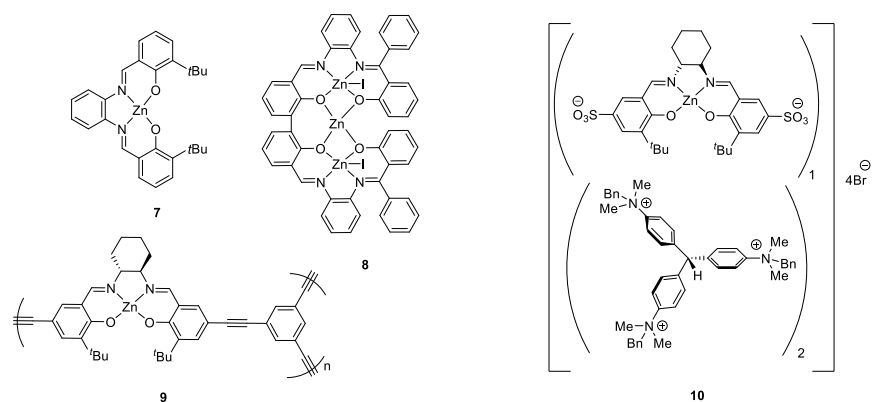
Catalyst	Conditions	Substrates	TON	TOF (h⁻¹)	Reference
1	PPNCl co-catalyst, 100 °C, 20 bar, 3 h	Propylene Oxide	920	307	23a
2	TBAB, rt, 1 bar, 48 h	Propylene Oxide	150	3	23b
3	TBAB, rt, 1 bar, 24 h	Propylene oxide	30.8	10.3	23c
		Epoxy hexane	34.8	11.6	
4	TBAB, rt, 1 bar, 24 h	Styrene Oxide	38.4	1.6	23d
5	TBAI, 23 °C, 1 bar, 18 h	Styrene Oxide	9.3	0.52	23e
6	25 °C, 6 h	Propylene Oxide	18	3	23f
2-pyridine-methanol	TBAI, rt, balloon, 20 h	Propylene Oxide	10.7	0.53	23g
6a	TBAI, rt, 1 bar, 24 h, **BLUE LED**	Propylene Oxide	142	8	This work
		Epoxy hexane	184	10	
		Styrene Oxide	174	7.2	
7	TBAI, 45 °C, 10 bar, 18	Epoxy hexane	32	1.77	23h

	h, DCM solvent				
7	TBAI, 45 °C, 80 bar, 3 h	Styrene oxide	38.4	12.8	23i
8	85 °C, 10 bar, 18 h	Glycidyl methyl ether	38.3	2.1	23j
9 (heterogeneous cat.)	TBAB, 120 °C, 30 bar, 1 h	Propylene oxide	11600	11600	23k
10	TBAB, 50 °C, 50 bar, 24 h	Styrene Oxide	49	2	23l

3A.4 Experimental section

3A.4.1 *General information*

All reagents and starting materials were purchased from Sigma-Aldrich, Alfa-Aesar, and Spectrochem chemical companies and used as received unless otherwise noted. Chlorinated solvents, acetonitrile, and DMF were distilled from CaH_2. THF and toluene were distilled from Na/benzophenone before use. All 400 MHz ^{1}H, 100 MHz ^{13}C, NMR spectra were recorded on a Bruker ARX 400 spectrometer operating at 400 MHz. All ^{1}H and ^{13}C NMR spectra were referenced internally to solvent signals. All NMR spectra were recorded at ambient temperature. ESI mass spectra were recorded on Bruker, micrOTOF-QII mass spectrometer. The absorbance spectra were recorded on a JASCO V-730 UV-Visible spectrometer. The fluorescence spectra were recorded using Edinburgh FS5 spectrofluorometer. Absolute fluorescence quantum yields of compounds **6a-6c** were measured by integrating sphere method using Edinburgh FS5 spectrofluorometer. The fluorescence spectra are corrected for the instrumental response. Single-crystal X-ray diffraction data for compounds **6a** and **8h** were collected on a

Rigaku SuperNova fine-focused dual diffractometer, with Cu Kα radiation (λ = 1.54178 Å) or Mo-Kα radiation (0.71073 Å) equipped with a PILATUS200K detector. Using Olex2, the structures were solved with the ShelXS structure solution program using Direct Methods and refined with the ShelXL refinement package using Least Squares minimization. All non-hydrogen atoms were refined with anisotropic displacement coefficients. The H atoms were placed at calculated positions and were refined as riding atoms. Crystallographic data for compounds **6a** and **8h** have been deposited with the Cambridge Crystallographic Data Center as supplementary publication no. CCDC-2091448-2091449. Copies of the data can be obtained free of charge on application to CCDC, 12 Union Road, Cambridge CB2 1EZ, UK (fax: (+44) 1223-336-033; email: deposit@ccdc.cam.ac.uk).
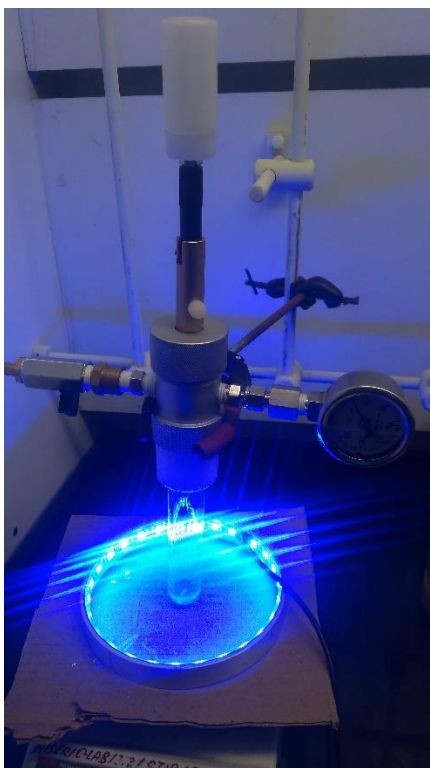
Figure 3A.7: A representative image of the CO_2 reaction set-up.

3A.4.2 *Synthetic procedure and spectral characterization*

Synthesis of compound 4a:
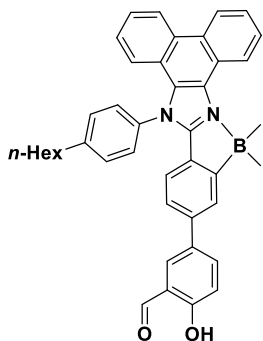
To an oven-dried two neck 250 mL RB, compound **2** (1.74 mmol, 1.00 g, 1.0 equiv.), compound **3**, (1.91 mmol, 0.476 g, 1.1 equiv.), Na_2CO_3 (5.23 mmol, 0.553 g, 3.0 equiv.) and $Pd(PPh_3)_4$ (0.0523 mmol, 0.060 g, 3 mol%) were loaded under nitrogen atmosphere. To this mixture, degassed THF (40 mL) and water (10 mL) in 4:1 ratio was added and the reaction mixture was refluxed for 24 h. The progress of the reaction was monitored through TLC. After completion of the reaction, the whole mixture is cooled to room temperature. Dichloromethane (50 mL) and water (50 mL) were added to the reaction mixture; the organic layer was separated and the aqueous layer was extracted using CH_2Cl_2 (3x20 mL). The combined organic layer was washed with brine, dried over Na_2SO_4, and concentrated under reduced pressure. The crude product was purified by column chromatography (1:20 of EtOAc: *n*-hexane) on silica gel to afford the corresponding coupled product **4a.** Yield = 64% (0.684 g). ^{1}H NMR (400 MHz, $CDCl_3$) δ 11.03 (s, 1H), 9.99 (s, 1H), 9.26 (d, *J* = 8.2 Hz, 1H), 8.77 (t, *J* = 8.0 Hz, 2H), 7.86 – 7.82 (m, 4H), 7.69 – 7.51 (m, 6H), 7.35 – 7.28 (m, 2H), 7.15 (dd, *J* = 8.1, 1.8 Hz, 1H), 7.08 (d, *J* = 9.3 Hz, 1H), 6.52 (d, *J* = 8.1 Hz, 1H), 2.92 (t, *J* = 7.7 Hz, 2H), 1.85 (p, *J* = 6.76 Hz, 2H), 1.52 – 1.36 (m, 6H), 0.97 (t, *J* = 8.0 Hz 3H), 0.49 (d, *J* = 2.1 Hz, 6H). ^{13}C NMR (101 MHz, $CDCl_3$) δ 7.36, 14.28, 22.82, 29.01, 31.29, 31.82, 35.96, 118.16, 120.76, 120.86, 121.52, 123.48, 123.63, 124.21, 125.68, 126.00, 126.73, 126.96, 127.11, 127.58, 128.25, 129.00, 129.35, 131.08, 132.30, 134.36, 136.15, 146.72, 161.14, 196.93. ^{11}B NMR (128 MHz, $CDCl_3$) δ 0.11 HRMS (ESI+, m/z) calcd for $C_{42}H_{40}BN_2O_2$, $[M+H]^+$ m/z = 615.3185, found = 615.3150

Synthesis of compound 5a:
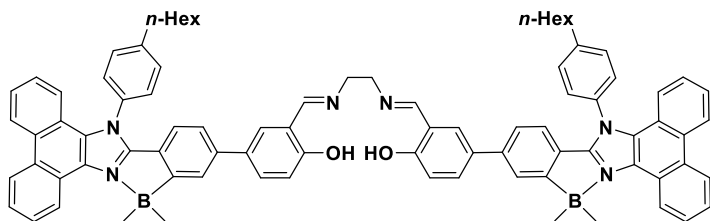
To 100 mL one neck RB, compound **4a** (0.81 mmol, 0.50 g, 2.0 equiv.) and ethylene diamine (0.40 mmol, 27 μL, 1.0 equiv.) were added to dry methanol and refluxed overnight. The reaction mixture was filtered and the resultant yellow precipitate of compound **5a** was collected. Yield: 93% (0.466 g) ^{1}H NMR (400 MHz, CDCl$_3$) δ 13.28 (s, 2H), 9.26 (dd, J = 8.2, 1.4 Hz, 2H), 8.76 (t, J = 8.0 Hz, 4H), 8.48 (s, 2H), 7.83 (t, J = 8.0 Hz, 2H), 7.80 (d, J = 1.88 Hz, 2H) 7.73 (t, J = 8.0 Hz, 2H), 7.68 – 7.52 (m, 14H), 7.32 – 7.27 (m, 4H), 7.12 (dd, J = 8.1, 1.8 Hz, 2H), 7.02 (d, J = 8.6 Hz, 2H), 6.48 (d, J = 8.1 Hz, 2H), 4.00 (s, 4H), 2.91 (t, J = 7.7 Hz, 4H), 1.84 (p, J = 7.5 Hz, 4H), 1.52 – 1.35 (m, 12H), 0.96 (t, J = 6.96 Hz, 6H), 0.46 (s, 12H). ^{13}C NMR (101 MHz, CDCl$_3$) δ 7.36, 14.25, 22.79, 28.98, 31.25, 31.80, 35.94, 59.99, 117.53, 118.86, 120.74, 121.42, 122.56, 123.35, 123.49, 123.70, 124.18, 125.74, 125.86, 125.98, 126.63, 126.90, 127.11, 127.51, 128.28, 128.98, 129.09, 129.29, 130.36, 131.02, 131.22, 131.62, 132.60, 134.43, 141.60, 146.63, 153.62, 160.82, 166.76, 174.36. ^{11}B NMR (128 MHz, CDCl$_3$) δ 0.69. HRMS (ESI+, m/z) calcd for C$_{86}$H$_{82}$B$_2$N$_6$O$_2$, [M]$^+$ m/z = 1253.6717, found 1253.6652

Synthesis of complex 6a:

To 100 mL one neck RB, compound **5a** (0.200 g, 0.16 mmol, 1.0 equiv.) was dissolved in 10 mL of CH$_2$Cl$_2$ and a solution of Zn(OAc)$_2$.2H$_2$O (0.039 g, 0.17 mmol, 1.1 equiv.) in 10 mL methanol was added dropwise. The greenish-yellow solution was refluxed for 12 h. Light green color crystals of complex **6a** with a coordinated solvent molecule were
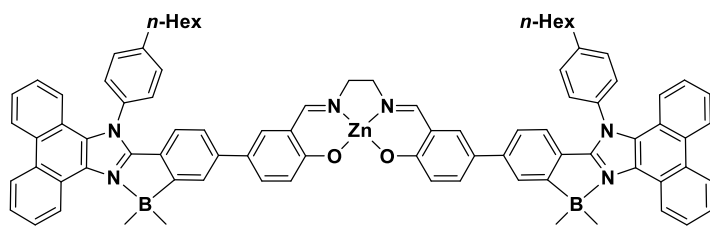
collected after 1 week. Yield: 84% (0.177 g). ^{1}H NMR (400 MHz, DMSO-d_6) δ 9.12 (d, J = 8.2 Hz, 2H), 8.94 (brs, 4H), 8.59 (s, 2H), 8.30 – 8.23 (m, 1H), 7.88 (brs, 5H), 7.77 (t, J = 7.9 Hz, 2H), 7.75 – 7.66 (m, 6H), 7.66 – 7.57 (m, 4H), 7.52 (d, J = 8.9 Hz, 2H), 7.36 (t, J = 7.88 Hz, 2H), 7.26 (d, J = 8.3 Hz, 2H), 7.17 (d, J = 8.2 Hz, 2H), 6.76 (d, J = 8.5 Hz, 2H), 6.38 (d, J = 8.0 Hz, 2H), 3.80 (s, 4H), 2.91 (t, J = 7.5 Hz, 4H), 1.80 (brs, 8H), 1.40 (brs, 12H), 0.93 (t, J = 6.7 Hz, 6H), 0.38 (s, 12H). ^{13}C NMR (101 MHz, DMSO-D_6) δ 7.42, 13.71, 14.89, 22.03, 28.14, 30.45, 31.00, 35.05, 55.84, 64.96, 118.91, 120.09, 120.91, 121.77, 121.87, 122.74, 123.17, 123.50, 123.74, 124.24, 124.80, 125.04, 126.17, 126.64, 126.87, 127.67, 128.17, 128.26, 128.37, 130.03, 130.58, 131.27, 132.65, 133.56, 141.27, 145.93, 153.18, 170.77. ^{11}B NMR (128 MHz, DMSO-D_6) δ 0.31. MALDI-MS Calcd for $C_{86}H_{80}B_2N_6O_2Zn$, $[M]^+$ m/z = 1314.5, found 1314.4. Anal. Calcd for $C_{86}H_{80}B_2N_6O_2Zn$: C, 78.45; H, 6.12; N, 6.38. Found: C, 78.12; H, 6.26; N, 6.44.

Synthesis of 4b:

To an oven-dried two neck 250 mL RB, compound **1** (1.87 mmol, 1.00 g, 1.0 equiv.), compound **3**, (2.06 mmol, 0.512 g, 1.1 equiv.), Na_2CO_3 (5.61 mmol, 0.595 g, 3.0 equiv.) and $Pd(PPh_3)_4$ (0.0561 mmol, 0.065 g, 3.0 mol%) were loaded under nitrogen atmosphere. To this mixture, degassed THF (40 mL) and water (10 mL) in the ratio of 4:1 was added and the reaction mixture was refluxed for 24 h. The completion of the reaction was monitored through TLC. After completion of the reaction, the whole mixture is cooled to room temperature. Dichloromethane (20 mL) and water (20 mL) were added,
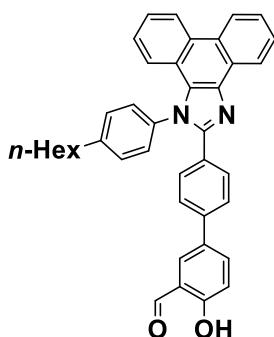
the organic layer was separated and the aqueous layer was extracted using dichloromethane (3x20 mL). The combined organic layer was washed with brine, and dried over Na_2SO_4 concentrated under reduced pressure. The crude product was purified by column chromatography (1:30 of EtOAc : *n*-hexane) on silica gel to afford the corresponding coupling product **4b.** Yield = 56% (0.602 g). ^{1}H NMR (400 MHz, CDCl3) δ 11.02 (s, 1H), 9.96 (s, 1H), 8.89 (d, *J* = 7.9 Hz, 1H), 8.77 (d, *J* = 8.4 Hz, 1H), 8.71 (d, *J* = 8.3 Hz, 1H), 7.79 – 7.73 (m, 3H), 7.72 – 7.62 (m, 3H), 7.56 – 7.38 (m, 7H), 7.30 – 7.19 (m, 2H), 7.06 (d, *J* = 9.0 Hz, 1H), 2.81 (t, *J* = 7.6 Hz, 2H), 1.76 (pent, *J* = 7.3 Hz, 2H), 1.45 - 1.26 (m, 6H), 0.92 (t, *J* = 6.6 Hz, 3H).^{13}C NMR (101 MHz, CDCl3) δ 14.25, 22.82, 28.89, 31.23, 31.83, 35.80, 118.31, 120.83, 121.03, 122.84, 123.22, 123.26, 124.20, 125.01, 125.73, 126.25, 126.35, 127.35, 127.40, 128.39, 128.52, 128.92, 129.39, 129.79, 129.95, 130.32, 131.81, 132.44, 135.60, 136.36, 137.57, 139.36, 145.07, 150.42, 161.29, 196.69. HRMS (ESI+, m/z) calcd for $C_{40}H_{35}N_2O_2$, $[M+H]^+$ m/z = 575.2684, found 575.2693

Synthesis of 5b:
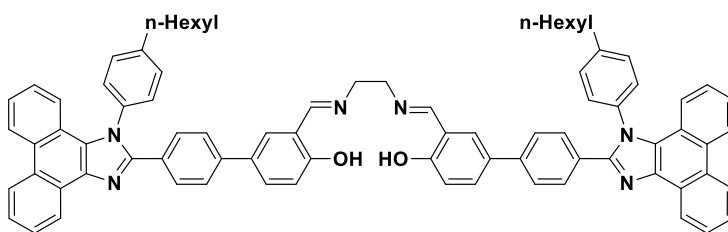
To 100 mL one neck RB, compound **4b** (0.86 mmol, 0.50 g, 2.0 equiv.) and ethylene diamine (0.43 mmol, 29 μL, 1.0 equiv.) were added to dry methanol and refluxed overnight. The reaction mixture was filtered and the resultant yellow solid of compound **5b** was collected. Yield: 91% (0.460 g). ^{1}H NMR (400 MHz, CDCl3) δ 13.26 (s, 2H), 8.88 (d, *J* = 8.0 Hz, 2H), 8.75 (d, *J* = 8.4 Hz, 2H), 8.69 (d, *J* = 8.3 Hz, 2H), 8.39 (s, 2H), 7.73 (t, *J* =

7.5 Hz, 2H), 7.68-7.58 (m, 6H), 7.54-7.45 (m, 4H), 7.45 – 7.34 (m, 14H), 7.27 – 7.14 (m,

4H), 6.99 (d, J = 8.5 Hz, 2H), 3.96 (s, 4H), 2.78 (t, J = 7.6 Hz, 4H), 1.79-1.68 (m, 4H),

1.44 – 1.26 (m, 12H), 0.91 (t, J = 6.4 Hz, 6H). ^{13}C NMR (101 MHz, CDCl$_3$) δ 14.26,

22.83, 28.90, 31.24, 31.84, 35.81, 59.89, 117.67, 118.84, 121.04, 122.87, 123.25, 124.19,

124.93, 125.67, 126.21, 126.33, 127.38, 128.38, 128.46, 128.94, 129.16, 129.36, 129.81,

129.92, 130.29, 131.17, 136.41, 137.56, 140.35, 145.01, 150.72, 160.97, 166.6. HRMS

(ESI+, m/z) calcd for C$_{82}$H$_{72}$N$_6$O$_2$, [M]$^+$ m/z = 1173.5604, found 1173.5790

Synthesis of 6b:
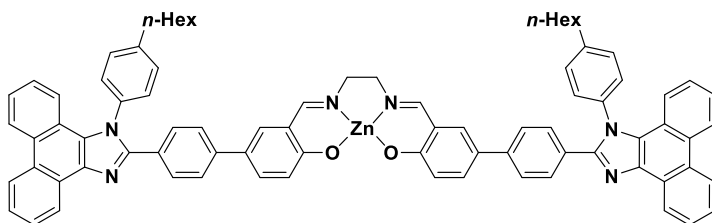
To 100 mL one neck RB, compound **5b** (0. 150 g, 0.12 mmol, 1.0 equiv.) was dissolved in 10 mL of

CH$_2$Cl$_2$ and a solution of Zn(OAc)$_2$.2H$_2$O (0.031 g, 0.14 mmol, 1.1 equiv.) in 10 mL dry

methanol was added dropwise. The greenish-yellow solution was refluxed for 12 h. The

precipitate formed was filtered and washed with diethyl to get compound **6b**. Yield: 79%

(0.117 g). ^{1}H NMR (400 MHz, DMSO) δ 8.88 (d, J = 8.5 Hz, 2H), 8.83 (d, J = 8.4 Hz,

2H), 8.71 (d, J = 7.9 Hz, 2H), 8.54 (s, 2H), 8.26 (s, 2H), 7.75 (t, J = 7.5 Hz, 2H), 7.67 (t,

J = 7.6 Hz, 2H), 7.63 – 7.47 (m, 20H), 7.28 (t, J = 7.7 Hz, 2H), 7.13 (d, J = 8.2 Hz, 2H),

6.75 (d, J = 8.7 Hz, 2H), 3.79 (s, 4H), 2.80 (t, J = 7.4 Hz, 4H), 1.73 (t, J = 7.3 Hz, 4H),

1.43-1.26 (m, 12H), 0.90 (t, J = 6.6 Hz, 6H) ppm. ^{13}C NMR (101 MHz, DMSO-D_6) δ

13.89, 22.14, 27.97, 30.52, 31.09, 34.76, 55.84, 119.27, 122.81, 123.43, 124.46, 124.96,

125.54, 126.34, 126.71, 127.25, 127.61, 127.78, 128.39, 128.77, 129.27, 130.16, 130.89,

132.73, 135.91, 136.51, 140.38, 168.12, 171.12 ppm. MALDI-MS Calcd for

C$_{82}$H$_{71}$N$_6$O$_2$Zn, [M+H]$^+$ m/z = 1235.4, found 1235.3. Anal. Calcd for C$_{82}$H$_{70}$N$_6$O$_2$Zn: C,

79.63; H, 5.70; N, 6.79. Found: C, 79.45; H, 6.30; N, 6.92.

General procedure for the cycloaddition reaction of epoxides with CO_2 at atmospheric pressure

The cycloaddition reaction of epoxides and CO_2 was conducted in a 20 mL Q-Tube equipped with a pressure gauge. In a typical reaction, the Q-tube was loaded with zinc catalyst (0.5 mol%), TBAI (2.5 mol%), and epoxide (1.8 mmol) at room temperature. The Q-tube was sealed with the pressure gauge and was evacuated by freeze-thaw cycles. After the process was completed, the Q-Tube was filled with CO_2 and the pressure was adjusted to 1 bar. The reaction set-up was kept at the center of a photochemical reactor (Sigma-Aldrich Micro Photochemical Reactor, blue LED lights at a distance of 7 cm from LED lights). A representative image of the set-up is shown in figure 3A.7. The reaction was then irradiated with 6 W blue LED with wavelength ranging between 435-445 nm and stirred for 24 hours. The conversion of epoxides and NMR yield of cyclic carbonates were determined using 1,3,5-trimethyl benzene as the internal standard in $CDCl_3$. Then, the reaction mixture was diluted with dichloromethane and the product was isolated by column chromatography using ethyl acetate/n-hexane as the eluent.

Analytical data of cyclic carbonates:

Compound 8a[19]**:** Yield: 91% (0.236 g). ^{1}H NMR (400 MHz, $CDCl_3$) δ 4.71 – 4.65 (m, 1H), 4.51 (t, J = 8.1 Hz, 1H), 4.05 (t, J = 8.24 Hz, 1H), 1.82 – 1.73 (m, 1H), 1.71 – 1.61 (m, 1H), 1.50 – 1.28 (m, 4H), 0.89 (t, J = 6.9 Hz, 3H). ^{13}C NMR (101 MHz, $CDCl_3$) δ 13.85, 22.29, 26.48, 33.58, 69.49, 77.18, 155.23.

 Compound 8b[19]**:** Yield: 71% (0.130 g). ^{1}H NMR (400 MHz, $CDCl_3$) δ 4.87 – 4.79 (m,

1H), 4.58 (t, $J = 7.8$ Hz, 1H), 4.04 (t, $J = 7.5$ Hz, 1H), 1.48 (d, $J = 6.1$ Hz, 3H). ^{13}C NMR (101 MHz, CDCl$_3$) δ 19.03, 70.55, 73.59, 155.05.

Compound 8c[19]**:** Yield: 87% (0.224 g).^{1}H NMR (400 MHz, CDCl$_3$) δ 5.03 – 4.91 (m, 1H), 4.61 (t, $J = 8.6$ Hz, 1H), 4.42 (dd, $J = 8.9, 5.7$ Hz, 1H), 3.84 (dd, $J = 12.2, 4.8$ Hz, 1H), 3.76 (dd, $J = 12.4, 3.6$ Hz, 1H). ^{13}C NMR (101 MHz, CDCl$_3$) δ 154.52, 154.48, 74.48, 74.43, 66.87, 66.83, 44.19, 44.15.

Compound 8d[19]**:** Yield: 88% (0.225 g).^{1}H NMR (400 MHz, CDCl$_3$) δ 5.82 – 5.61 (m, 1H), 5.09 – 4.87 (m, 2H), 4.76 – 4.60 (m, 1H), 4.47 (t, $J = 8.2$ Hz, 1H), 4.02 (t, $J = 7.7$ Hz, 1H), 2.25 – 2.02 (m, 2H), 1.90 – 1.77 (m, 1H), 1.77 – 1.65 (m, 1H). ^{13}C NMR (101 MHz, CDCl$_3$) δ 28.49, 32.77, 69.27, 76.36, 116.04, 136.13, 154.98.

Compound 8e[20]**:** Yield: 74% (0.152 g).^{1}H NMR (400 MHz, CDCl$_3$) δ 5.86 (ddd, $J = 17.2, 10.4, 6.9$ Hz, 1H), 5.46 (d, $J = 17$ Hz, 1H), 5.38 (d, $J = 10.48$ Hz, 1H), 5.15 – 5.03 (m, 1H), 4.56 (t, $J = 8.4$ Hz, 1H), 4.11 (dd, $J = 8.6, 7.4$ Hz, 1H). ^{13}C NMR (101 MHz, CDCl$_3$) δ 69.11, 77.38, 121.15, 132.19, 154.88.

Compound 8f[20]**:** Yield: 87% (0.257 g). ^{1}H NMR (400 MHz, CDCl$_3$) δ 7.44-7.34 (m, 3H), 7.34-7.25 (m, 2H), 5.64 (t, $J = 8.0$ Hz, 1H), 4.75 (t, $J = 8.5$ Hz, 1H), 4.26 (t, $J = 8.2$ Hz, 1H).^{13}C NMR (101 MHz, CDCl$_3$) δ 70.97, 77.84, 125.81, 128.91, 129.39, 135.69, 154.86.

Compound 8g[20]**:** Yield: 72% (0.251 g). ^{1}H NMR (400 MHz, CDCl$_3$) δ 7.35 – 7.28 (m, 2H), 7.02 (t, $J = 7.3$ Hz, 1H), 6.96 – 6.87 (m, 2H), 5.06 – 5.00 (m, 1H), 4.62 (t, $J = 8.4$ Hz, 1H), 4.54 (dd, $J = 8.5, 5.9$ Hz, 1H), 4.24 (dd, $J = 10.5, 4.2$ Hz, 1H), 4.15 (dd, $J = 10.6, 3.5$ Hz, 1H). ^{13}C NMR (101 MHz, CDCl$_3$) δ 157.86, 154.79, 129.83, 122.12, 114.71, 74.22, 66.96, 66.37.

Compound 8h[21]**:** Yield: 82% (0.331 g). X-ray quality crystals were grown from CHCl$_3$-

hexane solvent system. ^{1}H NMR (400 MHz, CDCl$_3$) δ 6.84 (s, 4H), 5.05 – 4.97 (m, 1H), 4.60 (t, J = 8.4 Hz, 1H), 4.53 (dd, J = 8.5, 5.9 Hz, 1H), 4.18 (dd, J = 10.6, 4.2 Hz, 1H), 4.10 (dd, J = 10.6, 3.6 Hz, 1H), 3.77 (s, 3H). ^{13}C NMR (101 MHz, CDCl$_3$) δ 55.84, 66.37, 67.91, 74.33, 114.91, 115.90, 152.03, 154.82

Compound 8i[22]**:** Yield: 89% (0.378 g). ^{1}H NMR (400 MHz, CDCl$_3$) δ 7.12 (d, J = 8.1 Hz, 2H), 6.82 (d, J = 8.3 Hz, 2H), 5.04 - 4.88 (m, 1H), 4.61 – 4.48 (m, 1H), 4.48 – 4.37 (m, 1H), 4.17 (d, J = 10.5 Hz, 1H), 4.05 (d, J = 10.4 Hz, 1H), 2.84 (sept, J = 6.8 Hz, 1H), 1.20 (d, J = 7.1 Hz, 6H). ^{13}C NMR (101 MHz, CDCl$_3$) δ 24.07, 33.17, 66.12, 67.00, 74.45, 114.38, 127.37, 142.21, 154.97, 155.87.

Compound 8j: Yield: 90% (0.366 g).^{1}H NMR (400 MHz, CDCl$_3$) δ 7.28 (dd, J = 8.4, 5.5 Hz, 2H), 7.01 (t, J = 8.6 Hz, 2H), 4.86 – 4.77 (m, 1H), 4.56 – 4.49 (m, 2H), 4.46 (t, J = 8.4 Hz, 1H), 4.34 (dd, J = 8.4, 5.9 Hz, 1H), 3.70 (dd, J = 11.2, 3.3 Hz, 1H), 3.58 (dd, J = 11.2, 3.7 Hz, 1H). ^{13}C NMR (101 MHz, CDCl$_3$) δ 66.06, 68.80, 72.53, 75.12, 115.11 (d, J_{C2-F} = 21 Hz), 129.33 (d, J_{C3-F} = 8 Hz), 133.06 (d, J_{C4-F} = 3 Hz), 155.03, 162.18 (d, J_{C1-F} = 244 Hz). ^{19}F NMR (376 MHz, CDCl$_3$) δ -113.93. HRMS (ESI+, m/z) calcd for C$_{11}$H$_{11}$FO$_4$Na, [M+Na]$^+$ m/z = 249.0534, found 249.0538

Compound 8k[19]**:** Yield: 88% (0.329 g). ^{1}H NMR (400 MHz, CDCl$_3$) δ 7.40 – 7.19 (m, 5H), 4.76 (m, 1H), 4.59 – 4.48 (m, 2H), 4.39 (t, J = 8.4 Hz, 1H), 4.30 (dd, J = 8.4, 6.1 Hz, 1H), 3.66 (dd, J = 11.2, 3.3 Hz, 1H), 3.54 (dd, J = 11.2, 3.8 Hz, 1H). ^{13}C NMR (101 MHz, CDCl$_3$) δ 66.05, 68.73, 73.26, 75.10, 127.49, 127.77, 128.33, 137.12, 155.05.

Compound 8l: Yield: 62% (0.252 g). ^{1}H NMR (400 MHz, CDCl$_3$) δ 7.36 (t, J = 7.7 Hz, 1H), 7.28 (dd, J = 7.4 Hz, 1H), 7.13 (t, J = 7.5 Hz, 1H), 7.03 (t, J = 9.2 Hz, 1H), 4.86 – 4.77 (m, 1H), 4.66 – 4.56 (m, 2H), 4.46 (t, J = 8.4 Hz, 1H), 4.35 (dd, J = 8.4, 6.1 Hz, 1H), 3.74 (dd, J = 11.2, 3.4 Hz, 1H), 3.62 (dd, J = 11.1, 3.7 Hz, 1H).^{13}C NMR (101 MHz,

CDCl$_3$) δ 66.09, 66.98, 67.01, 69.07, 75.08, 115.14 (d, $J_{C2\text{-}F}$ = 21 Hz), 124.15 (d, $J_{C3\text{-}F}$ = 15 Hz), 124.17 (d, $J_{C6\text{-}F}$ = 4 Hz), 129.75 (d, $J_{C4\text{-}F}$ = 8 Hz), 129.97 (d, $J_{C5\text{-}F}$ = 4 Hz), 155.07, 160.55 (d, $J_{C1\text{-}F}$ = 246 Hz). ^{19}F NMR (376 MHz, CDCl$_3$) δ -118.73. HRMS (ESI+, m/z) calcd for C$_{11}$H$_{12}$FO$_4$, [M+H]$^+$ m/z = 227.0725, found 227.0714

Compound 8m: Yield: 90% (0.359 g). ^{1}H NMR (400 MHz, CDCl$_3$) δ 7.19 – 7.12 (m, 1H), 7.12 – 7.01 (m, 3H), 4.68 – 4.58 (m, 1H), 4.49 – 4.35 (m, 2H), 4.28 (t, J = 8.4 Hz, 1H), 4.17 (t, J = 8.4, 1H), 3.57 (dd, J = 11.2, 3.3 Hz, 1H), 3.44 (dd, J = 11.2, 3.7 Hz, 1H), 2.19 (s, 3H). ^{13}C NMR (101 MHz, CDCl$_3$) δ 18.53, 66.04, 68.79, 71.80, 75.09, 125.63, 127.99, 128.45, 130.17, 135.01, 136.63, 155.02. HRMS (ESI+, m/z) calcd for C$_{12}$H$_{14}$O$_4$Na, [M+Na]$^+$ m/z = 245.0784, found 245.0796

Compound 8n: Yield: 76% (0.325 g). ^{1}H NMR (400 MHz, CDCl$_3$) δ 7.23 (d, J = 8.1 Hz, 2H), 6.87 (d, J = 8.0 Hz, 2H), 4.81 – 4.71 (m, 1H), 4.54 – 4.44 (m, 2H), 4.44 (t, J = 8.6 Hz, 1H), 4.30 (t, J = 7.1 Hz, 1H), 3.76 (s, 3H), 3.65 (dd, J = 11.3, 3.4 Hz, 1H), 3.53 (dd, J = 11.4, 3.8 Hz, 1H).^{13}C NMR (101 MHz, CDCl$_3$) δ 55.03, 66.08, 68.39, 72.93, 75.11, 113.65, 129.12, 129.21, 155.01, 159.19. HRMS (ESI+, m/z) calcd for C$_{12}$H$_{14}$O$_5$Na, [M+Na]$^+$ m/z = 261.0740, found 261.0733

Compound 8o: Yield: 83% (0.355 g). ^{1}H NMR (400 MHz, CDCl$_3$) δ 7.22 – 7.09 (m, 2H), 6.82 (t, J = 7.5 Hz, 1H), 6.74 (d, J = 8.3 Hz, 1H), 4.69 – 4.59 (m, 1H), 4.51 – 4.42 (m, 2H), 4.27 (t, J = 8.4 Hz, 1H), 4.20 (dd, J = 8.4, 6.0 Hz, 1H), 3.67 (s, 3H), 3.59 (dd, J = 11.3, 3.4 Hz, 1H), 3.47 (dd, J = 11.2, 3.8 Hz, 1H). ^{13}C NMR (101 MHz, CDCl$_3$) δ 55.00, 65.98, 68.19, 68.88, 75.14, 110.03, 120.14, 125.34, 128.64, 128.84, 154.99, 156.85. HRMS (ESI+, m/z) calcd for C$_{12}$H$_{14}$O$_5$Na, [M+Na]$^+$ m/z = 261.0741, found 261.0733

Compound 8p: Yield: 71% (0.283 g). ^{1}H NMR (400 MHz, CDCl$_3$) δ 7.08 (d, J = 8.0 Hz, 2H), 7.02 (d, J = 8.0 Hz, 2H), 4.69 – 4.59 (m, 1H), 4.46 – 4.33 (m, 2H), 4.29 (t, J = 8.4 Hz, 1H), 4.19 (t, J = 6.6 Hz, 1H), 3.54 (dd, J = 11.2, 3.5 Hz, 1H), 3.42 (dd, J = 11.1, 3.7 Hz, 1H), 2.21 (s, 3H). ^{13}C NMR (101 MHz, CDCl$_3$) δ 20.96, 66.10, 68.56, 73.20, 75.12, 127.69, 129.02, 134.06, 137.54, 155.03. HRMS (ESI+, m/z) calcd for C$_{12}$H$_{14}$O$_4$Na, [M+Na]$^+$ m/z = 245.0799, found 245.0784.

3A.5 References

1. (a) M. Bendikov, F. Wudl, D. F. Perepichka, *Chem. Rev.* **2004,** *104*, 4891-4945; (b) J. E. Anthony, *Chem. Rev.* **2006,** *106*, 5028-5048; (c) J. Wu, W. Pisula, K. Mullen, *Chem. Rev.* **2007,** *107*, 718-747.

2. (a) T. Baumgartner, F. Jäkle, John Wiley & Sons: Hoboken, NJ, **2018**. (b) F. Vidal, F. Jäkle, *Angew. Chem., Int. Ed.* **2019**, *58*, 5846−5870. (c) X. M. He, T. Baumgartner, *RSC Adv.* **2013**, *3*, 11334−11350. (d) A. M. Priegert, B. W. Rawe, S. C. Serin, D. P. Gates, *Chem. Soc. Rev.* **2016**, *45*, 922−953. (e) G. Y. Zhang, J. B. Zhao, P. C. Y. Chow, K. Jiang, J. Q. Zhang, Z. L. Zhu, J. Zhang, F. Huang, H. Yan, *Chem. Rev.* **2018**, *118*, 3447−3507. (f) M. Gon, K. Tanaka, Y. Chujo, *Polym. J.* **2018**, *50*, 109−126. (g) A. Fukazawa, S. Yamaguchi, *Chem. Asian. J.* **2009,** *4*, 1386-1400; (h) A. Narita, X. Y. Wang, X. Feng, K. Mullen, *Chem. Soc. Rev.* **2015,** *44*, 6616-6643 (i) M. Stepien, E. Gonka, M. Zyla, N. Sprutta, *Chem. Rev.* **2017,** *117*, 3479-3716. (j) E. von Grotthuss, A. John, T. Kaese, M. Wagner, *Asian J. Org. Chem.* **2018**, *7*, 37−53.

3. (a) M. Yusuf, K. Liu, F. Guo, R. A. Lalancette, F. Jäkle, *Dalton. Trans.* **2016,** *45*, 4580-4587 (b) Z. J. Zhao, Z. F. Chang, B. R. He, B. Chen, C. M. Deng, P. Lu, H.

Y. Qiu, B. Z. Tang, *Chem. - Eur. J.* **2013**, *19,* 11512−11517. (c) Y. L. Rao, C. Hörl, H. Braunschweig, S. N. Wang, *Angew. Chem., Int. Ed.* **2014**, *53*, 9086−9089. (d) M. S. Baranov, K. M. Solntsev, N. S. Baleeva, A. S. Mishin, S. A. Lukyanov, K. A. Lukyanov, I. V. Yampolsky, *Chem. - Eur. J.* **2014**, *20*, 13234−13241. (e) K. K. Neena, P. Sudhakar, P. Thilagar, *Angew. Chem. Int. Ed.* **2018**, 57, 16806–16810. (f) V. F. Pais, M. M. Alcaide, R. Lopez-Rodriguez, D. Collado, F. Najera, E. Perez-Inestrosa, E. Alvarez, J. M. Lassaletta, R. Fernandez, R, A. Ros, U. Pischel, *Chem. Eur. J.* **2015**, *21*, 15369−15376. (g) B. Y. W. Wong, H. L. Wong, Y. C. Wong, M. Y. Chan, V. W. W. Yam, *Chem. Eur. J.* **2016**, *22*, 15095−15106. (h) R. Y. Zhao, C. D. Dou, Z. Y. Xie, J. Liu, L. X. Wang, *Angew. Chem., Int. Ed.* **2016**, *55*, 5313−5317. (i) K. Matsuo, T. Yasuda, *Chem. Commun.* **2017**, *53*, 8723−8726. (j) R. Hecht, J. Kade, D. Schmidt, A. Nowak-Krol, *Chem. Eur. J.* **2017**, *23*, 11620−11628. (k) S. Pang, M. Mas-Montoya, M. Xiao, C.́ Duan, Z. Wang, X. Liu, R. Janssen, G. Yu, F. Huang, Y. Cao, *Chem. Eur. J.* **2018**, *25*, 564−572. (l) M. Grandl, B. Rudolf, Y. Sun, D. F. Bechtel, A. J. Pierik, F. Pammer, *Organometallics* **2017,** *36* (14), 2527-2535. (m) C. Zhu, X. Ji, D. You, T. L. Chen, A. U. Mu, K. P. Barker, L. M. Klivansky, Y. Liu, L. Fang, *J. Am. Chem. Soc.* **2018,** *140*, 18173-18182. (n) D. Kunchala, S. Sa, P. Nayak, S. J. Ponniah, K. Venkatasubbaiah, *Organometallics* **2019,** *38*, 870-878; (o) A. C. Murali, P. Nayak, K. Venkatasubbaiah, *Dalton Trans.* **2022**, *51***,** 5751-5771 (p) M. Gon, K. Tanaka, Y. Chujo, *Bull. Chem. Soc. of Jap.* **2019,** *92*, 7-18.

4. (a) Y.-L. Rao, H. Amarne, S. Wang, *Coord. Chem. Rev.* **2012,** *256*, 759-770. (b) D. Li, H. Zhang, Y. Wang, *Chem. Soc. Rev.* **2013,** *42*, 8416-8433. (c) D. L. Crossley, I. Vitorica-Yrezabal, M. J. Humphries, M. L. Turner, M. J. Ingleson,

Chem. - Eur. J. **2016**, *22*, 12439−12448. (d) D. L. Crossley, I. A. Cade, E. R. Clark, A. Escande, M. J. Humphries, S. M. King, I. Vitorica-Yrezabal, M. J. Ingleson, M. L. Turner, *Chem. Sci.* **2015,** *6*, 5144-5151. (e) K. Liu, R. A. Lalancette, F. Jäkle, *J. Am. Chem. Soc.* **2019**, *141*, 7453-7462. (f) K. Liu, R. A. Lalancette, F. Jäkle, *J. Am. Chem. Soc.* **2017**, *139*, 18170-18173. (g) S. K. Mellerup, C. Li, T. Peng, S. N. Wang, *Angew. Chem., Int. Ed.* **2017**, *56*, 6093−6097.

5. (a) M. Aresta, A. Dibenedetto, *Catal.* **2004,** *98* (4), 455-462; (b) I. Omae, *Catal.* **2006,** *115*, 33-52; (c) C. Song, *Catal.* **2006,** *115*, 2-32; (d) M. Aresta; A. Dibenedetto, *Dalton. Trans.* **2007,** 2975-2992; (e) J.-C. C. Toshiyasu Sakakura, Hiroyuki Yasuda, *Chem. Rev.* **2007,** *107*, 2365-2387. (f) E. S. Sanz-Perez, C. R. Murdock, S. A. Didas, C. W. Jones, *Chem. Rev.*, **2016**, *116*, 11840-11876.

6. (a) I. I. F. Boogaerts, S. P. Nolan, *Chem. Commun.* **2011,** *47*, 3021-3024; (b) M. Cokoja, C. Bruckmeier, B. Rieger, W. A. Herrmann, F. E. Kuhn, *Angew. Chem. Int. Ed. Engl.* **2011,** *50*, 8510-8537; (c) R. Martin, A. W. Kleij, *ChemSusChem* **2011,** *4*, 1259-1263; (d) M. Peters, B. Kohler, W. Kuckshinrichs, W. Leitner, P. Markewitz, T. E. Muller, *ChemSusChem* **2011,** *4*, 1216-1240; (e) Y. Tsuji, T. Fujihara, *Chem. Commun.* **2012,** *48*, 9956-9964; (f) N. Kielland, C. J. Whiteoak, A. W. Kleij, *Adv. Synth. Catal.* **2013,** *355*, 2115-2138. (g) D. C. Grills; M. Z. Ertem, M. McKinnon, K. T. Ngo, J. Rochford, *Coord. Chem. Rev.* **2018**, *374*, 173-217.

7. (a) A. Decortes, A. M. Castilla, A. W. Kleij, *Angew. Chem. Int. Ed. Engl.* **2010,** *49*, 9822-9837; (b) M. North, R. Pasquale, C. Young, *Green Chem.* **2010,** *12*, 1514-1539; (c) P. P. Pescarmona, M. Taherimehr, *Catal. Sci. Technol.* **2012,** *2*,

2169-2187; (d) C. J. Whiteoak, N. Kielland, V. Laserna, E. C. Escudero-Adan, E. Martin, A. W. Kleij, *J. Am. Chem. Soc.* **2013,** *135*, 1228-1231; (e) J. W. Comerford, I. D. V. Ingram, M. North, X. Wu, *Green Chem.* **2015,** *17*, 1966-1987; (f) V. D'Elia, J. D. A. Pelletier, J.-M. Basset, *ChemCatChem* **2015,** *7*, 1906-1917; (g) C. Martín, G. Fiorani, A. W. Kleij, *ACS Catalysis* **2015,** *5*, 1353-1370; (h) M. Alves, B. Grignard, R. Mereau, C. Jerome, T. Tassaing, C. Detrembleur, *Catal. Sci. Technol.* **2017,** *7*, 2651-2684; (i) F. Chen, N. Liu, B. Dai, *ACS Sustain. Chem. Eng.* **2017,** *5*, 9065-9075; (j) R. R. Shaikh, S. Pornpraprom, V. D'Elia, *ACS Catalysis* **2017,** *8*, 419-450; (k) Z. Zhao, J. Qin, C. Zhang, Y. Wang, D. Yuan, Y. Yao, *Inorg Chem* **2017,** *56*, 4569-4576; (l) H. Ullah, B. Mousavi, H. A. Younus, Z. A. K. Khattak, S. Chaemchuen, S. Suleman, F. Verpoort, *Commun. Chem.* **2019,** *2*, 42.

8. (a) X.-B. Lu, Y.-J. Zhang, B. Liang, X. Li, H. Wang, *J. Mol. Catal. A Chem.* **2004,** *210*, 31-34; (b) W. Clegg, R. W. Harrington, M. North, R. Pasquale, *Chem. - Eur. J.* **2010,** *16*, 6828-6843; (c) J. A. Castro-Osma, M. North, X. Wu, X., *Chem. - Eur. J.* **2016,** *22*, 2100-2107.

9. (a) W.-L. .D Yu-Mei Shen, Min Shi., *J. Org. Chem.* **2003,** *68*, 1559-1562 (b) A. Decortes, M. Martinez Belmonte, J. Benet-Buchholz, A. W. Kleij, *Chem. Commun.* **2010,** *46*, 4580-4582; (c) R. M. Haak, A. Decortes, E. C. Escudero-Adan, M. Martinez Belmonte, E. Martin, J. Benet-Buchholz, A. W. Kleij, *Inorg. Chem.* **2011,** *50*, 7934-7936; (d) M. Taherimehr, A. Decortes, S. M. Al-Amsyar, W. Lueangchaichaweng, C. J. Whiteoak, E. C. Escudero-Adán, A. W. Kleij, P. P. Pescarmona, *Catal. Sci. Technol.* **2012,** *2*, 2231-2237; (e) Y. Ren, J. Chen, C. Qi, H. Jiang, *ChemCatChem* **2015,** *7*, 1535-1538.

10. J. Donald, R. M. M. Darensbourg, *J. Am. Chem. Soc.* **2005,** *127*, 14026-14038.

11. (a) W.-L. D. Yu-Mei Shen, Min Shi, *J. Org. Chem.* **2003,** *68*, 1559-1562; (b) X. B. Lu, D. J. Darensbourg, *Chem. Soc. Rev.* **2012,** *41*, 1462-1484; (c) Y. A. Rulev, V. A. Larionov, A. V. Lokutova, M. A. Moskalenko, O. L. Lependina, V. I. Maleev, M. North, Y. N. Belokon, *ChemSusChem* **2016,** *9*, 216-222.

12. (a) M. V. Escarcega-Bobadilla, M. Martinez Belmonte, E. Martin, E. C. Escudero-Adan, A. W. Kleij, *Chem. - Eur. J.* **2013,** *19*, 2641-2648; (b) C. Martín, C. J. Whiteoak, E. Martin, M. Martínez Belmonte, E. C. Escudero-Adán, A. W. Kleij, *Catal. Sci. Technol.* **2014,** *4*, 1615-1621; (c) S. He, F. Wang, W. L. Tong, S. M. Yiu, M. C. Chan, *Chem. Commun.* **2016,** *52*, 1017-1020; (d) S. A. Kuznetsova, Y. A. Rulev, V. A. Larionov, A. F. Smol'yakov, Y. V. Zubavichus, V. I. Maleev, H. Li, M. North, A. S. Saghyan, Y. N. Belokon, *ChemCatChem* **2018,** *11*, 511-519. (e) K. Takaishi, B. D. Nath, Y. Yamada, H. Kosugi, T. Emma, *Angew. Chem. Int. Ed. Engl.*, **2019**, *58*, 9984-9988; (f) J. Liang, R-P. Chen, X.-Y. Wang, T.-T. Liu, X.-S. Wang, Y.-B. Huang, R. Cao, *Chem. Sci*, **2017**, *8*, 1570-1575.

13. M. Vanga, S. Sa, A. Kumari, A. C. Murali, P. Nayak, P, R. Das, K. Venkatasubbaiah, *Dalton. Trans.* **2020,** *49*, 7737-7746.

14. (a) A.L. Singer, D. A. A., *Inorg. Chim. Acta* **1998**, 157-162; (b) K. H. Chang, C. C. Huang, Y. H. Liu, Y. H. Hu, P. T. Chou, Y. C. Lin, *Dalton. Trans.* **2004,** 1731-1738.

15. K. Dhanunjayarao, S. Sa, B. P. R. Aradhyula, K. Venkatasubbaiah, *Tetrahedron* **2018,** *74*, 5819-5825.

16. A. D. Becke, *J. Chem. Phys.* **1993,** *98*, 5648-5652.

17. F. Dumur, E. Contal, G. Wantz, D. Gigmes, *Eur. J. Inorg. Chem.* **2014,** *2014*, 4186-4198.

18. A. Decortes, A. W. Kleij, *ChemCatChem* **2011,** *3*, 831-834.

19. Y. Hao, D. Yuan, Y. Yao, *ChemCatChem*, **2020**, *12*, 4346-4351.

20. K. Grollier, N. D. Vu, K. Onida, A. Akhdar, S. Norsic, F. D'Agosto, C. Boisson, N. Duguet, *Adv. Synth. Catal.,* **2020**, *362*, 1696-1705.

21. X. Guo, Z. Zhou, C. Chen, J. Bai, C. He, C. Duan, *ACS Appl Mater Interfaces*, **2016,** *8*, 31746-31756.

22. P. Heydari, A. Hafizi, M. R. Rahimpour, R. Khalifeh, *J. Environ. Chem. Eng*., **2020**, *8*, 104568-104578

23. (a) K. A. Andrea, F. M. Kerton, *ACS Catal.* **2019**, *9*, 1799−1809 (b) T.-T. Wang, Y. Xie, W.-Q. Deng, *J. Phys. Chem. A* **2014**, *118*, 39, 9239–9243 (c) J. Meléndez, M. North, R. Pasquale, *Eur. J. Inorg. Chem.* **2007**, *2007*, 3323−3326 (d) X. Wu, M. North, *ChemSusChem* **2017**, *10*, 74−78 (e) A. M. Hardman-Baldwin, A. E. Mattson, *ChemSusChem* **2014**, *7*, 3275-3278 (f) Y. Toda, T. Sakamoto, Y. Komiyama, A. Kikuchi, H. Suga, *ACS Catal.* **2017**, *7*, 9, 6150–6154 (g) L. Wang, G. Zhang, K. Kodama, T. Hirose, *Green Chem.* **2016**, *18*, 1229-1233 (h) A. Decortes, M. M. Belmonte, J. Benet-Buchholz, A. W. Kleij, *Chem. Commun.***, 2010**, *46*, 4580-4582 (i) M. Taherimehr, A. Decortes, S. M. Al-Amsyar, W. Lueangchaichaweng, C. J. Whiteoak, E. C. Escudero-Adán, A. W. Kleij, P. P. Pescarmona, *Catal. Sci. Technol.***, 2012**, *2*, 2231-2237 (j) M. V. Escárcega-Bobadilla, M. M. Belmonte, E. Martin, E. C. Escudero-Adán, A. W. Kleij, *Chem. Eur. J.* **2013**,*19*, 2641–2648 (k) Y. Xie, T.-T. Wang, R.-X. Yang, N.-Y. Huang, K. Zou, W.-Q. Deng, *ChemSusChem*, **2014**, *7*, 2110 – 2114

(l) S. A. Kuznetsova, Y. A. Rulev, V. A. Larionov, A. F. Smol'yakov, Y. V. Zubavichus, V. I. Maleev, H. Li, M. North, A. S. Saghyan, Y. N. Belokon, *ChemCatChem*, **2018**, *11*, 511-519

Chapter 3B

Four-coordinate boron functionalized phenanthroimidazole based zinc-salen as photocatalyst for the cycloaddition of CO_2 and aziridines

3B.1 Introduction

Boron-containing fluorophores have been evolving as innovative materials in the last decade.[1] Tunable optical properties and better luminescence quantum yields of these boron complexes increase their applicability in the fields of organic light-emitting diodes (OLEDs), photovoltaics, sensors, and organic field-effect transistors.[1l, 2] Among the different boron based fluorophores, boron-incorporated polycyclic aromatic hydrocarbons (PAHs), especially tetra-coordinated boron-embedded PAHs, have gained attraction owing to their tunable optical properties.[3] Recently we have reported monomers and dimers of tetracoordinate boron functionalized PAHs and studied their linear and non-linear properties.[4] We also reported the use of B-N coordinated PAH-based zinc-salen for the cycloaddition of CO_2 and epoxides.[5] Oxazolidinones are one of the important classes of organic compounds which act as chiral auxiliaries, intermediates in organic synthesis, and as pharmaceutical agents.[6] Some of the FDA-approved drugs such as Linezolid,[7] Tedizolid[8,] and Toloxatone[9] contain oxazolidinones motif in their structure. Conventionally, oxazolidinones were synthesized using toxic or reactive derivatives such as phosgene or carbonic acid which is not atom-economical.[10] Hence, much attention has been paid to the catalytic coupling of aziridines and CO_2. This methodology acts as an attractive alternative for the synthesis of oxazolidines which exploit the greenhouse gas CO_2 as a renewable C1 building block and a broad range of substituted aziridines. In the last decade, notable progress has been made in the design and synthesis of catalysts for the coupling of aziridines and CO_2 which includes superbases,[11] ionic liquids,[12] N-heterocyclic compounds,[13] metal complexes[14]. Catalyst-free and stoichiometric salts promoted CO_2/Aziridine coupling were also investigated with limited substrate scope at elevated temperature or high CO_2 pressure.[15] Although, a significant effort has been

made for the conversion of aziridines and CO_2 to oxazolidines; most of them operate at high pressure, high temperature, and/or high catalyst loading.[14a, 14c, 16]

Zinc-based complexes have been extensively used for the cycloaddition of CO_2 and epoxides[17] however, their use as a catalyst for the conversion of aziridines and CO_2 to oxazolidines is very scarcely reported. For instance, Park and co-workers[18] utilized a zinc-glutamate MOF, and Zhao and co-workers[11c] used a multicentered Zn(I)-Zn(I) bond-based MOF as a catalyst for the conversion of aziridines and CO_2 to oxazolidines. In this chapter, we report B-N coordinated phenanthroimidazole based zinc salen complex (Fig 3B.1) as a photocatalyst for the cycloaddition of CO_2 with aziridines.

3B.2 Results and discussion:
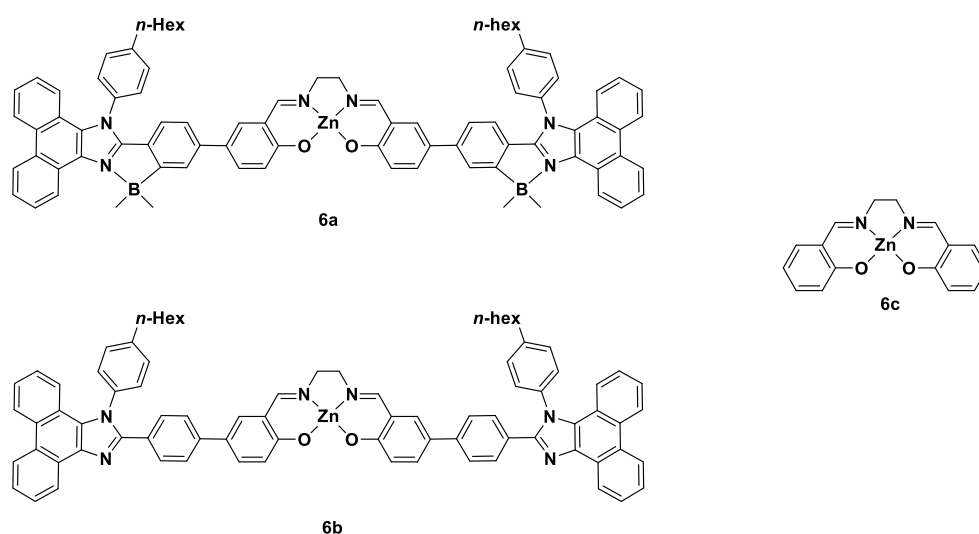
Figure 3B.1: Zn-salen's **6a-6c** used in this study

Motivated by the results presented in chapter 3A[5], we investigated the catalytic activity of **6a** (Fig**.** 3B.1) for the synthesis of oxazolidinone from 1-butyl-2-phenylaziridine under the irradiation of blue LED (6W, 435-445 nm) in solvent-free conditions with 1 bar carbon dioxide pressure. The reaction of 1-butyl-2-phenylaziridine with 0.5 mol% of **6a**, 2.5 mol% of tetrabutylammonium iodide

(TBAI) as a co-catalyst at 1 bar CO_2 pressure under blue light for 24 h resulted in 20 % of the 5-substituted oxazolidinone product with 100% regioselectivity (Table 3B.1, entry 1). With 3 mol% of TBAI, 63% of the desired product was observed (Table 3B.1, entry 3). However, further increase of the catalyst (**6a**) and TBAI loading did not show any significant impact on the catalytic activity (Table 3B.1, entries 2-8). Motivated by these results we further screened using tetrabutylammonium bromide (TBAB) as a co-catalyst. 5 mol% of TBAB and 1 mol% of **6a** resulted in 78% of the oxazolidinone product (Table 3B.1, entry 9). Finally, 1 mol% of **6a** and 7 mol% of TBAB with 1 bar CO_2 pressure under blue light for 24 h resulted in 95 % of 3-butyl-5-phenyloxazolidin-2-one product (Table 3B.1, entry 10). The significance of **6a** under blue light was realized when the reaction was performed under dark conditions, which resulted in 64 % of the product (Table 3B.1, entry 11). There was no significant impact on the catalytic activity on further varying the catalyst and co-catalyst loading (Table 3B.1, entry 12-14). Control reaction performed using catalyst **6a** (without TBAB) did not produce any product formation, (Table 3B.1, entry 23) however, 19% product formation was observed when the reaction was performed using TBAB (without catalyst **6a**) (Table 3B.1, entry 22). Other co-catalysts such as $^nBu_4NPF_6$, NaI, KBr, and Et_4NCl proved to be less efficient (Table 3B.1, entries 18 - 21). Increasing the pressure to 2 bar does not have a significant impact on the catalytic activity (Table 3B.1, entry 15). Decreasing the reaction time resulted in 84% of the product (Table 3B.1, entry 16). Efforts to use CH_2Cl_2, methanol, THF, or DMSO as a solvent under similar conditions did not yield the desired cyclic products in high yields (Table 3B.1, entry 24-27). The catalytic activity was reduced to half with simple zinc-salen catalyst **6c** (Table 3B.1, entry 29). The use of catalyst **6b** also gave a low yield of the desired product (Table 3B.1, entry 28) which shows the importance

of boron coordination. A high degree of planarity was achieved after boron coordination in **6a** which helps in effective conjugation. The effective conjugation plays a crucial role in driving the cycloaddition reaction between aziridine and CO_2.

Table 3B.1: Optimization of the cycloaddition of CO_2 and 1-butyl-2-phenylaziridine
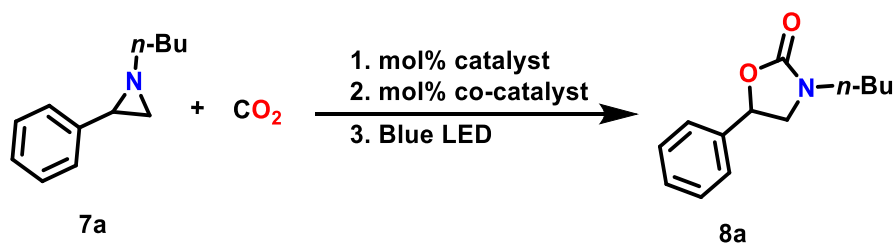
Sl. No.	Catalyst (mol %)	co-catalyst (mol %)	pCO_2 (bar)	Time	Yield[e] (%)
1.	**6a** (0.5)	TBAI (2.5)	1	24 h	20
2.	**6a** (0.5)	TBAI (2.5)	1	24 h	22
3.	**6a** (0.5)	TBAI (3)	1	24 h	63
4.	**6a** (0.5)	TBAI (4)	1	24 h	56
5.	**6a** (1.0)	TBAI (3)	1	24 h	61
6.	**6a** (1.0)	TBAI (5)	1	24 h	70
7.	**6a** (2.0)	TBAI (5)	1	24 h	55
8.	**6a** (2.0)	TBAI (10)	1	24 h	71
9.	**6a** (1.0)	TBAB (5)	1	24 h	78
10.	**6a (1.0)**	**TBAB (7)**	**1**	**24 h**	**95**
11.	**6a (1.0)**	**TBAB (7)**	**1**	**24 h**	**62 (dark)**
12.	**6a** (1.0)	TBAB (10)	1	24 h	85
13.	**6a** (1.5)	TBAB (7)	1	24 h	71

| 14.	**6a** (0.5)	TBAB (7)	1	24 h	76
15.	**6a** (1.0)	TBAB (7)	2	24 h	74
16.	**6a** (1.0)	TBAB (7)	1	20 h	84
17.	**6a** (1.0)	TBACl (7)	1	24 h	68
18.	**6a** (1.0)	$^{n}Bu_4NPF_6$ (7)	1	24 h	ND
19.	**6a** (1.0)	NaI (7)	1	24 h	57
20.	**6a** (1.0)	KBr (7)	1	24 h	09
21.	**6a** (1.0)	Et_4NCl (7)	1	24 h	ND
22.	------------	TBAB (7)	1	24 h	19
23.	**6a** (1.0)	-----------	1	24 h	ND
24[a].	**6a** (1.0)	TBAB (7)	1	24 h	73
25[b].	**6a** (1.0)	TBAB (7)	1	24 h	ND
26[c].	**6a** (1.0)	TBAB (7)	1	24 h	36
27[d].	**6a** (1.0)	TBAB (7)	1	24 h	42
28.	**6b** (1.0)	TBAB (7)	1	24 h	52
29.	**6c** (1.0)	TBAB (7)	1	24 h	51

[a]CH_2Cl_2, [b]THF, [c]DMSO, [d]Methanol, [e]NMR yield is calculated taking mesitylene as an internal standard.

As the photocatalyst **6a** absorbs between 325 - 425 nm, we further investigated the catalytic activity of the cycloaddition of 1-butyl-2-phenylaziridine and CO_2 using two different LEDs of different wavelengths, *viz*., 6W blue (435-445 nm) and 6W purple (400-410 nm) LEDs. Under the optimized conditions, we did not observe much difference in the catalytic activity when the reaction was performed under blue and purple LEDs (Fig 3B.2). In addition, the progress of the reaction of 1-butyl-2-phenylaziridine was monitored by NMR spectroscopy. The disappearance of

butyl peaks corresponding to the starting material was observed with the formation of the oxazolidinone product as the reaction progresses (Fig 3B.2). The NMR studies further reveal that only starting materials and/or the oxazolidinone product signals were present. Characteristic ^{1}H NMR peaks of the product appear between 3.5-6.0 ppm whereas the starting material peaks appear between 1.3 – 2.0 ppm (Fig 3B.2). Both blue and purple LEDs gave almost identical yields after 4h of the reaction (~54 %) and took 24h for the full conversion of the reactant. The percentage of yield *vs* time plot is provided in figure 3B.2 for both blue and purple LED reactions along with NMR spectra for the reaction mixture in different intervals of time. The reaction under UV light (365 nm) irradiation afforded 90% of the cyclic product.

To investigate the applicability of the photocatalyst **6a**, we screened different substrates under the optimized conditions. As shown in table 3B.2, different N-alkyl substituted phenylaziridines (*n*-butyl, *n*-hexyl, *n*-propyl, ethyl, and methyl) resulted in
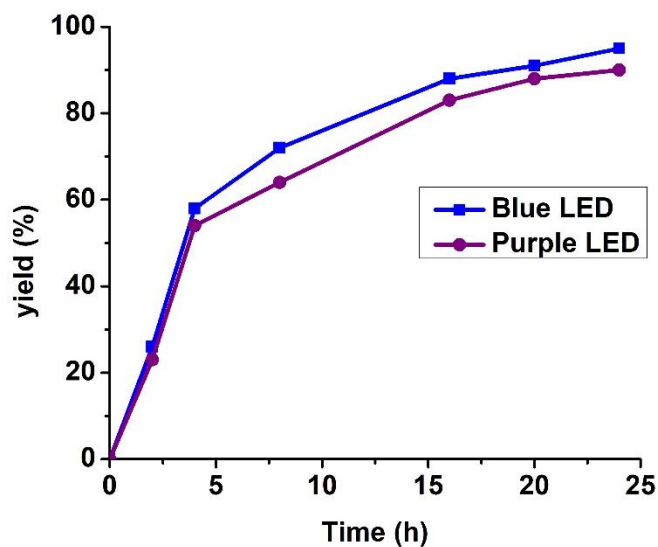
(a)
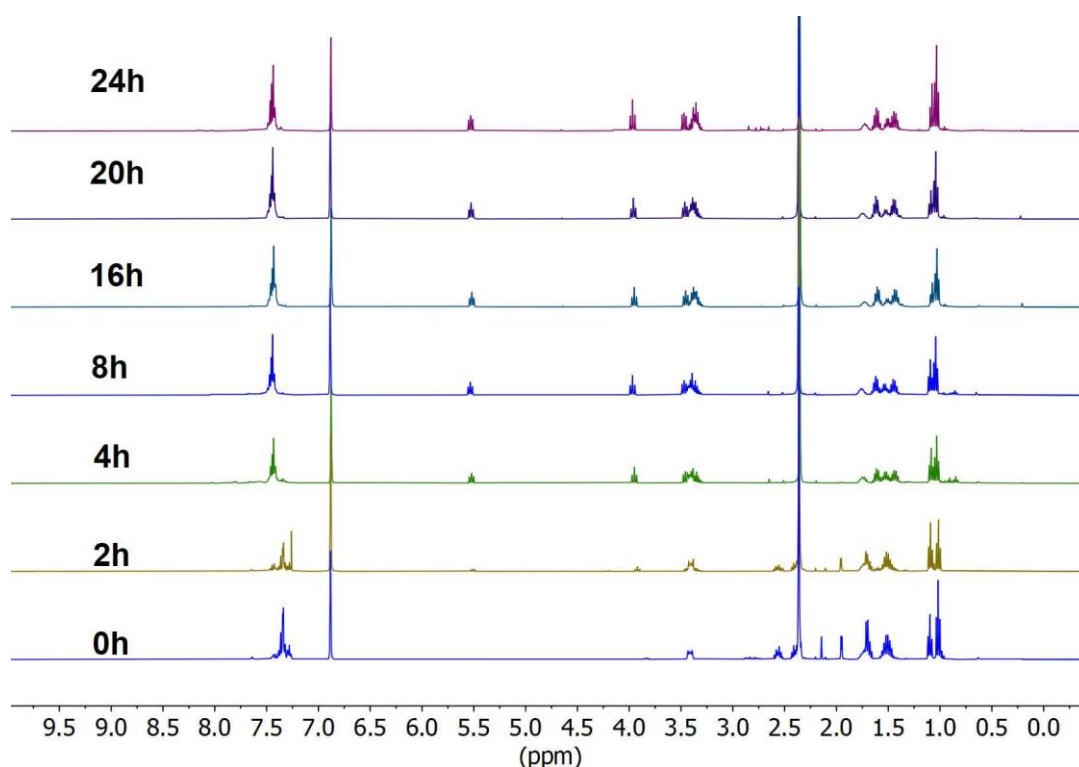
(b)

Figure 3B.2: (a) Stacked NMR spectra of the reaction mixture (mesitylene is used as an internal standard) in $CDCl_3$ at different time intervals (b) Yield (%) vs time plot of 1-butyl-2-phenylaziridine to 5-substituted oxazolidinone **8a** at 1 bar CO_2 pressure at room temperature (27 °C) under blue LED

respective oxazolidinones **8a**-**8e** in good to excellent yield. 2-Phenyl-1-(trifluoroethyl)aziridine on reaction with CO_2 under the optimized condition resulted moderate yield of 63% of the cyclic product (**8f**). Similarly, catalyst **6a** also showed good reactivity with different N-alkyl (*n*-hexyl, *n*-butyl, *n*-propyl, and ethyl) substituted 4-methylphenylaziridines to yield the desired products **8l**-**8o** in 92%, 81%, 94%, and 84% respectively. Aziridines with different benzyl derivatives at the nitrogen atom under similar conditions yielded the corresponding oxazolidinones (**8g**-**8k**) in 84%, 82%, 80%, 94%, and 95% respectively.

1-Benzyl-2-(4-(tert butyl)phenyl)aziridine, 1-benzyl-2-(4-fluorophenyl)aziridine and 1-benzyl-2-(4-chlorophenyl)aziridine on reaction with CO_2 yielded the corresponding oxazilidinones **8p**-**8r** in 81%, 76%, and 71% respectively. Due to steric factors in

substrates cyclopropyl and iso-propyl substituted phenylaziridines yielded 49% and 15% of cyclic product respectively (entry **8t** and **8u**) (Table 3B.2).
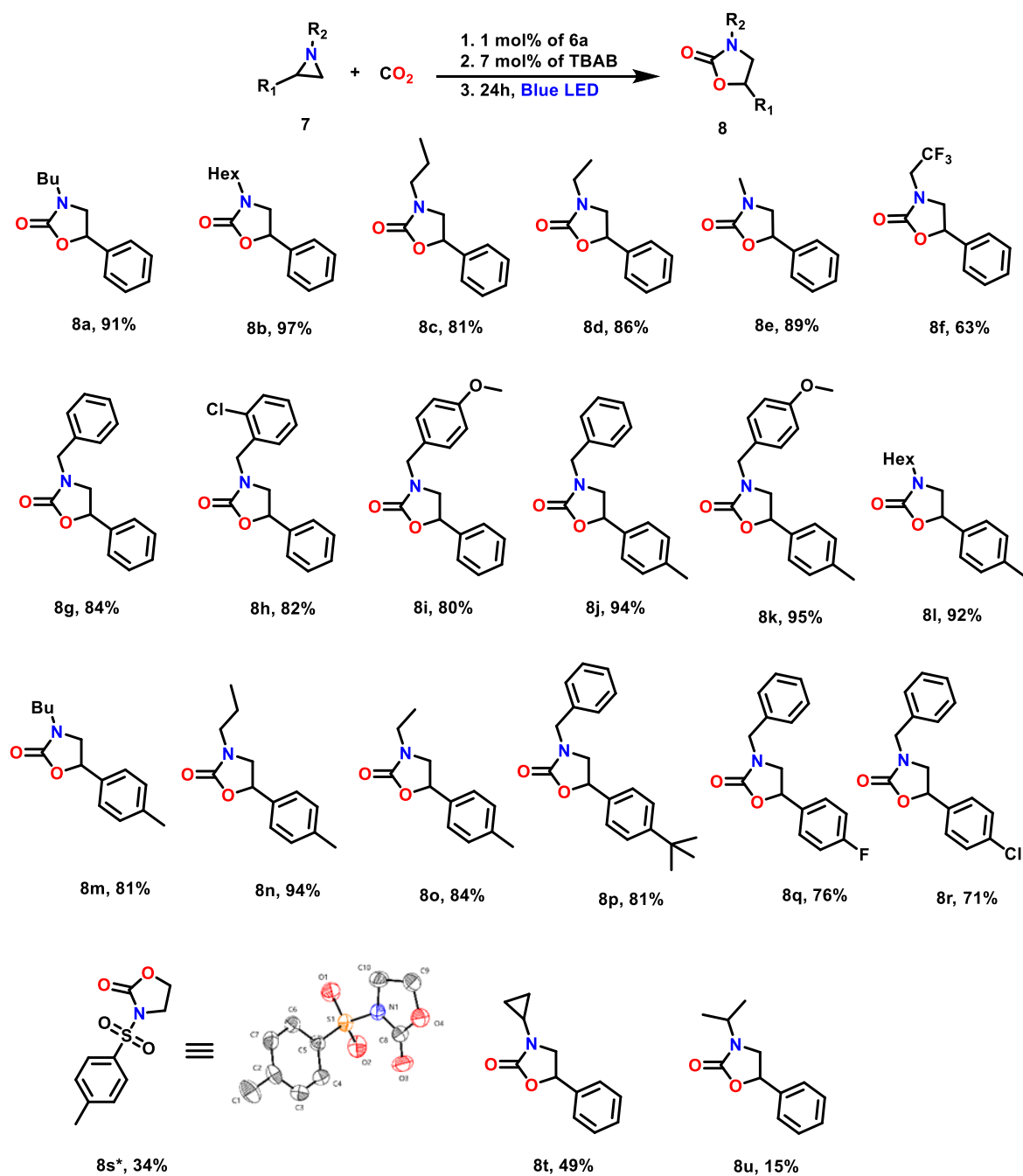
We have also isolated 3-butyl-5-phenyloxazolidin-2-one in gram scale under the optimized condition with 88% yield from 1 g of 1-butyl-2-phenylaziridine.(scheme 3B.1)
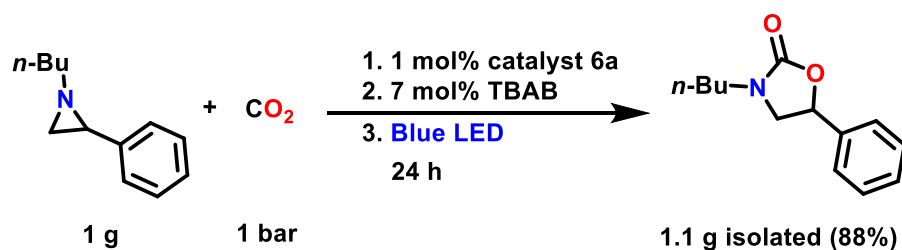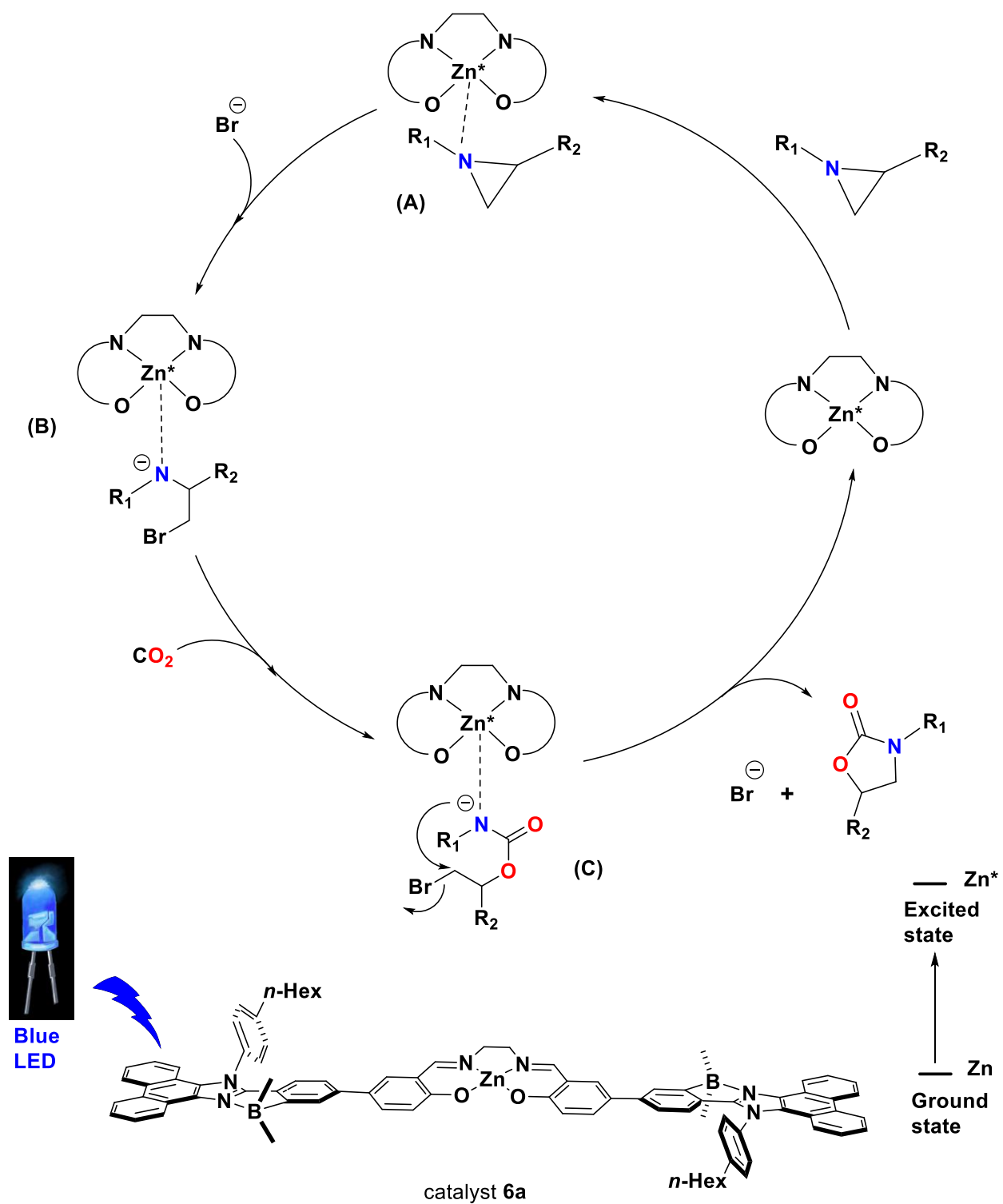

Scheme 3B.1: Gram scale reaction

A possible catalytic cycle for the cycloaddition of CO_2 and aziridines is proposed based on the literature (Scheme 3B.2). The catalytic cycle initiated with the binding of aziridine N-atom with the Lewis acidic zinc center in its excited state and thereby activating the aziridine ring to form the species A. Intramolecular nucleophilic attack by the bromine anion on the less-hindered side of the activated aziridine leads to the ring-opened aziridine, affording an intermediate of metal-bound alkylamide species B. CO_2 insertion allowed the formation of species C which subsequently undergoes intramolecular nucleophilic (S_N2) reaction to give the corresponding oxazolidinone and regenerates the excited state catalyst **6a**.

Table 3B.2: Substrate scope of the coupling of CO_2 with different aziridines catalyzed by photocatalyst **6a**.

8a, 91% 8b, 97% 8c, 81% 8d, 86% 8e, 89% 8f, 63%

8g, 84% 8h, 82% 8i, 80% 8j, 94% 8k, 95% 8l, 92%

8m, 81% 8n, 94% 8o, 84% 8p, 81% 8q, 76% 8r, 71%
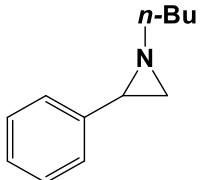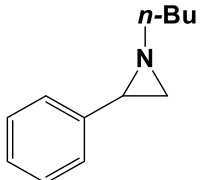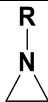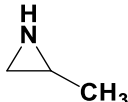
8s*, 34% 8t, 49% 8u, 15%

[a]Isolated yield, *CH_2Cl_2 solvent, pCO$_2$ = 1 bar

Scheme 3B.2: Proposed Catalytic Cycle
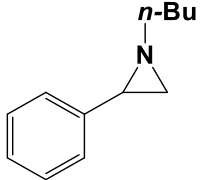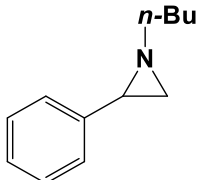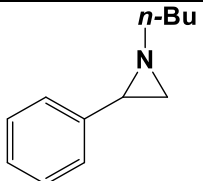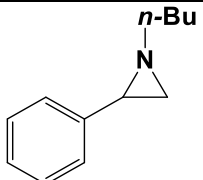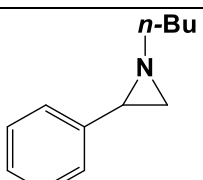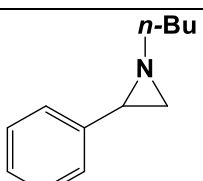
A brief comparison of the catalysts reported in the literature is presented in table 3B.3.

Although various catalysts with different ligand systems have been reported to

promote this conversion, most of these systems operate at high pressures and temperatures, in many instances the substrate scope is limited. The photocatalyst presented here helped to synthesize a variety of oxazolidinones by the cycloaddition of CO_2 and aziridines under mild conditions such as low pressure and low temperature.

Table 3B.3: A brief comparison of different catalysts studied for the coupling of CO_2 and aziridines.

Catalyst/co-catalyst	Substrate	pCO_2 (bar)	Temp. (°C)	Reaction Time (h)	Yield (%)	Reference
$PEG_{6000}(NBu_3Br)_2$	*n*-Bu N (phenyl aziridine)	80	100	0.41	94	25a
$ZrOCl_2.8H_2O$	*n*-Bu N (phenyl aziridine)	60	100	2	93	25b
Imidazolium-2-carboxylates	R N (aziridine)	50	90	20	R = $CH_2C_6H_5$ (92) $C(CH_3)_3$ (74)	16j
Zn-MOF/TBAB/H_2O	H N CH_3 (methyl aziridine)	10	rt	24	94	18

Catalyst	Product					Ref.
imidazolium-based ionic liquid (IL) functionalized zinc porphyrin	*n*-Bu substituted phenylaziridine	20	90	2	93	16e
Cr-MOF/TBAB	*n*-Bu substituted phenylaziridine	20	70	12	93	16b
Metallo-porphyrin/TBAB	*n*-Bu substituted phenylaziridine	20	100	10	99	19
[Ru(TPP)(NAr)$_2$]/ TBACl/benzene Ar = 3,5(CF$_3$)$_2$C$_6$H$_3$	*n*-Bu substituted phenylaziridine	30	100	6	79	16d
Heterometal-MOF/TBAB	*n*-Bu substituted phenylaziridine	10	70	10	91	16g
({L^{n}Ln[N(SiMe$_3$)$_2$]THF}$_2$) /DBU	*n*-Bu substituted phenylaziridine	balloon	50	48	88	14c
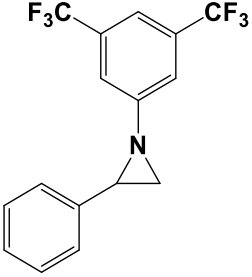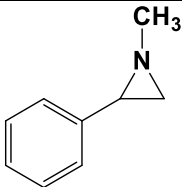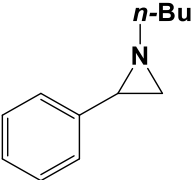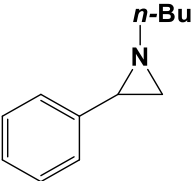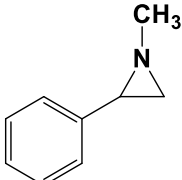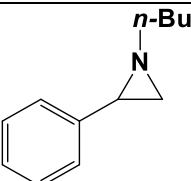
Catalyst	Structure					
Porphyrin/TBACl	1-(3,5-bis(trifluoromethyl)phenyl)-2-phenylaziridine	12	125	8	99	16i
[Et$_2$NH$_2$]I	1-methyl-2-phenylaziridine (N–CH$_3$)	1	21	24	82	20
Zn-MOF/TBAB	1-butyl-2-phenylaziridine (N–n-Bu)	20	70	12	87	16c
In-MOF/TBAB	1-butyl-2-phenylaziridine (N–n-Bu)	10	30	10	94	21
[NbCl$_3$(O$_2$CNEt$_2$)$_2$/ TBAI	1-methyl-2-phenylaziridine (N–CH$_3$)	1	25	24	86	25c
Catalyst 6a/TBAB/Blue LED	1-butyl-2-phenylaziridine (N–n-Bu)	**1**	**27**	**24**	**91**	**This Work**

Table 3B.4: Crystal data and structure refinement for compound **8s**

Identification code	Compound **8s**
Empirical formula	$C_{20}H_{22}N_2O_8S_2$
Formula weight	482.51
Temperature/K	300(1)
Crystal system	triclinic
Space group	P1
a/Å	5.9453(8)
b/Å	8.9006(11)
c/Å	11.0638(13)
α/°	86.52(2)
β/°	74.588(12)
γ/°	73.93(2)
Volume/Å^3	542.31(13)
Z	1
ρ_{calc}g/cm^3	1.477
μ/mm^{-1}	0.296
F(000)	252.0
Crystal size/mm^3	$0.16 \times 0.14 \times 0.12$
Radiation	MoKα ($\lambda = 0.71073$)
2Θ range for data collection/°	7.382 to 61.208
Index ranges	$-8 \leq h \leq 7$, $-12 \leq k \leq 11$, $-14 \leq l \leq 15$
Reflections collected	11494

Independent reflections	4654 [R_{int} = 0.1196, R_{sigma} = 0.0667]
Data/restraints/parameters	4654/527/291
Goodness-of-fit on F^2	1.161
Final R indexes [I>=2σ (I)]	R_1 = 0.0482, wR_2 = 0.1486
Final R indexes [all data]	R_1 = 0.0594, wR_2 = 0.1979
Largest diff. peak/hole / e Å^{-3}	0.46/-0.56
Flack parameter	0.00(7)
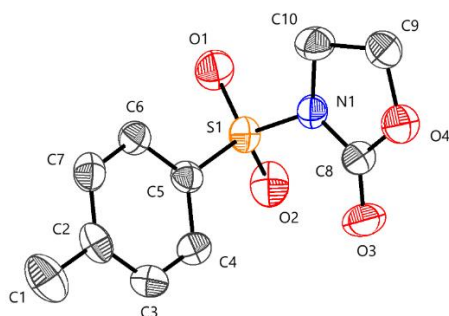
Figure 3B.3: Crystal Structure of **8s.** Thermal ellipsoids are drawn at 50% probability level. Hydrogens are removed for clarity. X-ray quality crystals were grown in CHCl$_3$-hexane solvent system.

3B.3 Conclusion

In summary, three different zinc-salens were screened under blue light irradiation for the coupling of CO$_2$ with 1-butyl-2-phenylaziridine. The zinc-salen (**6a**) with B-N coordinated motif showed superior activity over other zinc-salen's. A comparative study using blue and purple LEDs reveals that there is no significant effect on the activity of the coupling of CO$_2$ with 1-butyl-2-phenylaziridine. Importantly, catalyst

6a effectively promotes the conversion of various aziridines and CO_2 under blue light irradiation, atmospheric pressure, and room temperature to form their corresponding oxazolidinones.

3B.4 Experimental section:

3B.4.1 *General procedure for the cycloaddition of CO_2 into aziridines at atmospheric pressure*

The cycloaddition reaction of aziridines and CO_2 was conducted in a 20 mL Q-Tube equipped with a pressure gauge. In a typical reaction, zinc catalyst (1 mol%), TBAB (7 mol%), and aziridine were loaded in the Q-tube at room temperature. The Q-tube was sealed with the pressure gauge and was evacuated by freeze-thaw cycle. After the process was completed, the Q-Tube was filled with CO_2, and the pressure was adjusted to 1 bar. The reaction set-up was kept at the center of a photochemical reactor (Sigma-Aldrich Micro Photochemical Reactor, blue LED lights at a distance of 7 cm from LED). The reaction was then irradiated with 6 W blue LED with wavelength ranging between 435-445 nm and stirred for 24 hours. Then, the reaction mixture was diluted with dichloromethane and the product was isolated by column chromatography with ethyl acetate/hexane as the eluent.

3B.4.2 *Analytical data for substrate scope*

Compound 8a[16c]
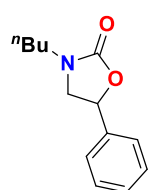
Prepared from 1-butyl-2-phenylaziridine (0.094 g, 0.50 mmol). After purification by column chromatography (n-hexane/EtOAc, 10/1), the product got isolated as a yellow liquid (0.107 g, 91%). ^{1}H NMR (400 MHz, CDCl$_3$) δ 7.45 - 7.21 (m, 5H), 5.46 (t, *J* = 8.0 Hz, 1H), 3.89 (t, *J* = 8.0 Hz, 1H),

3.41 (t, J = 8.0 Hz, 1H), 3.36 – 3.19 (m, 2H), 1.52 (p, J = 8.0 Hz, 2H), 1.32 – 1.24 (m, 2H), 0.84 (t, J = 8.0 Hz, 3H). ^{13}C NMR (101 MHz, CDCl$_3$) δ 158.00, 138.95, 128.94, 128.81, 125.55, 74.38, 52.20, 43.95, 29.44, 19.88, 13.75. HRMS (ESI+, m/z) calcd for C$_{13}$H$_{17}$NO$_2$Na, [M+Na]$^+$ m/z = 242.1148, found 242.1151

1g scale procedure: Prepared from 1-butyl-2-phenylaziridine (1g, 5.7 mmol). After purification by column chromatography (*n*-hexane/EtOAc, 10/1), the product got isolated as yellow liquid (1.1 g, 88%)

Compound 8b[19]

Prepared from 1-hexyl-2-phenylaziridine (0.088 g, 0.43 mmol). After purification by column chromatography (n-hexane/EtOAc, 10/1), the product got isolated as a yellow liquid Yield: 97% (0.105 g). ^{1}H NMR (400 MHz, CDCl$_3$) δ 7.44 – 7.21 (m, 5H), 5.48 (t, J = 8.0 Hz, 1H), 3.91 (t, J = 8.0 Hz, 1H), 3.42 (t, J = 8.0 Hz, 1H), 3.37 – 3.21 (m, 2H), 1.52 (p, J = 8.0 Hz, 2H), 1.37 – 1.20 (m, 6H), 0.88 (t, J = 8.0 Hz, 3H). ^{13}C NMR (101 MHz, CDCl$_3$) δ 157.99, 138.97, 128.93, 128.80, 125.54, 74.36, 52.19, 44.22, 31.43, 27.34, 26.31, 22.57, 14.04. HRMS (ESI+, m/z) calcd for C$_{15}$H$_{22}$NO$_2$, [M+H]$^+$ m/z = 248.1651, found 248.1637
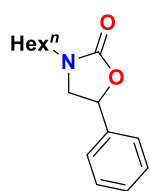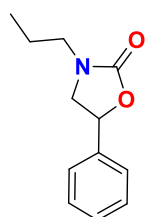
Compound 8c[16c]

Prepared from 1-propyl-2-phenylaziridine (0.097 g, 0.60 mmol). After purification by column chromatography (n-hexane/EtOAc, 10/1), the product got isolated as a yellow liquid Yield: 81% (0.100 g). ^{1}H NMR (400 MHz, CDCl$_3$) δ 7.41 – 7.28 (m, 5H), 5.45 (t, J = 8.0 Hz, 1H), 3.88 (t, J = 8.0 Hz, 1H), 3.39 (t, J = 8.0 Hz, 1H), 3.33 – 3.14 (m, 2H), 1.55 (sext, J = 8.0 Hz, 2H), 0.90 (t, J = 8.0 Hz, 3H). ^{13}C NMR (101 MHz, CDCl$_3$) δ 158.00, 138.93, 128.87, 125.49, 74.31, 52.11, 45.78, 20.63, 11.07. HRMS (ESI+, m/z) calcd for C$_{12}$H$_{16}$NO$_2$, [M+H]$^+$ m/z = 206.1181, found 206.1200

Compound 8d[16c]

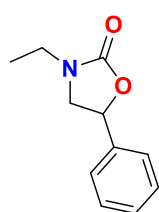Prepared from 1-ethyl-2-phenylaziridine (0.090 g, 0.61 mmol). After purification by column chromatography (n-hexane/EtOAc, 10/1), the product got isolated as a yellow liquid Yield: 86% (0.101g). ^{1}H NMR (400 MHz, CDCl$_3$) δ 7.46 – 7.29 (m, 5H), 5.48 (t, J = 8.0 Hz, 1H), 3.92 (t, J = 8.0 Hz, 1H), 3.46 - 3.26 (m, 3H), 1.17 (t, J = 8.0 Hz, 3H). ^{13}C NMR (101 MHz, CDCl$_3$) δ 157.78, 138.91, 128.97, 128.86, 125.60, 74.40, 51.66, 38.98, 12.66. HRMS (ESI+, m/z) calcd for C$_{11}$H$_{13}$NO$_2$Na, [M+Na]$^+$ m/z = 214.0829, found 214.0838
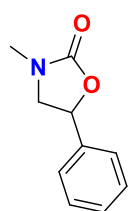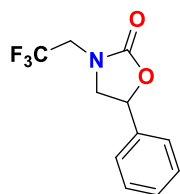
Compound 8e[19]

Prepared from 1-methyl-2-phenylaziridine (0.087 g, 0.65 mmol). After purification by column chromatography (n-hexane/EtOAc, 10/1), the product got isolated as a yellow liquid Yield: 89% (0.103g). ^{1}H NMR (400 MHz, CDCl$_3$) δ 7.34 (m, 5H), 5.44 (t, J = 8.0 Hz, 1H), 3.89 (t, J = 8.0 Hz, 1H), 3.41 (t, J = 8.0 Hz, 1H), 2.89 (s, 3H). ^{13}C NMR (101 MHz, CDCl$_3$) δ 158.21, 138.68, 128.86, 128.77, 125.53, 74.17, 54.38, 54.36, 31.05. HRMS (ESI+, m/z) calcd for C$_{10}$H$_{11}$NO$_2$Na, [M+Na]$^+$ m/z = 200.0681, found 200.0682

Compound 8f

Prepared from 2-phenyl-1-(2,2,2-trifluoroethyl)aziridine (0.122 g, 0.61 mmol). After purification by column chromatography (n-hexane/EtOAc, 10/1), the product got isolated as a colorless liquid Yield: 63% (0.094g). ^{1}H NMR (400 MHz, CDCl$_3$) δ 7.44 – 7.31 (m, 5H), 5.53 (t, J = 8.0 Hz, 1H), 4.06 (t, J = 8.0 Hz, 1H), 4.02 - 3.90 (m, 1H), 3.89 – 3.76 (m, 1H), 3.58 (t, J = 8.0 Hz, 1H). ^{13}C NMR (101 MHz, CDCl$_3$) δ 157.67, 137.67, 129.23, 129.06, 125.71, 75.18, 52.68, 46.57, 46.23, 45.88, 45.53. HRMS (ESI+, m/z) calcd for C$_{11}$H$_{11}$F$_3$NO$_2$, [M+H]$^+$ m/z = 246.0742, found 246.0741

Compound 8g[20]

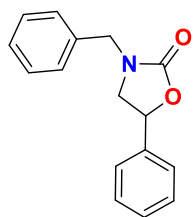
Prepared from 1-benzyl-2-phenylaziridine (0.107 g, 0.51 mmol). After purification by column chromatography (n-hexane/EtOAc, 5/1), the product got isolated as a yellow liquid Yield: 84% (0.109g). ^{1}H NMR (400 MHz, CDCl$_3$) δ 7.45 – 7.19 (m, 10H), 5.44 (t, J = 8.0 Hz, 1H), 4.52 (d, J = 16 Hz, 1H), 4.39 (d, J = 16 Hz, 1H), 3.75 (t, J = 8.0 Hz, 1H), 3.29 (t, J = 8.0 Hz, 1H). ^{13}C NMR (101 MHz, CDCl$_3$) δ 157.99, 138.57, 135.62, 128.88, 128.87, 128.80, 128.15, 128.03, 125.54, 74.54, 51.50, 48.35. HRMS (ESI+, m/z) calcd for C$_{16}$H$_{15}$NO$_2$Na, [M+Na]$^+$ m/z = 276.0995, found 276.1011

Compound 8h
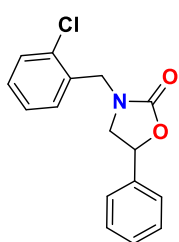
Prepared from 1-(2-chlorobenzyl)-2-phenylaziridine (0.108 g, 0.44 mmol). After purification by column chromatography (n-hexane/EtOAc, 5/1), the product got isolated as a yellow liquid Yield: 82% (0.105g). ^{1}H NMR (400 MHz, CDCl$_3$) δ 7.48 – 7.20 (m, 9H), 5.49 (t, J = 8.0 Hz, 1H), 4.69 (d, J = 16.0 Hz, 1H), 4.58 (d, J = 16.0 Hz, 1H), 3.85 (t, J = 8.0 Hz, 1H), 3.38 (t, J = 8.0 Hz, 1H). ^{13}C NMR (101 MHz, CDCl$_3$) δ 158.11, 138.40, 133.84, 133.14, 130.30, 129.78, 129.52, 128.90, 128.88, 127.42, 125.60, 51.92, 45.69, 20.91. HRMS (ESI+, m/z) calcd for C$_{16}$H$_{15}$ClNO$_2$, [M+H]$^+$ m/z = 288.0786, found 288.0781

Compound 8i[16f]
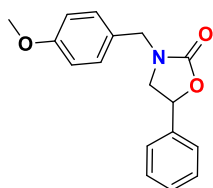
Prepared from 1-(4-methoxybenzyl)-2-phenylaziridine (0.102 g, 0.43 mmol). After purification by column chromatography (n-hexane/EtOAc, 5/1), the product got isolated as a yellow liquid Yield: 80% (0.097g). ^{1}H NMR (400 MHz, CDCl$_3$) δ 7.40 – 7.32 (m, 3H), 7.31 – 7.27

(m, 2H), 7.21 (d, J = 8.0 Hz, 2H), 6.87 (d, J = 8.0 Hz, 2H), 5.45 (t, J = 8.0 Hz, 1H), 4.47 (d, J = 16 Hz, 1H), 4.35 (d, J = 16.0 Hz, 1H), 3.79 (s, 3H), 3.74 (t, J = 8.0 Hz, 1H), 3.28 (d, J = 8.0 Hz, 1H). ^{13}C NMR (101 MHz, CDCl$_3$) δ 159.47, 158.03, 138.69, 129.68, 128.97, 128.89, 127.71, 125.63, 114.30, 74.62, 55.40, 51.50, 47.89. HRMS (ESI+, m/z) calcd for C$_{17}$H$_{19}$NO$_3$Na, [M+Na]$^+$ m/z = 306.1101, found 306.1089

Compound 8j[15a]
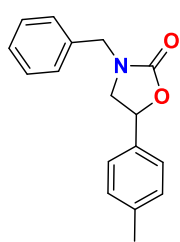
Prepared from 1-benzyl-2-(p-tolyl)aziridine (0.091 g, 0.41 mmol). After purification by column chromatography (n-hexane/EtOAc, 5/1), the product got isolated as a yellow liquid Yield: 94% (0.103g). $^1$H NMR (400 MHz, CDCl$_3$) δ 7.35 – 7.16 (m, 5H), 7.12 – 7.03 (m, 4H), 5.32 (t, J = 8.0 Hz, 1H), 4.44 (d, J = 16 Hz, 1H), 4.31 (d, J = 16 Hz, 1H), 3.64 (t, J = 8.0 Hz, 1H), 3.19 (t, J = 8.0 Hz, 1H), 2.24 (s, 3H). ^{13}C NMR (101 MHz, CDCl$_3$) δ 158.08, 138.72, 135.69, 135.54, 129.51, 128.88, 128.17, 128.02, 125.63, 74.61, 51.54, 48.36, 21.19. HRMS (ESI+, m/z) calcd for C$_{17}$H$_{17}$NO$_2$Na, [M+Na]$^+$ m/z = 290.1151, found 290.1163

Compound 8k[14b]

Prepared from 1-(4-methoxybenzyl)-2-(p-tolyl)aziridine (0.095 g, 0.37 mmol). After purification by column chromatography (n-hexane/EtOAc, 5/1), the product got isolated as a yellow liquid Yield: 95% (0.106g). ^{1}H NMR (400 MHz, CDCl$_3$) δ 7.16 – 7.02 (m, 6H), 6.76 (d, J = 8.0 Hz, 2H), 5.29 (t, J = 8.0 Hz, 1H), 4.35 (d, J = 15.0 Hz, 1H), 4.24 (d, J = 15.0 Hz, 1H), 3.68 (s, 3H), 3.61 (t, J = 8.0 Hz, 1H), 3.16 (t, J = 8.0 Hz, 1H), 2.23 (s, 3H). ^{13}C NMR (101 MHz, CDCl$_3$) δ 159.32, 157.97, 138.65, 135.57, 129.54, 129.46, 127.67, 125.60, 114.16, 74.55, 55.25, 51.37, 47.72, 21.14. HRMS (ESI+, m/z) calcd for C$_{18}$H$_{19}$NO$_3$Na, [M+Na]$^+$ m/z = 320.1257, found 320.1275

Compound 8l

Prepared from 1-hexyl-2-(p-tolyl)aziridine (0.085 g, 0.39 mmol). After purification by column chromatography (n-hexane/EtOAc, 10/1), the product got isolated as a yellow liquid Yield: 92% (0.094g). ^{1}H NMR (400 MHz, CDCl$_3$) δ 7.25 – 7.16 (m, 4H), 5.45 (t, J = 8.0 Hz, 1H), 3.88 (t, J = 8.0 Hz, 1H), 3.41 (t, J = 8.0 Hz, 1H), 3.37 – 3.20 (m, 2H), 2.36 (s, 3H), 1.59 – 1.48 (m, 2H), 1.37 – 1.19 (m, 7H), 0.88 (t, J = 8.0 Hz, 3H). ^{13}C NMR (101 MHz, CDCl$_3$) δ 158.55, 138.90, 136.47, 130.70, 126.20, 73.16, 52.77, 45.09, 30.98, 26.79, 26.38, 22.63, 20.42, 14.09. HRMS (ESI+, m/z) calcd for C$_{16}$H$_{24}$NO$_2$, [M+H]$^+$ m/z = 262.1802, found 262.1800
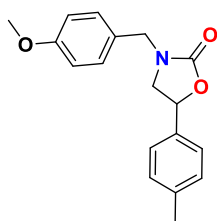
Compound 8m[27]
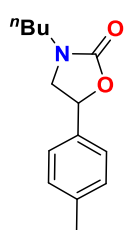
Prepared from 1-butyl-2-(p-tolyl)aziridine (0.098 g, 0.51 mmol). After purification by column chromatography (n-hexane/EtOAc, 10/1), the product got isolated as a yellow liquid Yield: 81% (0.098g). ^{1}H NMR (400 MHz, CDCl$_3$) δ 7.25 – 7.13 (m, 4H), 5.41 (t, J = 8.0 Hz, 1H), 3.86 (t, J = 8.0 Hz, 1H), 3.38 (t, J = 8.0 Hz, 1H), 3.34 – 3.18 (m, 2H), 2.33 (s, 3H), 1.51 (p, J = 8.0 Hz, 2H), 1.33 (h, J = 8.0 Hz, 2H), 0.91 (t, J = 8.0 Hz, 3H). ^{13}C NMR (101 MHz, CDCl$_3$) δ 157.97, 138.58, 135.84, 129.47, 125.54, 74.33, 52.10, 43.81, 29.34, 21.13, 19.78, 13.67. HRMS (ESI+, m/z) calcd for C$_{14}$H$_{20}$NO$_2$, [M+H]$^+$ m/z = 234.1489, found 234.1513

Compound 8n[21]
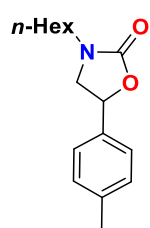
Prepared from 1-propyl-2-(p-tolyl)aziridine (0.090 g, 0.52 mmol). After purification by column chromatography (n-hexane/EtOAc, 10/1), the product got isolated as a yellow liquid Yield: 94% (0.107g). ^{1}H NMR (400 MHz, CDCl$_3$) δ 7.24 – 7.14 (m, 4H), 5.41 (t, J = 8.0 Hz, 1H), 3.85

(t, *J* = 8.0 Hz, 1H), 3.38 (t, *J* = 8.0 Hz, 1H), 3.32 – 3.13 (m, 2H), 2.32 (s, 3H), 1.55 (sext, *J* = 8.0 Hz, 2H), 0.90 (t, *J* = 8.0 Hz, 3H). ^{13}C NMR (101 MHz, CDCl$_3$) δ 158.03, 138.58, 135.88, 129.46, 125.53, 74.33, 52.10, 45.73, 21.11, 20.60, 11.04. HRMS (ESI+, m/z) calcd for C$_{13}$H$_{17}$NO$_2$Na, [M+Na]$^+$ m/z = 242.1151, found 242.1157
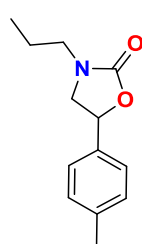
Compound 8o[16c]

Prepared from 1-ethyl-2-(p-tolyl)aziridine (0.100 g, 0.62 mmol). After purification by column chromatography (n-hexane/EtOAc, 10/1), the product got isolated as a yellow liquid Yield: 84% (0.107g). ^{1}H NMR (400 MHz, CDCl$_3$) δ 7.26 – 7.11 (m, 4H), 5.41 (t, *J* = 8.0 Hz, 1H), 3.87 (t, *J* = 8.0 Hz, 1H), 3.45 – 3.20 (m, 3H), 2.33 (s, 3H), 1.15 (t, *J* = 8.0 Hz, 3H). ^{13}C NMR (101 MHz, CDCl$_3$) δ 157.73, 138.62, 135.83, 129.48, 125.57, 74.34, 51.56, 38.85, 21.14, 12.53. HRMS (ESI+, m/z) calcd for C$_{12}$H$_{16}$NO$_2$, [M+H]$^+$ m/z = 206.1176, found 206.1172

Compound 8p

Prepared from 1-benzyl-2-(4-(tert-butyl)phenyl)aziridine (0.090 g, 0.34 mmol). After purification by column chromatography (n-hexane/EtOAc, 5/1), the product got isolated as a yellow liquid Yield: 81% (0.085g). ^{1}H NMR (400 MHz, CDCl$_3$) δ 7.33 – 7.11 (m, 9H), 5.34 (t, *J* = 8.0 Hz, 1H), 4.43 (d, *J* = 15.0 Hz, 1H), 4.31 (d, *J* = 15.0 Hz, 1H), 3.64 (t, *J* = 8.0 Hz, 1H), 3.22 (t, *J* = 8.0 Hz, 1H), 1.21 (s, 9H). ^{13}C NMR (101 MHz, CDCl$_3$) δ 158.08, 151.96, 135.75, 135.51, 128.88, 128.20, 128.03, 125.79, 125.46, 74.55, 51.46, 48.40, 34.65, 31.28. HRMS (ESI+, m/z) calcd for C$_{20}$H$_{23}$NO$_2$Na, [M+Na]$^+$ m/z = 332.1621, found 332.1624
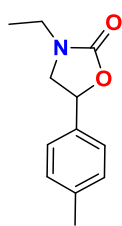
Compound 8q

Prepared from 1-benzyl-2-(4-fluorophenyl)aziridine (0.105 g, 0.46 mmol). After purification by column chromatography (n-hexane/EtOAc, 5/1), the product got isolated as a yellow liquid Yield: 76% (0.096g). ^{1}H NMR (400 MHz, CDCl$_3$) δ 7.42 – 7.25 (m, 7H), 7.05 (t, J = 8.0 Hz, 2H), 5.45 (t, J = 8.0 Hz, 1H), 4.53 (d, J = 16.0 Hz, 1H), 4.43 (d, J = 16.0 Hz, 1H), 3.78 (t, J = 8.0 Hz, 1H), 3.29 (t, J = 8.0 Hz, 1H). ^{13}C NMR (101 MHz, CDCl$_3$) δ 164.08, 161.62, 157.81, 135.58, 134.44, 134.41, 128.93, 128.17, 128.11, 127.62, 127.54, 115.98, 115.76, 74.00, 51.51, 48.38. ^{19}F NMR (377 MHz, CDCl$_3$) δ -112.64. HRMS (ESI+, m/z) calcd for C$_{16}$H$_{14}$FNO$_2$Na, [M+Na]$^+$ m/z = 294.0901, found 294.0911
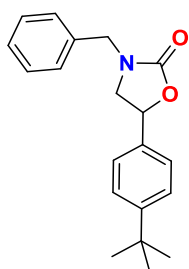
Compound 8r[15a]
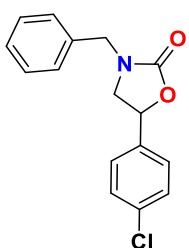
Prepared from 1-benzyl-2-(4-chlorophenyl)aziridine (0.118 g, 0.48 mmol). After purification by column chromatography (n-hexane/EtOAc, 5/1), the product got isolated as a yellow liquid Yield: 71% (0.099g). ^{1}H NMR (400 MHz, CDCl$_3$) δ 7.44 – 7.21 (m, 9H), 5.45 (t, J = 8.0 Hz, 1H), 4.53 (d, J = 16.0 Hz, 1H), 4.42 (d, J = 16.0 Hz, 1H), 3.78 (t, J = 8.0 Hz, 1H), 3.27 (t, J = 8.0 Hz, 1H). ^{13}C NMR (101 MHz, CDCl$_3$) δ 157.76, 137.12, 135.47, 134.66, 129.09, 128.94, 128.16, 128.14, 126.99, 73.84, 51.40, 48.38. HRMS (ESI+, m/z) calcd for C$_{16}$H$_{14}$ClNO$_2$Na, [M+Na]$^+$ m/z = 310.0652, found 310.0611

Compound 8s[22]

Prepared from 1-tosylaziridine (0.099 g, 0.50 mmol). After purification by column chromatography (n-hexane/EtOAc, 4/1), the product got isolated as white solid Yield: 34% (0.041g). ^{1}H NMR

(400 MHz, CDCl$_3$) δ 7.94 (d, J = 8.0 Hz, 2H), 7.37 (d, J = 8.0 Hz, 2H), 4.36 (t, J = 8.0 Hz, 2H), 4.05 (t, J = 8.0 Hz, 2H), 2.46 (s, 3H). ^{13}C NMR (101 MHz, CDCl$_3$) δ 152.17, 145.99, 133.92, 130.07, 128.47, 62.39, 44.74, 21.87. HRMS (ESI+, m/z) calcd for C$_{10}$H$_{11}$NO$_4$SNa, [M+Na]$^+$ m/z = 264.0289, found 264.0301
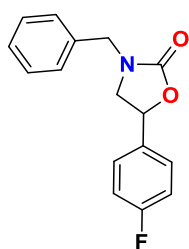
Compound 8t[14b]
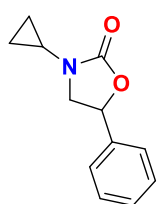
Prepared from 1-cyclopropyl-2-phenylaziridine (0.099 g, 0.62 mmol). After purification by column chromatography (n-hexane/EtOAc, 10/1), the product got isolated as a yellow liquid Yield: 49% (0.062g). ^{1}H NMR (400 MHz, CDCl$_3$) δ 7.43 – 7.29 (m, 5H), 5.42 (t, J = 8.0 Hz, 1H), 3.88 (t, J = 8.0 Hz, 1H), 3.43 (t, J = 8.0 Hz, 1H), 2.60 – 2.52 (m, 1H), 0.86 – 0.65 (m, 4H). ^{13}C NMR (101 MHz, CDCl$_3$) δ 158.19, 138.63, 128.96, 128.87, 125.57, 74.59, 53.56, 25.89, 6.18, 5.69. HRMS (ESI+, m/z) calcd for C$_{12}$H$_{13}$NO$_2$Na, [M+Na]$^+$ m/z = 226.0838, found 226.0813
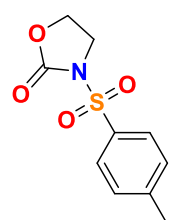
Compound 8u[20]
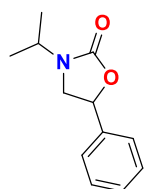
Prepared from 1-isopropyl-2-phenylaziridine (0.104 g, 0.65 mmol). After purification by column chromatography (n-hexane/EtOAc, 10/1), the product got isolated as a yellow liquid Yield: 15% (0.020g). ^{1}H NMR (400 MHz, CDCl$_3$) δ 7.46 – 7.30 (m, 5H), 5.47 (t, J = 8.0 Hz, 1H), 4.17 (hept, J = 8.0 Hz, 1H), 3.86 (t, J = 8.0 Hz, 1H), 3.37 (t, J = 8.0 Hz, 1H), 1.21 (d, J = 8.0 Hz, 3H), 1.16 (d, J = 8.0 Hz, 3H). ^{13}C NMR (101 MHz, CDCl$_3$) δ 157.27, 139.11, 129.01, 128.86, 125.59, 74.63, 47.51, 45.01, 20.14, 19.67. HRMS (ESI+, m/z) calcd for C$_{12}$H$_{15}$NO$_2$Na, [M+Na]$^+$ m/z = 228.0995, found 228.0970

3B.5 References:

1. (a) T. W. Hudnall; C.-W. Chiu; F. P. Gabbai, *Acc. Chem. Res.* **2008,** *42*, 388-397; (b) Z. M. Hudson; S. Wang, *Acc. Chem. Res.* **2009,** *42*, 1584-1596; (c) A. Lorbach, A. Hubner, M. Wagner, *Dalton Trans.* **2012,** *41*, 6048-6063; (d) C. D. Entwistle, T. B. Marder, *Chem. Mater.* **2004,** *16*, 4574-4585; (e) J. F. Araneda; W. E. Piers; B. Heyne; M. Parvez; R. McDonald, *Angew. Chem. Int. Ed.* **2011,** *50*, 12214-12217; (f) M. J. D. Bosdet; W. E. Piers; T. S. Sorensen; M. Parvez, *Angew. Chem. Int. Ed.* **2007,** *119*, 5028-5031; (g) J. He; F. Rauch; M. Finze; T. B. Marder, *Chem. Sci.* **2020,** *12*, 128-147; (h) F. Jäkle, *Coord. Chem. Rev.* **2006,** *250*, 1107-1121; (i) S. K. Mellerup; S. Wang, *Chem. Soc. Rev.* **2019,** *48*, 3537-3549; (j) A. Murali; P. Nayak; K. Venkatasubbaiah, *Dalton Trans.* **2022,** *51*, 5751-5771; (k) Y.-L. Rao; H. Amarne; S. Wang, S., *Coord. Chem. Rev.* **2012,** *256*, 759-770; (l) E. von Grotthuss; A. John; T. Kaese; M. Wagner, *Asian J. Org. Chem.* **2018,** *7*, 37-53; (m) S. Yamaguchi; A. Wakamiya, *Pure Appl. Chem.* **2006,** *78*, 1413-1424.

2. (a) Z. M. Hudson, S. Wang, *Acc. Chem. Res.* **2009,** *42*, 1584-1596; (b) C. R. Wade, E. J. Broomsgrove, S. Aldridge, F. P. Gabbai, *Chem. Rev.* **2010,** *110*, 3959-3964; (c) K. Dhanunjayarao; V. Mukundam; K. Venkatasubbaiah, *Inorg. Chem.* **2016,** *55*, 11153-11159; (d) L. Ji; S. Griesbeck; T. B. Marder, *Chem. Sci.* **2017,** *8*, 846-863; (e) M. Kinoshita; H. Kita; Y. Shirota, *Adv. Funct. Mater.* **2002,** *12*, 780-786; (f) D. Li; H. Zhang; Y. Wang, *Chem. Soc. Rev.* **2013,** *42*, 8416-33; (g) P. Nayak; A. C. Murali; V. Chandrasekhar; K. Venkatasubbaiah, *Mater. Adv.* **2022,** *3*, 5893-5899; (h) T. Noda; H. Ogawa; Y. Shirota, *Adv. Mater.* **1999,** *11*, 283-285; (i) Y. L. Rao; S. Wang, *Inorg. Chem.* **2011,** *50*, 12263-74; (j) S. Sa; A. C. Murali; P. Nayak; K. Venkatasubbaiah,

Chem. Commun. **2021,** *57*, 10170-10173; (k) G. Turkoglu; M. E. Cinar; T. Ozturk, *Molecules* **2017**, *22*, 1522 ; (l) C. R. Wade; F. P. Gabbai, *Inorg. Chem.* **2010,** *49*, 714-720.

3. (a) M. A. Filatov; S. Karuthedath; P. M. Polestshuk; H. Savoie; K. J. Flanagan; C. Sy; E. Sitte; M. Telitchko; F. Laquai; R. W. Boyle; M. O. Senge, *J. Am. Chem. Soc.* **2017,** *139*, 6282-6285; (b) D. Frath; J. Massue; G. Ulrich; R. Ziessel, *Angew. Chem. Int. Ed.* **2014,** *53*, 2290-310; (c) D. Kunchala; S. Sa; P. Nayak; S. J. Ponniah; K. Venkatasubbaiah, *Organometallics* **2019,** *38*, 870-878.

4. M. Vanga; S. Sa; A. Kumari; A. C. Murali; P. Nayak; R. Das; K. Venkatasubbaiah, *Dalton Trans.* **2020,** *49*, 7737-7746.

5. P. Nayak; A. C. Murali; P. K. Pal; U. D. Priyakumar; V. Chandrasekhar; K. Venkatasubbaiah, *Inorg. Chem.* **2022,** *61*, 14511-14516.

6. (a) A. Bhushan; N. J. Martucci; O. B. Usta; M. L. Yarmush, *Expert Opin. Drug Metab. Toxicol.* **2016,** *12*, 475-7; (b) N. Pandit; R. K. Singla; B. Shrivastava, *Int. J. Med. Chem.* **2012,** *2012*, 159285; (c) C. Roger; J. A. Roberts; L. Muller, *Clin. Pharmacokinet.* **2018,** *57*, 559-575; (d) V. Zadsirjan; M. M. Heravi, *Curr. Org. Synth.* **2018,** *15*, 3-20.

7. A. Zahedi Bialvaei; M. Rahbar; M. Yousefi; M. Asgharzadeh; H. Samadi Kafil, *J. Antimicrob. Chemother.* **2017,** *72*, 354-364.

8. D. McBride; T. Krekel; K. Hsueh; M. J. Durkin, *Expert Opin. Drug Metab. Toxicol.* **2017,** *13*, 331-337.

9. F. M. Wouters, DP. Vercauteren, S. Collin, G. Evrard, F. Durant, F. Ducrey, JJ. Koenig, FX. Jarreau, *Eur. J. Med. Chem.* **1992,** *27*, 939-948.

10. (a) D. J. Ager, I. Prakash, D. R. Schaad, *Chem. Rev.* **1996,** *96*, 835-875; (b) J. R. Gage, D. A. Evans, *Org. Synth.* **1990,** *68.*

11. (a) Y. Wu; G. Liu, *Tetrahedron Lett.* **2011,** *52* (48), 6450-6452; (b) Z.-Z. Yang; Y.-N. Li; Y.-Y. Wei; L.-N. He, *Green Chem.* **2011,** *13,* 2351-2353.

12. Z.-Z. Yang; L.-N. He; S.-Y. Peng; A.-H. Liu, *Green Chem.* **2010,** *12*, 1850-1854.

13. (a) A.-H. Liu; Y.-L. Dang; H. Zhou; J.-J. Zhang; X.-B. Lu, *ChemCatChem.* **2018,** *10*, 2686-2692; (b) V. B. Saptal; B. M. Bhanage, *ChemSusChem.* **2016,** *9*, 1980-1985.

14. (a) A. W. Miller, S. T. Nguyen, *Org. Lett.* **2004,** *6*, 2301-2304; (b) M. Sengoden; M. North; A. C. Whitwood, *ChemSusChem.* **2019,** *12*, 3296-3303; (c) Y. Xie; C. Lu; B. Zhao; Q. Wang; Y. Yao, *J. Org. Chem.* **2019,** *84*, 1951-1958; (d) F. Zhou; S.-L. Xie; X-T. Gao; R. Zhang; C.-H. Wang; G.-Q. Yin; J. Zhou, *Green Chem.* **2017,** *19*, 3908-3915.

15. (a) G. Bresciani; E. Antico; G. Ciancaleoni; S. Zacchini; G. Pampaloni; F. Marchetti, *ChemSusChem.* **2020,** *13*, 5586-5594; (b) M. T. Hancock; A. R. Pinhas, *Tetrahedron Lett.* **2003,** *44*, 5457-5460; (c) C. Phung; A. R. Pinhas, *Tetrahedron Lett.* **2010,** *51*, 4552-4554; (d) C. Phung; R. M. Ulrich; M. Ibrahim; N. T. G. Tighe; D. L. Lieberman; A.R. Pinhas, *Green Chem.* **2011,** *13*, 3224-3229.

16. (a) G. Bresciani; S. Zacchini; F. Marchetti; G. Pampaloni, *Dalton Trans.* **2021,** *50*, 5351-5359; (b) C. S. Cao; Y. Shi; H. Xu; B. Zhao, *Dalton Trans.* **2018,** *47*, 4545-4553; (c) C. S. Cao; Y. Shi; H. Xu; B. Zhao, *Chem. Commun.* **2021,** *57*, 7537-7540; (d) D. Carminati; E. Gallo; C. Damiano; A. Caselli; D. Intrieri, *Eur. J. Inorg. Chem.* **2018,** *2018*, 5258-5262; (e) Y. Chen; R. Luo; Z. Yang;

X. Zhou; H. Ji, *Sustainable Energy & Fuels* **2018,** *2*, 125-132; (f) C. Damiano; P. Sonzini; G. Manca; E. Gallo, *Eur. J. Org. Chem.* **2021,** *2021*, 2807-2814; (g) X. M. Kang; L. H. Yao; Z. H. Jiao; B. Zhao, *Chem. Asian. J.* **2019,** *14*, 3668-3674; (h) A. Rostami; A. Ebrahimi; J. Husband; M. U. Anwar; R. Csuk; A. Al-Harrasi, *Eur. J. Org. Chem.* **2020,** *2020*, 1881-1895; (i) P. Sonzini; C. Damiano; D. Intrieri; G. Manca; E. Gallo, *Adv. Synth. & Catal.* **2020,** *362*, 2961-2969; (j) A. Ueno; Y. Kayaki; T. Ikariya, *Green Chem.* **2013,** *15*, 425-430.

17. (a) Y.-M. Shen; W-L. Duan, M. Shi, *J. Org. Chem.* **2003,** *68*, 1559-1562; (b) A. Decortes; M. Martinez Belmonte; J. Benet-Buchholz; A. W. Kleij, *Chem. Commun.* **2010,** *46*, 4580-2; (c) R. M. Haak; A. Decortes; E. C. Escudero-Adan; M. Martinez Belmonte; E. Martin; J. Benet-Buchholz; A. W. Kleij, *Inorg. Chem.* **2011,** *50*, 7934-6; (d) Y. Ren; J. Chen; C. Qi; H. Jiang, *ChemCatChem.* **2015,** *7*, 1535-1538; (e) M. Taherimehr; A. Decortes; S. M. Al-Amsyar; W. Lueangchaichaweng; C. J. Whiteoak; E. C. Escudero-Adán; A. W. Kleij; P. P. Pescarmona, *Catal. Sci. Technol.* **2012,** *2*, 2231-2237.

18. A. C. Kathalikkattil; R. Roshan; J. Tharun; R. Babu; G. S. Jeong; D. W. Kim; S. J. Cho; D. W. Park, *Chem. Commun.* **2016,** *52*, 280-3.

19. X. Wang; W. Y. Gao; Z. Niu; L. Wojtas; J. A. Perman; Y. S. Chen; Z. Li; B. Aguila; S. Ma, *Chem Commun.* **2018,** *54*, 1170-1173.

20. G. Bresciani; M. Bortoluzzi; G. Pampaloni; F. Marchetti, *Org. Biomol. Chem.* **2021,** *19*, 4152-4161.

21. X. R. Tian; Y. Shi; S. L. Hou; Y. Ma; B. Zhao, *Inorg. Chem.* **2021,** *60*, 15383-15389.

22. S. Carrasco; A. Sanz-Marco; B. Martín-Matute, *Organometallics* **2019,** *38*, 3429-3435.

23. D. Adhikari; A. W. Miller; M. H. Baik; S. T. Nguyen, *Chem. Sci.* **2015,** *6*, 1293-1300.

24. J. W. McFarland; C.E. Hayes; E. B. Blair; K. R. Stuhlmacher, *J. Het. Chem.* **1980,** *17*, 271-272.

25. *(a)* Y. Du; Y. Wu; A-H. Liu; L-N. He, *J. Org. Chem.* **2008**, *73*, 4709–4712; (b) Y. Wu; L-N. He; Y. Du; J-Q. Wang; C-X. Miao, W. Li, *Tetrahedron*, **2009**, *65*, 6204-6210; (c) G. Bresciani; S. Zacchini; F. Marchetti; G. Pampaloni, *Dalton Trans.,* **2021**, *50*, 5351–5359

Chapter 4

Tetra-coordinated boron functionalized pyrazole-based chiral zinc sensors for enantioselective recognition of phenylalanine, alanine, and cysteine

4.1 Introduction

Proteins are made up of amino acids (AAs), which are essential for many chemical and biological activities. The concentration of amino acids affects the metabolism of peptides and proteins. In recent years, there has been an increase in demand for the differentiation of amino acids in a number of disciplines, including the diagnosis of disease and nutritional screening.[1, 2] *L*-enantiomers are predominant in natural amino acids but in recent years more *D*-enantiomers are found in plants, animals, microbes and food. Different biological processes are connected with *D*-amino acids.[3, 4] For instance, many *D*-amino acids are now recognized as a new class of neuromodulators, as there is an increase in the concentration of *D*-amino acids in food due to microbial contamination or high temperature or extreme pH. Therefore, there is a growing demand for techniques that can enantioselectively discriminate amino acids. Among the different techniques, fluorescent techniques have attracted significant interest owing to their simplicity, real-time analysis, low cost, high sensitivity, non-invasive and non-destructive nature, and diverse signal output modes.[5] In the last decade, many small-molecule fluorescent sensors have been synthesized to sense and discriminate bio-thiols like cysteine, homocysteine, and glutathione.[6-11] A limited number of fluorescent sensors are available for the detection of non-thiol group amino acids.[12-15] Metal complexes have been used as fluorescent sensors for the enantioselective sensing of biologically important small molecules such as ribonucleosides,[16] saccharides[17-19], and amino acids.[14, 20-25] Smart and rational design of metal complexes can help in the effective sensing of amino acids. The metal centers in these complexes serve as active sites for amino acids,[14, 20-27] and the unique spatial structure of these complexes limits their interaction with some special amino acids through supramolecular interaction.[28-34] These distinct properties of metal complexes make it

possible to sense amino acids. In this regard, chiral complexes have been developed for enantioselective recognition of enantiomers.[28, 30, 31, 33, 35] However, most of the complexes were able to sense derivatives of amino acids[30, 36-39] but not sense free amino acids. Similarly, modified chiral zinc salen complexes have been developed for the enantioselective discrimination of chiral amines,[40, 41] saccharides[17-19], and hydroxycarboxylic acids.[28, 42] However there are limited reports on zinc salen complexes for the discrimination of chiral amino acids.[28] Therefore, it is very challenging to effectively sense natural amino acids.

Motivated by these findings we have rationally designed and synthesized a pair of tetra coordinated boron-based chiral zinc complexes, (*S,S*)-**Zn** and (*R,R*)-**Zn** in which the tetracoordinated boron functionalized pyrazole chromophore is coupled with chiral zinc salen to enhance the emissive property. These chiral zinc complexes are well characterized by multinuclear NMR spectroscopy, MALDI-MS and X-ray crystallography methods. In solution medium, our newly synthesized zinc salen complexes can discriminate *D*- & *L*-phenylalanine, *D*- & *L*-alanine and *D*- & *L*-cysteine with moderate enantiomeric fluorescence ratio.

4.2 Result and Discussions:

4.2.1 *Synthesis:*

Compound **4** was prepared according to the procedure mentioned in chapter 2 (Scheme 2.1).[43] The synthetic route to pyrazole-based B-N coordinated imine ligands (*S,S*)-**L** and (*R,R*)-**L** and their corresponding Zn(II) complexes (*S,S*)-**Zn** and (*R,R*)-**Zn** is out-lined in Scheme 4.1.
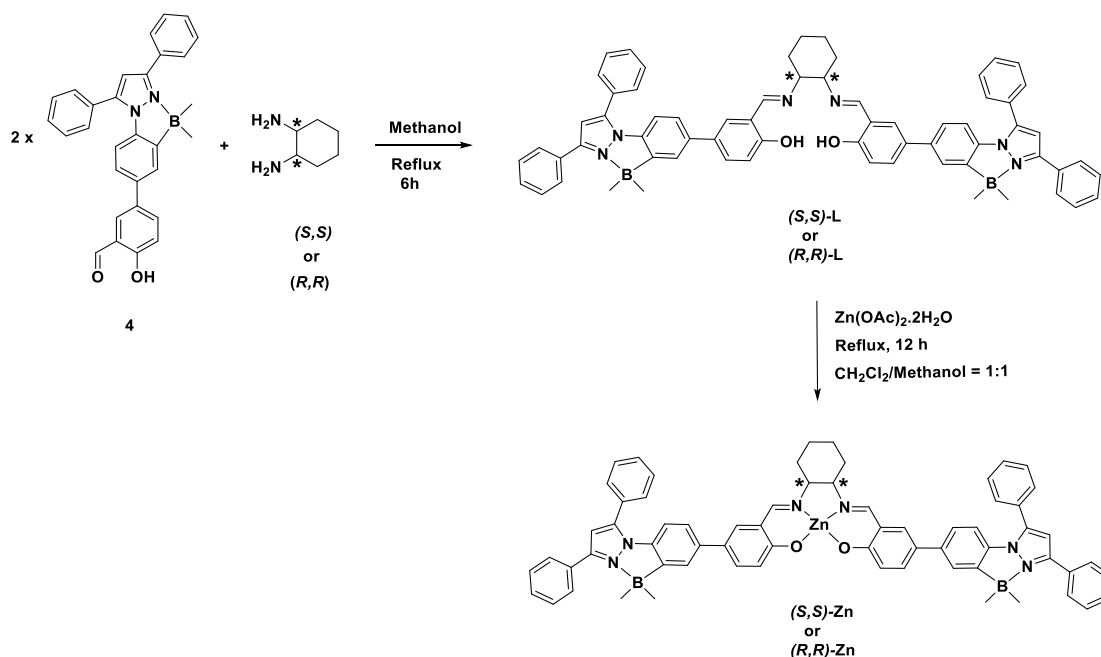
Scheme 4.1: Synthesis of **(S,S)-Zn** and **(R,R)-Zn**

The ligand **(S,S)-L** was synthesized in excellent yield (88%) by a simple condensation reaction of compound **4** with (*1S,2S*)-1,2-diaminocyclohexane in dry methanol. Similarly **(R,R)-L** was synthesized from the condensation reaction of **4** with (*1R,2R*)-1,2-diaminocyclohexane. The Zn(II) complexes **(S,S)-Zn** and **(R,R)-Zn** were synthesized in good yield by reacting equimolar amounts of **(S,S)-L** and **(R,R)-L** respectively with Zn(OAc)$_2$.2H$_2$O in CH$_2$Cl$_2$/CH$_3$OH under reflux condition for 12 hours. Ligands **(S,S)-L/(R,R)-L** and complexes **(S,S)-Zn/(R,R)-Zn** were characterized by multi-nuclear NMR, HRMS (for ligands), MALDI-MS, and X-ray crystallography (for complexes). Boron coordination in ligands and complexes was confirmed by ^{11}B-NMR. Singlets at 0.09 ppm in the ^{1}H-NMR of **(R,R)-Zn** and **(S,S)-Zn** complex respectively represents 12 protons from four methyl groups attached to the B center.

4.2.2 *X-ray Crystal Structure Analysis:*

Single crystals of *(S,S)*-**Zn** and *(R,R)*-**Zn** complexes suitable for X-ray diffraction were grown by slow evaporation of the $DMSO/CH_2Cl_2/Methanol$ solvent system. The structures were determined by X-ray crystallography. The crystallographic data of both the zinc enantiomers are given in Table 4.1. Both the complexes *(S,S)*-**Zn** and *(R,R)*-**Zn** crystallized in a monoclinic space group $P2_1$. The molecular structures of *(S,S)* and *(R,R)*-**Zn** are shown in Figures 4.1 and 4.2 respectively. Selected bond angles and bond lengths are summarized in Table 4.2. The boron center in both complexes exhibits distorted tetrahedral geometry with the formation of a five-membered ring with the pyrazole ligand system. The zinc center exhibits a distorted square pyramidal geometry in both enantiomers.

Table 4.1: Crystal data and structure refinement for chiral Zn complexes

Identification code	*(S,S)*-**Zn**	*(R,R)*-**Zn**
Empirical formula	$C_{68}H_{64}B_2N_6O_3SZn$	$C_{69}H_{66}B_2Cl_2N_6O_3SZn$
Formula weight	1132.30	1217.22
Temperature/K	100.00(10)	100.00(10)
Crystal system	monoclinic	monoclinic
Space group	$P2_1$	$P2_1$
a/Å	10.5446(2)	10.56100(10)
b/Å	25.4701(5)	25.5010(3)
c/Å	22.9828(6)	22.8758(3)

α/°	90	90
β/°	95.860(2)	95.7870(10)
γ/°	90	90
Volume/$\mathring{A}^3$	6140.3(2)	6129.42(12)
Z	4	4
ρ_{calc}g/cm^3	1.225	1.319
μ/mm^{-1}	1.267	2.090
F(000)	2376.0	2544.0
Crystal size/mm^3	$0.24 \times 0.22 \times 0.2$	$0.25 \times 0.23 \times 0.2$
Radiation	CuKα (λ = 1.54184)	CuKα (λ = 1.54184)
2Θ range for data collection/°	6.942 to 150.98	7.77 to 149.006
Index ranges	-13 ≤ h ≤ 13, -30 ≤ k ≤ 31, -19 ≤ l ≤ 28	-13 ≤ h ≤ 8, -31 ≤ k ≤ 30, -28 ≤ l ≤ 28
Reflections collected	47851	53687
Independent reflections	21346 [R_{int} = 0.0372, R_{sigma} = 0.0367]	23075 [R_{int} = 0.0373, R_{sigma} = 0.0389]
Data/restraints/parameters	21346/3071/1471	23075/1/1526
Goodness-of-fit on F^2	1.104	1.061
Final R indexes [I>=2σ (I)]	R_1 = 0.0637, wR_2 = 0.1823	R_1 = 0.0565, wR_2 = 0.1582
Final R indexes [all data]	R_1 = 0.0681, wR_2 = 0.1862	R_1 = 0.0605, wR_2 = 0.1615
Largest diff. peak/hole / e $\mathring{A}^{-3}$	2.03/-1.08	1.40/-0.91
Flack parameter	0.04(3)	0.06(2)

Table 4.2: Some selected bond lengths [A] and bond angles [º] for complexes (*R,R*)-Zn and (*S,S*)-Zn

	(*R,R*)-Zn	(*S,S*)-Zn		(*R,R*)-Zn	(*S,S*)-Zn
Zn1-O1	1.980(4)	2.000(5)	O2-Zn1-O3	95.6(2)	100.8(2)
Zn1-O2	1.981(5)	1.970(5)	O2-Zn1-N3	163.85(2)	148.6(2)
Zn1-N3	2.087(4)	2.117(5)	O2-Zn1-N4	89.86(2)	90.0(2)
Zn1-N4	2.101(4)	2.078(6)	O3-Zn1-N3	99.96(2)	110.5(2)
Zn1-O3	2.064(5)	2.054(5)	O3-Zn1-N4	117.13(2)	107.2(2)
B1-N2	1.642(9)	1.656(1)	N3-Zn1-N4	79.26(2)	78.5(2)
B1-C85	1.622(1)	1.627(1)	C87-B1-N2	115.9(5)	114.0(7)
B1-C87	1.599(1)	1.606(1)	C87-B1-C85	115.3(6)	112.6(7)
B1-C88	1.617(1)	1.591(1)	C87-B1-C88	112.8(6)	116.2(8)
B2-N6	1.669(9)	1.665(1)	C85-B1-N2	94.0(5)	94.0(6)
B2-C117	1.612(9)	1.609(1)	C88-B1-N2	105.9(6)	106.7(7)
B2-C121	1.616(9)	1.604(1)	C88-B1-C85	111.4(6)	111.1(7)
B2-C122	1.622(9)	1.635(1)	C121-B2-N6	108.3(5)	109.6(7)
O1-Zn1-O2	93.91(2)	93.0(2)	C121-B2-C122	113.1(5)	114.1(6)
O1-Zn1-O3	96.5(2)	92.1(2)	C117-B2-N6	94.4(4)	95.3(5)
O1-Zn1-N3	88.61(2)	88.6(2)	C117-B2-C121	115.1(5)	114.3(6)
O1-Zn1-N4	145.6(2)	159.5	C117-B2-C122	111.3(5)	109.8(7)

Figure 4.1: Molecular structure of (*S*,*S*)-**Zn**. Thermal ellipsoids are drawn at 50% probability level. Hydrogen atoms are removed for clarity (except H71 and H106)
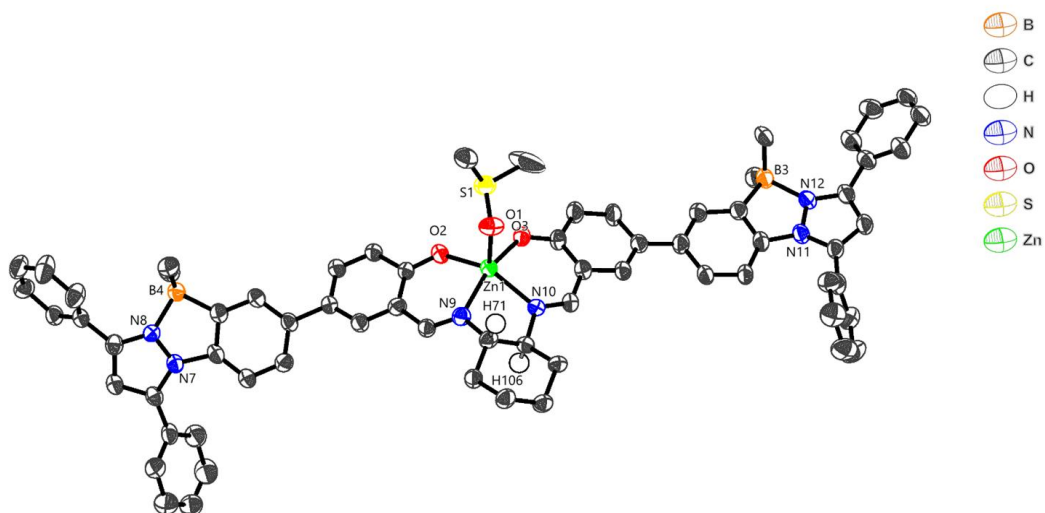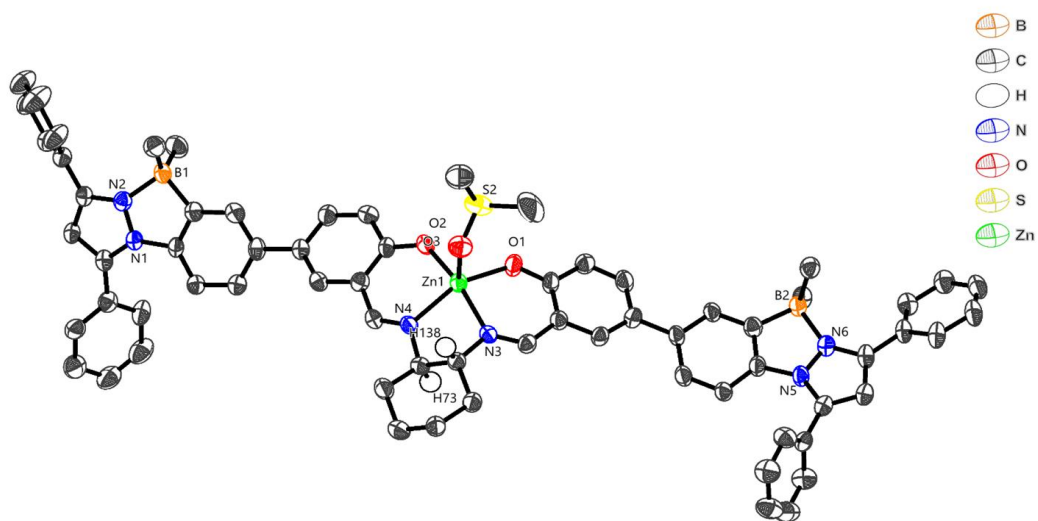

Figure 4.2: Molecular structure of (*R*,*R*)-**Zn**. Thermal ellipsoids are drawn at 50% probability level. Hydrogen atoms are removed for clarity (except H73 and H138)
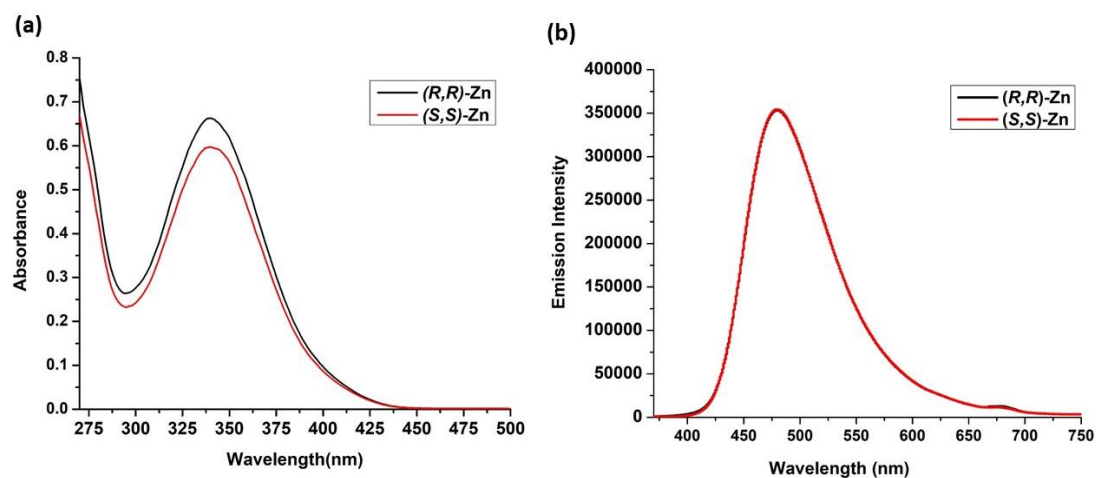
4.2.3 *Photophysical Studies:*

Figure 4.3: (a) Absorption and (b) Emission spectra of **(*S,S*)-Zn** and **(*R,R*)-Zn** in THF at 1 x 10^{-5} M concentration

The photophysical data of complexes **(*R,R*)-Zn** and **(*S,S*)-Zn** in different solvents is given in table 4.3 and their absorption and emission spectra in THF are displayed in figure 4.3. Both the enantiomers in different solvents displayed absorption maxima at ca. 345−350 nm, with a moderate molar extinction coefficient of ca. 22500-66300 M^{-1} cm^{-1}. (Table 4.3). The **(*S,S*)-Zn** and **(*R,R*)-Zn** complexes showed similar absorption profiles in coordinating and non-coordinating solvents. In coordinating solvents like in DMF, DMSO, and THF the absorption maximum was around 340 nm to 355 nm and in non-coordinating CH_2Cl_2, the adsorption maximum was at 332 nm. Emission spectra of both the enantiomers showed similar profiles in THF with the presence of a sharp peak at 480 nm. Both the enantiomers showed similar quantum yields in both coordinating and non-coordinating solvents. The fluorescence lifetime of **(*R,R*)-Zn** and **(*S,S*)-Zn** complexes are 2.45 ns and 2.46 nm respectively in THF solvent (Figure 4.4 and table 4.3).
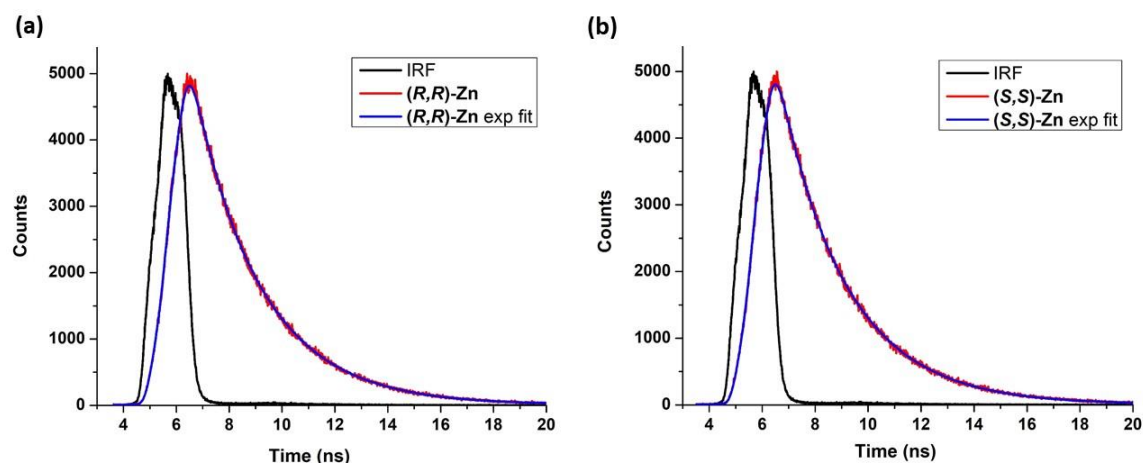
Figure 4.4: Fluorescence decay profile of (**R,R**)-**Zn** and (**S,S**)-**Zn** in THF

Table 4.3: Summary of photophysical data of (**R,R**)-**Zn** and (**S,S**)-**Zn**.

Solvent	Complex	λ_{max} (nm)	$\varepsilon \times 10^4$ (mol^{-1} L cm^{-1})	λ_{ems} (nm)	ΔE (cm^{-1}) Stokes shift	QY[a]
THF	(*S,S*)-**Zn**	340	5.97	480	8578	11.13 % (2.46 ns)
	(*R,R*)-**Zn**	340	6.63	480	8578	12.72 % (2.45 ns)
DCM	(*S,S*)-**Zn**	332	2.48	476	9112	4.44 %
	(*R,R*)-**Zn**	332	2.25	476	9112	5.06 %
DMF	(*S,S*)-**Zn**	354	5.32	548	10000	2.23 %
	(*R,R*)-**Zn**	354	4.54	548	10000	2.46 %
DMSO	(*S,S*)-**Zn**	355	5.85	555	10150	4.25 %
	(*R,R*)-**Zn**	355	4.39	555	10150	4.48 %

[a]Absolute quantum yield using integrating sphere module

4.2.4 *CD Spectroscopy:*

The circular dichroism (CD) spectra in THF show the chirality of ligands and zinc complexes (Figure 4.5). As shown in figure 4.5, the CD spectra of **(*S,S*)-L** shows a negative Cotton effect at 256 nm and 333 nm while **(*R,R*)-L** shows a positive cotton effect at 256 nm and 333 nm which confirmed that **(*S,S*)-L** and **(*R,R*)-L** are perfect mirror images of each other. As expected the CD spectra of zinc complexes were different from the ligand systems and both the enantiomers exhibited mirror images in CD spectra. **(*S,S*)-Zn** and **(*R,R*)-Zn** (Figure 4.5(b)) showed opposite Cotton effects at 299 nm and 409 nm. The results confirmed the successful synthesis of chiral zinc complexes from chiral ligand systems.
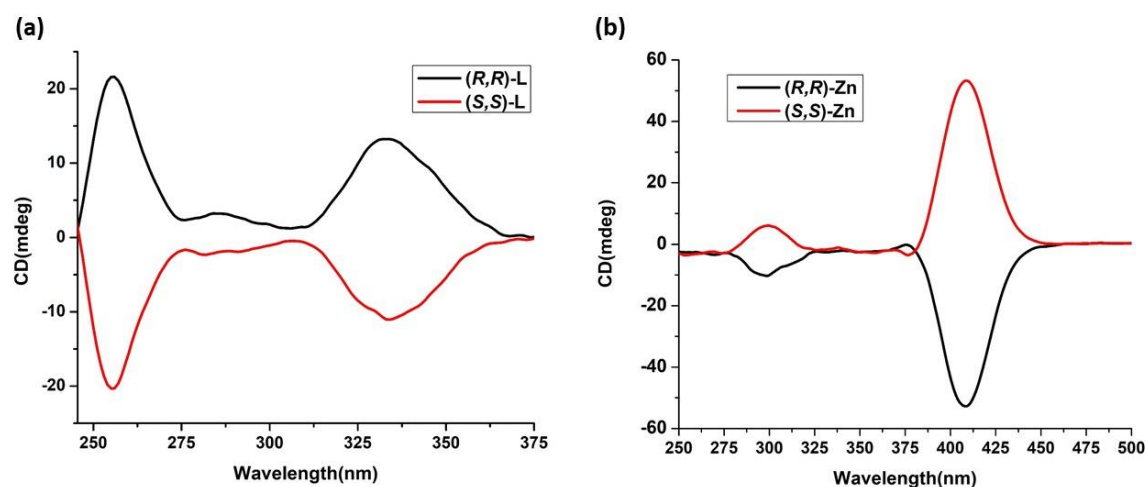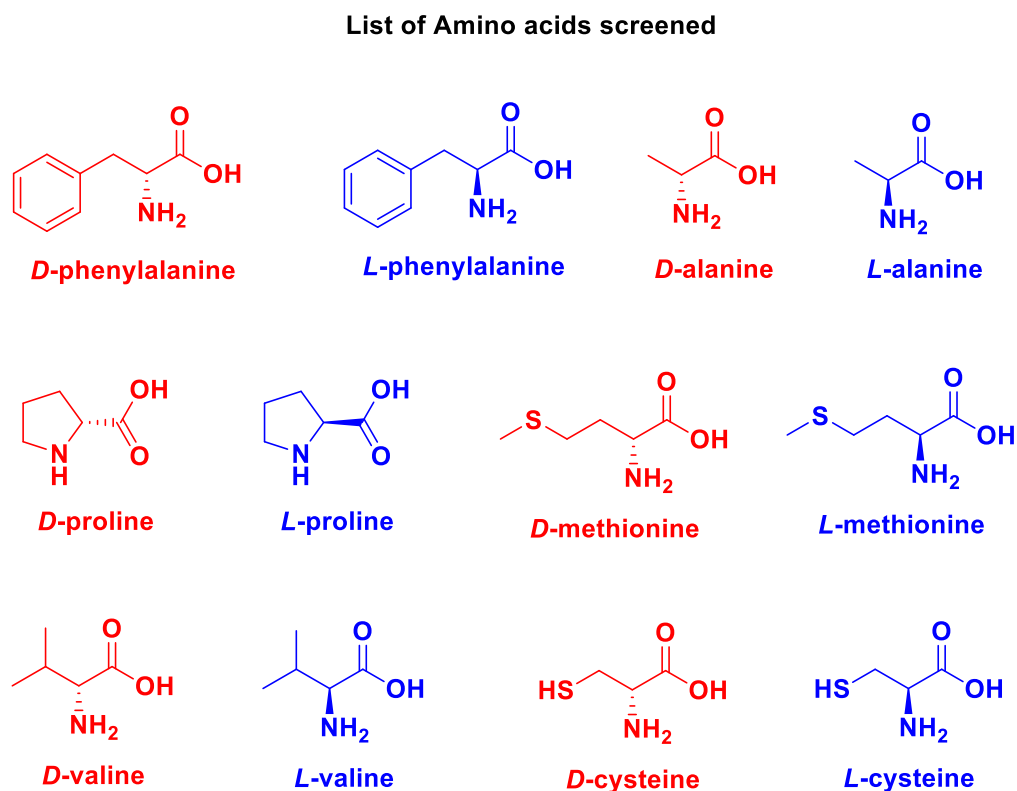

Figure 4.5: Circular Dichromism (CD) spectra of (a) **(*S,S*)/(*R,R*)-L** (b) **(*S,S*)/(*R,R*)-Zn** at 1 x 10^{-4} M concentration in THF solution

4.2.5 Enantioselective Sensing of Amino Acids

A THF solution of (**R,R**)-**Zn**/(**S,S**)-**Zn** (1.0 x 10^{-5} mol L^{-1}) was treated with the individual enantiomers of amino acids in water over the concentration range 1.67 x 10^{-6} – 3.0 x 10^{-5} mol L^{-1}. The enantioselectivity of ((**R,R**)-**Zn**/(**S,S**)-**Zn**) toward various amino acids can be represented by the ratio of the fluorescence intensity for the emission of the zinc enantiomers (I_D/I_L or I_L/I_D). The list of amino acids that were screened to determine enantioselectivity is presented in Table 4.4.

Table 4.4: List of amino acids screened

List of Amino acids screened

D-phenylalanine · L-phenylalanine · D-alanine · L-alanine

D-proline · L-proline · D-methionine · L-methionine

D-valine · L-valine · D-cysteine · L-cysteine

4.2.5.1 D- and L-phenylalanine

The effect of the concentration of enantiomers of phenylalanine on the fluorescent response of the (**R,R**)-**Zn** sensor in solution is shown in Figure 4.6. As the concentration of the enantiomers of the chiral phenylalanine (1.67 x 10^{-6} – 2.3 x 10^{-5}

176

M) increased, the fluorescent intensity at 481 nm gradually decreased. We observed that adding 70 μL of *L*-phenylalanine (1 x 10^{-3} M) quenches the emission of **(*R,R*)-Zn** more than that of *D*-phenylalanine (1 x 10^{-3} M, 70 μL). Figure 4.7 plots the fluorescence intensity
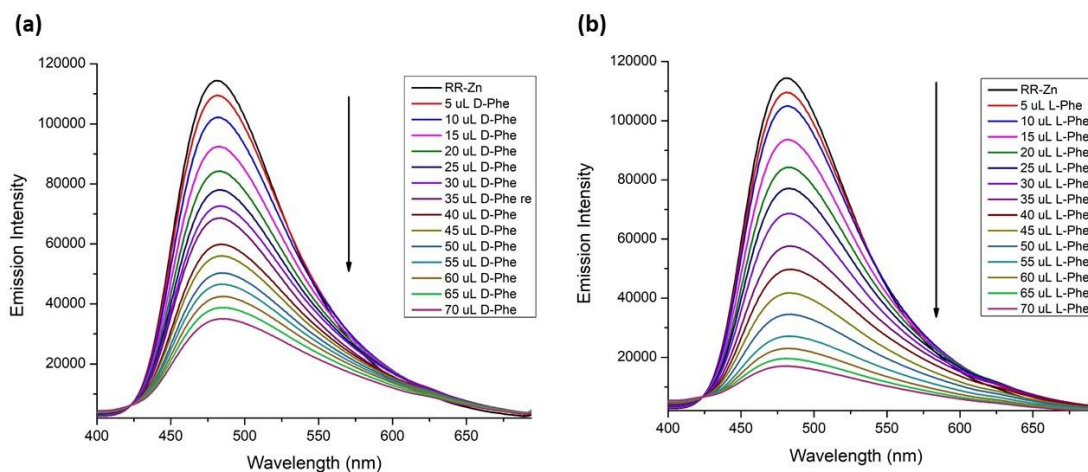

Figure 4.6: Fluorescence titration spectra of **(*R,R*)-Zn** (1.0×10^{-5} mol/L) in THF with (a) (*D*)- and (b) (*L*)-phenylalanine (1.0×10^{-3} mol/L) in water
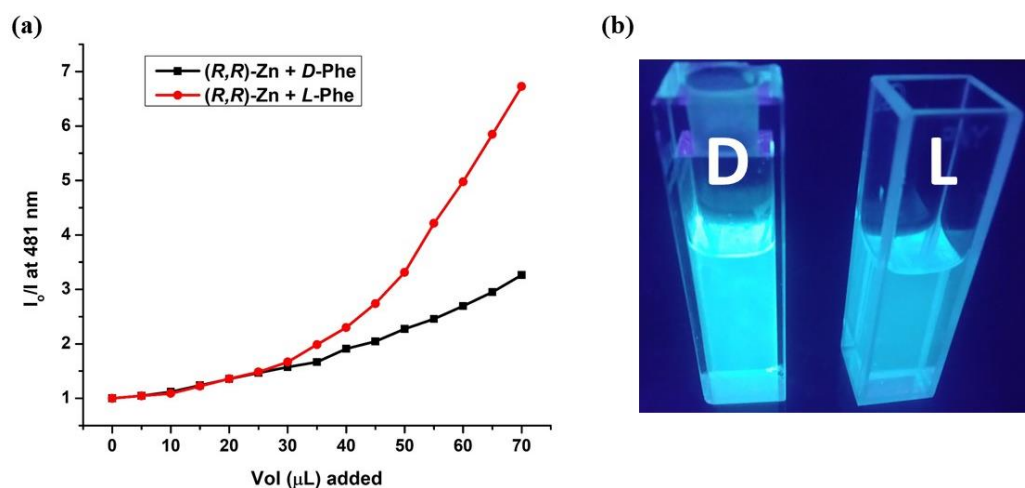

Figure 4.7: (a) Fluorescence quenching of **(*R,R*)-Zn** (1.0×10^{-5} mol/L in THF) with (*D*)- and (*L*)-phenylalanine (1.0×10^{-3} mol/L in water) at λ_{em} = 481 nm (b) Fluorescence image of **(*R,R*)-Zn** (1.0×10^{-5} mol/L) with the addition of 70 μL of (*L*)- and (*D*)-phenylalanine (1.0×10^{-3} mol/L in water) taken under hand-held UV-Lamp

ratio I_0/I_{481} versus the volume of the chiral phenylalanine (1×10^{-3} M) added, which shows a highly enantioselective fluorescent response. The ratio I_0/I_{481} for *D*-phenylalanine and *L*-phenylalanine remains the same up to the addition of 30 μL, and the subsequent addition of *D*- or *L*-phenylalanine exhibits enantioselectivity (Figure 4.7). We noted an enantioselective fluorescence ratio (I_D/I_L) of 2.06 for **(R,R)-Zn** at 2.3×10^{-5} M concentration addition of phenylalanine.
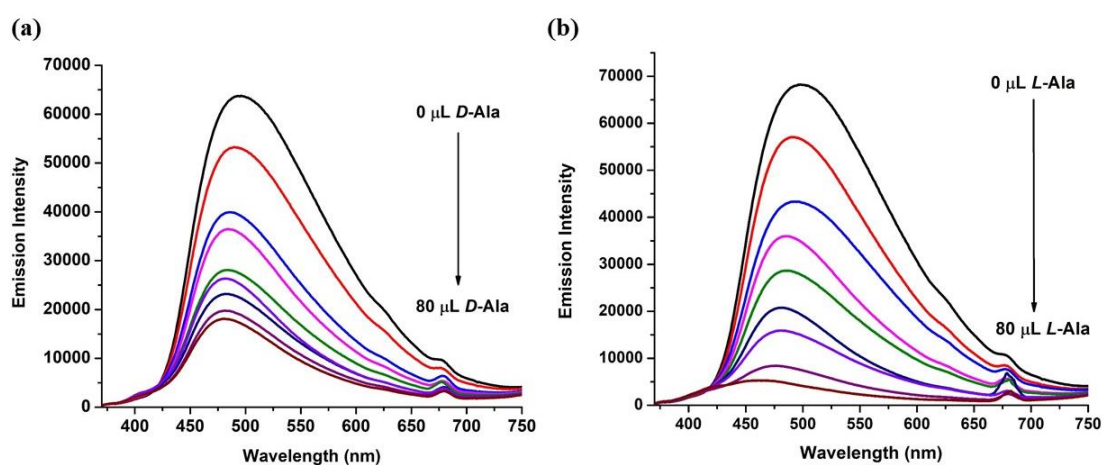
4.2.5.2 *D*- and *L*-Alanine

Figure 4.8: Fluorescence titration spectra of **(R,R)-Zn** (1.0×10^{-5} mol/L) in THF with (a) (*D*)- and (b) (*L*)-alanine (1.0×10^{-3} mol/L) in water

The effect of the concentration of enantiomers of alanine on the fluorescent response of the **(R,R)-Zn** sensor in solution is shown in figure 4.8. As the concentrations of the enantiomers of the chiral phenylalanine ($1.67 \times 10^{-6} - 2.67 \times 10^{-5}$ M) increased, the fluorescent intensity at 481 nm gradually decreased. We observed that adding 80 μL of *L*-alanine (1×10^{-3} M) quenches the emission of **(R,R)-Zn** more than adding 80 μL of *D*-alanine (1×10^{-3} M). Figure 4.9 plots the fluorescence intensity ratio I_0/I_{481} versus the volume of the chiral phenylalanine (1×10^{-3} M) added, which shows a highly enantioselective fluorescent response. The ratio I_0/I_{481} for *D*-alanine

and *L*-alanine remains the same up to the addition of 40 µL, and subsequent addition of *D*- or *L*-alanine exhibits enantioselectivity (figure 4.9).   We noted a high enantioselective fluorescence ratio (I_D/I_L) of 3.95 for **(*R,R*)-Zn** at 2.67 x 10^{-5} M concentration upon addition of alanine.
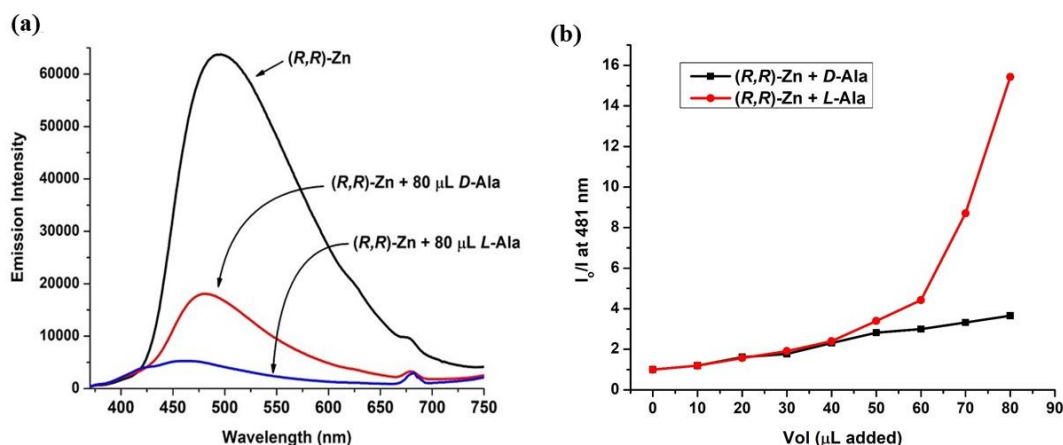

Figure 4.9: (a) Fluorescence spectra of **(*R,R*)-Zn** (1.0×10^{-5} mol/L) in THF with and without (*D*)- and (*L*)-alanine (1.0×10^{-3} mol/L in water) (b) I_o/I at 481 nm of **(*R,R*)-Zn** (1.0×10^{-5} mol/L in THF; $\lambda_{ex} = 340$ nm) versus the increasing volume of *L*-alanine or *D*-alanine (1.0×10^{-3} mol/L in water)

We observed a mirror image response for **(*S,S*)-Zn** interaction with D-/L-alanine in comparison to **(*R,R*)-Zn**. The effect of the concentration of enantiomers of alanine on the fluorescent response of the **(*S,S*)-Zn** sensor in solution is shown in figure 4.10. As the concentrations of the enantiomers of the chiral alanine (1.67×10^{-6} – 2.83×10^{-5} M) increased, the fluorescent intensity at 481 nm gradually decreased. We observed that adding 85 µL of *D*-alanine (1×10^{-3} M) quenches the emission of **(*S,S*)-Zn** more than adding 85 µL of *L*-alanine does (1×10^{-3} M). Figure 4.11 plots the fluorescence intensity ratio I_o/I_{481} versus the volume of the chiral alanine (1×10^{-3} M)
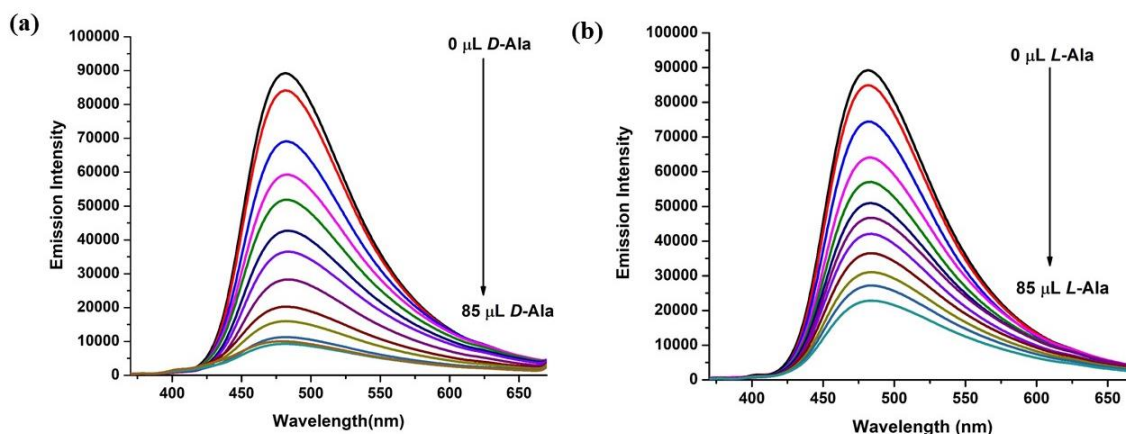
Figure 4.10: Fluorescence titration spectra of **(S,S)-Zn** $(1.0 \times 10^{-5}$ mol/L) in THF with (a) D- and (b) L-alanine $(1.0 \times 10^{-3}$ mol/L) in water
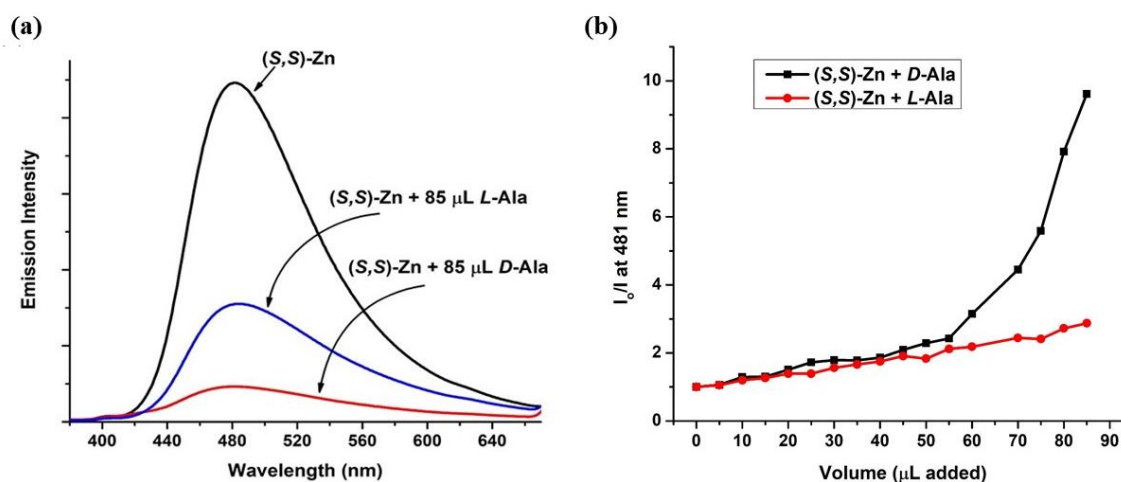

Figure 4.11: (a) Fluorescence titration spectra of **(S,S)-Zn** $(1.0 \times 10^{-5}$ mol/L in THF with and without (D)- and (L)-alanine $(1.0 \times 10^{-3}$ mol/L in water) (b) I_o/I at 483 nm of **(S,S)-Zn** $(1.0 \times 10^{-5}$ mol/L in THF; $\lambda_{ex} = 340$ nm) versus the increasing volume of L-alanine or D-alanine $(1.0 \times 10^{-3}$ mol/L in water)

added, which shows high enantioselective fluorescent response. The ratio I_o/I_{481} for D-alanine and L-alanine remains the same up to the addition of 55 μL of D- or L-alanine, and the subsequent addition of D- or L-alanine exhibits enantioselectivity

(figure 4.11).   We noted a high enantioselective fluorescence ratio (I_L/I_D) of 3.44 for **(S,S)-Zn** at 2.83 x 10^{-5} M concentration addition of alanine.

4.2.5.3 D- and L-Cysteine

The effect of the concentration of enantiomers of cysteine on the fluorescent response of the **(R,R)-Zn** sensor in solution is shown in figure 4.12. As the concentrations of the enantiomers of the chiral cysteine (1.67 x 10^{-6} – 1.34 x 10^{-5} M) increased, the fluorescent intensity at 481 nm gradually decreased. We observed that adding 40 µL of D-cysteine (1 x 10^{-3} M) quenches the emission of **(R,R)-Zn** more than adding 40 µL of L-cysteine does (1 x 10^{-3} M). Figure 4.13 plots the fluorescence intensity ratio I_o/I_{481} versus the volume of the chiral cysteine (1 x 10^{-3} M) added, which shows a highly enantioselective fluorescent response. The ratio I_o/I_{481} for D-cysteine and L-cysteine remains the same up to the addition of 40 µL, and the subsequent addition of D- or L-alanine exhibits enantioselectivity (figure 4.13). We noted an enantioselective fluorescence ratio (I_L/I_D) of 2.51 for **(R,R)-Zn** at 1.34 x 10^{-5} M concentration upon addition of cysteine.
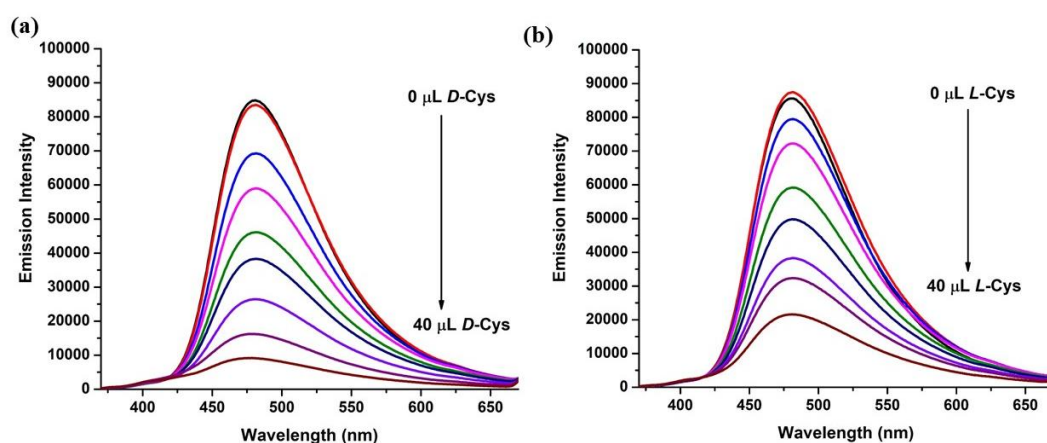

Figure 4.12: Fluorescence titration spectra of **(R,R)-Zn** (1.0 × 10^{-5} mol/L) in THF with (a) (D)- and (b) (L)-cysteine (1.0 × 10^{-3} mol/L) in water
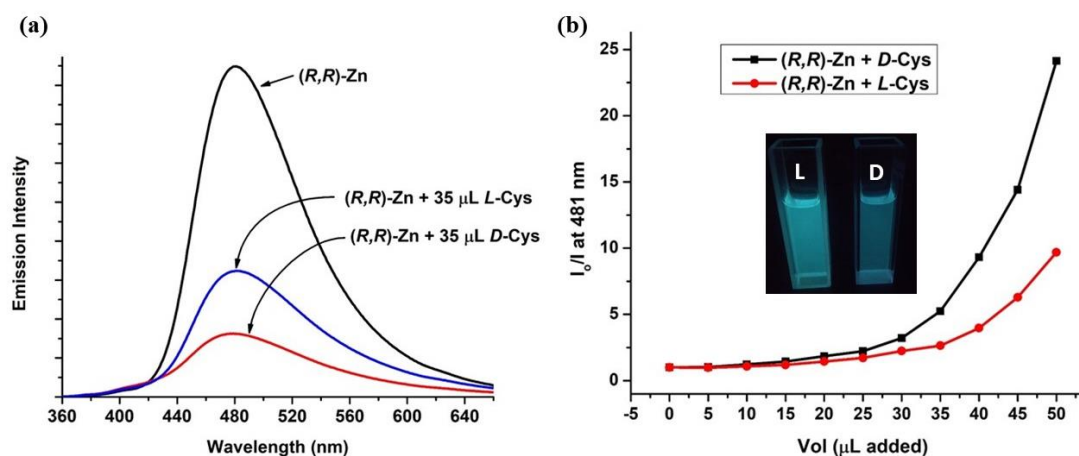
Figure 4.13: (a) Fluorescence titration spectra of **(R,R)-Zn** (1.0×10^{-5} mol/L in THF with and without (*D*)- and (*L*)-cysteine (1.0×10^{-3} mol/L in water) (b) I_o/I at 481 nm of **(R,R)-Zn** (1.0×10^{-5} mol/L in THF; $\lambda_{ex} = 340$ nm) versus the increasing volume of *L*-cysteine or *D*-cysteine (1.0×10^{-3} mol/L in water)
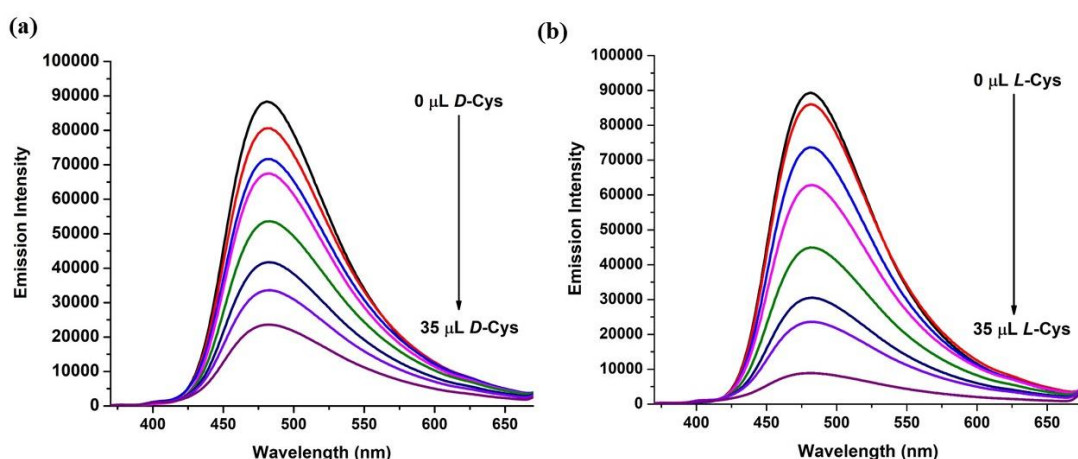

Figure 4.14: Fluorescence titration spectra of **(S,S)-Zn** (1.0×10^{-5} mol/L) in THF with (a) (*D*)- and (b) (*L*)-cysteine (1.0×10^{-3} mol/L) in water

The effect of the concentration of enantiomers of cysteine on the fluorescent response of the **(S,S)-Zn** sensor in solution is shown in Figure 4.14. As the concentrations of the enantiomers of the chiral cysteine (1.67×10^{-6} – 1.67×10^{-5} M) increased, the

fluorescent intensity at 481 nm gradually decreased. We observed that adding 35 μL

of D-cysteine (1 x 10^{-3} M) quenches the emission of (S,S)-Zn more than adding 35 μL

of L-cysteine does (1 x 10^{-3} M). Figure 4.15 plots the fluorescence intensity

ratio I_o/I_{481} versus the volume of the chiral cysteine (1 x 10^{-3} M) added, which shows

a high enantioselective fluorescent response. The ratio I_o/I_{481} for D-cysteine and L-

cysteine remains the same up to the addition of 25 μL, and the subsequent upon

addition of D- or L-cysteine exhibits enantioselectivity (figure 4.15).   We noted an

enantioselective fluorescence ratio (I_D/I_L) of 2.60 for (S,S)-Zn at 1.67 x 10^{-5} M
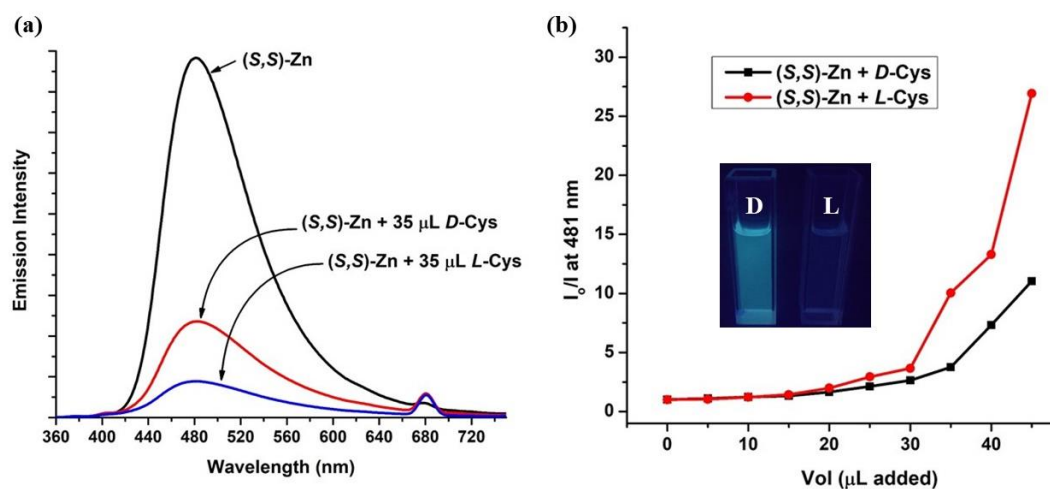
concentration addition of cysteine

Figure 4.15: (a) Fluorescence titration spectra of (S,S)-Zn (1.0×10^{-5} mol/L in THF

with and without (D)- and (L)-cysteine (1.0×10^{-3} mol/L in water) (b) I_o/I at 481 nm of

(S,S)-Zn (1.0×10^{-5} mol/L in THF; λ_{ex} = 340 nm) versus the increasing volume of L-

cysteine or D-cysteine (1.0 x 10^{-3} mol/L in water)

4.2.5.4 D- and L-Methionine

The effect of the concentration of enantiomers of methionine on the fluorescent

response of the (R,R)-Zn sensor in solution is shown in figure 4.16. As the

concentrations of the enantiomers of the chiral methionine (1.67 x 10^{-6} – 1.83 x 10^{-5}

M) increased, the fluorescent intensity at 481 nm gradually decreased. However we did not observe any enantioselective fluorescence response even after adding 60 μL of D- or L-methionine (1 x 10^{-3} M) to **(R,R)-Zn** (1 x 10^{-5} M). Figure 4.16(b) plots the fluorescence intensity ratio I_o/I_{481} versus the volume of the chiral methionine (1 x 10^{-3} M) added, which shows no enantioselective fluorescent response. The ratio I_o/I_{481} for D-methionine and L-methionine remains the same up to the addition of 60 μL and the subsequent addition of D- or L-methionine does not exhibit any enantioselectivity.(figure 4.16) We noted an enantioselective fluorescence ratio (I_D/I_L) of 1.03 for **(R,R)-Zn** at 1.34 x 10^{-5} M concentration addition of methionine.

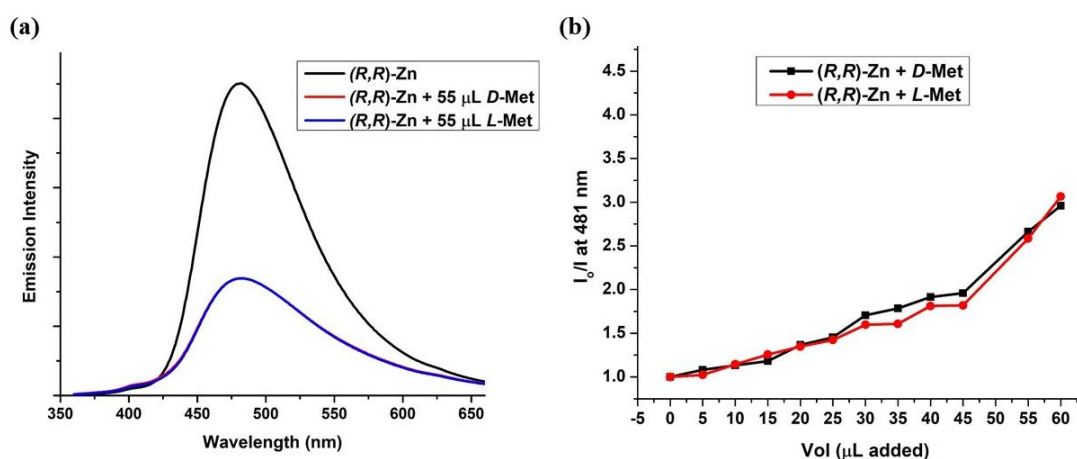**Figure 4.16:** (a) Fluorescence titration spectra of **(R,R)-Zn** (1.0 × 10^{-5} mol/L in THF with and without (D)- and (L)-methionine (1.0 ×10^{-3} mol/L in water) (b) I_o/I at 481 nm of **(R,R)-Zn** (1.0 × 10^{-5} mol/L in THF; λ_{ex} = 340 nm) versus the increasing volume of L-methionine or D-methionine (1.0 x 10^{-3} mol/L in water)

The effect of the concentration of enantiomers of methionine on the fluorescent response of the **(S,S)-Zn** sensor in solution is shown in Figure xx. Similar findings to those seen with **(R,R)-Zn** were also seen in **(S,S)-Zn**. The ratio I_o/I_{481} for D-methionine and L-methionine remains the same up to the addition of 55 μL, and the

subsequent addition of *D*- or *L*-methionine does not exhibit any enantioselectivity (figure 4.17). We noted an enantioselective fluorescence ratio (I_L/I_D) of 1.01 for **(*S,S*)-Zn** at 1.83 x 10^{-5} M concentration addition of methionine.
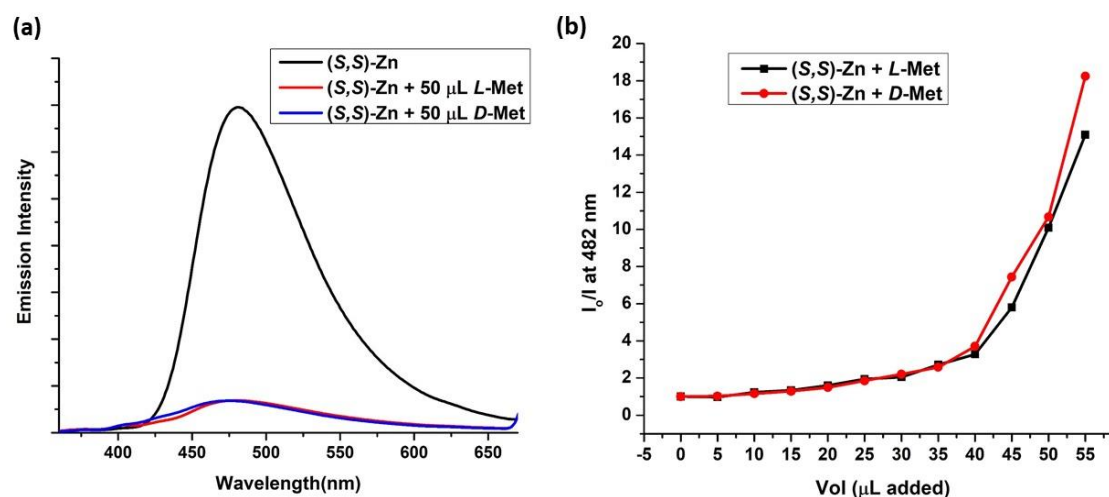
.

Figure 4.17: (a) Fluorescence titration spectra of **(*S,S*)-Zn** (1.0×10^{-5} mol/L in THF with and without (*D*)- and (*L*)-methionine (1.0×10^{-3} mol/L in water) (b) I_o/I at 481 nm of **(*S,S*)-Zn** (1.0×10^{-5} mol/L in THF; $\lambda_{ex} = 340$ nm) versus the increasing volume of *L*-methionine or *D*-methionine (1.0×10^{-3} mol/L in water)

4.2.5.5 D- and *L*-Valine

The effect of the concentration of enantiomers of valine on the fluorescent response of the **(*R,R*)-Zn** sensor in solution is shown in figure 4.18. As the concentrations of the enantiomers of the chiral valine (1.67 x 10^{-6} – 1.83 x 10^{-5} M) increased, the fluorescent intensity at 481 nm gradually decreased. However we observed low enantioselective fluorescence response after adding 55 µL of *D*- or *L*-valine (1 x 10^{-3} M) to **(*R,R*)-Zn** (1 x 10^{-5} M). Figure 4.18(b) plots the fluorescence intensity

ratio I_o/I_{481} versus the volume of the chiral valine (1 x 10^{-3} M) added, which shows low enantioselective fluorescent response. The ratio I_o/I_{481} for *D*-valine and *L*-valine remains the same up to the addition of 35 µL, and subsequent addition of *D*- or *L*-valine exhibit low enantioselectivity (figure 4.18). We noted an enantioselective fluorescence ratio (I_D/I_L) of 1.35 for **(*R,R*)-Zn** at 1.83 x 10^{-5} M concentration addition of valine.
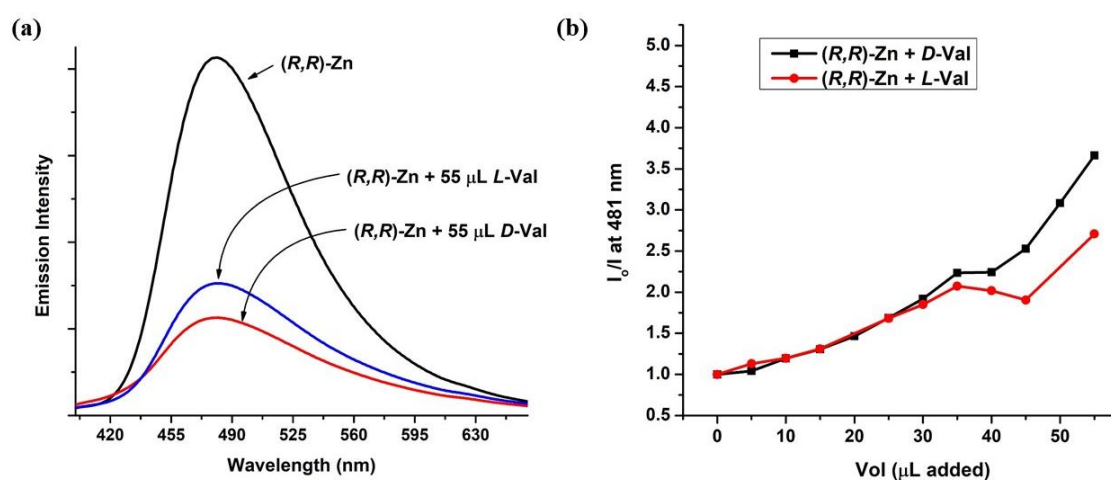

Figure 4.18: (a) Fluorescence titration spectra of **(*R,R*)-Zn** (1.0×10^{-5} mol/L in THF with and without (*D*)- and (*L*)-valine (1.0×10^{-3} mol/L in water) (b) I_o/I at 481 nm of **(*R,R*)-Zn** (1.0×10^{-5} mol/L in THF; λ_{ex} = 340 nm) versus the increasing volume of *L*-valine or *D*-valine (1.0×10^{-3} mol/L in water)

The effect of the concentration of enantiomers of valine on the fluorescent response of the **(*S,S*)-Zn** sensor in solution is shown in figure 4.19. As the concentrations of the enantiomers of the chiral valine (1.67 x 10^{-6} – 1.83 x 10^{-5} M) increased, the fluorescent intensity at 481 nm gradually decreased. However, we observe low enantioselective fluorescence response after adding 55 µL of *D*- or *L*-valine (1 x 10^{-3}

M) to **(S,S)-Zn** (1 x 10^{-5} M). Figure 4.19(b) plots the fluorescence intensity ratio I_o/I_{481} versus the volume of the chiral valine (1 x 10^{-3} M) added, which shows a low enantioselective fluorescent response. The ratio I_o/I_{481} for *D*-valine and *L*-valine remains the same up to the addition of 20 μL, and subsequent addition of *D*- or *L*-valine exhibit low enantioselectivity (figure 4.19). We noted an enantioselective fluorescence ratio (I_D/I_L) of 1.40 for **(S,S)-Zn** at 1.83 x 10^{-5} M concentration addition of valine.
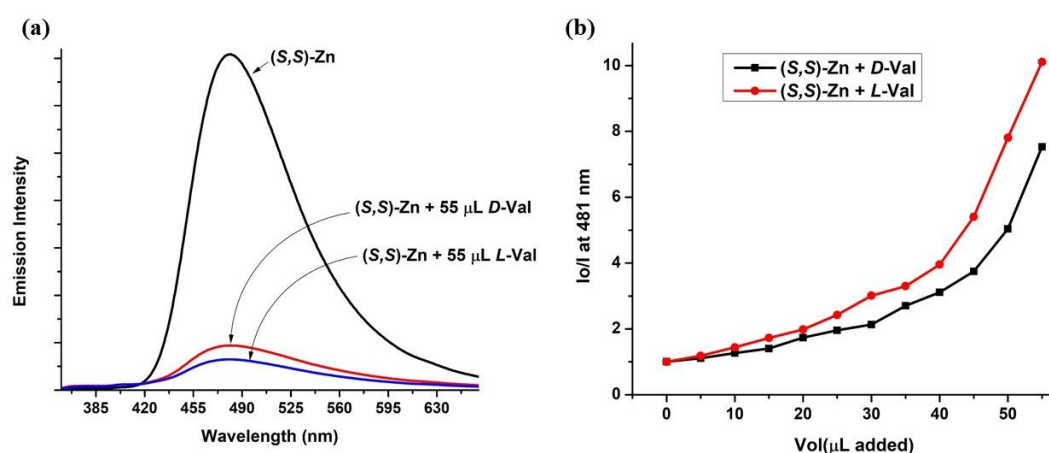

Figure 4.19: (a) Fluorescence titration spectra of **(S,S)-Zn** (1.0×10^{-5} mol/L in THF with and without (*D*)- and (*L*)-valine (1.0×10^{-3} mol/L in water) (b) I_o/I at 481 nm of **(S,S)-Zn** (1.0×10^{-5} mol/L in THF; λ_{ex} = 340 nm) versus the increasing volume of *L*-valine or *D*-valine (1.0 x 10^{-3} mol/L in water)

The fluorescent responses of **(R,R)**- and **(S,S)-Zn** towards a variety of amino acids are summarized in table 4.5.

Table 4.5: The fluorescent responses of (**R,R**)- and (**S,S**)-**Zn** towards a variety of amino acids

Amino acid	Amino acid conc. (M)	(*R,R*)-Zn or (*S,S*)-Zn conc. (M)	(*R,R*)-Zn (I_D/I_L or I_L/I_D)	(*S,S*)-Zn (I_D/I_L or I_L/I_D)
Alanine	2.67×10^{-5}	1×10^{-5}	3.95	3.44
Cysteine	1.34×10^{-5}	1×10^{-5}	2.51	2.60
Valine	$1,83 \times 10^{-5}$	1×10^{-5}	1.35	1.40
Methionine	1.83×10^{-5}	1×10^{-5}	1.03	1.01
Leucine	1.34×10^{-5}	1×10^{-5}	1.08	1.02

4.3 Conclusion:

In summary, we have synthesized and characterized tetra-coordinated boron functionalized pyrazole-based chiral zinc salen complexes. The synthesized chiral zinc complexes serve as fluorescent sensors for the enantioselective recognition of *D/L*-phenylalanine, *D/L*-alanine and *D/L*-cysteine.

4.4 Experimental Section:

4.4.1 General Information

All reagents and starting materials were purchased from Sigma-Aldrich, Alfa-Aesar, and Spectrochem chemical companies and used as received unless otherwise noted.

Chlorinated solvents, acetonitrile, and DMF were distilled from CaH_2. THF and toluene were distilled from Na/benzophenone before use. All 400 MHz ^1H, 100 MHz ^{13}C, and NMR spectra were recorded on a Bruker ARX 400 spectrometer operating at 400 MHz. All ^1H and ^{13}C NMR spectra were referenced internally to solvent signals. All NMR spectra were recorded at ambient temperature. ESI mass spectra were recorded on Bruker, micrOTOF-QII mass spectrometer. MALDI was recorded on Applied Biosystems Q10 4800 MALDI TOF/TOF analyzer using 4000 series explorer software for acquisition and GPS explorer software, version 3.6 for analysis. Elemental analyses were performed in a Euro Vector EA 3000 CHNS analyzer. The absorbance spectra were recorded on a JASCO V-730 UV-Visible spectrometer. The fluorescence spectra were recorded using an Edinburgh FS5 spectrofluorometer. Absolute fluorescence quantum yields of complexes were measured by integrating sphere method using an Edinburgh FS5 spectrofluorometer. The fluorescence spectra were corrected for the instrumental response. Single-crystal X-ray diffraction data for compounds (*S,S*)-**Zn** and (*R,R*)-**Zn** were collected on a Rigaku SuperNova fine-focused dual diffractometer, with Cu Kα radiation (λ = 1.54178 Å) or Mo-Kα radiation (0.71073 Å) equipped with a PILATUS200K detector. Using Olex2, the structures were solved with the ShelXS structure solution program using Direct Methods and refined with the ShelXL refinement package using Least Squares minimization. All non-hydrogen atoms were refined with anisotropic displacement coefficients. The H atoms were placed at calculated positions and were refined as riding atoms.

4.4.1.2 Preparation of samples for fluorescence measurements

Materials: The synthesized zinc complexes were purified by recrystallization and then

stored in a refrigerator. The amino acid derivatives were purchased from Aldrich. Dry

THF stock solutions of the sensors were freshly prepared for each measurement. A

0.001 M stock solution of the amino acid was freshly prepared by using water. For the

fluorescence quenching study, a sensor solution was mixed with amino acid solution

at room temperature in a glass vial and diluted to the desired concentration. The

resulting solution was allowed to stand at room temperature for 4 h before the

fluorescence measurement.

### 4.4.2 Synthetic procedure and spectral characterization

Synthesis of compound (*S,S*)-L:
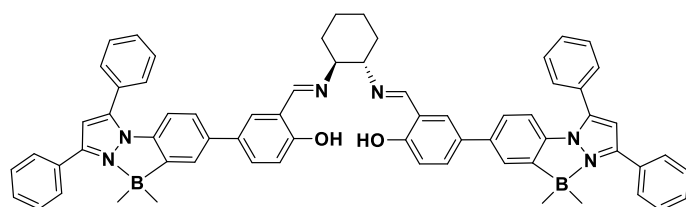
To 150 mL two neck RB, compound **4** (1.09 mmol, 0.5 g, 2 equiv.) and (1*S*,2*S*)-1,2-diaminocyclohexane (0.55 mmol, 62.5 mg, 1 equiv.) were added to dry methanol and refluxed overnight under nitrogen. The reaction mixture was filtered and a yellow precipitate of compound **(*S,S*)-L** was collected. Yield: 88% (480 mg) ^{1}H NMR (400 MHz, DMSO-d_6): δ = 13.39 (s, 2H), 8.58 (s, 2H), 7.92 – 7.85 (m, 4H), 7.79 – 7.72 (m, 4H), 7.70 – 7.62 (m, 9H), 7.61 – 7.42 (m, 6H), 7.53 – 7.45 (m, 5H), 7.17 – 7.09 (m, 4H) 6.84 (d, J = 8.0 Hz, 2H), 6.69 (d, J = 8.0 Hz, 2H), 3.46 – 3.39 (m, 2H), 1.95 – 1.86 (m, 2H), 1.83 – 1.75 (m, 2H), 1.70 – 1.57 (m, 2H), 1.53 – 1.40 (m, 2H), 0.06 (s, 12H). ^{13}C NMR (101 MHz, DMSO-d_6) δ 165.3, 159.9, 155.7, 147.9, 140.1, 137.5, 136.8, 130.7, 130.5, 129.6, 129.1, 128.9, 128.5, 127.9, 126.6, 123.0, 118.6, 116.8, 111.5, 111.2, 71.2, 32.4, 23.7, 9.6 ppm. ^{11}B NMR (128 MHz, DMSO-d_6) δ -2.83 ppm.

HRMS (ESI+, m/z) calcd for $C_{66}H_{60}B_2N_6O_2$, [M+H] $^+$ m/z = 991.5056, found = 991.5000

Synthesis of compound (*R,R*)-L:
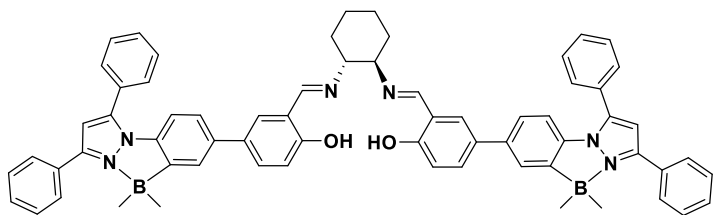
To 150 mL two neck RB, compound **4** (1.09 mmol, 0.5 g, 2 equiv.) and (1*R*, 2*R*)-1,2-

diaminocyclohexane (0.55 mmol, 62.5 mg, 1 equiv.) were added to dry methanol and refluxed overnight under nitrogen. The reaction mixture was filtered and a yellow precipitate of compound **5a** was collected. Yield: 93% (507 mg) ^{1}H NMR (400 MHz, DMSO-d_6): δ 13.39 (s, 2H), 8.58 (s, 2H), 7.92 – 7.84 (m, 4H), 7.78 – 7.73 (m, 4H), 7.71 – 7.62 (m, 9H), 7.62 – 7.54 (m, 6H), 7.53 – 7.46 (m, 4H), 7.19 – 7.11 (m, 4H), 6.84 (d, *J* = 8.0 Hz, 2H), 6.69 (d, *J* = 8.0 Hz, 2H), 3.46 – 3.39 (m, 2H), 1.96 – 1.86 (m, 2H), 1.86 – 1.76 (m, 2H), 1.70 – 1.57 (m, 2H), 1.53 – 1.40 (m, 2H), 0.06 (s, 12H) ppm. ^{13}C NMR (101 MHz, DMSO-d_6) δ 165.3, 159.9, 155.7, 147.9, 140.1, 137.5, 136.8, 130.7, 130.5, 129.6, 129.1, 128.9, 128.5, 127.9, 126.6, 123.0, 118.6, 116.8, 111.5, 111.2, 71.2, 32.4, 23.7, 9.6 ppm. ^{11}B NMR (128 MHz, DMSO-d_6) δ -2.26 ppm. HRMS (ESI+, m/z) calcd for $C_{66}H_{60}B2N_6O_2$, [M+H] + m/z = 991.5056, found = 991.5036
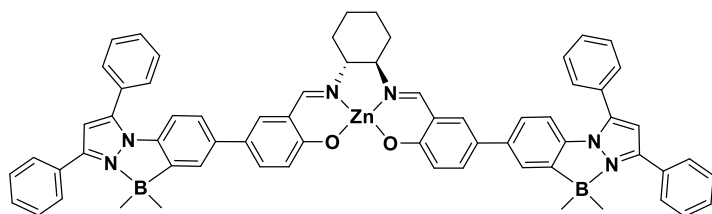
Synthesis of complex (*S,S*)-Zn:
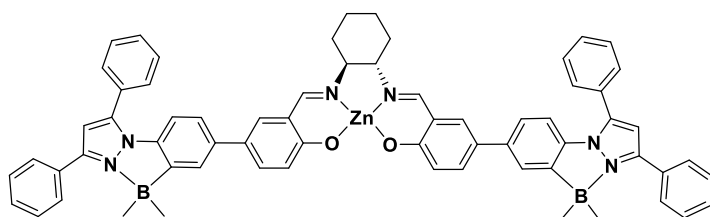
To 150 mL two neck RB, compound (*S,S*)-L (300mg, 0.3 mmol, 1 equiv.) was dissolved in 15 mL CH_2CL_2 and a solution of Zn(OAc)$_2$.2H$_2$O (72 mg, 0.33 mmol, 1.1 equiv.) in 15 mL dry methanol was added dropwise under nitrogen. The greenish-

yellow solution was refluxed for 12 h. Light green color crystals of complex **(S,S)-Zn** with a coordinated DMSO molecule were collected in DMSO/CH₂Cl₂/Methanol solvent system after 1 week. Yield: 65% (206 mg) ^{1}H NMR (400 MHz, DMSO-d_6) δ 8.48 (s, 2H), 7.95 – 7.83 (m, 4H), 7.82 – 7.72 (m, 4H), 7.71 – 7.62 (m, 8H), 7.61 – 7.51 (m, 8H), 7.50 – 7.40 (m, 2H), 7.20 (d, J = 8.0 Hz, 2H), 7.10 (s, 2H), 6.68 (d, J = 8.0 Hz, 4H), 3.27 – 3.16 (m, 2H), 1.97 – 1.86 (m, 2H), 1.83 – 1.69 (m, 6H), 1.46 - 1.28 (m, 2H), 0.09 (s, 12H). ^{13}C NMR (101 MHz, DMSO-D_6) δ 170.4, 165.1, 155.5, 147.8, 139.8, 138.4, 135.9, 133.2, 131.0, 130.5, 129.6, 129.1, 129.0, 128.5, 128.0, 125.7, 124.0, 123.1, 122.1, 119.3, 111.5, 111.1, 67.0, 27.7, 25.1, 23.8, 22.4, 9.8 ppm. ^{11}B NMR (128 MHz, DMSO-d_6) δ -3.39 ppm. MALDI-MS calcd for C₆₆H₅₈B₂N₆O₂Zn, [M]⁺ m/z = 1054.2, found 1054.4. Anal. Calcd for C₆₆H₅₈B₂N₆O₂Zn: C, 75.19; H, 5.55; N, 7.97. Found: C, 75.42; H, 6.18; N, 8.48

Synthesis of complex (R,R)-Zn:

To 150 mL two neck RB, compound **(R,R)-L** (300 mg, 0.3 mmol, 1 equiv.) was dissolved in 15 mL CH₂Cl₂ and a solution of Zn(OAc)₂.2H₂O (72 mg, 0.33 mmol, 1.1 equiv.) in 15 mL dry methanol was added dropwise under nitrogen. The greenish-yellow solution was refluxed for 12 h. Light green color crystals of complex **(R,R)-Zn** with a coordinated DMSO molecule were collected after 1 week from DMSO/CH₂Cl₂/Methanol solvent system. Yield: 53% (168 mg) ^{1}H NMR (400 MHz, DMSO-d_6) δ 8.48 (s, 2H), 7.99 – 7.83 (m, 4H), 7.82 – 7.73 (m, 4H), 7.72 – 7.62 (m, 8H), 7.61 – 7.50 (m, 8H), 7.50 – 7.36 (m, 2H), 7.20 (d, J = 8.0 Hz, 2H), 7.10 (s, 2H), 6.69 (d, J = 8.0 Hz, 4H), 3.27 – 3.13 (m, 2H), 1.97 – 1.86 (m, 2H), 1.83 – 1.69 (m, 6H), 1.46 - 1.28 (m, 2H), 0.09 (s,

12H) ^{13}C NMR (101 MHz, DMSO-D_6) δ 170.4, 165.1, 147.8, 139.8, 138.4, 135.9, 133.2, 131.0, 130.5, 129.7, 129.1, 129.0, 128.5, 128.0, 125.7, 124.0, 123.1, 122.1, 119.3, 111.5, 111.1, 64.6, 27.7, 23.8, 22.3, 9.81 ppm. ^{11}B NMR (128 MHz, DMSO-d_6) δ -2.26 ppm. MALDI-MS calcd for $C_{66}H_{58}B_2N_6O_2Zn$, $[M]^+$ m/z = 1054.2, found 1054.4. Anal. Calcd for $C_{66}H_{58}B_2N_6O_2Zn$: C, 75.19; H, 5.55; N, 7.97. Found: C, 74.91; H, 5.89; N, 8.72

4.5 References:

1.　L. Mutihac, J. H. Lee, J. S. Kim and J. Vicens, *Chem. Soc. Rev.*, **2011**, *40*, 2777-2796.

2.　Y. Zhou and J. Yoon, *Chem. Soc. Rev.*, **2012**, *41*, 52-67.

3.　C. Zeng, X. Zhang and L. Pu, *Chem. Eur. J.*, **2017**, *23*, 2432-2438.

4.　F. Zhao, Y. Du, J. Tian, D. Shi, Y. Wang, L. Hu, S. Yu, X. Yu and L. Pu, *Eur. J. Org. Chem.*, **2018**, *2018*, 1891-1895.

5.　J. Wang, H.-B. Liu, Z. Tong and C.-S. Ha, *Coord. Chem. Rev.*, **2015**, *303*, 139-184.

6.　L. He, X. Yang, K. Xu, X. Kong and W. Lin, *Chem. Sci.*, **2017**, *8*, 6257-6265.

7.　M. Hu, J. Fan, H. Li, K. Song, S. Wang, G. Cheng and X. Peng, *Org. Biomol. Chem.*, **2011**, *9*, 980-983.

8.　K. Wu, K. Li, Y. J. Hou, M. Pan, L. Y. Zhang, L. Chen and C. Y. Su, *Nat. Commun.*, **2016**, *7*, 10487.

9.　C. X. Yin, K. M. Xiong, F. J. Huo, J. C. Salamanca and R. M. Strongin, *Angew. Chem. Int. Ed.*, **2017**, *56*, 13188-13198.

10.   J. Yin, Y. Kwon, D. Kim, D. Lee, G. Kim, Y. Hu, J. H. Ryu and J. Yoon, *J. Am. Chem. Soc.*, **2014**, *136*, 5351-5358.

11.   M. Zhang, M. L. Saha, M. Wang, Z. Zhou, B. Song, C. Lu, X. Yan, X. Li, F. Huang, S. Yin and P. J. Stang, *J. Am. Chem. Soc.*, **2017**, *139*, 5067-5074.

12.   L. He, V. L. L. So and J. H. Xin, *Sens. Act. B Chem.*, **2014**, *192*, 496-502.

13.   E. Oliveira, C. Santos, P. Poeta, J. L. Capelo and C. Lodeiro, *Analyst*, **2013**, *138*, 3642-3645.

14.   G. Sivaraman, T. Anand and D. Chellappa, *ChemPlusChem*, **2014**, DOI: 10.1002/cplu.201402217, n/a-n/a.

15.   T.-B. Wei, J.-F. Chen, X.-B. Cheng, H. Li, B.-B. Han, Y.-M. Zhang, H. Yao and Q. Lin, *Org. Chem. Front.*, **2017**, *4*, 210-213.

16.   Y. Liu, X. Wu, C. He, Z. Li and C. Duan, *Dalton Trans.*, **2010**, *39*, 7727-7732.

17.   C. He, Z. Lin, Z. He, C. Duan, C. Xu, Z. Wang and C. Yan, *Angew. Chem. Int. Ed.*, **2008**, *47*, 877-881.

18.   Y. Jiao, J. Zhang, L. Zhang, Z. Lin, C. He and C. Duan, *Chem. Commun.*, **2012**, *48*, 6022-6024.

19.   Y. Liu, X. Wu, C. He, Y. Jiao and C. Duan, *Chem. Commun.*, **2009**, DOI: 10.1039/b915358f, 7554-7556.

20.   X. He, Q. Zhang, X. Liu, L. Lin and X. Feng, *Chem. Commun.*, **2011**, *47*, 11641-11643.

21.   S. Y. Jiao, L. L. Peng, K. Li, Y. M. Xie, M. Z. Ao, X. Wang and X. Q. Yu, *Analyst*, **2013**, *138*, 5762-5768.

22. R. Joseph, B. Ramanujam, A. Acharya and C. P. Rao, *J. Org. Chem.*, **2009**, *74*, 8181-8190.

23. R. K. Pathak, K. Tabbasum, A. Rai, D. Panda and C. P. Rao, *Analyst*, **2012**, *137*, 4069-4075.

24. X. Wu, H. B. Zhang, Z. X. Xu and J. Zhang, *Chem. Commun.*, **2015**, *51*, 16331-16333.

25. Q. H. You, A. W. Lee, W. H. Chan, X. M. Zhu and K. C. Leung, *Chem. Commun.*, **2014**, *50*, 6207-6210.

26. J. T. Hou, K. Li, K. K. Yu, M. Y. Wu and X. Q. Yu, *Org. Biomol. Chem.*, **2013**, *11*, 717-720.

27. Z. Huang, S. Yu, K. Wen, X. Yu and L. Pu, *Chem. Sci.*, **2014**, *5*, 3457-3462.

28. J. Dong, C. Tan, K. Zhang, Y. Liu, P. J. Low, J. Jiang and Y. Cui, *J. Am. Chem. Soc.*, **2017**, *139*, 1554-1564.

29. C. He, J. Wang, P. Wu, L. Jia, Y. Bai, Z. Zhang and C. Duan, *Chem. Commun.*, **2012**, *48*, 11880-11882.

30. J. Hou, F. Song, L. Wang, G. Wei, Y. Cheng and C. Zhu, *Macromolecules*, **2012**, *45*, 7835-7842.

31. M. M. Wanderley, C. Wang, C. D. Wu and W. Lin, *J. Am. Chem. Soc.*, **2012**, *134*, 9050-9053.

32. P. Wu, M. Jiang, X. Hu, J. Wang, G. He, Y. Shi, Y. Li, W. Liu and J. Wang, *RSC Adv.*, **2016**, *6*, 27944-27951.

33.   W. Xuan, M. Zhang, Y. Liu, Z. Chen and Y. Cui, *J. Am. Chem. Soc.*, **2012**, *134,* 6904-6907.

34.   Y. Yang, Q. Zhao, W. Feng and F. Li, *Chem. Rev.*, **2013**, *113*, 192-270.

35.   S. K. Mellerup and S. Wang, *Chem. Soc. Rev.*, **2019**, *48*, 3537-3549.

36.   H. Jintoku, M. Takafuji, R. Oda and H. Ihara, *Chem. Commun.*, **2012**, *48*, 4881-4883.

37.   N. Zhou, S. Wang, Y. Xiao and X. Li, *Chem. Asian J.*, **2018**, *13*, 81-88.

38.   A. S. Mahadevi and G. N. Sastry, *Chem. Rev.*, **2016**, *116*, 2775-2825.

39.   Z. Xing, Y. Fu, J. Zhou, C. Zhu and Y. Cheng, *Org. Biomol. Chem.*, **2012**, *10*, 4024-4028.

40.   J. Dong, Y. Zhou, F. Zhang and Y. Cui, *Chem. Eur. J.*, **2014**, *20*, 6455-6461.

41.   R. Puglisi, F. P. Ballistreri, C. M. A. Gangemi, R. M. Toscano, G. A. Tomaselli, A. Pappalardo and G. T. Sfrazzetto, *New J. Chem.*, **2017**, *41*, 911-915.

42.   F. Song, G. Wei, L. Wang, J. Jiao, Y. Cheng and C. Zhu, *J. Org. Chem.*, **2012**, *77*, 4759-4764.

43.   P. Nayak, A. C. Murali, V. Chandrasekhar and K. Venkatasubbaiah, *Mater. Adv.*, **2022**, *3*, 5893-5899.

Chapter 5

Synthesis of B←N coordinated phenanthroimidazole based diphenyl-borane dimers and study of their photophysical and electrochemical properties

5.1 Introduction

Conjugated polycyclic aromatic hydrocarbons (PAHs), have gained popularity due to their potential uses in organic light-emitting diodes, organic photovoltaics, and organic field-effect transistors.[1] PAHs have shown reduced HOMO-LUMO gap which is useful in making materials for optoelectronic applications. Recent research has demonstrated that main-group elements such as N, P, S, B, and Si can be included in the backbone of PAHs to modify their electronic properties.[2, 3] Among different main-group embedded PAHs, tri- and tetra-coordinated boron-embedded PAHs exhibit phosphorescence, strong fluorescence, thermally induced delayed fluorescence, and photo-switchable molecules.[4-23] Although several tetra-coordinated boron compounds have been discovered, B←N coordinated compounds have drawn a lot of attention due to their ability to adopt a planar conformation and the rigidity of their structure, both of which contribute to the materials' enhanced ability to receive electrons.[5, 11, 12, 14, 24-33] Owing to these interesting properties, the B-N coordinated compounds are used as photochromic materials,[21] oxygen sensors,[34] mechanochromic materials, photocatalysts,[35] and so on.

Recently, nitrogen-containing PAHs have attracted interest and are considered potential candidates for optical sensors because of their great thermal stability, high extinction coefficients, and programmable photophysical properties.[36-44] Due to their high quantum efficiency and effective electron transport properties, phenanthroimidazoles, one of the nitrogen-containing PAHs, have been employed in organic light-emitting diodes (OLEDs) or as photosensitizers in dye-sensitized solar cells.[36, 37, 39, 40, 44] Different methods have been used to synthesize π-extended phenanthroimidazoles, which favorably change the photophysical properties and broaden the range of applications for photonic and optoelectronic devices.[40] These

methods aid in achieving strong UV-Vis absorption, improved fluorescence quantum yield, a long excited state lifetime, and good solubility in organic solvents.[45] Recent research has revealed that the optoelectronic characteristics of phenanthroimidazoles can be tuned by boron coordination.[46-49] Li and co-workers, for instance, prepared a number of phenanthroimidazole-quinoline-based boron dyes that exhibit strong red fluorescence both in solution and in the solid state.[47] Lee and coworkers demonstrated the use of phenanthroimidazole-based triaryl boranes as sensors for the detection of fluoride ions.[50] Ziessel[51] and Zhang[49] studied the photophysical properties of 2-(2-hydroxyphenyl)phenanthroimidazole based boron compounds. Although π-conjugated phenanthroimidazole dimers that work well as fluorescent materials have been reported, boron-embedded π-conjugated phenanthroimidazole dimers has not been investigated. The charge-withdrawing ability of parent species (imidazole, pyridine, *etc.*).) is significantly improved by B N coordination in general.[52] This allows for effective intramolecular charge transfer, resulting in a significant change in dipole moment upon activation. Recently, we examined the effects of structural organization on nonlinear optical (NLO) properties and reported the synthesis and characterization of π-conjugated dimethyl-boron doped phenanthroimidazole dimers.[53] By lowering the rotational degrees of freedom, the presence of B-N coordination also increases the posibility of attaining coplanar chromophores. Herein, we report the synthesis and photophysical properties of highly emissive π-extended diphenyl-borane doped phenanthroimidazole dimers.

5.2 Results and Discussion

5.2.1 *Synthesis*

Scheme 5.1 shows the synthesis of B-N coordinated phenanthroimidazole dimers with and without a spacer. The starting materials **1** and **2** were synthesized by following the literature procedure.[35] Compounds **3** and **4** were obtained in moderate yield by the electrophilic aromatic borylation reaction of **1** (or) **2** with BBr_3. The reaction of compounds 3 or 4 with PhMgBr affords compounds **5** or **6**. The reaction of compound **6** with bis(pinacolato)diboron and a catalytic amount of $Pd(dppf)Cl_2$ under Miyaura borylation conditions afforded compound **8** in 78% yield. The ^{11}B NMR spectrum of compound **8** shows two peaks; the peak at -0.2 ppm corresponds to a tetra-coordinate boron center and the peak at 30.1 ppm corresponds to the boronate ester boron center (Fig. 5.1). Compound **9** was synthesized by Pd-catalyzed Suzuki coupling between compound **8** and compound **6**. The Suzuki coupling between compound **6** and 2,2'-(9,9-dihexyl-9H-fluorene-2,7-diyl)bis(4,4,5,5-tetramethyl-1,3,2-dioxaborolane) (or) 9-hexyl-2,7-bis(4,4,5,5-tetramethyl-1,3,2-dioxaborolan-2-yl)-9H-carbazole afforded compound **10** (or) **11**, respectively, in moderate yields. All the dimers were purified by silica gel column chromatography and characterized by ^{1}H, ^{13}C, and ^{11}B NMR spectroscopy.
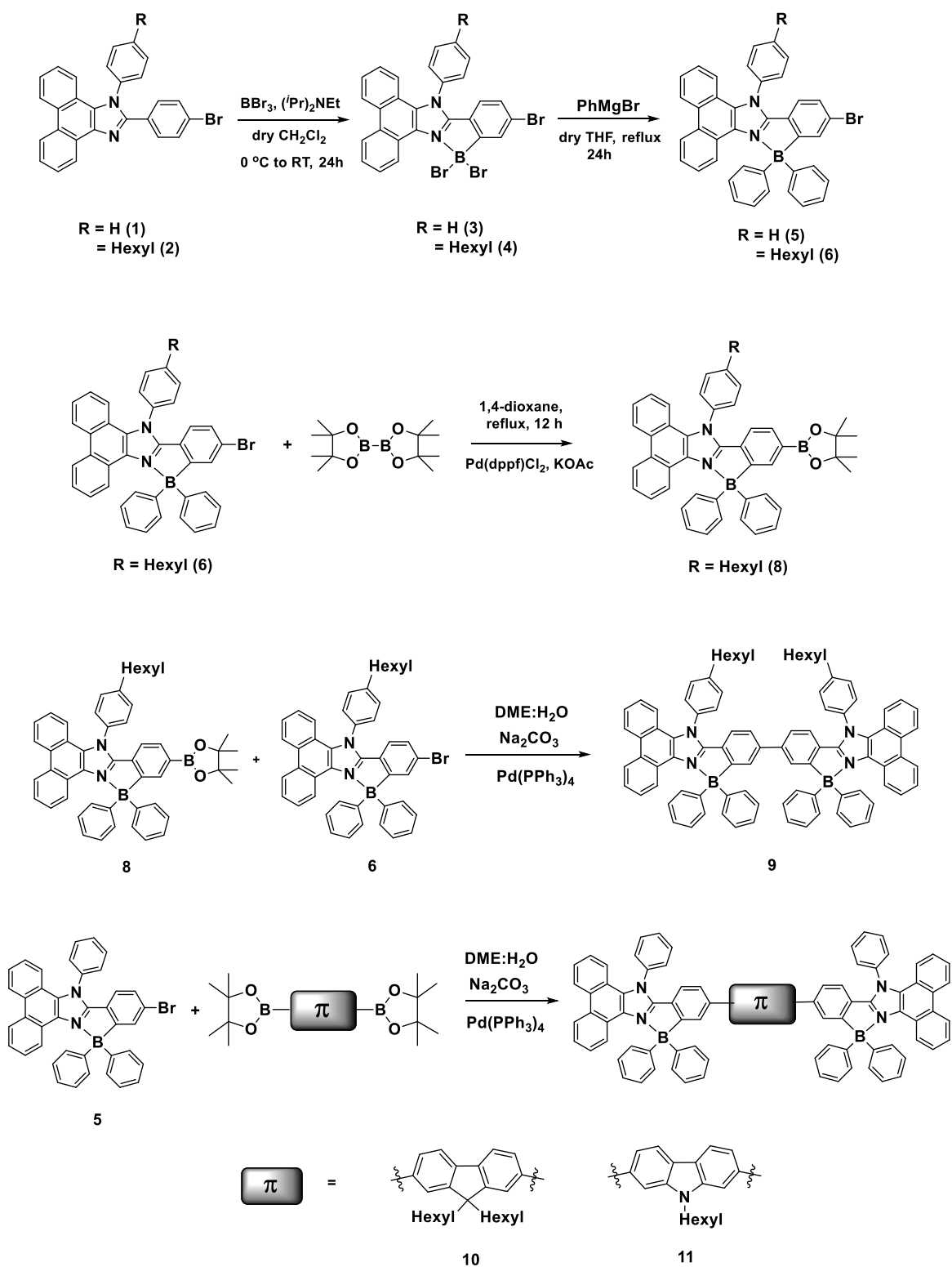
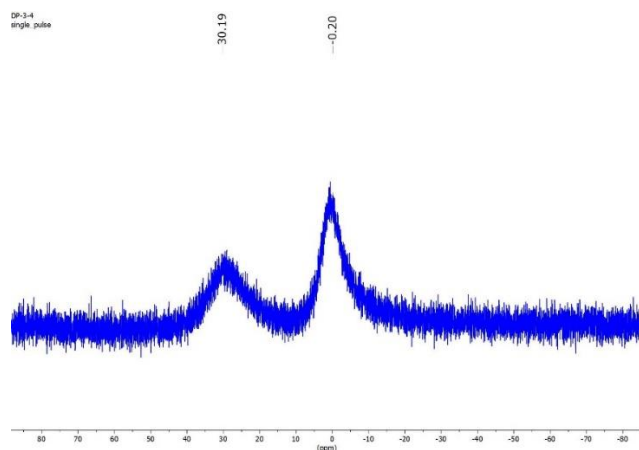**Scheme 5.1:** Synthesis of compounds **5-11**

Figure 5.1: ^{11}B NMR of compound **8** in CDCl$_3$

5.2.2 *X-ray crystal structure analysis*

Single crystal of compound **6** suitable for X-ray diffraction was obtained by slow evaporation of the respective solutions using CHCl$_3$/*n*-hexane mixture. The molecular structure of compound **6** is shown in Fig 5.2; the bond distances and bond angles of compound **6** are presented in table 5.2. In compound **6**, the tetra-coordinate boron center adopts a typical distorted tetrahedral geometry with bond lengths and bond angles ranging between 1.622 Å to 1.637 Å and 96.25º to 117.51º respectively. The B–N and B–C distances are consistent with those of other reported B ← N chelated tetra-coordinated boron complexes.[53] (Table 5.2).

A single crystal of compound **9** suitable for X-ray diffraction was obtained by slow evaporation of the respective solutions using a CHCl$_3$/diethyl ether mixture. The molecular structure of compound **9** is shown in Fig 5.2; bond angles and bond lengths of compound **9** are presented in table 5.2. In compound **9**, the tetra-coordinate boron center adopts a typical distorted tetrahedral geometry with bond lengths and bond angles ranging between 1.619 Å to 1.629 Å and 96.27º to 115.4º respectively. The B–N and B–C distances are consistent with those of other reported B ← N chelated tetra-coordinate boron compounds in the literature.[35]
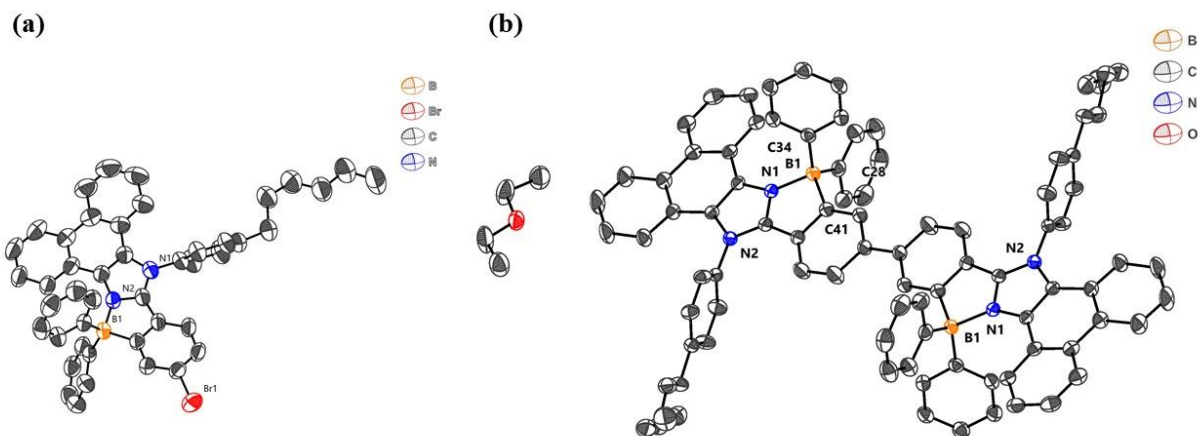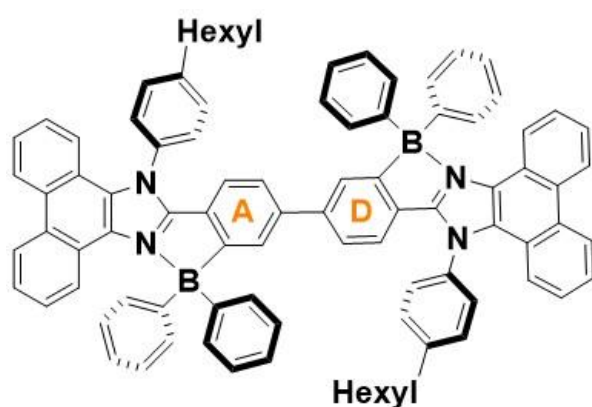
Figure 5.2: Crystal structure of compounds (a) **6** and (b) **9.** (Thermal ellipsoids at 50% probability). Hydrogen atoms are removed for clarity.

Compound **9** shows a crystallographic inversion center in which both the boron centers are *anti* to each other. The interplanar angle between Plane A and Plane D in compound **9** is 0.78° which indicates near planarity within the system. Boron coordination helps in the planarization of the phenanthrene imidazole plane with phenyl ring A and subsequently, complete planarization is achieved in the dimeric system.
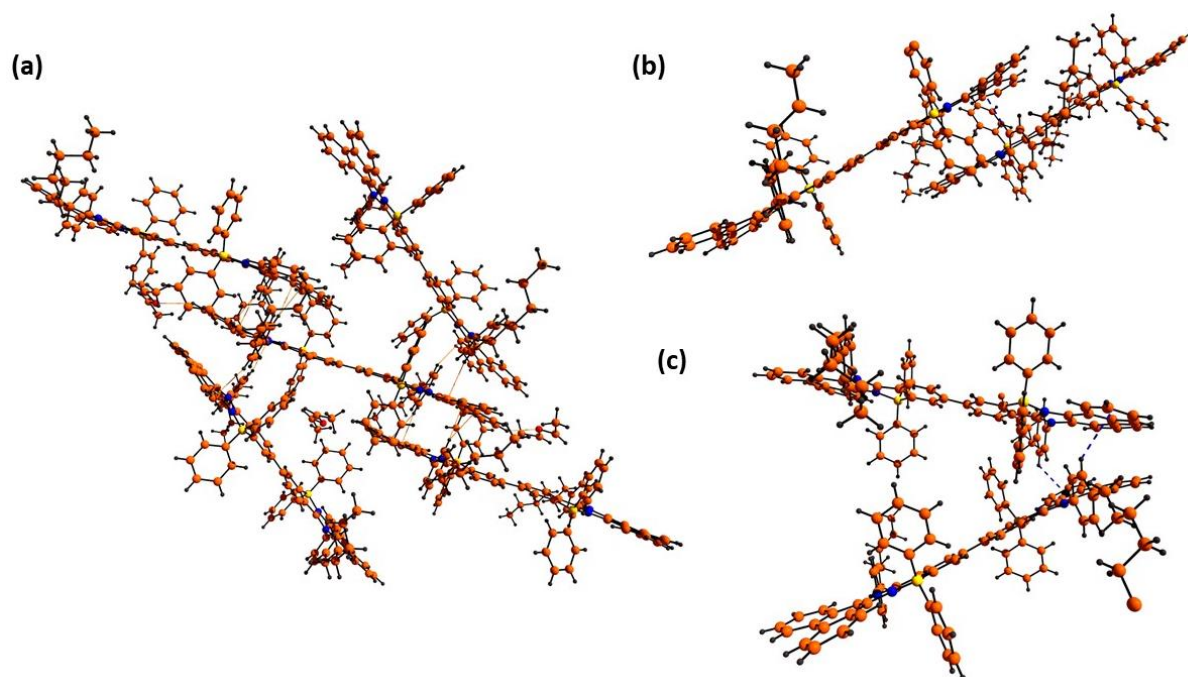
Figure 5.3: C-H….π interactions in compound **9**

Table 5.1: Crystal data and structure refinement for compounds **6** and **9**

Identification code	Compound **6**	Compound **9**
Empirical formula	$C_{45}H_{38}BBrN_2$	$C_{94}H_{84}B_2N_4O$
Formula weight	697.49	653.63
Temperature/K	299.8(4)	100.01(10)
Crystal system	triclinic	monoclinic
Space group	P-1	C2/c
a/Å	10.02640(10)	27.7707(7)
b/Å	12.17750(10)	14.7767(4)
c/Å	16.18720(10)	17.8187(5)
α/°	108.6550(10)	90
β/°	90.5560(10)	101.874(2)
γ/°	105.8170(10)	90
Volume/Å^3	1791.46(3)	7155.6(3)

Z	2	8
ρ_{calc}g/cm^3	1.293	1.213
μ/mm^{-1}	1.815	0.070
F(000)	724.0	2776.0
Crystal size/mm^3	$0.16 \times 0.15 \times 0.12$	$0.19 \times 0.17 \times 0.15$
Radiation	CuKα (λ = 1.54184)	MoKα (λ = 0.71073)
2Θ range for data collection/°	8.01 to 151.17	6.802 to 60.686
Index ranges	$-12 \le h \le 12, -15 \le k \le 15, -20 \le l \le 18$	$-34 \le h \le 37, -19 \le k \le 16, -22 \le l \le 23$
Reflections collected	33142	33359
Independent reflections	7245 [R_{int} = 0.0347, R_{sigma} = 0.0200]	8353 [R_{int} = 0.0296, R_{sigma} = 0.0239]
Data/restraints/parameters	7245/903/443	8353/0/458
Goodness-of-fit on F^2	1.046	1.048
Final R indexes [I>=2σ (I)]	R_1 = 0.0577, wR_2 = 0.1764	R_1 = 0.0643, wR_2 = 0.1786
Final R indexes [all data]	R_1 = 0.0622, wR_2 = 0.1818	R_1 = 0.0697, wR_2 = 0.1826
Largest diff. peak/hole / e Å^{-3}	0.53/-0.85	0.78/-0.43

Table 5.2: Selected bond lengths and bond angles of compounds **6** and **9**

Compound **6**	**Bond Length (Å)**	Compound **9**	**Bond Length (Å)**
N2-B1	1.625 (3)	N1-B1	1.629 (2)

C17-B1	1.637 (3)	C34-B1	1.619 (2)
C34-B1	1.622 (3)	C41-B1	1.629 (2)
C40-B1	1.632 (3)	C28-B1	1.625 (3)
	Bond Angles (°)		**Bond Angles (°)**
N2-B1-C17	96.25 (15)	C34-B1-N1	110.30 (13)
N2-B1-C40	110.70 (18)	C34-B1-C28	115.44 (13)
C34-B1-N2	107.67 (18)	C34-B1-C41	109.95 (13)
C34-B1-C17	113.10 (18)	C28-B1-N1	109.04 (13)
C34-B1-C40	117.51 (17)	C28-B1-C41	114.16 (14)
C40-B1-C17	109.52 (18)	C41-B1-N1	96.27 (12)

5.2.3 *Photophysical properties*

Compounds **9-11** are insoluble in non-polar and protic solvents; hence, the UV-Vis absorption and emission properties were studied in CH_2Cl_2, DMF, and THF solvents, and the relevant data are presented in Table 5.3. The UV-Vis absorption and fluorescence spectra of compounds **9-11** in THF are depicted in Fig. 5.4. As shown in table 5.3, compound **9** absorbs at a lower wavelength ($\lambda_{max} = 380$ nm) whereas compound **11** absorbs at a higher wavelength ($\lambda_{max} = 389$ nm) in CH_2Cl_2 solution with a molar extinction coefficient of 87000 & 78000 $M^{-1} cm^{-1}$ for compounds **9** & **11** respectively.

All compounds **9-11** exhibit negligible absorption maximum shifts in different solvents with different polarities. These results suggest that all the boron compounds are less solvated by polar solvents in the ground state and also the B ← N coordinated bond present in these compounds may not be replaced with strong nucleophiles such as DMF. The absorption maximum of compound **11 is slightly** red-shifted compared

to those of other compounds, which can be attributed to the better conjugation nature of carbazole over fluorene spacer, in other words, carbazole acts as a better spacer to extend the conjugation in the dimers. Furthermore, all the dimers exhibited a substantial redshift in emission over the monomeric borylated phenanthroimidazole owing to the increased conjugation length. (Fig. 5.5)
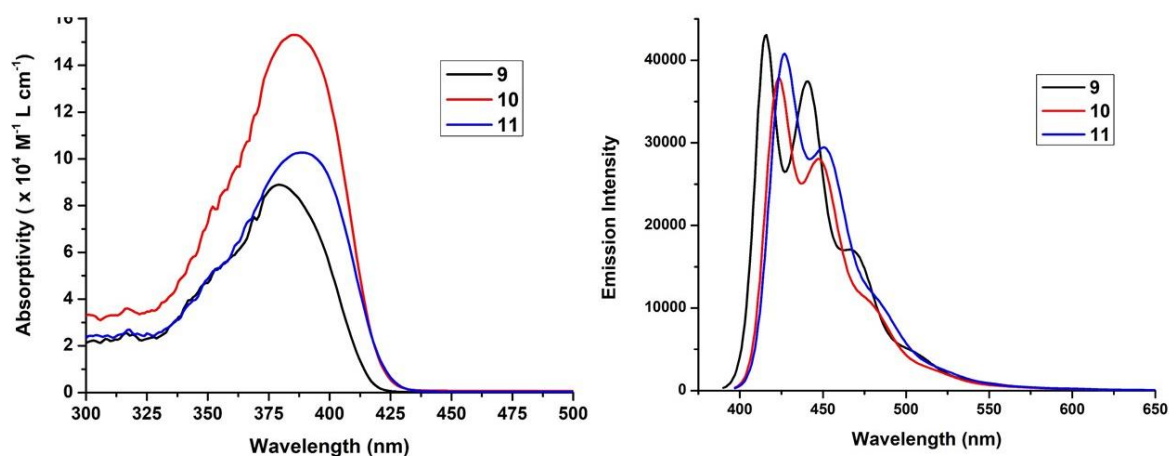

Figure 5.4: Absorption and emission spectra of compounds **9**, **10,** and **11** in THF at 1 x 10^{-5} M concentration

Table 5.3: Summary of photophysical properties of compounds **9,10** and **11** in different solvents

	Solvent	λ_{max} (nm)	ε x 10^5 (mol^{-1} L cm^{-1})	λ_{ems} (nm)	Stokes Shift (cm^{-1})	ϕ^c	Lifetime (ns)
Compound **9**	CH$_2$Cl$_2$	380	0.87	418, 443	3742	0.99	1.01
	CHCl$_3$	380	1.29	418, 443	3742	0.79	0.95
	THF	379	0.89	416, 441	3709	0.92	1.01
	DMF	381	1.08	419, 444	3724	0.88	1.06
	Solid			462, 491		0.38	

Compound **10**	CH$_2$Cl$_2$	386	1.02	424, 448	3585	0.99	0.72
	CHCl$_3$	387	0.88	425, 449	3568	0.86	0.69
	THF	386	1.53	424, 447	3535	0.95	0.71
	DMF	387	1.13	426, 449	3568	0.76	0.71
	Solid			457, 485		0.11	
Compound **11**	CH$_2$Cl$_2$	389	0.78	429, 452	3583	0.99	0.75
	CHCl$_3$	388	0.88	428, 452	3649	0.83	0.71
	THF	389	1.02	427, 451	3533	0.91	0.75
	DMF	391	0.84	429, 452	3451	0.70	0.80
	Solid			479		0.23	

[c] Absolute quantum yield using integrating sphere module

The steady-state fluorescence spectra of compounds **9-11** were recorded upon excitation at their absorption maxima and the relevant data are summarised in Table 5.3. All the complexes show intense emission with a maximum at 418 nm (for **9**), 424 nm (for **10**), and 429 nm (for **11**) in CH$_2$Cl$_2$ (Fig 5.4), and the emission maxima of the dimers are slightly affected by solvent polarity.

Compounds **11** exhibit red-shifted emission maxima over compounds **9 and 10** due to an increase in the conjugation length. Interestingly, all these compounds exhibit very high fluorescence quantum yields (0.99 for **9**, 0.99 for **10,** and 0.99 for **11** in CH$_2$Cl$_2$) compared to other reported B ← N coordinated boron compounds[5, 11, 12, 14, 24-33] which suggests that the energy loss through a non-radiative process is minimum in the dimers. We believe that the B ← N coordination plays a major role in reinforcing the planarity by inhibiting the free rotation between the phenanthroimidazole unit and the phenyl ring.
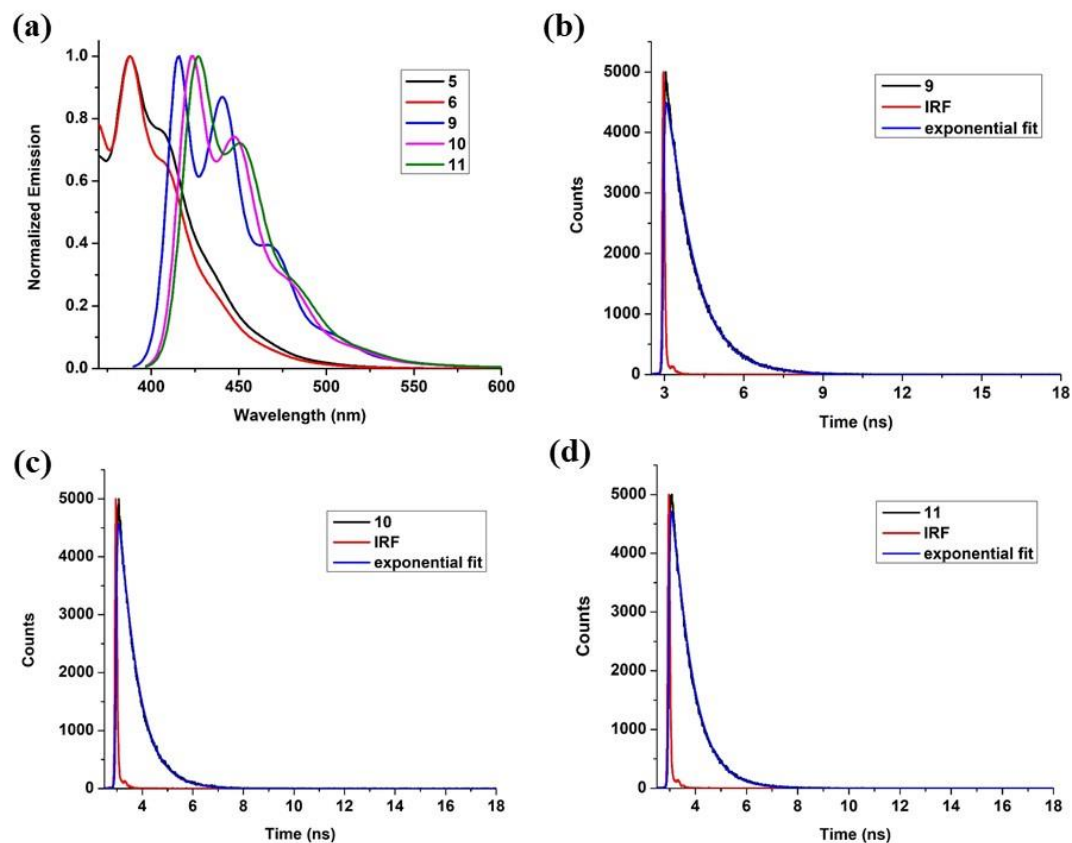
Figure 5.5: (a) Normalized emission of compounds **5, 6, 9, 10,** and **11** in THF at 1 x 10^{-5} M. Fluorescence lifetime decay profiles of compounds (b) **9** (c) **10** and (d) **11** in THF

Compounds **9-11** also exhibit bright solid-state emission (Fig 5.6) with red-shifted emission maxima in comparison with their emission in the solution state (table 5.3). The solid-state quantum yields of 0.38 for **9**, 0.11 for **10,** and 0.23 for **11** are significantly lower than their solution-state quantum yields. The observed red-shifted emissions and lower quantum yields in the solid state might be because of the increased intermolecular interactions in the solid state. (Fig. 5.3)
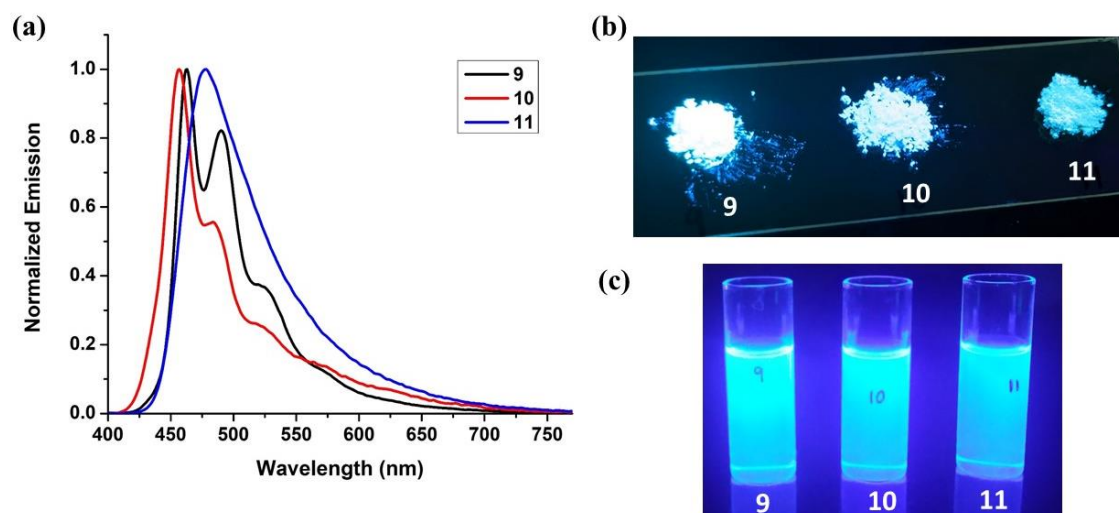
Figure 5.6: (a) Solid emission spectra of compounds **9**, **10** and **11** excited at 380 nm. Photographic images of compounds **9**, **10**, **11** in (b) solid state (c) THF at 1 x 10^{-5} M concentration

5.2.4 *Electrochemical Properties*

Table 5.4: Electrochemical data of **9-11**

Compounds	E_{red}[#] (V)
9	-2.26, -2.43
10	-2.35, -2.78
11	-2.40, -2.76

Cathodic peak potential

The electrochemical properties of compounds **9-11** were investigated by cyclic voltammetry (CV) in deoxygenated N, N-Dimethylformamide (DMF) at room temperature (Figure 5.7 and Table 5.4). Within the DMF electrochemical window, all the compounds display two-electron reduction reactions. While compounds **10** and **11** had two quasi-reversible reduction peaks, compound **9** showed two reversible

reduction peaks. Compound **9** has less negative reduction potentials than compounds **10** and **11**. Increased π-conjugation resulted in a highly negative cathodic peak potential of compound **11**.
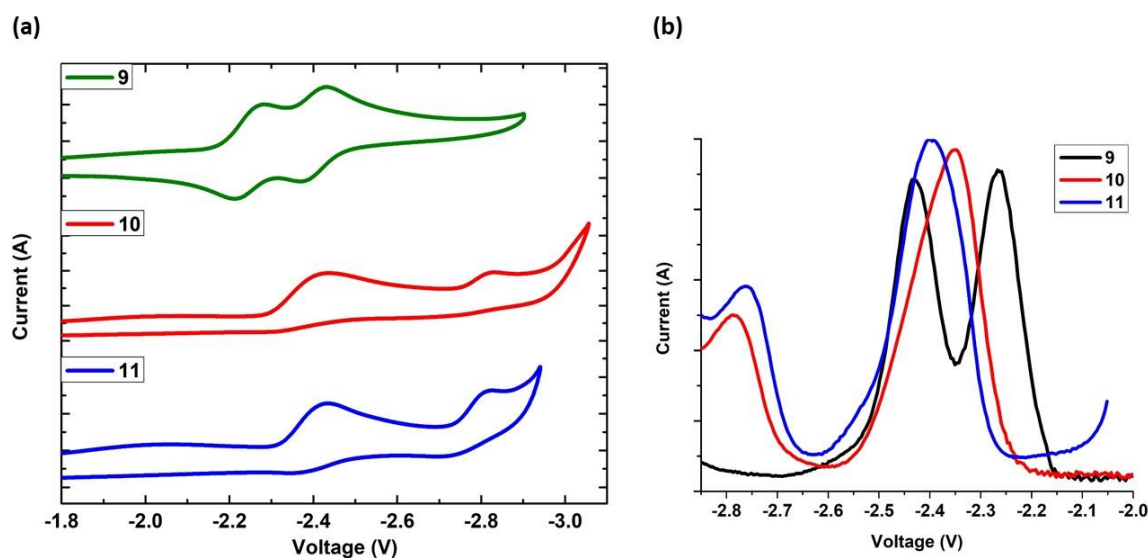
Figure 5.7: (a) Cyclic voltammograms of compounds **9** - **11** (vs. Ferrocene/Ferrocenium) with 0.1 M Bu$_4$NPF$_6$ in DMF as the supporting electrolyte (scan rate 100 mV/s) (b) Differential Pulse Voltammetry (DPV) of compounds **9** – **11** (vs Ferrocene/Ferrocenium) with 0.1 M Bu$_4$NPF$_6$ in DMF as the supporting electrolyte

5.2.5 *Theoretical calculations*

To gain more insight into the electronic properties, we performed DFT calculations at the B3LYP/6-31G(d) level. Electronic excitations were computed using time-dependent density functional theory (TD-DFT) calculations with the optimized geometries. The HOMO and LUMO levels along with the band gaps are presented in Tables 5.5 and 5.6. For all compounds **9–11**, the HOMO and LUMO levels involve contributions from the entire molecule and can be considered as π–π* transition which
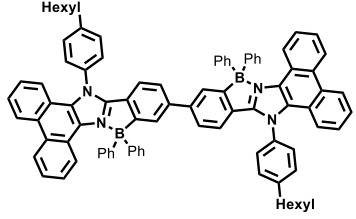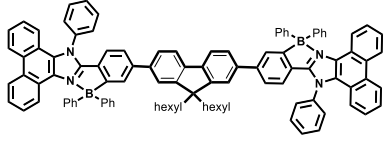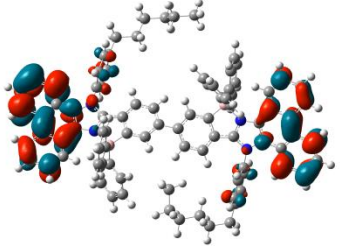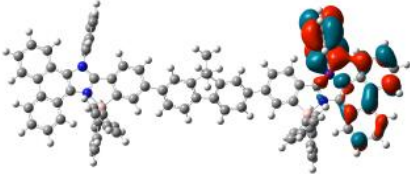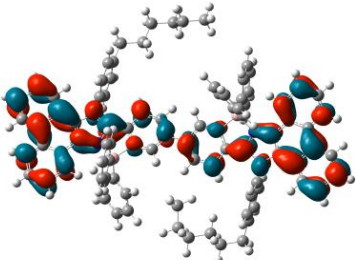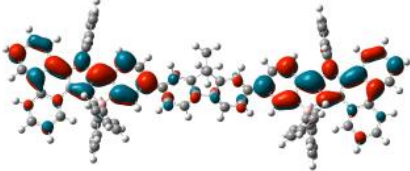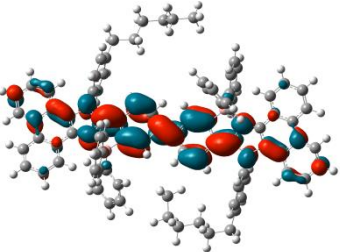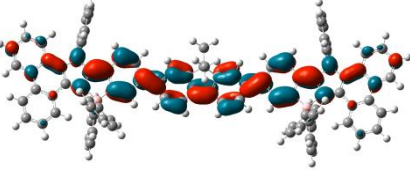
is the lowest electronic transition. The HOMO–LUMO gaps of compounds **9** (3.60 eV), **10** (3.52 eV), **11** (3.54 eV), and **12** (3.61 eV) remain nearly unchanged.
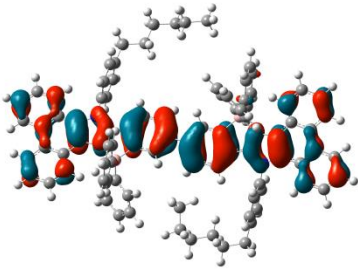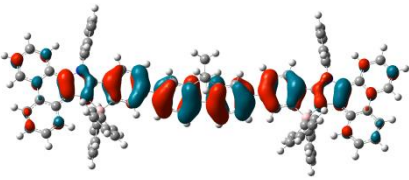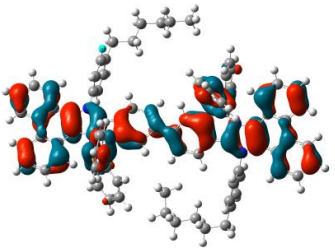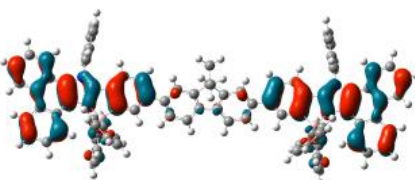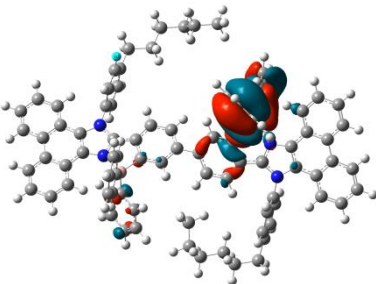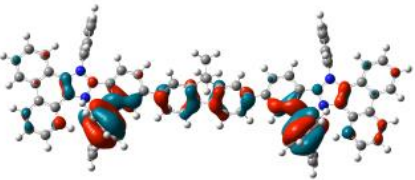
Table 5.5: Calculated electronic transitions for compounds **9**, **10** and **11** from TD-DFT (B3LYP) calculations
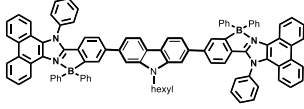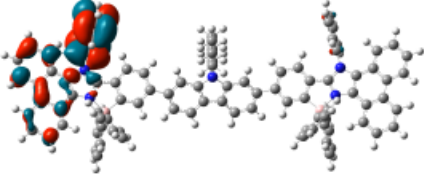
Compound	Transition	MO contributions	Energy gap eV (nm)	Oscillator strength/f
9	$S_0 \rightarrow S_1$	HOMO→LUMO	3.16 (391)	1.5339
	$S_0 \rightarrow S_2$	HOMO-2→LUMO	3.49 (354)	0.0034
		HOMO-1→LUMO		
	$S_0 \rightarrow S_3$	HOMO-5→LUMO	3.55 (348)	0.0053
		HOMO-2→LUMO		
		HOMO-1→LUMO		
10	$S_0 \rightarrow S_1$	HOMO-1→LUMO+1	3.0882 (401)	2.5646
		HOMO→LUMO		
	$S_0 \rightarrow S_2$	HOMO-1→LUMO	3.42 (361)	0.0127
		HOMO→LUMO+1		
	$S_0 \rightarrow S_3$	HOMO-3→LUMO	3.51 (352)	0.0035
		HOMO-2→LUMO+1		
		HOMO-1→LUMO		
		HOMO→LUMO+1		
11	$S_0 \rightarrow S_1$	HOMO-2→LUMO+1	3.10 (398)	2.6668
		HOMO→LUMO		
	$S_0 \rightarrow S_2$	HOMO-1→LUMO	3.27 (378)	0.0108
	$S_0 \rightarrow S_3$	HOMO-2→LUMO	3.47 (361)	0.0249
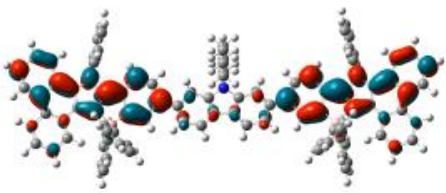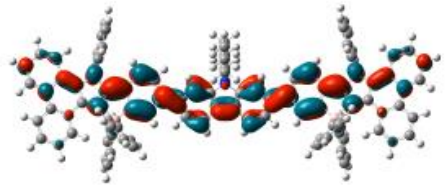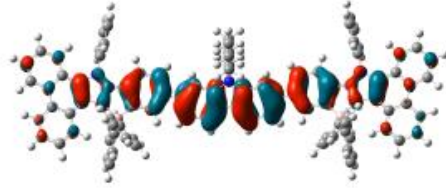
		HOMO→LUMO+1		

Table 5.6. Computed orbitals for compounds **9-11**

Compound	**9**	**10**
LUMO+2	-0.9813 eV	-1.0501 eV
LUMO+1	-1.0686 eV	-1.3521 eV
LUMO	-1.5879 eV	-1.5996 eV

HOMO	-5.1957 eV	-5.1212 eV
HOMO-1	-5.4884 eV	-5.4122 eV
HOMO-2	-5.6508 eV	-5.6342 eV

Compound	**11**
LUMO+2	

	-1.0491 eV	
LUMO+1	-1.3341 eV	
LUMO	-1.5495 eV	
HOMO	-5.0902 eV	
HOMO-1	-5.2501 eV	
HOMO-2	-5.4013 eV	

5.3 Conclusion

In conclusion, we have synthesized a series of phenanthroimidazole based dinuclear boron compounds (**9–11**) starting from different phenanthroimidazole structural motifs using Suzuki coupling. The photophysical properties of these compounds greatly depend on the π-conjugation length (no spacer-compound **9**; 9,9-dihexyl-9*H*-fluorene-compound **10**; 9-hexyl-9*H*-carbazole-compound **11**). The B ← N coordination reinforces the coplanarity between plane A (D) and the phenanthroimidazole, which makes them act as better conjugating materials and thus helps to achieve more desirable optical properties. In general, all the dimers showed an enhanced molar absorption coefficient and substantial redshift over the monomeric borylated phenanthroimidazole due to the increased conjugation length. Furthermore, all the dinuclear boron compounds exhibited strong fluorescence emission with 99% quantum yield in solution and moderate emission in the solid state. The electrochemical and rich photophysical properties make these compounds potential candidates for use in OLEDs as electron-transporting materials.

5.4 Experimental section

5.4.1 *General information*

All reagents and starting materials were purchased from Sigma-Aldrich, Alfa-Aesar, and Spectrochem chemical companies and used as received unless otherwise noted. Chlorinated solvents, acetonitrile, and DMF were distilled from CaH_2. THF and toluene were distilled from Na/benzophenone before use. All 400 MHz ^{1}H, 100 MHz ^{13}C, and NMR spectra were recorded on a Bruker ARX 400 spectrometer operating at 400 MHz. All ^{1}H and ^{13}C NMR spectra were referenced internally to solvent signals.

All NMR spectra were recorded at ambient temperature. ESI mass spectra were recorded on Bruker, micrOTOF-QII mass spectrometer. MALDI was recorded on Applied Biosystems Q10 4800 MALDI TOF/TOF analyzer using 4000 series explorer software for acquisition and GPS explorer software, version 3.6 for analysis. Elemental analyses were performed in a Euro Vector EA 3000 CHNS analyzer. The absorbance spectra were recorded on a JASCO V-730 UV-Visible spectrometer. The fluorescence spectra were recorded using an Edinburgh FS5 spectrofluorometer. Absolute fluorescence quantum yields of compounds **9-11** were measured by integrating sphere method using an Edinburgh FS5 spectrofluorometer. The fluorescence spectra are corrected for the instrumental response. Cyclic voltammetric measurements were performed with a conventional three-electrode cell using an electrochemical workstation (CH Instrument, Model: 1100A) The three-electrode system consisted of a Glassy carbon working electrode, a Pt wire as the secondary electrode, and an Ag wire as the reference electrode. The voltammograms were recorded in deoxygenated THF containing Bu_4NPF_6 (0.1 M) as the supporting electrolyte. The scans were referenced after the addition of a small amount of ferrocene as the internal standard. Single-crystal X-ray diffraction data for compounds **6** and **9** were collected on a Rigaku SuperNova fine-focused dual diffractometer, with Cu Kα radiation (λ = 1.54178 Å) or Mo-Kα radiation (0.71073 Å) equipped with a PILATUS200K detector. Using Olex2, the structures were solved with the ShelXS structure solution program using Direct Methods and refined with the ShelXL refinement package using Least Squares minimization. All non-hydrogen atoms were refined with anisotropic displacement coefficients. The H atoms were placed at calculated positions and were refined as riding atoms. DFT calculations were performed with the Gaussian09 program.[54] The structures were optimized using 6-

31G(d,p) (B3LYP) as the basis set. Frequency calculations confirmed the optimized structures to be local minimum structures. Excitation data were determined using TD-DFT (B3LYP) calculations.

### 5.4.2 *Synthetic procedure and spectral characterization*

Compound 5
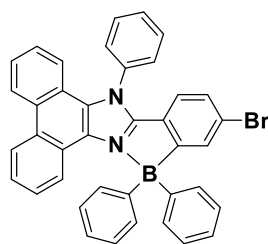
To a stirred solution of compound **1** (5.0 g, 11.1 mmol), N,N-diisopropylethylamine (1.94 mL, 11.1 mmol) in 150 mL dichloromethane at 0 °C was added BBr_3 (3.15 mL, 33.3 mmol) under nitrogen. After being stirred at room temperature for 24 h, the reaction was quenched by adding ice water and extracted with CH_2Cl_2. The combined organic layers were washed with water, dried over Na_2SO_4, and concentrated under vacuum to afford the crude complex **3**. Without further isolation, PhMgBr (1.0 M in THF, 27.75 ml, 27.75 mmol) was added to the stirred solution of complex **3** in dry THF at 0 °C. After the addition of PhMgBr, the reaction was refluxed and progress was monitored by TLC. After being refluxed for 32 h, it was quenched with ice-cold water and extracted with ethyl acetate. The combined organic layer was washed with water, and brine, and dried over Na_2SO_4, and concentrated under vacuum. The residue was purified by silica gel column chromatography using *n*-hexane/dichloromethane as eluent. Yield: 4.6 g (67%). ^{1}H NMR (400 MHz, CDCl$_3$) δ 8.76 (d, *J* = 8.0 Hz, 1H), 8.65 (d, *J* = 8.0 Hz, 1H), 8.44 (d, *J* = 8.0 Hz, 1H), 7.96 – 7.77 (m, 6H), 7.67 – 7.48 (m, 6H), 7.40 – 7.27 (m, 3H), 7.23 – 7.08 (m, 7H), 7.05 (dd, *J* = 8.0, 2.4 Hz, 1H), 6.26 (d, *J* = 8.0 Hz, 1H). ^{13}C NMR (101 MHz, CDCl$_3$) δ 154.5, 136.5, 133.5, 133.3, 131.8, 131.4, 130.9, 129.8, 129.1, 128.6, 128.4, 127.4, 127.1, 127.0, 126.8, 126.6, 126.5, 125.6, 124.3, 122.8, 122.7, 122.2, 122.1, 120.7. ^{11}B NMR

(128 MHz, CDCl$_3$) δ 0.79. HRMS (ESI+, m/z) calcd for C$_{39}$H$_{27}$BBrN$_2$, [M+H]$^+$ m/z = 614.3725, found 614.3693

Compound 6
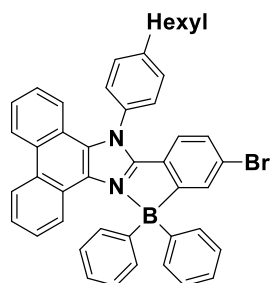
Compound 6 was synthesized by adopting a similar protocol used for the synthesis of compound 5. The quantities involved are compound **2** (5.0 g, 9.37 mmol), N,N-diisopropylethylamine (1.63 ml, 9.37 mmol), BBr$_3$ (2.66 mL, 28.11 mmol), PhMgBr (1.0 M in THF, 23.42 ml, 23.42 mmol). Yield: 4.76g (73%).^{1}H NMR (400 MHz, CDCl$_3$) δ 8.76 (d, J = 8.0 Hz, 1H), 8.64 (d, J = 8.0 Hz, 1H), 8.44 (d, J = 8.0 Hz, 1H), 7.86 – 7.79 (m, 1H), 7.73 – 7.49 (m, 10H), 7.39 – 7.27 (m, 3H), 7.22 – 7.09 (m, 6H), 7.08 – 7.01 (m, 1H), 6.32-6.26 (m, 1H), 2.94 (t, J = 8.0 Hz, 2H), 1.92 – 1.79 (m, 2H), 1.54 – 1.34 (m, 8H), 0.97 (t, J = 8.0 Hz, 3H). ^{13}C NMR (101 MHz, CDCl$_3$) δ 154.6, 147.1, 133.8, 133.4, 133.3, 131.2, 130.8, 129.7, 129.3, 129.0, 128.6, 128.0, 127.3, 127.1, 126.9, 126.6, 126.4, 125.8, 125.5, 124.2, 122.7, 122.3, 122.1, 120.7, 35.9, 31.7, 31.2, 28.9, 22.7, 14.1. ^{11}B NMR (128 MHz, CDCl$_3$) δ 1.79. HRMS (ESI+, m/z) calcd for C$_{45}$H$_{39}$BBrN$_2$, [M+H]$^+$ m/z = 698.2270, found 698.2256
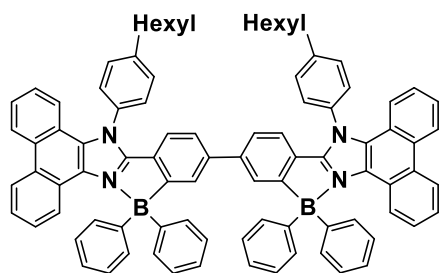
Compound 8
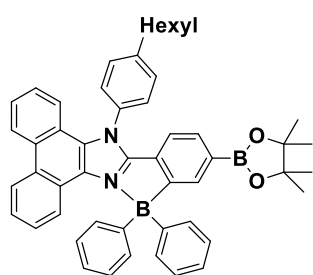
Degassed 1,4-dioxane was added to a mixture of compound **5** (4.0 g, 6.52 mmol), potassium acetate (1.92 g, 19.57 mmol), bis(pinacolato)diborane (1.82 g, 7.17 mmol), Pd(dppf)Cl$_2$ (143 mg, 0.19 mmol, 3 mol%) under nitrogen atmosphere in a two necked round bottom flask fitted with refluxing condenser. The reaction was refluxed and the progress was monitored by TLC. After 24 h, the reaction mixture was poured into water and extracted with CH$_2$Cl$_2$. The combined organic layer was washed with brine solution, dried over Na$_2$SO$_4$, and concentrated

under vacuum. The residue was purified by silica gel column chromatography using

n-hexane/ethyl acetate mixture as eluent. Yield: 3.78 (78%) ^{1}H NMR (400 MHz,

CDCl$_3$) δ 8.75 (d, *J* = 8.0 Hz, 1H), 8.63 (d, *J* = 8.0 Hz, 1H), 8.47 (d, *J* = 8.0 Hz, 1H),

8.14 (s, 1H), 7.73 – 7.65 (m, 2H), 7.65 – 7.56 (m, 7H), 7.55 – 7.49 (m, 1H), 7.41 –

7.27 (m, 4H), 7.19 – 7.12 (m, 4H), 7.12 – 7.04 (m, 2H), 6.42 (d, *J* = 8.0 Hz, 1H), 2.92

(t, *J* = 8.0 Hz, 2H), 1.83 (p, *J* = 7.6 Hz, 2H), 1.53 – 1.37 (m, 5H), 0.97 (t, *J* = 8.0 Hz,

3H). ^{13}C NMR (101 MHz, CDCl$_3$) δ 136.5, 133.4, 131.9, 131.1, 129.7, 128.1, 127.2,

127.0, 126.8, 126.3, 125.2, 124.2, 122.9, 122.7, 122.2, 120.8, 120.0, 83.7, 35.9, 31.7,

31.4, 29.0, 24.9, 22.7, 14.2. ^{11}B NMR (128 MHz, CDCl$_3$) δ 30.19, -0.20. Anal. Calcd

for C$_{51}$H$_{50}$B$_2$N$_2$O$_2$: C, 82.27; H, 6.77; N, 3.76. Found: C, 81.55; H, 7.42; N, 4.32
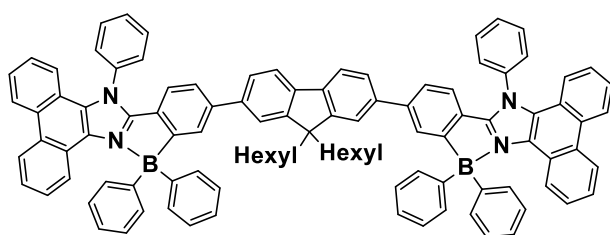
Compound 9

To an oven-dried two neck 250 mL RB, compound **6** (1.0 g, 1.43 mmol), compound **8** (1.17 g, 1.57 mmol), Na$_2$CO$_3$ (0.454 g, 4.29 mmol) and Pd(PPh$_3$)$_4$ (0.05 g, 0.043 mmol) were

loaded under nitrogen atmosphere. To this mixture, degassed DME (40 mL) and water

(10 mL) in 4:1 ratio were added and the reaction mixture was refluxed for 24 h. The

progress of the reaction was monitored through TLC. After completion of the

reaction, the whole mixture is cooled to room temperature. Dichloromethane (50 mL)

and water (50 mL) were added to the reaction mixture; the organic layer was

separated and the aqueous layer was extracted using CH$_2$Cl$_2$ (3x20 mL). The

combined organic layer was washed with brine, dried over Na$_2$SO$_4$, and concentrated

under reduced pressure. The crude product was purified by column chromatography

using *n*-hexane/dichloromethane on neutral alumina to afford the corresponding

product **9**. Yield: 55% (0.917 g). ^{1}H NMR (400 MHz, CDCl$_3$) δ 8.75 (d, *J* = 8.0 Hz, 2H), 8.63 (d, *J* = 8.0 Hz, 2H), 8.47 (d, *J* = 8.0 Hz, 2H), 7.78 (s, 2H), 7.70 (d, *J* = 8.0 Hz, 4H), 7.63 (d, *J* = 8.0 Hz, 4H), 7.60 – 7.47 (m, 12H), 7.40 – 7.30 (m, 4H), 7.28 (s, 1H), 7.24 (s, 1H), 7.12 (t, *J* = 8.0 Hz, 10H), 7.08 – 7.01 (m, 4H), 6.47 (d, *J* = 8.0 Hz, 2H), 2.94 (t, *J* = 8.0 Hz, 4H), 1.92 – 1.81 (m, 4H), 1.53 – 1.35 (m, 12H), 0.97 (t, *J* = 8.0 Hz, 6H). ^{13}C NMR (101 MHz, CDCl$_3$) δ 169.9, 155.4, 148.2, 146.9, 143.7, 134.0, 133.3, 131.1, 131.0, 129.6, 129.2, 129.2, 128.9, 128.1, 127.2, 127.0, 126.8, 126.7, 126.3, 126.2, 125.2, 125.0, 124.2, 122.9, 122.7, 122.3, 121.2, 120.8, 35.9, 31.7, 31.2, 29.0, 22.8, 14.2. ^{11}B NMR (128 MHz, CDCl$_3$) δ 1.59. Anal. Calcd for C$_{90}$H$_{76}$B$_2$N$_4$: C, 87.51; H, 6.20; N, 4.54. Found: C, 87.08; H, 6.94; N, 4.22
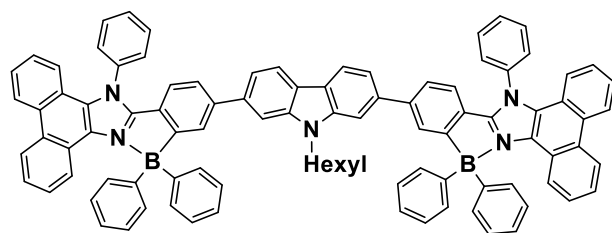
Compound 10

To an oven-dried two neck 250 mL RB, compound **5** (1.00 g, 1.63 mmol), 2,2'-(9,9-dihexyl-9H-fluorene-2,7-diyl)bis(4,4,5,5-tetramethyl-1,3,2-dioxaborolane) (0.477 g, 0.81 mmol), Na$_2$CO$_3$ (0.518 g, 4.89 mmol) and Pd(PPh$_3$)$_4$ (0.056g, 0.049 mmol) were loaded under nitrogen atmosphere. To this mixture, degassed DME (40 mL) and water (10 mL) in 4:1 ratio were added and the reaction mixture was refluxed for 24 h. The progress of the reaction was monitored through TLC. After completion of the reaction, the whole mixture is cooled to room temperature. Dichloromethane (50 mL) and water (50 mL) were added to the reaction mixture; the organic layer was separated and the aqueous layer was extracted using CH$_2$Cl$_2$ (3x20 mL). The combined organic layer was washed with brine, dried over Na$_2$SO$_4$, and concentrated under reduced pressure. The crude product was purified by

column chromatography using *n*-hexane/dichloromethane on neutral alumina to afford the corresponding product **10**. Yield: 41% (0.464 g). ^{1}H NMR (400 MHz, CDCl$_3$) δ 8.77 (d, *J* = 8.0 Hz, 2H), 8.65 (d, *J* = 8.0 Hz, 2H), 8.50 (d, *J* = 8.0 Hz, 2H), 7.99 (s, 2H), 7.98 – 7.78 (m, 10H), 7.69 – 7.64 (m, 10H), 7.62 – 7.47 (m, 6H), 7.43 (s, 2H), 7.37 – 7.27 (m, 6H), 7.25 – 7.17 (m, 10H), 7.17 – 7.07 (m, 4H), 6.53 (d, *J* = 8.0 Hz, 2H), 2.04 – 1.86 (m, 4H), 1.30 – 1.22 (m, 2H), 1.15 – 0.96 (m, 12H), 0.74 (t, *J* = 8.0 Hz, 6H). ^{13}C NMR (101 MHz, CDCl$_3$) δ 155.3, 151.6, 144.1, 140.3, 140.2, 136.8, 133.4, 131.6, 131.3, 131.0, 129.6, 129.2, 129.0, 128.6, 127.3, 127.0, 126.8, 126.7, 126.5, 126.2, 126.0, 125.4, 124.8, 124.2, 122.8, 122.2, 121.7, 121.2, 120.7, 119.9, 55.2, 40.4, 31.5, 29.8, 23.8, 22.7, 14.0. ^{11}B NMR (128 MHz, CDCl$_3$) δ 2.34. Anal. Calcd for C$_{103}$H$_{84}$B$_2$N$_4$: C, 88.40; H, 6.05; N, 4.00. Found: C, 87.68; H, 6.45; N, 3.95

Compound 11

To an oven-dried two neck 250 mL RB, compound **5** (1.00 g, 1.63 mmol), 9-hexyl-2,7-bis(4,4,5,5-tetramethyl-1,3,2-dioxaborolan-2-yl)-9H-carbazole (0.450 g, 0.81 mmol), Na$_2$CO$_3$ (0.518 g, 4.89 mmol) and Pd(PPh$_3$)$_4$ (0.056 g, 0.049 mmol) were loaded under nitrogen atmosphere. To this mixture, degassed DME (40 mL) and water (10 mL) in 4:1 ratio were added and the reaction mixture was refluxed for 24 h. The progress of the reaction was monitored through TLC. After completion of the reaction, the whole mixture is cooled to room temperature. Dichloromethane (50 mL) and water (50 mL) were added to the reaction mixture; the organic layer was separated and the aqueous layer was extracted using CH$_2$Cl$_2$ (3x20 mL). The combined organic layer was washed with brine, dried over MgSO$_4$, and concentrated under reduced pressure. The crude product was purified by

column chromatography (1:20 of EtOAc: *n*-hexane) on silica gel to afford the corresponding coupled product **11**. Yield: 37% (0.394 g).^{1}H NMR (400 MHz, CDCl$_3$) δ 8.77 (d, *J* = 8.0 Hz, 2H), 8.66 (d, *J* = 8.0 Hz, 2H), 8.53 (d, *J* = 8.0 Hz, 2H), 8.10 – 8.01 (m, 4H), 7.98 – 7.84 (m, 10H), 7.73 – 7.65 (m, 8H), 7.63 – 7.51 (m, 4H), 7.48 (s, 2H), 7.43 – 7.26 (m, 10H), 7.24 – 7.17 (m, 8H), 7.16 – 7.10 (m, 4H), 6.56 (d, *J* = 8.0 Hz, 2H), 4.29 (t, *J* = 8.0 Hz, 2H), 1.89 – 1.76 (m, 2H), 1.36 – 1.21 (m, 6H), 0.87 (t, *J* = 8.0 Hz, 3H). ^{13}C NMR (101 MHz, CDCl$_3$) δ 170.1, 155.4, 148.3, 144.7, 141.4, 139.5, 136.8, 133.4, 131.6, 131.3, 131.1, 129.6, 129.6, 129.2, 129.0, 128.6, 127.3, 127.0, 126.9, 126.8, 126.3, 126.0, 125.4, 125.2, 124.3, 122.8, 122.8, 122.2, 122.0, 121.2, 120.7, 120.5, 119.1, 107.6, 43.2, 31.7, 29.8, 29.0, 27.1, 22.7, 14.1. ^{11}B NMR (128 MHz, CDCl$_3$) δ 2.57. Anal. Calcd for C$_{96}$H$_{71}$B$_2$N$_5$: C, 87.60; H, 5.44; N, 5.32. Found: C, 87.66; H, 5.59; N, 6.04

5.5 References

1.   J. Wu, W. Pisula and K. Müllen, *Chem. Rev.*, **2007**, *107*, 718-747.

2.   A. Narita, X.-Y. Wang, X. Feng and K. Müllen, *Chem. Soc. Rev.*, **2015**, *44*, 6616-6643.

3.   M. Stepien, E. Gonka, M. Zyla and N. Sprutta, *Chem. Rev.*, **2017**, *117*, 3479-3716.

4.   R. R. Cloke, T. Marangoni, G. D. Nguyen, T. Joshi, D. J. Rizzo, C. Bronner, T. Cao, S. G. Louie, M. F. Crommie and F. R. Fischer, *J. Am. Chem. Soc.*, **2015**, *137*, 8872-8875.

5. D. L. Crossley, I. A. Cade, E. R. Clark, A. Escande, M. J. Humphries, S. M. King, I. Vitorica-Yrezabal, M. J. Ingleson and M. L. Turner, *Chem. Sci*, **2015**, *6*, 5144-5151.

6. A. Escande and M. J. Ingleson, *Chem. Comm.*, **2015**, *51*, 6257-6274.

7. K. Hu, Z. Zhang, J. Burke and Y. Qin, *J. Am. Chem. Soc.*, **2017**, *139*, 11004-11007.

8. L. Ji, S. Griesbeck and T. B. Marder, *Chem. Sci.*, **2017**, *8*, 846-863.

9. S. Kawai, S. Saito, S. Osumi, S. Yamaguchi, A. S. Foster, P. Spijker and E. Meyer, *Nat. Commun.*, **2015**, *6*, 8098.

10. T. Kushida, S. Shirai, N. Ando, T. Okamoto, H. Ishii, H. Matsui, M. Yamagishi, T. Uemura, J. Tsurumi, S. Watanabe, J. Takeya and S. Yamaguchi, *J. Am. Chem. Soc.*, **2017**, *139*, 14336-14339.

11. K. Matsuo and T. Yasuda, *Chem. Comm.*, **2017**, *53*, 8723-8726.

12. S. K. Mellerup and S. Wang, *Chem. Soc. Rev.*, **2019**, *48*, 3537-3549.

13. F. Miyamoto, S. Nakatsuka, K. Yamada, K.-i. Nakayama and T. Hatakeyama, *Org. Lett.*, **2015**, *17*, 6158-6161.

14. V. Mukundam, S. Sa, A. Kumari, R. Das and K. Venkatasubbaiah, *J. Mater. Chem. C.*, **2019**, *7*, 12725-12737.

15. K. K. Neena, P. Sudhakar, K. Dipak and P. Thilagar, *Chem. Comm.*, **2017**, *53*, 3641-3644.

16. K. K. Neena and P. Thilagar, *J. Mater. Chem. C.*, **2016**, *4*, 11465-11473.

17. M. Numata, T. Yasuda and C. Adachi, *Chem. Comm.*, **2015**, *51*, 9443-9446.

18. V. F. Pais, M. M. Alcaide, R. Lopez-Rodriguez, D. Collado, F. Najera, E. Perez-Inestrosa, E. Alvarez, J. M. Lassaletta, R. Fernandez, A. Ros and U. Pischel, *Chem. Eur. J.*, **2015**, *21*, 15369-15376.

19. E. v. Grotthuss, A. John, T. Kaese and M. Wagner, *Asian J. Org. Chem.*, **2018**, *7*, 37-53.

20. X.-Y. Wang, J.-Y. Wang and J. Pei, *Chem. Eur. J.*, **2015**, *21*, 3528-3539.

21. D.-T. Yang, S. K. Mellerup, J.-B. Peng, X. Wang, Q.-S. Li and S. Wang, *J. Am. Chem. Soc.*, **2016**, *138*, 11513-11516.

22. S. Yruegas, J. J. Martinez and C. D. Martin, *Chem. Comm.*, **2018**, *54*, 6808-6811.

23. C. Zhu, X. Ji, D. You, T. L. Chen, A. U. Mu, K. P. Barker, L. M. Klivansky, Y. Liu and L. Fang, *J. Am. Chem. Soc.*, **2018**, *140*, 18173-18182.

24. M. Grandl, T. Kaese, A. Krautsieder, Y. Sun and F. Pammer, *Chem. Eur. J.*, **2016**, *22*, 14373-14382.

25. K. Liu, R. A. Lalancette and F. Jäkle, *J. Am. Chem. Soc.*, **2017**, *139*, 18170-18173.

26. V. F. Pais, M. M. Alcaide, R. López-Rodríguez , D. Collado, F. Nájera, E. Pérez-Inestrosa, E. Álvarez, J. M. Lassaletta, R. Fernández, A. Ros and U. Pischel, *Chem. Eur. J.*, **2015**, *21*, 15369-15376.

27. C. Shen, M. Srebro-Hooper, M. Jean, N. Vanthuyne, L. Toupet, J. A. G. Williams, A. R. Torres, A. J. Riives, G. Muller, J. Autschbach and J. Crassous, *Chem. Eur. J.*, **2017**, *23*, 407-418.

28. B. Y.-W. Wong, H.-L. Wong, Y.-C. Wong, M.-Y. Chan and V. W.-W. Yam, *Chem. Eur. J.*, **2016**, *22*, 15095-15106.

29. D.-T. Yang, S. K. Mellerup, J.-B. Peng, X. Wang, Q.-S. Li and S. Wang, *J. Am. Chem. Soc.*, **2016**, *138*, 11513-11516.

30. R. Yoshii, A. Nagai, K. Tanaka and Y. Chujo, *Chem. Eur. J.*, **2013**, *19*, 4506-4512.
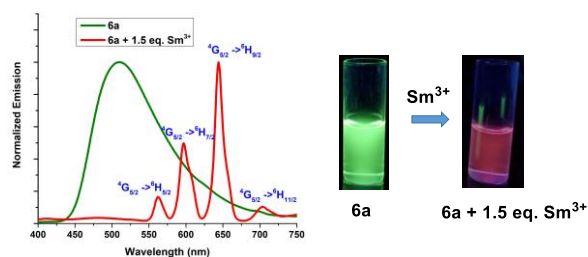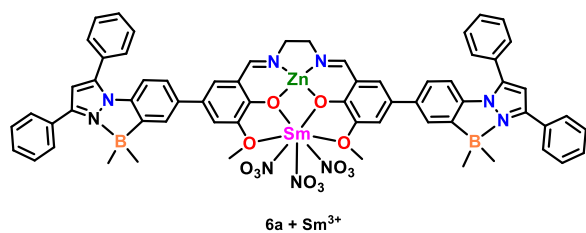
31. M. Yusuf, K. Liu, F. Guo, R. A. Lalancette and F. Jцₚkle, *Dalton Trans.*, **2016**, *45*, 4580-4587.

32. R. Zhao, C. Dou, Z. Xie, J. Liu and L. Wang, *Angew. Chem. Int. Ed.*, 2016, **55**, 5313-5317.

33. C. Zhu, X. Ji, D. You, T. L. Chen, A. U. Mu, K. P. Barker, L. M. Klivansky, Y. Liu and L. Fang, *J. Am. Chem. Soc.*, **2018**, *140*, 18173-18182.

34. K. Liu, R. A. Lalancette and F. Jakle, *J. Am. Chem. Soc.*, **2017**, *139*, 18170-18173.

35. P. Nayak, A. C. Murali, P. K. Pal, U. D. Priyakumar, V. Chandrasekhar and K. Venkatasubbaiah, *Inorg. Chem.*, **2022**, *61*, 14511-14516.

36. W.-C. Chen, Y. Yuan, S.-F. Ni, Q.-X. Tong, F.-L. Wong and C.-S. Lee, *Chem. Sci.*, **2017**, *8*, 3599-3608.

37. R. Francke and R. D. Little, *J. Am. Chem. Soc.*, **2014**, *136*, 427-435.

38. H. Huang, Y. Wang, S. Zhuang, X. Yang, L. Wang and C. Yang, *J. Phys. Chem. C*, **2012**, *116*, 19458-19466.

39. J. E. Kwon, S. Park and S. Y. Park, *J. Am. Chem. Soc.*, **2013**, *135*, 11239-11246.

40. J. Tagare and S. Vaidyanathan, *J. Mater. Chem. C*, **2018**, *6*, 10138-10173.

41. Z. Wang, P. Lu, S. Chen, Z. Gao, F. Shen, W. Zhang, Y. Xu, H. S. Kwok and Y. Ma, *J. Mater. Chem*, **2011**, *21*, 5451-5456.

42. Y. Zhang, S.-L. Lai, Q.-X. Tong, M.-Y. Chan, T.-W. Ng, Z.-C. Wen, G.-Q. Zhang, S.-T. Lee, H.-L. Kwong and C.-S. Lee, *J. Mater. Chem.*, **2011**, *21*, 8206-8214.

43. Y. Zhang, S.-L. Lai, Q.-X. Tong, M.-F. Lo, T.-W. Ng, M.-Y. Chan, Z.-C. Wen, J. He, K.-S. Jeff, X.-L. Tang, W.-M. Liu, C.-C. Ko, P.-F. Wang and C.-S. Lee, *Chem. Mater.*, **2012**, *24*, 61-70.

44. N. Zhou, S. Wang, Y. Xiao and X. Li, *Chem. Asian J.*, **2018**, *13*, 81-88.

45. B. Jędrzejewska, M. Gordel, J. Szeremeta, I. Grela and M. Samoć, *Dyes Pigm*, **2017**, *136*, 150-160.

46. K. Benelhadj, J. Massue, P. Retailleau, G. Ulrich and R. Ziessel, *Org. Lett.*, **2013**, *15*, 2918-2921.

47. W. Li, W. Lin, J. Wang and X. Guan, *Org. Lett.*, **2013**, *15*, 1768-1771.

48. D. K. You, S. H. Lee, J. H. Lee, S. W. Kwak, H. Hwang, J. Lee, Y. Chung, M. H. Park and K. M. Lee, *RSC Adv.*, **2017**, *7*, 10345-10352.

49. Z. Zhang, Z. Zhang, H. Zhang and Y. Wang, *Dalton Trans.*, **2018**, *47*, 127-134.

50. D. K. You, S. H. Lee, J. H. Lee, S. W. Kwak, H. Hwang, J. Lee, Y. Chung, M. H. Park and K. M. Lee, *RSC Adv.*, **2017**, *7*, 10345-10352.

51. K. Benelhadj, J. Massue, P. Retailleau, G. Ulrich and R. Ziessel, *Org. Lett.*, **2013**, *15*, 2918-2921.

52. C. C. Jimenez, A. Enriquez-Cabrera, O. Gonzalez-Antonio, J. Ordonez-Hernandez, P. G. Lacroix, P. Labra-Vazquez, N. Farfan and R. Santillan, *Inorganics*, **2018**, *6,* 131.

53. M. Vanga, S. Sa, A. Kumari, A. C. Murali, P. Nayak, R. Das and K. Venkatasubbaiah, *Dalton Trans.*, **2020**, *49*, 7737-7746.

54. Gaussian 16, Revision A.03, M. J. Frisch, G. W. Trucks, H. B. Schlegel, G. E. Scuseria, M. A. Robb, J. R. Cheeseman, G. Scalmani, V. Barone, G. A. Petersson, H. Nakatsuji, X. Li, M. Caricato, A. V. Marenich, J. Bloino, B. G.
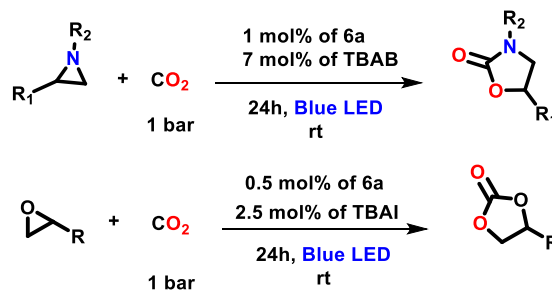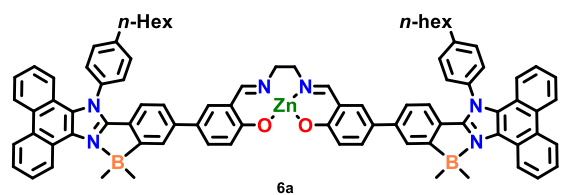
Janesko, R. Gomperts, B. Mennucci, H. P. Hratchian, J. V. Ortiz, A. F. Izmaylov, J. L. Sonnenberg, D. Williams-Young, F. Ding, F. Lipparini, F. Egidi, J. Goings, B. Peng, A. Petrone, T. Henderson, D. Ranasinghe, V. G. Zakrzewski, J. Gao, N. Rega, G. Zheng, W. Liang, M. Hada, M. Ehara, K. Toyota, R. Fukuda, J. Hasegawa, M. Ishida, T. Nakajima, Y. Honda, O. Kitao, H. Nakai, T. Vreven, K. Throssell, J. A. Montgomery, Jr., J. E. Peralta, F. Ogliaro, M. J. Bearpark, J. J. Heyd, E. N. Brothers, K. N. Kudin, V. N. Staroverov, T. A. Keith, R. Kobayashi, J. Normand, K. Raghavachari, A. P. Rendell, J. C. Burant, S. S. Iyengar, J. Tomasi, M. Cossi, J. M. Millam, M. Klene, C. Adamo, R. Cammi, J. W. Ochterski, R. L. Martin, K. Morokuma, O. Farkas, J. B. Foresman, and D. J. Fox, Gaussian, Inc., Wallingford CT, 2016.
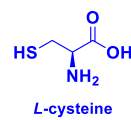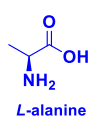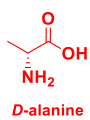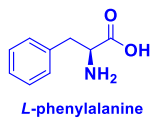
Summary

Chapter 2

6a + Sm³⁺

Chapter 3

6a

$$R_1 \xrightarrow{R_2} + CO_2 \xrightarrow[\text{24h, Blue LED}]{\substack{1 \text{ mol\% of 6a} \\ 7 \text{ mol\% of TBAB}}} \text{oxazolidinone}$$

1 bar   rt

$$\text{epoxide} + CO_2 \xrightarrow[\text{24h, Blue LED}]{\substack{0.5 \text{ mol\% of 6a} \\ 2.5 \text{ mol\% of TBAI}}} \text{cyclic carbonate}$$

1 bar   rt

Chapter 4

(S,S)-Zn
or
(R,R)-Zn

D-phenylalanine   L-phenylalanine   D-alanine   L-alanine   D-cysteine   L-cysteine

Chapter 5

9

π =

10   11